University of South Florida

Digital Commons @ University of South Florida

USF Tampa Graduate Theses and Dissertations

USF Graduate Theses and Dissertations

11-3-2008

Discrete Linear Constrained Multivariate Optimization for Power Sources of Mobile Systems

Stelios G. Ioannou
University of South Florida

Follow this and additional works at: https://digitalcommons.usf.edu/etd

Part of the American Studies Commons

Discrete Linear Constrained Multivariate Optimization

for Power Sources of Mobile Systems

by

Stelios G. Ioannou

A dissertation submitted in partial fulfillment
of the requirements for the degree of
Doctor of Philosophy
Department of Electrical Engineering
College of Engineering
University of South Florida

Co-Major Professor: Elias. K. Stefanakos, Ph.D.
Co-Major Professor: Kimon P. Valavanis, Ph.D.
Paris H. Wiley, Ph.D.
Kenneth A. Buckle, Ph.D.
Richard Wallace, Ph.D.

Date of Approval:
November 03, 2008

Keywords: gimball platform, lithium batteries, lead acid batteries, fuel cells, super-capacitors, Peukert, UGV, ATRV

DEDICATION / ΑΦΙΕΡΩΣΗ

Dedicated to my parents George and Epistimi Ioannou

Αφιερωμένο στους γονείς μου Γιώργο και Επιστήμη Ιωάννου

Thank you for your moral and financial support throughout the years.

This doctorate degree is testimony of good upbringing.

Ευχαριστώ για την ηθική και οικονομική υποστήριξη ανά τα έτη.

Αυτός ο διδακτορικός τίτλος είναι μαρτυρία καλής ανατροφής.

ACKNOWLEDGEMENTS

TABLE OF CONTENTS

LIST OF TABLES

viii

LIST OF FIGURES

NOMENCLATURE

a	Alpha Value of Variable Exponent Proposed Model
A	Surface Area in Meters Squared (m^2)
b	Beta Value of Variable Exponent Proposed Model
B	Vehicle Track in Meters (m)
C	Capacitance in Farads (F)
C_p	Peukert's Battery Capacity in Amperes-Hours (Ah)
CP	Units Connected in Parallel
CS	Units Connected in Series
D	Separation Distance in Meters (m)
E	Energy in Joules (J)
e	Efficiency
e$^-$	Electron
ESR	Effective Series Resistance in Ohms (Ω)
F	Tractive Force in Newton (N)
g	Acceleration of Gravity (9.81m/s^2)
h_{CG}	Height of Center of Gravity in meters (m)
H$^+$	Protons
I	Discharge Current in Amperes (A)
i	Wheel slippage
I_z	Moment of Inertia for Rotation Around the z-axis in (Kgm^2)
L	Vehicle Wheelbase in Meters (m)
l	Fuel Cell Fuel Consumption at Rated Power
m	Mass in Kilograms (Kg)
M_r	Moment of Turning Resistance

p	Peukert's Exponent
P	Electrical Power in Watts (W)
R	Electrical Resistance in Ohms (Ω)
r	Wheel Radius in Meters (m)
R'	Vehicle Turn Radius in Meters (m)
t	Runtime in Hours (Hrs)
T	Torque in Newton-Meters (Nm)
V	Voltage in Volts (V)
v	Vehicle Longitudinal Velocity in Meters per Second (m/s)
W	Weight Force in Newton (N)
ε	Permittivity of a Medium, $\varepsilon_o\varepsilon_r$, in ($CV^{-1}m^{-1}$ of Fm^{-1})
ε_o	Permittivity of Free Apace, 8.8542x10-12 $CV^{-1}m^{-1}$
ε_r	Relative Permittivity or Dielectric Constant
η	Gear Ratio
θ	Road Gradient in Degrees
μ_{rr}	Rolling Resistance Coefficient
μ_t	Lateral Friction Coefficient
ω	Angular Velocity in Radians per Second (rad/s)

Subscripts

-b	Battery Cell
-can	Canisters
-f	Front
-i	Inner
-L	Load
-m	Motor
-o	Outer
-p	Peukert
-PA	Battery Pack
-r	Rear

-ref	Reference or Advertised Discharge Time
-v	Vehicle
-w	Wheels

ABBREVIATIONS

AC	Alternate Current
AFC	Alkaline Fuel Cell
AGM	Absorbed Glass Mat
ATRV	All Terrain Robot Vehicle
CERC	Clean Energy Research Center
DC	Direct Current
DMFC	Direct Methanol Fuel Cell
DOE	Department of Energy
EMF (emf)	Electromotive Force
FC	Fuel Cell
GPS	Global Positioning System
HFC	Hydrogen Fuel Cell
IMU	Inertia Measurement Unit
iSTAR	Intelligence, Surveillance, Target Acquisition and Reconnaissance
Li-Ion	Lithium Ion
Li-Po	Lithium Polymer
NiCad	Nickel Cadmium
NREL	National Renewable Energy Laboratories
PEMFC	Proton Exchange Membrane Fuel Cell
PV	Photovoltaic
RMFC	Reformed Methanol Fuel Cell
SLA	Sealed Lead Acid
SOFC	Solid Oxide Fuel Cell
SPAWAR	Space and Naval Warfare

UAMS	Autonomous UAV Mission System
UAV	Unmanned Aerial Vehicle
UGV	Unmanned Ground Vehicle
USF	University of South Florida
USL	Unmanned Systems Lab
VRLA	Valve Regulate Rechargeable Lead Acid
VTOL	Vertical Take Off and Landing

DISCRETE LINEAR CONSTRAINED MULTIVARIATE OPTIMIZATION FOR POWER SOURCES OF MOBILE SYSTEMS

Stelios G. Ioannou

ABSTRACT

Unmanned ground and aerial vehicles (UGVs and UAVs) have strict payload limitations, limited free space affecting on board power availability resulting in limited endurance and operational range. This limitation is exacerbated by the addition of sensors, actuators and other related equipment needed to accomplish mission objectives in diverse applications.

Two energy sources are mainly available for mobile applications; batteries and fuel cells. Batteries are a relatively cheap, tested technology with good performance under varying loads. On the other hand, fuel cells offer fast and easy refueling solutions. Furthermore, preliminary studies have shown that a hybrid system can combine the advantages of both technologies offering a superior system.

It is true that for most outdoors applications, payload needs, sensor suite utilization and energy requirements are apriori unpredictable. This makes proper sizing of energy storage devices and the prediction of remaining available energy rather difficult tasks.

This research proposes an indirect way of improving the operational range for UAVs of Vertical Take Off and Landing (VTOLs), since the VTOL vehicle is transported to the mission site without the need to fly. The proposed gimballed platform, which will be a power source itself, rotates around two axes perpendicular to each other, allowing the

VTOL to take-off and land, regardless of the position of the UGV, while securing it during transportation. The UGV can also serve as a charging station for the VTOL.

Furthermore, this research proposes a Matlab Simulation tool that can simulate the energy and power demand of small to mid-sized robotic vehicles. This model will simulate the power consumption in the motors based on Skid steering, road gradient, linear and angular velocity.

With the energy and power requirements estimated, a Matlab optimization tool is proposed to be used to determine the optimal configuration of a power system for mobile applications under constraints relating to capacity/runtime, weight, volume, cost, and system complexity. The configuration will be based on commercially available batteries, and fuel cells to significantly reduce cost and delivery time. The optimization tool can be used for any mobile application.

Finally, a new model is proposed for the accurate prediction of battery runtime and remaining energy for single battery discharge. This model reformulates Peukert's equation and achieves higher accuracy by introducing a new concept of variable exponent which is a function of battery capacity and discharge current.

CHAPTER 1. BACKGROUND AND LITERATURE REVIEW

1.1 Motivation

Unmanned ground and aerial vehicles (UGVs and UAVs) have strict payload limitations, limited free space affecting on board power availability resulting in limited endurance and operational range. This limitation is exacerbated by the addition of sensors, actuators and other related equipment needed to accomplish mission objectives in diverse applications.

Two energy sources are available for mobile applications; batteries and fuel cells. Batteries are a relatively cheap, tested technology with good performance under varying loads. On the other hand, fuel cells offer fast and easy refueling solutions. Furthermore, preliminary studies have shown that a hybrid system can combine the advantages of both technologies offering a superior system.

It is true that for most outdoor applications, payload needs, sensor suite utilization and energy requirements are a priori unpredictable. This makes proper sizing of energy storage devices and the prediction of remaining available energy rather difficult tasks.

1.2 Proposed Work

This research proposes an indirect way of improving the operational range of Vertical Take Off and Landing (VTOL, UAVs), since the VTOL vehicle may be transported to the mission site without the need to fly. The proposed gimballed platform, which will be a power source itself, rotates around two axes perpendicular to each other, allowing the VTOL to take-off and land, regardless of the position of the UGV, while securing it during transportation. The UGV can also serve as a charging station for the VTOL.

Furthermore, this research proposes a Matlab Simulation tool that can simulate the energy and power demand of small to mid-sized UGVs. This model will simulate the power consumption in the motors based on Skid steering, road gradient, linear and angular velocity.

With the energy and power requirements estimated, a Matlab optimization tool is proposed to be used to determine the optimal configuration of the power system for mobile applications under constraints related to capacity/runtime, weight, volume, cost, and system complexity. The configuration will be based on commercially available batteries and fuel cells to significantly reduce cost and delivery time. The optimization tool can be used for any mobile application.

Finally, a new model is proposed for the accurate prediction of battery runtime and remaining energy for single battery discharge. This model reformulates Peukert's equation and achieves higher accuracy by introducing a new concept of variable exponent which is a function of battery capacity and discharge current.

1.3 Contributions

- A new model is proposed for accurate prediction of battery runtime and remaining energy for single battery discharge. This model reformulates Peukert's equation and achieves higher accuracy by introducing a new concept of variable exponent which is a function of battery capacity and discharge current.

- A new method is derived to determine the optimal configuration of a hybrid power system for mobile applications under constraints related to capacity/runtime, weight, volume and cost. The configuration will be based on commercially available batteries and fuel cells to reduce cost and delivery time.

- A proof is given showing that Peukert's equation can be used for accurate runtime and remaining energy prediction for lithium batteries.

- An additional contribution is that a Matlab model simulating the energy demand of small to mid-sized robotic vehicles for both indoor and outdoor applications is also part of this thesis. This model simulates the power consumption in the motors based on skid steering, road gradient, linear and angular velocity.

1.4 Novelty and Benefits

Mathematical modeling of power systems is not a new field, especially for batteries. Based on the application, design engineers have used these models for optimal power management algorithms as well as customizing power sources under volume and weight constraints. Nevertheless a literature review has yielded no previous work in the field of sizing hybrid systems.

Fuel cells are currently in the early stages of commercialization. They typically require hybridization by incorporating a battery that will supply start-up and peak power. As a result a need for sizing hybrid systems is already present. This work will benefit the penetration of fuel cells in the market as well as the endurance of mobile systems in both civilian and military applications.

The new concept of variable exponent which is a function of battery capacity and discharge current model achieves higher accuracy in battery runtime and remaining energy prediction than Peukert's equation without the need of more than two experiments that can be done in an hour. This work will benefit mobile applications for more accurate real time runtime and remaining energy prediction, as well as critical backup applications where the backup system can not be offline for more than an hour for accurate battery characterization. In addition this work will benefit lithium battery applications.

1.5 Background

Mathematical modeling of power systems is not a new field, especially for batteries. Such mathematical models are divided into 4 major categories; physical, empirical, abstract and mixed models. Mathematical models are evaluated based on accuracy, computational

complexity, configuration and analytical insight. Based on the application, design engineers have used these models for optimal power management algorithms as well as customizing power sources under volume and weight constraints [1]-[4].

Other software with graphical user interface such, as HOMER® and ADVISOR®, were developed produced by the US Department of Energy (DOE) and the National Renewable Energy Laboratories (NREL). HOMER software is used for static applications and, using a micro-power optimization model, it explores the role of generator sets in small solar power systems. With battery, photo-voltaic and diesel prices as inputs it explores the best cost effective solution at the present time for an increased load demand. For example, is it more cost-effective to include a diesel generator than to increase the size of the battery bank or photo-voltaic (PV) array? The Sri Lanka case study is an elaborate study available online on this.

ADVISOR on the other hand is a simulation tool for vehicle evaluation and testing. With elaborate car models which include wheels, engine, power-train and other car components, ADVISOR helps engineers determine how to increase the life of components, improve vehicle performance, optimize vehicle system designs, and reduce development times. However, models already available on ADVISOR software are mostly for products used in the automotive industry where weight constraints are not as critical as in mobile applications involving small unmanned ground and aerial vehicles (UGV and UAV).

In 1897, W. Peukert established a relationship between battery capacity and discharge current for Lead Acid batteries. His equation predicts the amount of energy you can have from a battery. At higher discharge currents (high discharge rate) the battery efficiency decreases and as a result less energy is delivered [5]-[8].

There are three main models of measuring energy delivered by a battery and hence estimate the remaining battery capacity [9]. The first model takes a linear approach

where the battery capacity loss due to high discharge currents is neglected. Hence, it is assumed that the advertised capacity is always delivered independent of discharge current.

The second model accounts for the loss of battery capacity due to discharge current by introducing a battery efficiency factor, *e*, which is a function of load and rated battery currents and can be derived from battery datasheets. More data will lead to more accurate efficiency estimation.

The third model accounts for the battery relaxation effect which gives the battery the chance to recover the high current lost capacity. This model however, is very analytical and difficult to implement.

Accuracy of both battery runtime and remaining energy prediction increases with increased available data.

1.6 List of References

[1]   R. Rao, S. Vrudhula, D. N. Rakhamatov, "Battery Modeling for Energy Aware System Design", IEEE Computer Society, December 2003.

[2]   M. Chin and G. A. Rincon-Mora, " Accurate Electrical Battery model Capable of Predicting Runtime and I-V Performance", IEEE transactions of energy conversion, Vol.21, No. 2. June 2006.

[3]   S. Parchicha and S. R. Shaw, "A Dynamic PEM Fuel Cell Model", IEEE transactions of energy conversion, Vol.21, No. 2. June 2006.

[4]   F. Rafik, H. Gualous, R. Gallay, A. Crausaz and A. Berthon, "Supercapacitors characterization fro hybrid vehicle applications", IEEE, 2006.

[5]   Smart Gauge, "A proper explanation of Peukert's Equation", Online Posting: http://www.smartgauge.co.uk/peukert.html (January 20, 2008).

[6]   W. Peukert, "About the Dependence of the Capacity of the Discharge Current Magnitude and Lead Acid Batteries", Elektrotechnische Zeitschrift, Volume 20, 1897.

[7]   James Larminie and John Lowry, "Electric Vehicle Technology Explained", 1st Edition, John Wiley and Sons Ltd., pp. 65, ISBN 0-470-85163-5, 2003.

[8]   Dennis Doerffel and Suleiman Abu Sharkh, "A critical review of using the Peukert equation for determining the remaining capacity of lead acid and lithium ion batteries", Journal of Power Sources, pp 395 – 400, 155, 2006.

[9]   Sung Park, Andreas Savvides and Mani B. Srivastava, "Battery Capacity Measurement and Analysis using Lithium Coin Cell battery", Low Power Electronics and Design, International Symposium on, 6-7 Aug. 2001 Page(s):382 – 387.

CHAPTER 2. STATE OF THE ART IN ENERGY AND POWER SYSTEM
TECHNOLOGIES

2.1 Batteries

2.1.1 Technology Overview

Battery is a device that stores electrical charge to be used by electrical devices. Batteries are composed of two electrodes and an electrolyte. By oxidation and reduction of the electrodes, chemical energy is converted to electrical energy. When an electrical device is connected between the cathode (positive electrode) and the anode (negative electrode), there is an electron flow from the anode to the cathode. The loss of electrons causes oxidation at the anode and the gain of electrons causes reduction at the cathode. The rate of change of charge between the electrodes is defined as current, and it is proportional to the chemical energy stored in the battery.

There are two types of batteries; rechargeable and non-rechargeable. Rechargeable batteries also known as secondary batteries are reusable, whereas non-rechargeable batteries are also known as primary or non-reusable. Recharging is the ability to convert electrical energy back to chemical energy and is achieved by an external device called a charger. By reversing the oxidation and reduction reactions occurring during discharge, a charger can force current into the battery. During discharge, anions flow from the cathode to the anode, and cat-ions from the anode to the cathode. The same reactions occur during charging, with the exception that the anode is now the positive electrode and the cathode is the negative electrode.

Battery technology profiles are summarized in table 2-1, with NiCad being the oldest technology. Its high life cycle, low internal resistance, and high load current

characteristics make it an attractive choice for power tools, two way radios and biomedical instruments. Reusable alkaline batteries on the other hand are very cheap, but their high internal resistance limits their use to only very low current applications. Furthermore, despite the low energy density, low price makes sealed lead acid (SLA) batteries attractive for applications where volume and weight is not a problem. Lithium ion batteries are the most expensive. With high energy density and cell voltage, lithium technology is an attractive choice for electronic devices where dimensions and weight are critical, such as consumer electronics and mobile applications. Furthermore, material technology advancements have enabled manufacturing of scaled up lithium batteries for satellite and electric vehicle applications. Since, the purpose of this research is mostly intended for mobile applications then lithium batteries will be primarily investigated. Sections 2.1.2 to 2.1.5 are devoted to lithium batteries.

Table 2-1: Battery Technology Profile from [1], [2]

	NiCad	NiMH	SLA	Li-Ion	Reusable Alkaline
Energy Density (Wh/Kg)	40-60	60-80	30	165	80 (initial)
Internal Resistance (mΩ)	100-300	200-800	<100	300-500	200-2000
Cycle Life	1500	500	200-300	500-1000	10000
Cell Voltage	1.2	1.2	2	3.6	1.5
Load Current	>2C	0.5-1C	0.2C	2C	0.2C
Operating Temperature (^{o}C)	-40 to +60	-20 to +60	-20 to +60	-20 to +60	0 to 65
Cost	$50	$70	$25	$100	$5
In Commercial Use Since	1950	1990	1970	1991	1992

2.1.2 Lithium Batteries

Lithium technology batteries are a good candidate for portable and mobile applications where weight and volume are major restrictions. With high cell voltage and energy densities lithium batteries are one-third the weight and one-half the volume of lead acid batteries and one-half the weight and two-thirds the volume of nickel metal hydride (NiMH) batteries [1]-[4].

2.1.2.1 Technology Overview

Lithium metal has a specific energy of 3800Ah/Kg (1727Ah/lb), which is much higher than lead at 260Ah/Kg, and cadmium at 480Ah/Kg [5]. Unfortunately lithium batteries are susceptible to catastrophic failures that can lead to fire or explosion. This problem necessitates the use of electronic safety designs to control the charging and discharging processes as well as the operating temperature [2], [6].

Lithium batteries have undergone rapid advancements in materials and processing techniques. Besides the Li-MnO$_2$ which is the most common type of lithium battery in use, other cathode materials have also been used [7], [8]. The somewhat newer Lithium Ion and Lithium Ion Polymer batteries have dominated the rechargeable lithium battery market and they feature higher energy and power densities, cell voltages as high as 3.85V, improved stability at voltages higher than 4.2V as well as higher discharge rates with discharge currents as high as 40 times their rated capacities. However, a major bottleneck to their advancement is the price of materials currently used [7]. For example, due to higher cost, than lithium ion and lithium polymer batteries are limited to mass production applications mostly for cell phones that come in a "credit card" like shape [2].

2.1.2.2 Charging Process

The three stages for charging lithium ion batteries are shown in figure 2-1. Most of the time, the charging process is referred to as the constant voltage/constant current method (CV/CC). In stage 1 constant current is applied until the cell open circuit voltage reaches 4.2 volts. Then in stage 2, voltage is kept constant and charging current is gradually decreased to 3% of rated current which indicates that the cell is fully charged to rated capacity. Finally, stage 3 compensates for some cell self discharge. Most lithium ion cells have a maximum open circuit voltage (OCV) of 4.2V (Panasonic – CGP30486 OCV is 4.1V [9]). Safety circuits will prevent higher voltages as long as the appropriate charger is used. Specified chargers should be used not only for safety reasons, but also for performance; if a cell with 4.2V OCV is only charged to 4.1V then its capacity is

reduced by 10% [2]. Depending on the cell type, the charging current varies; smaller cell phone batteries are charged at approximately 1C, whereas larger 18650 type cells are charged at 0.8C or less. Safety circuits monitor and control overcharge, over-discharge, and operating temperatures, thus making lithium ion operation safe.

Usually, the charging process of lithium ion and polymer batteries takes 1 to 3 hours. However, on March 29, 2005, Toshiba announced the release of a new rechargeable lithium ion battery which has the ability to recharge to 80% of its capacity in only one minute [10]. The prototype uses the latest advancements in nano-material technology and is 3.8mm thick, 62mm high and 35mm deep, with a capacity of 600mAh. According to Toshiba, during tests, the prototype battery was charged and discharged fully for 1000 times at a temperature of $25^{o}C$ and lost only 1% of its capacity. Furthermore, at $-40^{o}C$, its capacity is 80%, whereas at $45^{o}C$ it is 100%. After 1000 cycles it suffers a 5% capacity loss at these extreme temperatures. The battery was expected to be commercially available in 2006.
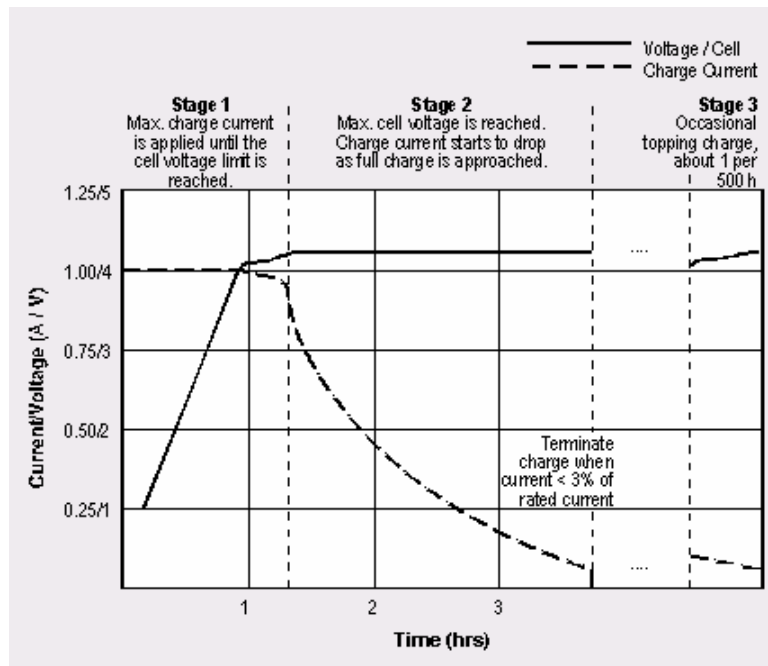
Figure 2-1: Three Stage Charging Process of Lithium Ion Batteries from [2], [6].

2.1.2.3 Performance Characteristics

The discharge versus temperature characteristics of figure 2-2 shows lower cell voltage at an operating temperature of -10°C than at 60°C. Performance of lithium ion batteries erodes drastically at temperatures below 0°C and above 65°C [11], [12] and [13]. Temperature variations lead to different internal resistances [11], [14]. At lower temperatures, internal resistance is higher, thus causing a higher voltage drop. At a discharge rate of 1C represented in figure 2-3, the increased internal resistance affects the cell capacity; at -10°C cell capacity is less than 1400mAh whereas at operating temperatures between 20°C and 60°C, the capacity is approximately 1500mAh.
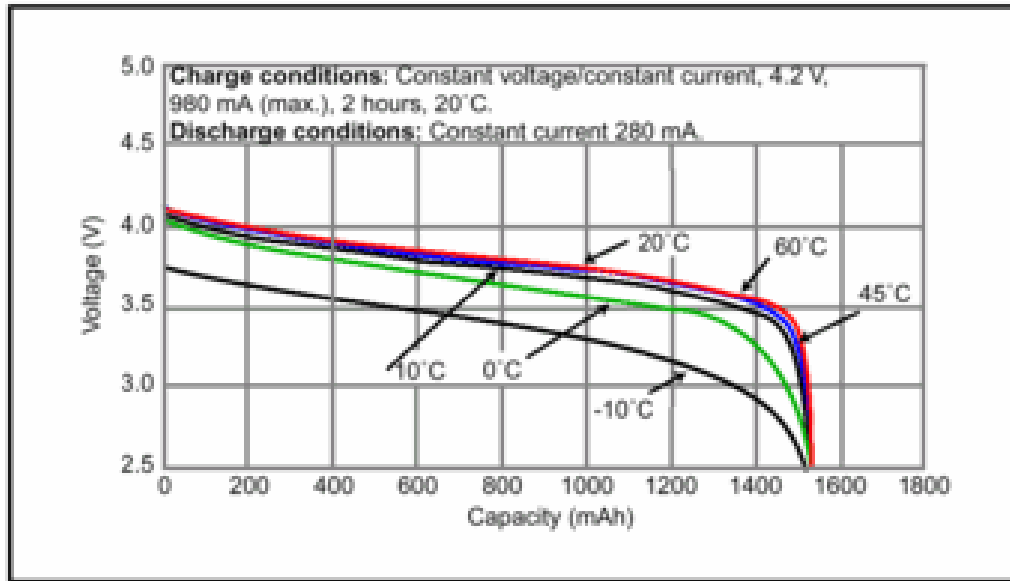
Figure 2-2: Discharge Versus Temperature Characteristics of a Typical Lithium Ion 18650 Cell from [15].

The voltage versus discharge current characteristics represented in figure 2-4 show an output power of 2 watts for this cell, with an end voltage of 3V.
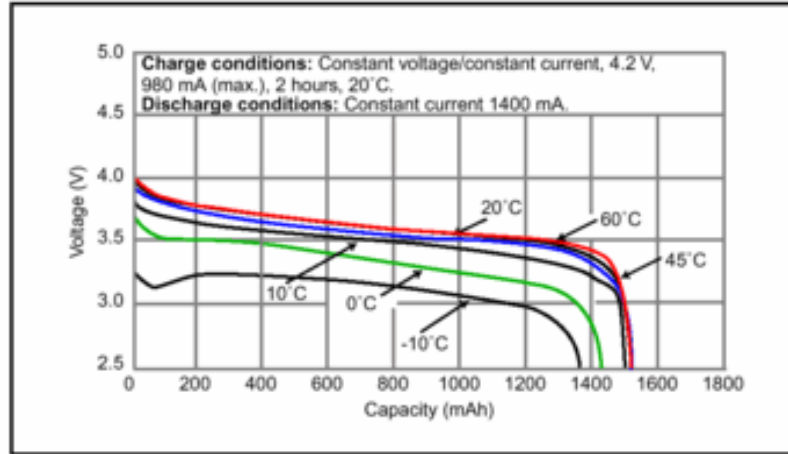
Figure 2-3: High Rate Discharge Characteristics of Typical Lithium Ion 18650 Cell from [15].
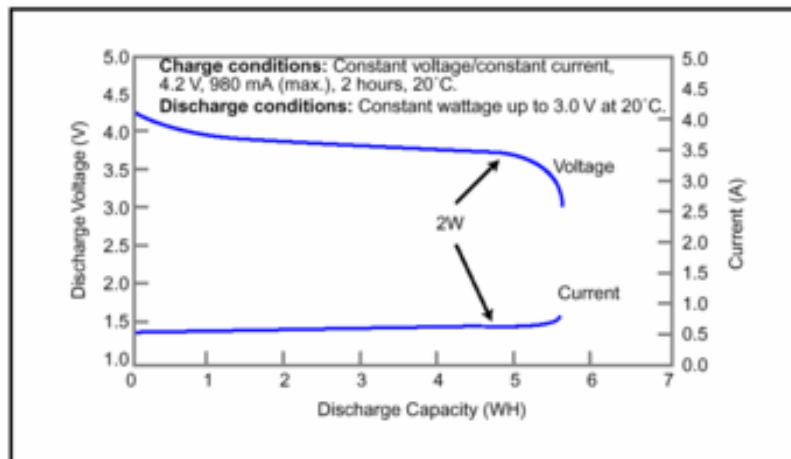
Figure 2-4: Constant Power Discharge for Typical Lithium Ion 18650 Cell from [15].

In summary, lithium ion batteries have high energy densities, do not need prolonged priming when new, have relatively low self discharge (less than 10% per month), require low maintenance and do not have any memory effect. However, lithium ion batteries are expensive to manufacture. The required protection circuits to maintain voltage, current and temperature within safe limits add more cost and complexity. Aging does not depend

on usage; aging takes place as soon as the battery is manufactured. The life of lithium ion batteries is estimated to be approximately to 2-3 years from the time of manufacture. Aging and low temperatures cause an increase in the cell internal impedance leading to power loss [6]. In addition, most lithium ion batteries are not suitable for heavy loads due to their moderate discharge currents. Higher discharge currents are available at the expense of higher weights and volumes as shown in Chapter 3 and Chapter 4.

On the other hand, lithium polymer batteries are easier to manufacture in any shape and size than lithium ion batteries. The gelled electrolytes result in improved safety by being more resistant to overcharge and electrolyte leakage, as well as resulting in simplified and lightweight packaging. However, lithium polymer batteries have lower electrolyte ionic conductivity (higher internal impedance) [16], decreased cycle count, and are more expensive than lithium ion. Similar to lithium-ion, higher discharge currents are available for lithium polymer batteries at the expense of higher weights and volumes as shown in Chapter 3 and Chapter 4.

2.1.3 Primary Lithium Batteries

There are some differences worth noting between secondary and primary lithium batteries. Many primary lithium batteries are currently available in the market: Lithium/ Poly-Carbon Monofluoride, Lithium/Manganese Dioxide, Lithium Thionyl Chloride, Lithium/ Sulphur Dioxide, etc. [15], [17]-[24]. Primary lithium batteries are more expensive than secondary lithium ion and polymer, have one time use and have higher service life than secondary batteries due to low discharge currents.

The constant voltage and high service life represented by the discharge characteristics of figure 9 are the results of very low discharge currents and do not necessarily represent a better quality than the Li-Ion 18650 cell discussed earlier. For example, from figure 2-5, with cell voltage of 3.6V and loads of 300, 1K, 3.6K and 36KΩ, the discharge currents are 12mA, 3.6mA, 1mA and 100μA, respectively. At 2000mAh rated capacity, the discharge rates for the 12mA and 3.6mA discharge currents would be as low as 0.006C at

167 hours discharge time and 0.0018C at 556 hours, respectively. Similarly, the Li-Ion 18650 cell, at 1400mAh capacity and 12mA load current, would result in a discharge rate of 0.0086C at 117 hours discharge time, which is very similar performance. Likewise, at such a small load current, the voltage drop of the internal resistance would be very small, resulting in no obvious operating voltage deviation.
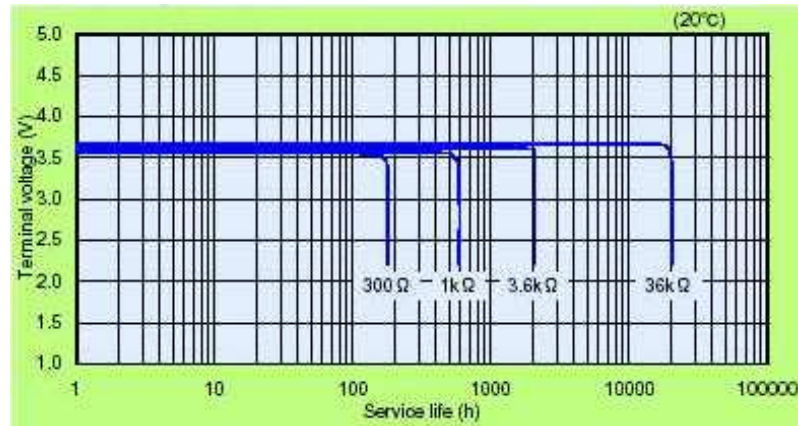
Figure 2-5: Discharge Characteristics of Toshiba (ER6VP) Thionyl Chloride Lithium Battery With 3.6V Nominal Voltage and 2000mAh Capacity and 16gr. Weight from [9].
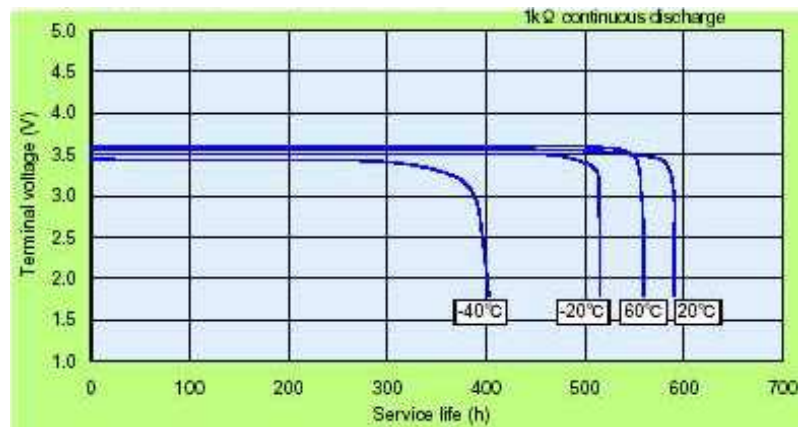
Figure 2-6: Discharge Versus Temperature Characteristics for Toshiba (ER6VP) Thionyl Chloride Lithium Battery With 3.6V Nominal Voltage and 2000mAh Capacity and 16gr. Weight from [9].

14

Similar to secondary batteries, primary batteries experience a loss of power at low temperatures due to an increase in the internal resistance.

2.1.4 Scaled Up Secondary Lithium Ion Batteries

Lithium ion batteries have been an attractive source of power because of their high energy density, high power density, low self discharge rates and good cycle life. At this time, lithium ion batteries are used mostly in consumer electronics, supplying less that 100Wh of energy, at limited load currents. However, recent advancements in materials and processes resulted in the manufacture of scaled-up lithium ion batteries to meet the requirements of satellites and automobile applications. For satellite applications the batteries have to be able to provide 1200-2400 cycles at 60% depth-of-discharge (DOD) over a period of 15 years, or 35,000 cycles at 25% DOD over seven years, for geo-synchronous orbit (GEO) and low earth orbit (LEO) respectively [6]. Ni-H2 (INTELSAT V) with energy densities of 40-50Wh/Kg and cell voltage of 1.2v had a total weight of 24.03Kg [6], whereas lithium ion batteries with energy densities of 90-140Wh/Kg and cell voltage of 3.6V would only weigh 12Kg. Older models of Electric and Hybrid Electric Vehicles (EV and HEV) are using 148V batteries whereas newer models use as high as 330-500V [2], [25]. High voltage batteries have the advantage of keeping the conductor and switch sizes small and hence minimizing copper losses.

For 450V operating voltage, 90 Lithium Ion cells of 3.7 volts each have to be connected in series (also known as string connection). More than two series cells form a module and more than two modules in parallel form a battery pack. A common problem faced by all chemistry modules is that when a series cell fails as a short, the terminal voltage drops, whereas if it fails as an open then the module current is cut off. The higher the number of string cells per module, the higher the possibility of module failure. For this reason, smaller modules are connected in series to achieve the desired terminal voltage. To achieve higher battery capacity (Ah), more than two cells are connected in parallel forming a pack. However, all parallel cells must have the same rated capacity and

voltage. The pack terminal voltage does not change. A cell failing as an open circuit will have a less severe impact on a pack as it would on a module; it would only shorten the runtime. To meet the voltage and current requirements for electric vehicles, modules are connected in series and parallel. For example, Toyota Prius uses Ni-MH cells with 1.2V and 6.5Ah. Six cells are used per module and a total of 38 modules give a terminal voltage of 273.6V, 1778Wh; with 1.04Kg per module the total battery weight is 53.3Kg [11]. Using the 18650 Li-Ion cells with 3.7V and 8Ah as proposed in [11] would take only 4 cells per module; 70 modules for a terminal voltage of 259V. However, with this configuration the energy capacity would be increased to 20072Wh, and with a module weight of only 0.24Kg, the battery weight would be dropped to 20Kg.

The advantages of using Li-Ion batteries in electric vehicle and satellite applications are obvious. However, building modules and packs is a tricky process. When more and more modules are connected in series or parallel, it causes the internal temperature of the battery pack to rise, which reduces the battery life and can lead to thermal runaway [6]. Uneven internal battery pack heat transfer raises an even more severe problem for Li-Ion batteries, as they can catch fire when overcharged. Heat variations lead to different internal resistances for different cells [2], [12]. When identical cells are charged in parallel, the cell with the lowest impedance will receive more current [6]. For this reason, temperatures and charging voltages are monitored and controlled by safety circuits. Thermal management is provided for improved battery performance. Cooling is used to prevent overheating whereas heating improves low temperature performance. Toyota Prius uses parallel-flow air-cooling [12] whereas Nissan Tino uses passenger air to cool down the batteries [6]. Leading companies in Li-Ion cells and battery packs for electric vehicle applications are Shin-Kobe Electric Machinery Co., Ltd., Japan Storage Battery Co., Ltd., and Saft.

2.1.5 Performance Metrics

A metric of battery performance is its capacity in ampere hours (Ah) from which other metrics can be derived like its energy density with respect to weight (also known as gravimetric or specific energy density) and with respect to volume (also known as volumetric). Battery capacity is depended on the discharge current, the latter usually expressed as a fraction of the numerical value of the capacity. At higher discharge currents (high discharge rate) the battery efficiency decreases and as a result less energy is delivered. The first mathematical model that captures this effect also known as Peukert's equation, is given by:

$$C_p = I^p t \qquad\qquad (2.1)$$

where C_p is the Peukert's battery capacity, I the discharge current, t the time and p Peukert's exponent usually between 1.1 and 1.4 dependent on the battery [26]. Unfortunately battery manufacturers use different discharge currents to calculate their battery capacities making straightforward comparison troublesome. This problem affects the other performance measures since they are derived from battery capacity. More explanations on Peukert's equation and exponent values can be found in Chapter 10.

Energy density either with respect to weight or volume is a very common performance measure which is widely used during battery sizing for a specific application, since it is easy to derive the weight and volume under a specific load. As it has already been mentioned the energy density suffers from the same drawback as battery capacity and therefore the discharge current needs to be taken into account in order to accurately estimate battery run time.

2.2 Fuel Cells

2.2.1 Technology Overview

Secondary batteries have limited runtime that is directly proportional to energy density and inversely proportional to load characteristics, with the recharging process requiring

several hours. On the other hand, fuel cells are capable of providing power for as long as fuel (usually hydrogen) is available.

Furthermore, the refueling process can take less than a few minutes, which presents a significant improvement over the hours usually required for recharging of batteries.

Table 2-2: Fuel Cell Technology Profile from [25]

	PAFC	AFC	MCFC	SOFC	SPFC	DMFC
Operating Temperature (^{o}C)	150-210	60-100	600-700	900-1000	50-100	50-100
Power Density (W/ cm^2)	0.2-0.25	0.2-0.3	0.1-0.2	0.24-0.3	0.35-0.6	0.04-0.23
Projected Life (hrs)	40,000	10,000	40,000	40,000	40,000	10,000
Projected Cost (US$/KW)	1000	200	1000	1500	200	200

Table 2-2 summarizes some of the characteristics of the various fuel cell technologies currently available. From these technologies the Proton Exchange Membrane Fuel Cells (PEMFCs) are the most attractive choice for portable applications because of their low operating temperatures. The primary fuel used in PEMFCs is hydrogen which entails an added complexity regarding storage and handling [27]. A subset of PEMFCs, the Direct Methanol Fuel Cells (DMFCs), uses methanol as a fuel. Although in general DMFCs are considered to be less efficient than PEMFCs, they are very attractive for sub-kilowatt, portable applications. This is due to the fact that they feature high energy densities and use a liquid fuel that although toxic is easier to handle.

Fuel Cells (FCs) share the same basic principle of operation as batteries [25], but instead of storing the energy, they are on-site energy production devices. Currently there are several fuel cell types in the market: Proton Exchange Membrane Fuel Cell (PEMFC), Alkaline Fuel Cell (AFC), Direct Methanol Fuel Cell (DMFC), Solid Oxide Fuel Cell (SOFC), Molten Carbonate Fuel Cell (MCFC) and Phosphoric Acid Fuel Cell (PAFC). Each of these types of FCs is named after the electrolyte or fuel used. In the range of 20

to 100W the market is currently dominated by hydrogen burning PEMFCs and their methanol counterparts, although there are a few alternative options based on SOFC and AFC.

The basic hydrogen fuel cell operation is given by two reactions that occur concurrently. At the anode of an acid electrolyte, hydrogen gas ionizes releasing two electrons, two mobile protons (H^+) and energy.

$$2H_2 \rightarrow 4H^+ + 4e^- \tag{2.2}$$

The mobile protons will travel through the acid electrolyte to the cathode, whereas the electrons can not go through and are forced to travel through an external connection provided by the load. At the cathode, oxygen reacts with the proton taken from the electrolyte and electrons arriving externally, to form water.

$$O_2 + 4e^- + 4H^+ \rightarrow 2H_2O \tag{2.3}$$

In the meantime, the electron flow between the electrodes is defined as electrical current, which provides electrical power the load.

Other fuel cell chemistries operate under similar principles although the anode and cathode reactions differ. Based on the fuel cell type, a cell has an operating voltage between 0.6 to 0.875V [28], although higher cell voltages are possible using different anode/cathode reactants. To reach the 12 or 24V terminal voltages usually needed, many cells are connected in series forming a stack.

The performance of fuel cells is affected by pressure and temperature. The voltage and current characteristics of a typical HFC are shown in figure 2-7. At low temperature and air pressure the theoretical or "No loss" cell voltage is 1.2V. However, the actual open circuit voltage is approximately 1V, and when a load is connected there is a steep drop in the voltage to approximately 0.9V. As the current density increases, there is a linear

voltage drop, whereas at current densities higher than 800mA/cm^2 the voltage drop decreases rapidly.
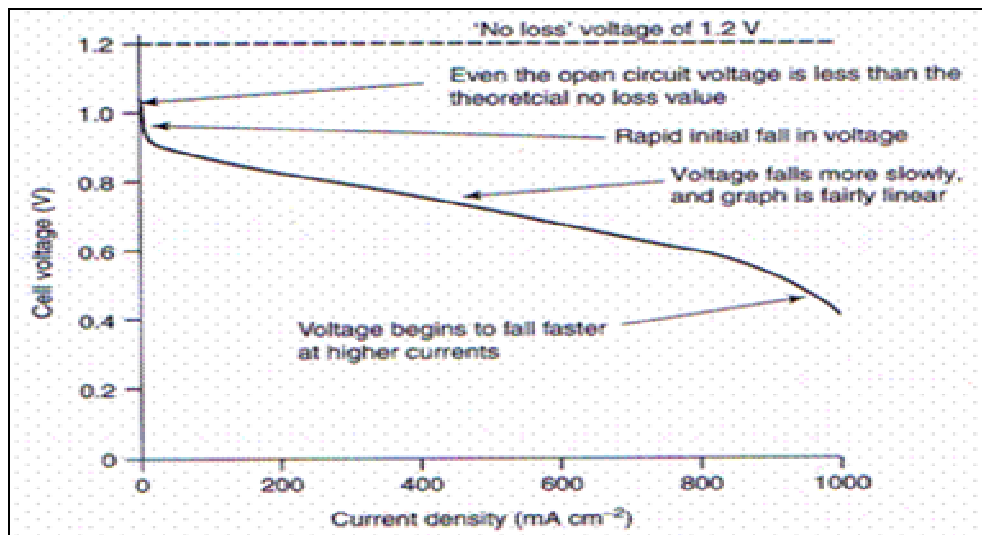
Figure 2-7: Voltage and Current Characteristics of a Typical Hydrogen Fuel Cell at Low Temperature and Air Pressure from [28].
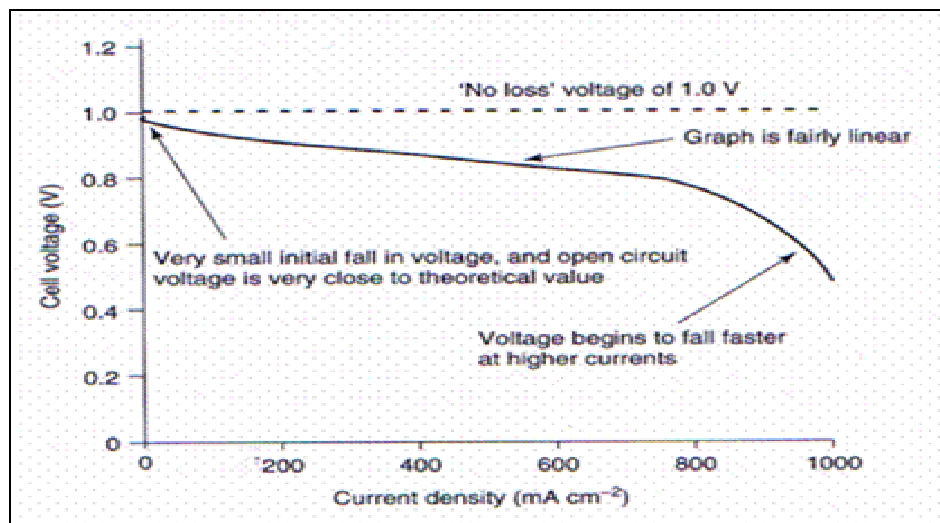
Figure 2-8: Voltage and Current Characteristics of a Typical SOFC at 800^{0}C and Air Pressure from [28].

Comparing the current and voltage characteristics of figure 2-7 with the characteristics of a SOFC operating at the higher temperature of 800°C (figure 2-8) it can be seen that at higher temperatures the actual open circuit voltage is very close to the theoretical value. Furthermore, the initial fall is smaller and the graph is more linear. These differences are due to four major "irreversibilities", that is, activation losses, fuel crossover and internal currents, ohmic losses and mass transport or concentration losses.

2.2.2 Performance Metrics

The evaluation of FCs with measures such as energy density is not as straightforward as in the case of batteries. This is because a typical fuel cell system will comprise of the stack which makes a significant contribution to the total system weight and the fuel which can be varied. Therefore, the quantity of the fuel determines the system energy density which as a result can vary. Things are further complicated from the fact that during the operation of the FC the weight of the fuel changes. As a consequence the energy density of a fuel cell can only be evaluated based on the apparent fuel to energy conversion. Figure 2-9 shows that the SOFC reviewed achieved a fuel energy density of around 3000 Wh/kg, while the DMFCs have on the average half that energy density. Hydrogen FCs seems to be inferior to DMFCs since their calculated fuel density is almost 100 times smaller.
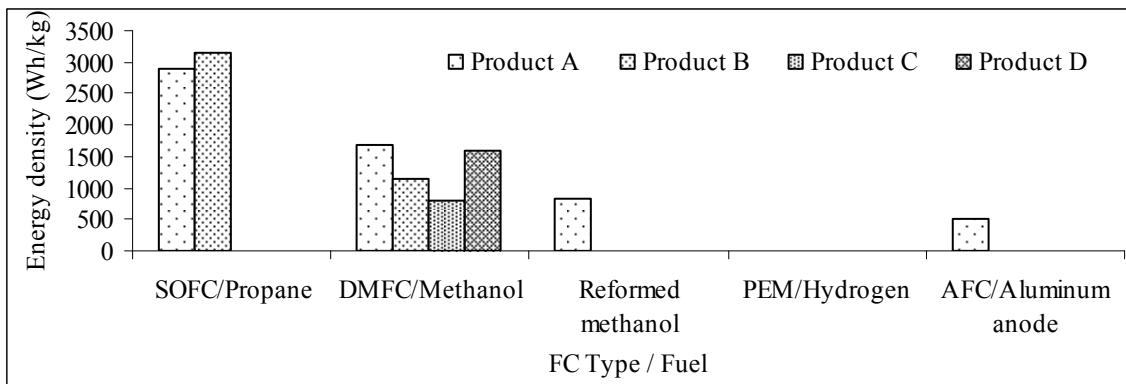
Figure 2-9: Fuel Energy Density for Various Fuel Cell Technologies.

To overcome these problems, the energy density of the systems reviewed is calculated based on 1, 3 and 10 days of continuous operation under their rated power and using the initial weight of the system that includes the fuel required and its container under each scenario.

2.3 Super-Capacitors

2.3.1 Technology Overview

Super-Capacitors, also known as ultra-capacitors, are a relatively new category of energy storage devices. Super-Capacitors exhibit higher power densities, lower effective series resistance (ESR), higher efficiency, lower RC time constant, and lower temperature dependency than batteries [29]-[35]. However, super-capacitors' relative smaller energy density and high cost does not make them an attractive battery replacement so far. When paralleled to a high energy density device, a super-capacitor can supply short-term over-the-average power demand, thus preventing excessive over-sizing of the battery pack and providing higher battery efficiency and life [36], [37].

A super-capacitor composition of two electrodes separated by an electrolyte is very similar to electrolytic capacitors, with capacitance being directly proportional to electrode surface area, A in m^2 and inversely proportional to the separation distance between the electrodes, d in meters.

$$C = \frac{A\varepsilon}{d}$$
(2.4)

However, super-capacitors exhibit much higher capacitance [30]-[38] (several Farads) than electrolytic capacitors (milli-farads), thus storing a significant higher amount of energy.

$$E_C = \frac{1}{2}CV^2$$
(2.5)

This major difference is attributed to the electrode composition used which yields a higher effective surface area and smaller electrode separation [29]-[35]. Electrodes used for electrolytic capacitors are metallic plates of finite dimensions and surface area. On the other hand, porous activated carbon electrodes are used for super-capacitors, which have a much higher effective surface area. In addition, with a proper electrolyte selection, a pore-size optimization can be achieved yielding higher capacitance for super-capacitors [29], [31].

The energy storage mechanisms divide super-capacitors to double layer and redox. Double layer super-capacitors store charge at the double layer interface between the electrodes and electrolyte, and capacitance is electrostatic. Redox super-capacitors, on the other hand, as implied by their name, store energy through a redox reaction. This is a reversible process between multiple oxidation states in the electrode material, as in batteries, and give rise to what is called pseudo-capacitance [31], [37].

2.3.1.1 Redox Super-Capacitors

Redox super-capacitors store energy through a redox reaction which is a reversible process between multiple oxidation states in the electrode material, as in batteries, and give rise to what is called pseudo-capacitance. Two classes of pseudo-capacitive materials have been investigated and developed: Conducting polymers and metal oxides.

2.3.1.2 Double Layer Super-Capacitors

Double layer super-capacitors are the most advanced version of super-capacitors present in the market. Double layer super-capacitors store charge at the double layer interface between the electrodes and electrolyte, and capacitance is electrostatic.

Figure 2-10 represents a double layer super-capacitor – two porous activated carbon electrodes emerged in an electrolyte solution that flows into and around the electrodes. The electrolyte is a conductive path linking the two capacitors together and also serves as an "effective conductive plate" for one side of each capacitor that is formed at the liquid

electrolyte/electrode interface. The DC electrical model of the double layer super-capacitor – two capacitors in series with the electrolyte resistance is represented in figure 2-11. The series resistance is much lower than the effective internal resistance of batteries.
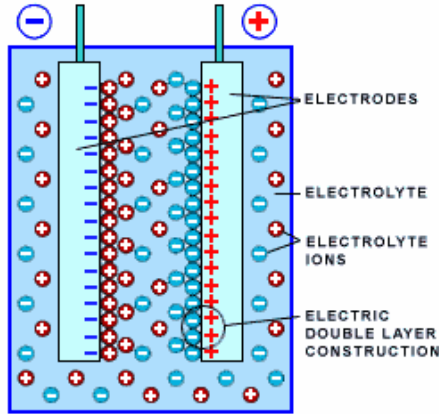
Figure 2-10: Double Layer Super-Capacitor from [30], [32].

Carbon electrodes have been mostly studied despite the fact that they are readily polarized and electrical conductivity depends on carbon preparation. Carbon and its various forms have been extremely attractive for accessibility, process-ability, low cost and non-toxicity. Carbon electrodes have been available as active powders, felts and cloths, xerogels, aerogels, and nanotubes. Electrolytes for double layer super-capacitors can be organic or aqueous [30], [33].
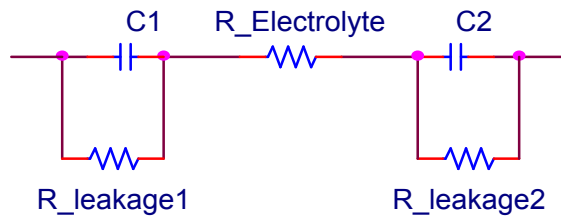
Figure 2-11: DC Electrical Model of a Double Layer Super-Capacitor from [29], [30].

Organic electrolytes display lower capacitance values than aqueous electrolytes. In addition, organic electrolytes have operating voltage above 2.5V, while the voltage of aqueous systems is approximately 1.2V [32], [33]. As a result of higher operating voltage, organic electrolytes provide a higher amount of stored energy which is directly proportional to the square of the voltage as shown by equation (2.5). On the other hand, organic electrolytes have higher ESR than aqueous electrolytes which limits the maximum output power of the device according to equation,

$$P = \frac{V^2}{4R} \tag{2.6}$$

where R equals ESR [31], [33]. The components of carbon resistance that contribute to ESR value are mostly the electronic and ionic components for charging the pores of small size, and to a lesser extent, the ionic resistance between the electrodes.

Table 2-3: List of Various Brands of Double Layer Super-Capacitors in the Market

Brand	Voltage (Volts)	Capacitance (Farads)	ESR (mΩ)		Energy Wh/Kg	Power W/Kg	Weight (gram)	RC Time Const. (Sec.)
			DC	AC				
Single Cell								
EPCOS	2.5	1800	0.6	0.3	2.9	2300	540	1.08
EPCOS	2.3	5	330	200	0.7	1200	5.5	1.65
NESS	2.3	20	55	40	3.7	6600	4	1.10
NESS	2.3	120	30	20	5.2	2600	17	3.60
Maxwell	2.7	2600	0.4	0.28	5.6	10400	470	1.04
Maxwell	2.5	2700	1	0.7	3.2	2.2	725	2.70
Skeleton	3	47	5.5	-	11.5	9600	5	0.26
MODULES								
EPCOS	14	200	5	2.6	1.9	1700	2800	2.50
EPCOS	42	67	15	8	2	1700	8200	1.01
NESS	5.4	1.5	200	150	1.74	10410	3.5	0.30
NESS	90	2.8	500	400	2.1	2800	1700	1.40
Maxwell	16.2	430	3.5	2.5	3.1	5200	5000	1.51

There are currently many companies manufacturing double layer super-capacitors: Maxwell, Skeleton, EPCOS, NESS, Matsushita etc. Double layer super-capacitors in the

market are available as single cells for low voltage applications and as modules for higher voltages. Double layer super-capacitors are not categorized by their electrode and electrolyte composition because that varies between companies. They are categorized by specific energy and power densities.

Table 2-3 lists various double layer super-capacitors already present in the market from different manufacturers. As it can be seen, products come in different operating voltages, capacitance, weight, and electrical characteristics. Applications of these devices vary from consumer electronics as primary and back-up power supply for LED displays, toys, electric buzzers, hand-held scanners, etc. to peak power supply for vehicles, voltage compensators, and car audio. The NESS 2.3V, 120F is manufactured for consumer electronics [39], whereas the MAXWELL 2.5V, 2700F is for automotive subsystems, power quality and rail system power applications [33]. Single cells can be connected in series to achieve a higher operating voltage, whereas desired capacitance is achieved by series and parallel connections. For example the NESS 90V, 2.8F was achieved by connecting 36 units of 2.7V and 100F each. Similarly, a 17.5V and 57F unit can be achieved by a matrix connection of 7 serial and 4 parallel cells of 2.7V and 100F each [39].

Worth noting that currently the highest single cell operating voltage is 3V and is offered by the Skeleton Technologies. Furthermore, the 3V, 47F Skeleton super-capacitor has a specific energy of 41400J/Kg which is 3 times higher than the best available super-capacitor from other manufacturers.

From table 2-3, it can be seen that the highest gravimetric energy density is 11.5Wh/Kg and is offered by the Skeleton super-capacitor whereas the highest power density is 10410W/Kg and is offered by NESS super-capacitor module.
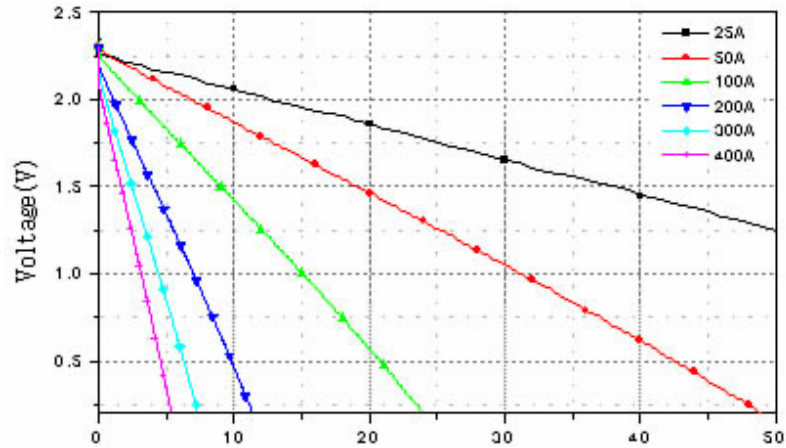
Figure 2-12: Double Layer Super-Capacitor Constant Discharge Current Characteristics (NESSCAP1200P) from [39].

2.4 Battery and Super-Capacitor Combination

Portable consumer electronics nowadays have gained a lot of computing and processing capabilities which require higher power. On the other hand, consumers are demanding portable devices to be light weight, compact and have longer runtime. Batteries and fuel cells have limited power densities that limit fast response to greater than average load power demands. This power quality problem may cause the computer to reset and motors to stall. A common solution to this increased energy and power demand would be to oversize the battery to meet these requirements. However, over-sizing a battery would raise the cost, weight and volume of the device. The later two factors are very critical for portable applications thus making this solution unattractive.

A quest for a better solution [36] showed that portable electronic devices, telecommunications and electric vehicles have very similar load profiles [36]. That is they have a low average power but high pulse power demands. Depending on the application, a pulse can range from milliseconds to seconds. Research [31]-[35] has shown that a more effective approach to this problem would be the use of hybrid power which would be a combination of battery and super-capacitor. The battery having a

higher energy density would provide longer runtime and the super-capacitor with higher power density and lower discharge time constant, will provide the pulse power demand. The combination of battery and super-capacitor achieves a higher specific power, charge to discharge efficiency and longer runtime than a battery alone. The battery and super-capacitor hybrid system has two major configurations; passive and active.

A passive system is the direct parallel connection between the battery and the super-capacitor. This configuration is very simple and keeps the cost to minimum since no other parts are required. Simulating the GSM telecom profile with 0.5ms pulses, research [37] has concluded that the passive hybrid configuration had voltage sag of only 0.1V whereas the battery alone had voltage sag of 1.1V. Furthermore, the battery alone with drain current of 2A had a higher losses and internal heating (I^2R) whereas with the hybrid configuration he battery drain current was minimized to 0.2A. The hybrid system deliver pulse power between 5-8W whereas the battery alone system was only 3.5-4W which is approximately 40% less. In addition the hybrid system had peak pulse power of 35W whereas the battery alone system was only 15W. However, due to higher drain currents achieved with the hybrid system the runtime was shorter than the battery alone system. Furthermore, besides higher peak power, research [40] reported higher efficiency and longer battery life with the battery and super-capacitor combination.

Some major disadvantages of the passive hybrid system are the following: First, the power sharing is determined by the ESR of the battery and the super-capacitor; during pulsed operation the battery current can have high ripple values which may activate some internal protection schemes common in lithium-ion technology batteries resulting in shutting off of the battery. Second, the voltage is not regulated; it follows the battery discharge curve and since it can vary significantly between fully charged and discharged then the super-capacitor full energy capabilities (equation (2.5)) can not be utilized.

An active system has a DC to DC converter connected between the battery and the super-capacitor. Adding the DC to DC converter between the battery and super-capacitor

configuration can eliminate all the negative effects mentioned for the passive configuration. In addition the super-capacitor voltage can be different from the battery voltage, thus giving more design flexibility [40] and also the DC-DC converter can act as a battery charging regulator while the passive system would require a separate battery charger. Research [40] reported that and active hybrid system has 3.2 times higher peak and 2.7 times higher specific energy than a passive system. Furthermore, an active system has lower battery currents with smaller ripple, than the passive system which results in a lower battery temperature and longer battery lifetime. Due to the added converter and increased super-capacitor losses, an active system has less discharge cycle time than a passive system.

2.5 List of References

[1]   Isidor Buchmann, "Understanding your Batteries in a Portable World", Article on Battery Choice and Maximize Service Life, IEEE Proc. of the Fourteenth Annual Battery Conference on Applications and Advances, pp 369–373, 1999.

[2]   Isidor Buchmann, "Batteries in Portable World", Second Edition, ISBN 0-9682118-2-8, 2001.

[3]   Walter A. Van Schalkwijk, "Lithium Rechargeable Batteries".

[4]   M. Broussely, M. Perelle, J. McDowal and G. Sarre, "Lithium Ion: The Next Generation of Long Life Batteries – Characteristics, Life Predictions and Integration into Telecom Systems", IEEE, 2000.

[5]   C. Robillard, A. Vallee, H. Wilkinson, "The Impact of Lithium-Metal-Polymer Battery Characteristics on Telecom Power System Design", AVESTOR, 2003.

[6]   W. Van Schalkwijk and B. Scrosati, "Advances in Lithium Ion Batteries, Kluwer Academic/Plenum Publishers, 2002.

[7]   E. Humbert, "Lithium Rechargeable Batteries in Standby but not for Power", June 17 2004, N.565, Batteries News, Newsletter, No.2, May 2005.

[8]   N. Hideyuki, "Alternative Cathode Material for Cobalt", Portable Power Conference and Expo, 2004.

[9]   Panasonic, "Lithium Ion Application Notes – Overcharge/ Over Discharge/ Over Current Safety Circuits, January 2000.

[10]   Toshiba Battery Co., Ltd., "Press Release, 29 March, 2005 – Toshiba's New Rechargeable Lithium-Ion Battery Recharges in only 1 Minute", Online Posting: http://www.toshiba.co.jp/about/press/2005_03/ pr2901.htm (July 19, 2005).

[11]   S. M. Lukic, S. A. Khateeb, S. Al-Hallaj, J. R. Selman, A. Emadi, "On the Suitability of a New High Power Lithium Ion Battery for Hybrid Electric Vehicle Applications", SAE International, 2003.

[12]   Sony Co., "US18650 Lithium Ion Battery Manual", Sony Co., 1993.

[13]   S. Al-Hallaj, J. Prakash, J. R. Selman, "Charatcerization of Commercial Li-Ion Batteries Using Electrochemical-Calometric Measurement", J of Power Sources, 87 (1/2), 2000.

[14]   S. Al-Hallaj, and J. R. Selman," Thermal Modelling of Secondary Lithium Batteries for Electric Vehicle/Hybrid Electric Vehicle Applications", J of Power Sources, 110, 341-348, 2002.

[15]   House of Batteries, "Design Assistance- How to Select the Right Kind of Battery for your Application", Online Posting: http://www.houseofbatteries.com/articletoc.asp (February 13, 2007).

[16]   D. Morrison, "Batteries Seek Higher Capacity, Power and Safety", Power Electronics Technology, October 1, 2004.

[17]   Battery Design Co., "Battery Companies", Online Posting: http://www.batdesign.com/links.htm#Battery%20Companies (February 13, 2007).

[18]   Matsushita Battery Industrial Co., Ltd., "Panasonic – Battery World, Product Information, Lithium Ion", Online Posting: http://industrial.panasonic.com/www-ctlg/ctlg/qACA4000_WW.html (February 6, 2007).

[19]   Sanyo Electric Co., Ltd., "Lithium-Ion and Lithium-Polymer Batteries", Online Posting: http://www.sanyo.co.jp/energy/english/ (February 6, 2007).

[20]   Samsung, "Rechargeable Battery Products – Lithium Polymer", Online Posting: www.samsungsdi.co.kr/contents/en/product/battery/battery.html (July 13, 2005).

[21]   Saft – High Tech Batteries for Industry, "Products by Technology – Lithium", Online Posting: http://www.saftbatteries.com/120-Techno/20-10_Lithium_system.asp (February 13, 2007).

[22]   Japan Storage Battery Co., Ltd., "Major Products – Lithium Ion", Online Posting:
        http://www.nippondenchi.co.jp/npd_e/lithium/ lithium.html (February 13, 2007).

[23]   Skin Kobe Electric Machinery Co., Ltd., "Automotive and Industrial Batteries-
        Lithium-Ion batteries for Hybrdi Electric Vehicles", Online Posting:
        http://www.shinkobe-denki.co.jp/e/products/ fcar_bat.htm (February 13, 2007).

[24]   Toshiba Battery Co., Ltd., "List of Primary Batteries – Ultra Lithium", Online
        Posting: http://www.tbcl.co.jp/tb_e/index_e.htm (February 13, 2007).

[25]   C. C. Chan, "The State of the Art of Electric Vehicles", Department of Electrical
        and Electronic Engineering, University of Hong Kong, Journal of Asian Electric
        Vehicles, Volume 2, Number 2, December 2004.

[26]   Wikipedia, "Peukert's_Law", Online Posting:
        http://en.wikipedia.org/wiki/Peukert's_Law (January 25, 2007).

[27]   The University of Hong Kong and Friends of the Earth, "Feasibility Study of
        Renewable Hydrogen in Hong Kong", October 2004.

[28]   J. Larminie and A. Dicks, "Fuel Cell Systems Explained, Second Edition", ISBN:
        0-470-84857-X, Wiley, Reprinted May 2003.

[29]   Baker P. Philip, "Ultra-Capacitors for Use in Power Quality and Distributed
        Resource Applications", IEEE, 2002.

[30]   Skeleton Technologies Group, "Breakthrough in Super-Capacitors", October
        2003.

[31]   W. Van Schalkwijk and B. Scrosati, "Advances in Lithium Ion Batteries, Chapter
        16, Electrochemical Supercapacitors", Kluwer Academic/Plenum Publishers,
        2002.

[32]   EPCOS, Electronic Parts and Components, "General Technical Information –
        Ultra-Capacitor Technology", Online Posting: www.epcos.com/ultracapacitor.htm
        (June 29, 2005).

[33]   Maxwell Technologies, "Ultra-Capacitor Application Notes", Online Posting:
        www.maxwell.com/ultracapacitors/support/ app_notes.html (June 29, 2005).

[34]   B. E. Conway, "Electrochemical Super-Capacitors: Scientific Fundamentals and
        Technological Applications", New York: Plenum, 1999.

[35]   G. L Bullard, H. B. Sierra-Alcazar, H. L. Lee, J. L. Morris, "Operating Principles of Ultra-Capacitor", IEEE, 25:102–106, January 1989.

[36]   Lijun Gao, "Power Enhancement of an Actively Controlled Battery/Ultra-Capacitor Hybrid", IEEE January 2005.

[37]   H. W. Brandhorst, Jr. and Z. Chen, "Achieving a High Pulse Power System through and Engineering Battery-Capacitor Combination", IEEE, 2001.

[38]   Miller, John R., "Fundamentals and Applications of Electrochemical Capacitors", Technology Tutorial, January 3, 2002.

[39]   Ionix Power Systems, "Electrochemical Capacitors", Online Posting: http://www.ionixpower.com/ electrochemical_capacitors.htm (June 29, 2005).

[40]   R. A. Dougal, S, Liu and R. E. White, "Power and Life Extension of Battery-Ultra-Capacitor hybrids", IEEE, 25:120–131, March 2002.

CHAPTER 3. COMMERCIALLY AVAILABLE ENERGY PRODUCTION AND STORAGE PRODUCTS

3.1 Introduction

This chapter analyzes commercially available energy production and storage options suitable for mobile applications with small payload capabilities such as small unmanned ground and aerial vehicles. Commercially available products are investigated for they are cheaper and have faster delivery time compared to custom made solutions. Furthermore, products made for military applications usually have better performance than consumer counterparts and also military products have a lot more online data which makes such an analysis possible. The review includes fuel cells, primary and secondary lithium batteries as well as super-capacitors for loads between 20 and 100W and total energy of up to 4800 Watt-hours.

Due to the completely different characteristics of the aforementioned power sources, a straightforward comparison between them is impossible. Therefore this survey will first compare the major technologies individually and in the end only top products from technology will be summarized.

3.2 Weight and Volume Packing Factors

This study reviews the state of the art of lithium technology batteries suitable to be used as power sources for mobile applications. The range of power considered is between 20 and 100W, hence for 24 and 48 hour runtime the range of energy capacity is between 480Wh and 4800Wh. Already available military packs are easy to analyze and compare with each other, however, a problem that arises is how newly developed cells are compared to these packs. Power and energy densities are a very good measure, but at the

same time a relationship should be established of cell volume and weight with a pack volume and weight. For example, when cells are connected in series and/or parallel to form packs, how are the performances change due to the extra weight and volume added?

There is not a lot of online data available for such a study. For this reason, a concept relationship is established from data available for Saft batteries. These data were collected from the Saft primary selector guide and involves a commonly used Saft lithium cell, LO26SX, which weighs 85grams and has a volume of 0.05 liters. This D-type cell has a nominal voltage of 2.8V and a capacity of 7.75Ah at a discharge current of 250mA or 0.0323C which is equivalent to a discharge time of 31 hours. Maximum current is 2.5A or C/3. This specific cell has been used by Saft in the following military packs: BA 5847B/U, BA 5599A/U, BT 5790, BT 5791, BA5590B/U. Most of the companies that produce military packs report the primary battery capacities at a discharge current of 250mA which makes comparison possible.

Table 3-1: Volume and Weight Comparison for Packs of LO26SX Cells

Model	Pack Construction	Number of Cells	Weight (Kg)	Volume (L)
LO 26 SX	1 cell	1	0.085	0.05
BA 5847B/U	2s1pLO 26 SX	2	0.240	0.23
BA 5599A/U	3s1pLO 26 SX	3	0.450	0.37
BT 5790	5s1pLO 26 SX	5	0.630	0.44
BT 5791	5s2pLO 26 SX	10	1.200	0.85
BA5590B/U	10s1pLO 26 SX	10	1.020	0.88

The normalized weight and volumes for the above configuration are presented in figure 3-1. Using Curve Experts 1.3 software, the weight relationship is best fit by a Rational Function whereas the volume by a Modified Geometric.

$$Weight_{norm} = \frac{a + bx}{1 + cx + dx^2} \qquad (3.1)$$

where a = -0.015585, b = 0.347896, c = -0.448238 and d = 0.208714.

$$Volume_{norm} = ax^{b/x} \qquad\qquad (3.2)$$

where $\alpha = 0.9625177$ and $b = 2.4009066$.
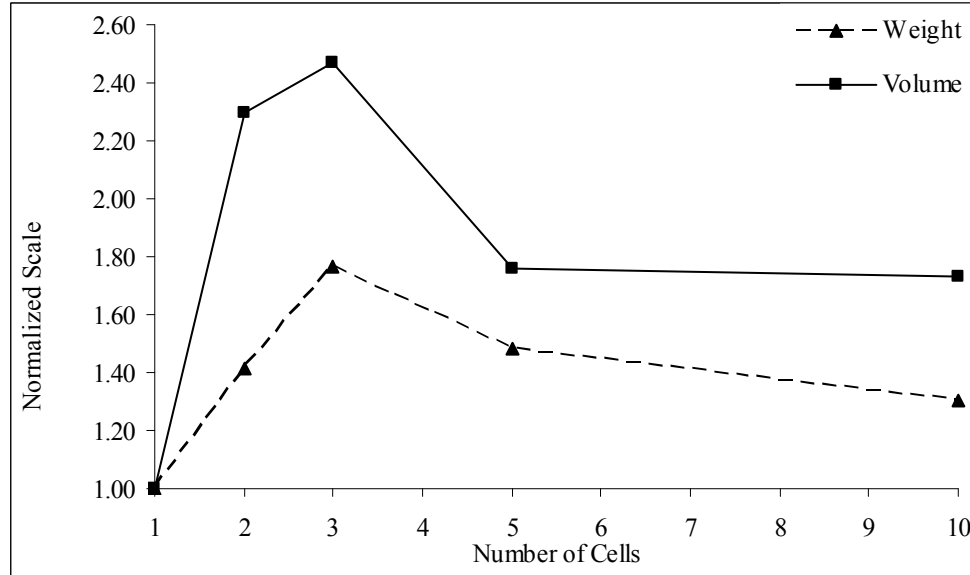
Figure 3-1: Normalized Weight and Volume Versus Number of LO26SX Cells.

From the data analysis of figure 3-1 it can be concluded that the volume and weight of 2 to 4 cells packed together is affected a lot more than a pack of 5 or more cells. As a result packs of 2 to 4 cells will have lower energy and power densities. It is therefore recommended to use as many cells as possible so that the extra package weight and volume does not affect the cell performance as much. However, based on the application, the number of cells will be restricted, as too many cells will add complexity to the design. Furthermore, the packing factor is more complicated and can not be generalized for all products. As it can be seen from table 3-1, both the BT5791 and BA5590 packs use the same cell type and number, and yet different weights and volumes are reported. A space utilization relationship should also be established by considering the cell and the pack geometries. Unfortunately, as mentioned earlier, there is not a lot of online data available which makes such a study impossible.

3.3 Analysis of Primary Lithium Battery Packs and Cells Combined

Several companies are actively developing battery solutions based on lithium technology. Some of the largest in this sector that also have a product line for military applications are Bren-tronics, Saft, Ultralife, MilPower and Tadiran. As it can be shown later on this survey Tadiran mostly produces high power lithium cells with very low energy densities whereas all other companies have a wider product selection with both high energy and high power. This study will focus on military packs since these often show better performance than their civilian applications counterparts.

Primary lithium technology batteries are more suitable for emergency response than secondary due to no maintenance, low self discharge and no charging needed. For this reason primary batteries will be considered in this report too. All primary lithium battery packs under comparison are tabulated in table A-1. The data were either directly obtained or derived from product datasheets downloaded from manufacturers' websites.

Something worth remembering when comparing off the shelf products is that for each battery the capacity, discharge time and discharge current are more accurately described by equation (2.1). However, many times for simplicity Peukert's exponent is chosen with a value of 1 which leads to a linear relationship of equation (3.3) where the battery capacity is the product of discharge current and time and the effects of capacity loss due to high discharge currents are ignored:

$$C = It \qquad (3.3)$$

The reciprocal of discharge time is called discharge rate and it is often noted as C-Rate. This means that for a discharge rate of 1C the discharge current would be equal to the rated capacity and a discharge time of 1 hour, whereas 0.2C denotes a discharge current of 0.2 times the rated capacity and discharge time of 5 hours. Based on this, the "Sophie" pack of table A-1 has a rated capacity of 5.8Ah and nominal voltage of 13V. This means that theoretically with a discharge rate of 1 hour, this pack would deliver 75.4 watts.

However, looking more closely to the datasheet, the maximum recommended current is 1.5A, which means that the fastest time this battery pack could be discharge is 3.9 hours or 0.26C and the maximum power would be 19.5W. In addition, when two such batteries are connected in parallel then maximum current and power would be doubled but the energy and power densities will remain the same.

Comparing energy and power densities does not show the total required weights and volumes for a complete mission. Even the battery with the highest energy and power density might not meet the payload capabilities of an unmanned ground vehicle, in which case other sources might have to be investigated or even redefine the mission total energy requirements. Therefore, all primary batteries compared and tabulated on table A-1, are compared based on a hypothetical mission scenario with a total energy requirement in the range of 480Wh.

In most of the cases examined the volumetric densities of power and energy tend to be higher than the gravimetric. In table A-1 all products are compared for a 480Wh mission and the data are sorted with respect to the highest energy density. For all products the total weight, volume and number of cells necessary are shown. The energy density varies between 15 to 572Wh/Kg. At the top of the table the Lithopack C by Saft offers the highest energy density of 572Wh/Kg but has the lowest power density of 5W/Kg. On the other hand the Tadiran cell TLM1550HP offers the highest power density of 970W/Kg but with energy density of 97Wh/Kg then 4.95Kg weight is required to meet a 480Wh mission. In addition, 247 Tadiran cells are required would make the design too complicated; even if 20 cells were added per module then approximately 120 modules would be required which logistically is not desirable.

With energy density directly proportional to runtime as shown in equation (3.3) and with optimum given with the least required weight possible then to avoid over-sizing a more detail analysis by separating the batteries in power ranges of less than 30W/Kg, between 30 and 70W/Kg and over 71W/Kg are provided in tables 3-2 to 3-4 respectively.

Table 3-2: Battery Packs With Power Density Less Than 30W/Kg

Brand	Model	Power Density (W/Kg)	Power Density (W/L)	Energy Density (Wh/Kg)	Energy Density (Wh/L)	Number Cells for 480Wh	Total Weight Kg	Total Volume Liters
Saft	Lithopack C	5	6	572	628	24.69	0.84	0.76
Saft	Lithopack	28	30	519	570	27.21	0.93	0.84
Saft	LSC 9V	5	2	372	175	44.44	1.29	2.74
Saft	LS 9V	12	6	341	161	48.48	1.41	2.99
Saft	G15-127	24	28	272	315	0.50	1.76	1.52
Saft	G15-127	24	28	272	315	0.50	1.76	1.52
MILPower	BA-5347/U	14	104	15	116	17.65	31.76	4.14

Grey 10% - High power density and low weight for a 480Wh mission
Grey 20% - Rejected due to weight; higher than 9Kg for a 480Wh mission

From table 3-2 it can be seen that for load power demands lower than 30W then the optimum solution would be the Lithopack by Saft which offers a power density of 28W/Kg and at the same time only 0.93Kg is required for a 480Wh mission. The 27 cells required would not be a big problem as it could be easily divided into 3 modules of 9 cells. Furthermore, the MILPower / BA5347 pack is the heaviest solution with 31.76Kg.

Table 3-3: Battery Packs With Power Density Between 30 and 70W/Kg

Brand	Model	Power Density (W/Kg)	Power Density (W/L)	Energy Density (Wh/Kg)	Energy Density (Wh/L)	Number Cells 480Wh	Total Weight Kg	Total Volume Liters
Saft	PS 52 A	58	76	400	529	5.33	1.20	0.91
Saft	PS 53 B	53	70	365	485	1.83	1.32	0.99
Saft	PS 48 B	55	60	274	298	1.52	1.75	1.61
Saft	PS 42 A	55	79	274	394	7.62	1.75	1.22
UltaLife	BA5390U	46	68	256	377	1.44	1.87	1.27
UltaLife	BA5390U	46	68	256	377	1.44	1.87	1.27
Saft	BA 5590HC	68	77	246	279	1.95	1.95	1.72
Saft	BA 5590HC	68	77	246	279	1.95	1.95	1.72
Saft	PS 40 A	64	53	226	187	7.45	2.12	2.56
MILPower	MIL/C0109	34	42	218	266	1.00	2.20	1.80
UltaLife	U2550HCE-CF-UFA	60	136	215	488	37.21	2.23	0.98
MILPower	BA-5590/U	59	66	211	239	2.22	2.28	2.01

Table 3-3 (Continued)

Brand	Model	Power Density		Energy Density		Number Cells 480Wh	Total Weight Kg	Total Volume Liters
		(W/Kg)	(W/L)	(Wh/Kg)	(Wh/L)			
MILPower	BA-5590/U	59	66	211	239	2.22	2.28	2.01
Saft	G6-104	70	110	210	330	11.43	2.29	1.45
Saft	C,D,E,F,G,H	70	110	210	330	11.43	2.29	1.45
MILPower	BA-5290/U	45	65	205	291	1.78	2.35	1.65
MILPower	BA-5290/U	45	65	205	291	1.78	2.35	1.65
Saft	BA5590B/U	66	77	199	230	2.37	2.42	2.09
Saft	BA5590B/U	66	77	199	230	2.37	2.42	2.09
MILPower	MIL/C4430	63	71	188	213	2.13	2.56	2.25
MILPower	BA-5600/U	62	96	186	289	7.11	2.58	1.66
Saft	BA 5800A/U	60	104	181	313	12.08	2.66	1.54
Saft	G30-102/B	34	47	179	253	1.07	2.68	1.90
UltaLife	BA-5367/U	52	118	177	405	123.08	2.71	1.18
UltaLife	BA-5347U	47	77	175	283	7.21	2.74	1.70
Saft	BT 5791	58	82	175	246	2.29	2.74	1.95
Saft	PS 31 A	58	196	173	588	111.11	2.78	0.82
UltaLife	5380	38	117	171	521	7.21	2.81	0.92
Saft	G9-124	59	57	170	164	7.62	2.82	2.92
Saft	BA 5600A/U	56	89	169	268	7.90	2.84	1.79
MIL Power	BA-5598/U	55	67	168	202	4.21	2.86	2.37
Saft	BT 5790	56	79	167	236	4.57	2.88	2.03
Saft	BA 5847B/U	55	57	166	170	12.08	2.90	2.82
Saft	BA 5598A/U	51	58	165	187	4.29	2.91	2.57
UltaLife	Sophie	42	42	160	160	6.37	2.99	3.00
UltaLife	BA-5368/U	51	104	158	324	40.00	3.04	1.48
UltaLife	BA-5372/U	48	138	150	430	160.00	3.20	1.12
UltaLife	1/2AA	48	109	150	340	320.00	3.20	1.41
Saft	G18-115	49	37	148	112	3.81	3.24	4.29
MIL Power	BA-5800/U	46	122	141	375	10.39	3.40	1.28
Saft	Li/3	47	173	140	520	7.62	3.43	0.92
Saft	G30-101	49	67	140	194	2.29	3.43	2.48
Saft	PS 38 A	45	59	135	177	22.86	3.54	2.72
Saft	BA 5599A/U	45	55	135	164	7.90	3.56	2.92
Saft	G15-114	52	54	99	103	18.05	4.87	4.68
Brentronics	BA-5368/U	59	93	80	127	80.80	5.98	3.77
Saft	BA 5368/U	33	111	74	250	44.44	6.44	1.92
Saft	XSG 1493/1	62	90	70	102	40.34	6.86	4.71

Grey 10% - High power density and low weight for a 480Wh mission
Grey 20% - Rejected due to weight; higher than 9Kg for a 480Wh mission
Grey 30% - Rejected due to complexity of design; too many cells required

For 50W average power demand, as shown in table 3-3, two packs by Saft, PS52A and PS53B, offer power densities of 58 and 53W/Kg and meet the 480Wh mission requirements with only 1.2 and 1.32Kg respectively. On the other hand for 70W power demand then the least weight for the 480Wh mission is 2.29Kg offered by Saft / G6-104.

Table 3-4: Battery Packs With Power Density Higher Than 71W/Kg

| Brand | Model | Power Density | | Energy Density | | 480Wh Mission | | |
		(W/Kg)	(W/L)	(Wh/Kg)	(Wh/L)	Number Cells	Weight (Kg)	Volume (Liters)
Brentronics	BA5347/U	78	89	222	256	8.00	2.16	1.88
MILPower	1794AS0953U	132	208	185	292	9.52	2.59	1.64
Saft	BA5567A/U	175	348	175	348	171.43	2.74	1.38
Saft	BA5588A/U	95	105	166	183	9.80	2.89	2.62
Saft	BT5313	92	NA	165	NA	2.65	2.91	NA
Saft	G6-105	127	162	163	207	26.79	2.95	2.32
Saft	BA5372/U	90	255	150	425	160.00	3.20	1.13
Brentronics	BA5374/U	NA	NA	148	617	57.14	3.24	0.78
MIL Power	BA5374/U	NA	NA	147	617	57.14	3.26	0.78
Brentronics	BA5372/U	90	255	144	408	166.67	3.33	1.18
Saft	BA5112A/U	124	129	143	148	18.63	3.35	3.24
Tadiran	TLM1550MP	776	1770	136	310	176.73	3.53	1.55
MIL Power	MIL/BA5567/U	150	407	129	350	186.05	3.72	1.37
Saft	BA5557A/U	112	322	123	354	7.79	3.90	1.36
Saft	BA5557A/U	112	141	123	155	7.79	3.90	3.09
Tadiran	TLM1530MP	696	1626	104	244	417.75	4.60	1.97
Tadiran	TLM1550HP	970	2212	97	221	247.42	4.95	2.17
Tadiran	TLM1520MP	428	1120	73	190	733.38	6.60	2.52
MIL Power	MIL150483	NA	NA	63	138	29.72	7.58	3.47
Tadiran	TLM1520HP	525	1374	53	137	1015.87	9.14	3.49
Tadiran	TLM1530HP	87.05	2032.33	8.01	186.97	544.90	59.94	2.57

Grey 10% - High power density and low weight for a 480Wh mission
Grey 20% - Rejected due to weight; higher than 9Kg for a 480Wh mission
Grey 30% - Rejected due to complexity of design; too many cells required

Finally, from table 3-4 the 480Wh energy requirement can be met with least weights of 2.16Kg and 2.59Kg with the Bren-tronics / BA5347 and the MILPower / 1794AS0953U respectively. The MILPower pack is 20% heavier solution that the Bren-tronics but at the same time it offers 70% higher power density. For higher power demand than 132W the suggested solutions require more complicated designs with more than 160 cells. As

mentioned in section 2.1.4 higher the number of cells used significantly increases the possibility of a failure. When more and more modules are connected in series or parallel, it causes the internal temperature of the battery pack to rise, which reduces the battery life and can lead to thermal runaway.

3.3.1 Suggested Primary Lithium Battery Packs for Mobile Applications

Lithium primary batteries are analyzed and compared in section 3.3 and to avoid over-sizing the results are separated and tabulated based on range of power. Since, this survey is concerned with commercially available power sources in the range of 20 to 100W then the suggested solutions are tabulated in table 3-5. Desired optimum is defined as highest energy density with least weight. Hence, the following suggested solutions cover the 480Whr energy requirement with less than 3Kg total weight, offer power density range between 28 and 132 W/Kg and does not require more than 28 cells.

Table 3-5: Suggested Battery Packs for Mobile Applications

| Brand | Model | Power Density | | Energy Density | | 480Wh Mission | | |
		(W/Kg)	(W/L)	(Wh/Kg)	(Wh/L)	Number Cells	Weight (Kg)	Volume (Liters)
Saft	Lithopack	28	30	519	570	27.21	0.93	0.84
Saft	PS 52 A	58	76	400	529	5.33	1.20	0.91
Saft	PS 53 B	53	70	365	485	1.83	1.32	0.99
Brentronics	BA-5347/U	78	89	222	256	8.00	2.16	1.88
MILPower	1794AS0953U	132	208	185	292	9.52	2.59	1.64

3.4 Secondary Lithium Batteries

Secondary lithium technology batteries are listed in table B-1. For logistical reasons, these products were limited to companies that also provided primary lithium military packs, that is, Bren-tronics, Saft, Ultralife, MilPower. The data were either directly obtained or derived from product datasheets downloaded from manufacturers' websites.

Secondary batteries were analyzed in a way similar to that of primary batteries. Table B-2 shows the total weight and volume required by each battery for a 480Wh mission. As it

can be seen at the top of the table, with the blue color 5 batteries are marked for meeting the 480Wh mission with least weight, whereas at the bottom of the table, two batteries are marked with red for requiring more than 10Kg for the 480Wh mission. It is worth noting that the top 5 batteries require 3Kg or less for the mission and can have peak power of more than 400W.

3.4.1 Suggested Secondary Lithium Batteries for Mobile Applications

To sum up for mobile applications the secondary batteries suggested by this study are tabulated in table 3-6. The following batteries can cover a 480Wh mission with a total weight of approximately 3Kg and a power density that varies between 132 and 343 Wh/Kg. These batteries can provide a maximum power in the range of 400 to 998W.

State of the art secondary lithium batteries offer higher power density than energy density. For mobile applications that require low power, state of the art secondary lithium batteries require more weight than primary batteries. From table 3-5 and table 3-6, it can be seen that primary lithium batteries have higher energy densities whereas secondary lithium batteries offer higher power densities.

Table 3-6: Suggested Secondary Lithium Battery Packs

| Brand | Model | C-rate | W/Kg | W/L | Wh/Kg | Wh/L | 480Whr mission | | |
							Number Cells	Weight Kg	Volume L
Saft	MP 176065	C/5	343	687	165	375	20.00	2.91	1.28
Saft	MP 174865	C/5	333	696	163	380	25.26	2.94	1.26
Saft	VL 34570	C/5	330	758	160	380	24.00	3.00	1.26
MIL Power	BB-2590/U	C/4	132	201	159	241	2.22	3.02	1.99
MILPower	BB-2590/U	C/4	132	201	159	241	2.22	3.02	1.99

3.5 Suggestions for Super-Capacitors as Mobile Power Sources

For mobile applications as mention earlier weight and volume are very critical. Therefore, volumetric and gravimetric energy densities of power sources have been compared. From table 2-3, it can be seen that the highest gravimetric energy density is

11.5Wh/Kg and is offered by the Skeleton super-capacitor whereas the highest power density is 10410W/Kg and is offered by NESS super-capacitor module.

The best super-capacitor, with an energy density of 11.5Wh/Kg would require 41.73Kg for a 480Wh mission. Therefore, this report concludes that state of the art super-capacitors can not replace batteries or fuel cells. However, research has shown a lot benefits offered by battery and super-capacitors offer. Therefore, hybrid systems in general should be examined in more detailed for man-portable military applications.

3.6 Commercially Available Fuel Cell Products

A selection of currently commercially available FCs and their physical and electrical characteristics are summarized in tables C-1 and C-2. These FCs have been developed as portable charging stations or direct power sources. Some of them have been developed for military applications and feature very small volumes and weights. In addition, for Hydrogen Fuel Cells, table C-3 provides hydrogen tanks and regulators that are commercially available.

3.7 Assumptions

For fuel cell comparison purposes as mentioned earlier, the energy and power densities have to be calculated. The necessary information was either available or derived from manufacturer datasheets that were downloaded directly form the official websites. For volumetric and gravimetric energy density, the volume and weight of both fuel cell and fuel were considered. In the case of hydrogen fuel, the hydrogen storage units are tabulated in table C-3. Calculating the energy density for a fuel cell system it is necessary to know the fuel consumption at a given power. Some fuel cell products tabulated in table C-2, such as BCS and SRE, were not included in the analysis and comparison because the fuel consumption was not available in the datasheet and the manufacturer did not provide any further requested information. Table C-4 gives the fuel consumption for the fuel cells under consideration.

Gravimetric and Volumetric energy densities are also presented in figures 3-2 to 3-7 for all fuel cell systems under consideration. Volumetric information for some cartridges was not available so some entries were left blank. Furthermore, the initial comparison and analysis divided the products into 3 different power ranges, less than 30W, 35 to 75W and 100W. As it can be seen in figures 3-2 to 3-7 for all power ranges the energy density increases with continuous operation at rated power, reaching the highest energy density value at 240 hours.
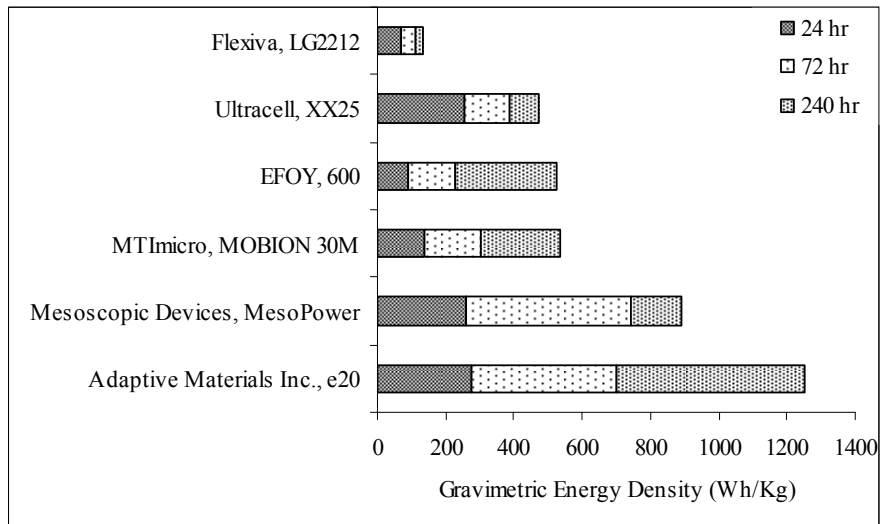
Figure 3-2: Gravimetric Energy Density for Fuel Cells of Less Than 30W.

The e20 by Adaptive Materials Inc of figure 3-2 provides the highest gravimetric energy density of 1250Wh/Kg whereas the Mesopower by Mesoscopic Devices, shown in figure 3-3, offers the highest volumetric energy density which approaches 2000Wh/L.
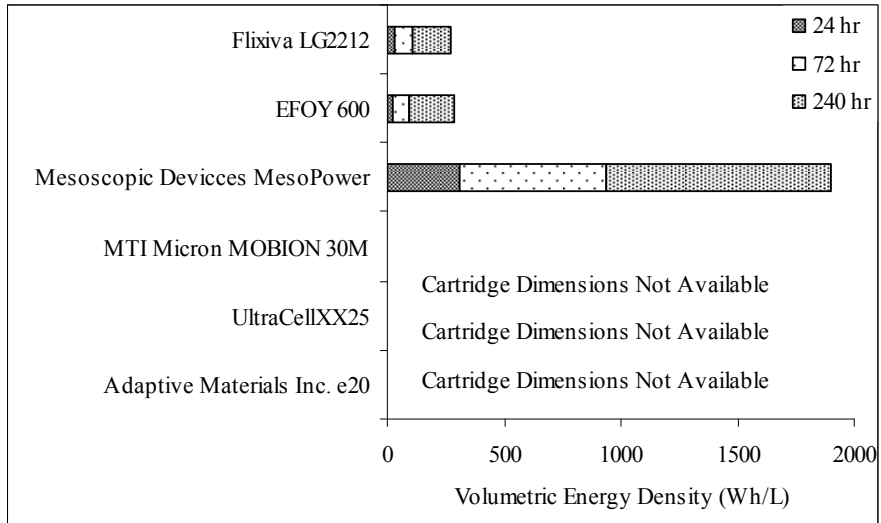
Figure 3-3: Volumetric Energy Density for Fuel Cells of Less Than 30W.
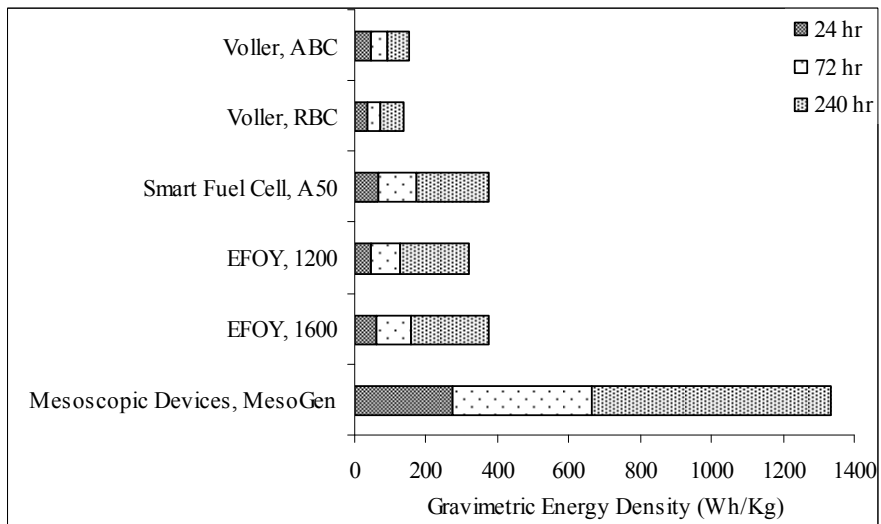
Figure 3-4: Gravimetric Energy Density for Fuel Cells Between 35W to 75W.

At higher rated power, the energy density of the fuel cells drops significantly mostly due to the higher weight and volume of the stack. In the range of 35 to 75W, the MesoGen by Mesoscopic devices, shown in figure 3-4 and figure 3-5 offers the highest gravimetric and volumetric energy density of 1801Wh/Kg and 1332Wh/L respectively, whereas in

the 100W range (figure 3-6 and figure 3-7) the APS100 by Altek offers 488Wh/Kg (volumetric density is not available because the cartridge dimensions were not provided). However, Altek reports in the datasheet that cartridges can have customized dimensions based on application and volume availability.
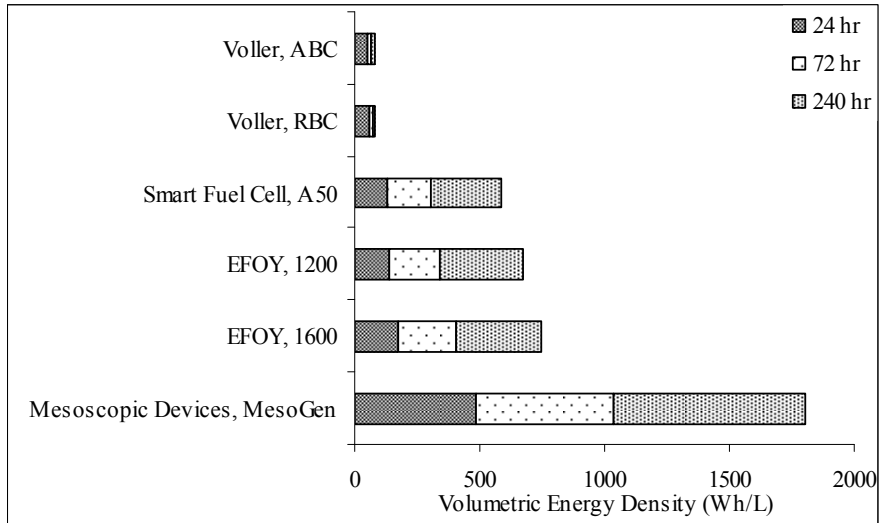
Figure 3-5: Volumetric Energy Density for Fuel Cells Between 35W to 75W.
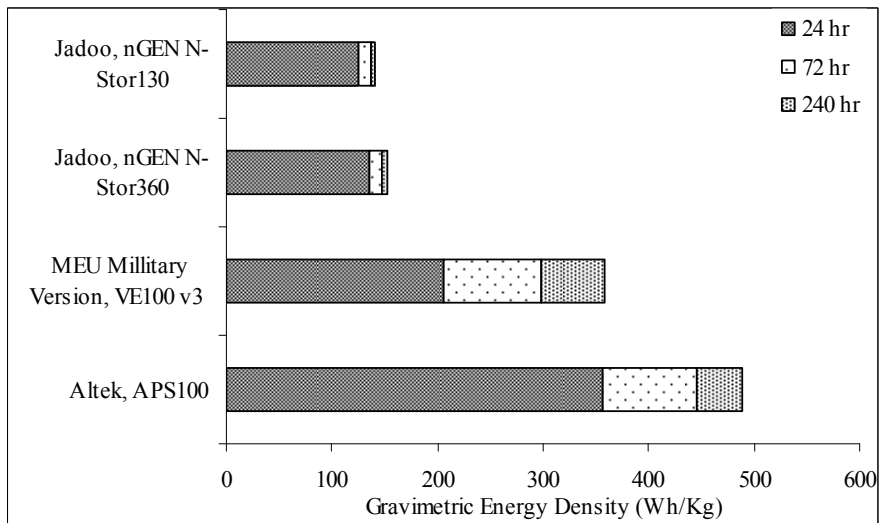
Figure 3-6: Gravimetric Energy Density for Fuel Cells of 100W.
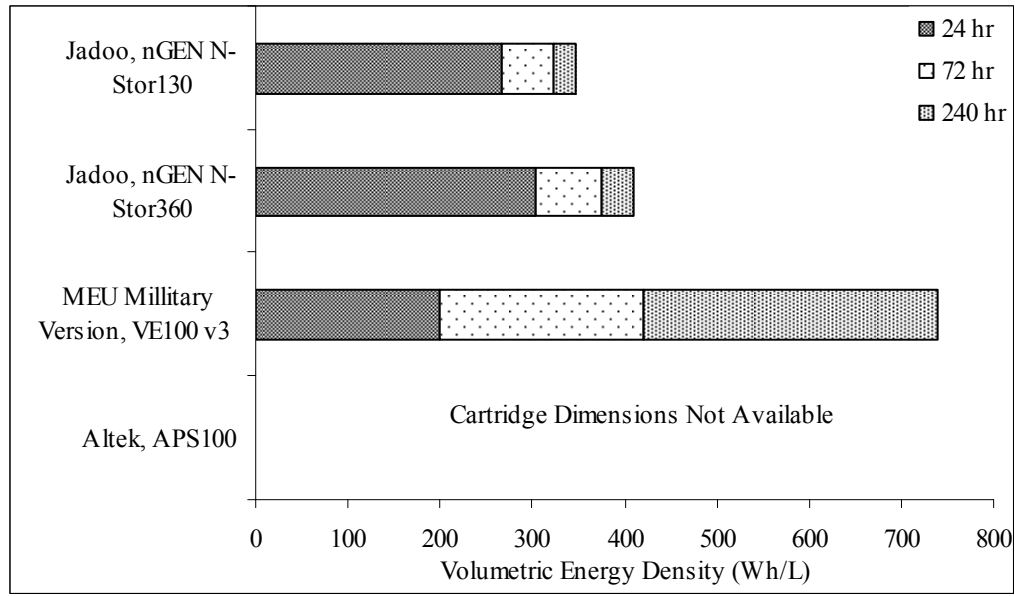
Figure 3-7: Volumetric Energy Density for Fuel Cells of 100W.

High gravimetric energy density does not guarantee that for a 24 hour or higher continuous operation of the fuel cell will provide minimum total weight, including the fuel cell and fuel weight. This is due to different fuel cell weights, nominal power and fuel. For example, a 100W fuel cell tends to be heavier than a 20W one. However, over a 24 hour period the 100W fuel cell provides 2400Wh of energy whereas the 20W only provides 480Wh. For this reason, all fuel cells under consideration should be compared for continues operation and then the total weight can be calculated. This analysis is shown in tables 3-7 to 3-9.

For 24 hour operation at rated power as shown in figure 3-8, the MesoGen by Mesoscopic Devices offers the highest energy density, whereas the APS100 by Altek, offers the second highest and the e20 by Adaptive Materials Inc offers the third highest. On the other hand, from table 3-7 the e20 requires a total weight of 1.73Kg for 24 hour continuous operation whereas the MesoGen requires 3.73Kg and the APS100 requires 6.72Kg.
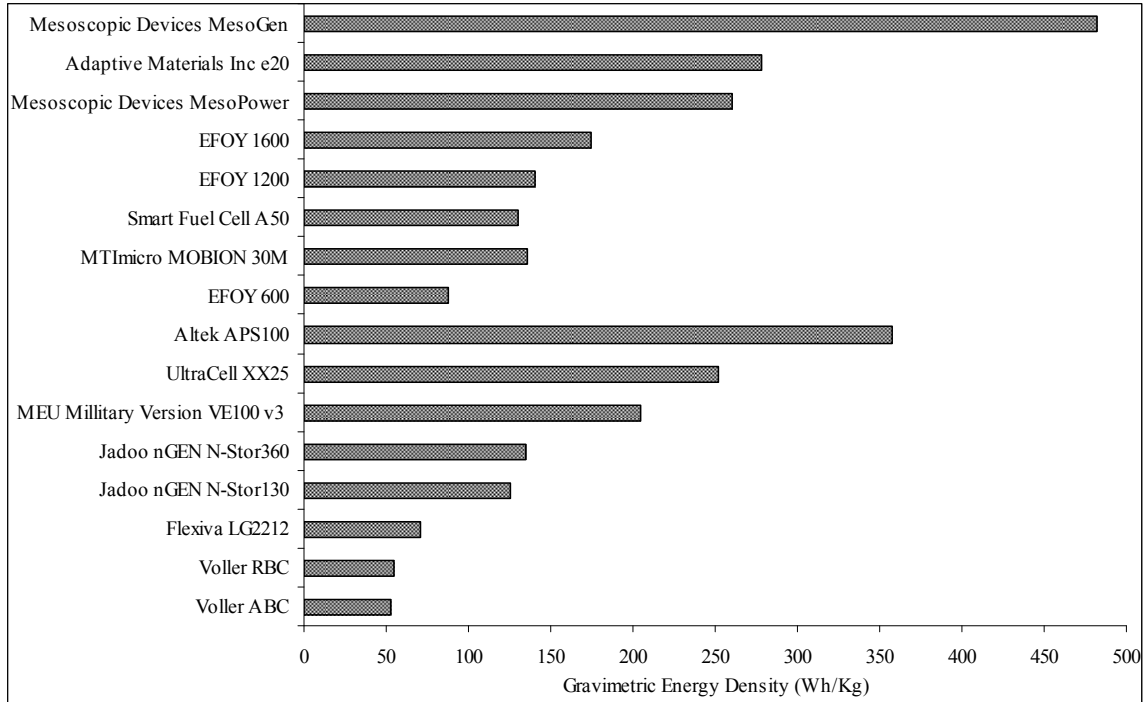
Figure 3-8: Gravimetric Energy Density for 24 Hour Operation at Rated Power.

Table 3-7: Total Weight (FC+Fuel) Required for a 24 Hour Mission at Rated Power

Brand	Model	Power (W)	Weight Kg	Comments/Complexity
Adaptive Materials Inc.	e20	20	1.73	0.17Kg (Solid Oxide)
Mesoscopic Devices	MesoPower	20	1.85	0.3Kg methanol (0.38L)
Ultracell	XX25	25	2.38	3.33 cartridges: 1.15Kg
Mesoscopic Devices	MesoGen	75	3.73	0.73Kg Solid Oxide
Flexiva	LG2212	15	5.07	1 H2 Tank: CL370
MTImicro	MOBION 30M	30	5.30	1 Cartridge 0.9Kg
Altek	APS100	100	6.72	Appro. 2 cartridges: 4.72Kg
EFOY	600	25	6.82	0.5Kg methanol (0.66L)
EFOY	1200	50	8.53	1.03Kg methanol (1.3L)
EFOY	1600	65	8.94	1.34Kg methanol (1.7L)
Smart Fuel Cell	A50	50	9.23	1.23Kg Methanol (1.56L)
MEU Millitary Version	VE100 v3	100	11.71	4 H_2 Tanks: CanV3
Jadoo	nGEN N-Stor360	100	17.77	7 H_2 Tanks: N-Stor360
Jadoo	nGEN N-Stor130	100	19.10	18 H_2 Tanks: N-Stor130
Voller	RBC	50	21.82	3 H_2 Tanks: BL750
Voller	ABC	50	22.64	3 H_2 Tanks: BL750

For 72 hour operation at rated power as shown in figure 3-9, the results are different. The MesoGen and Mesopower both by Mesoscopic Devices offer the first and second highest energy densities respectively, whereas the e20 by Adaptive Materials Inc offers the third highest and the APS100 offers the fourth highest energy density. However, from table 3-8 the Mesopower requires a total weight of 1.95Kg whereas the e20 requires a total weight of 2.06Kg for 72 hour continuous operation. The MesoGen is the fourth heaviest solution requiring 5.21Kg.
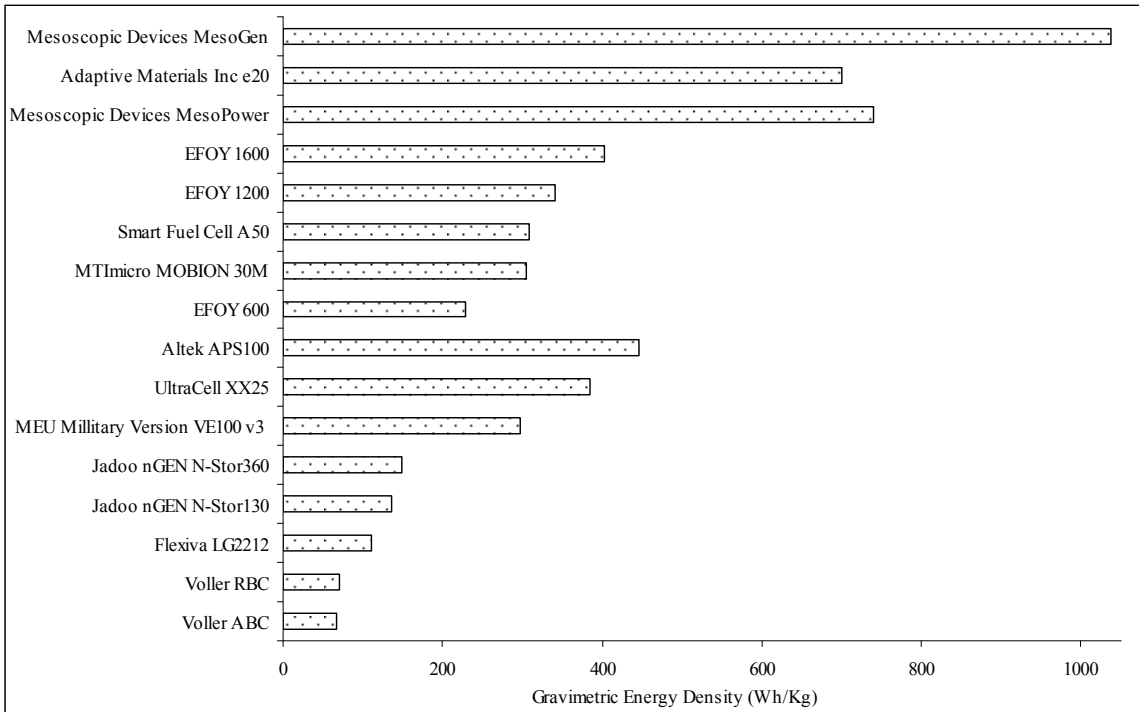
Figure 3-9: Gravimetric Energy Density for 72 Hour Operation at Rated Power.

Comparing the required weight for the 24 and 72 hour mission at rated power summarized table 3-7 and table 3-8 respectively, it can be seen that at 72 hour runtime more weight is required because of additional fuel weight. On the other hand, as shown in figure 3-8 and figure 3-9, the energy densities increase significantly at 72 hour operation because the energy density provided by the fuel offsets the device weight.

Table 3-8: Total Weight (FC+Fuel) Required for a 72 Hour Mission at Rated Power

Brand	Model	Power (W)	Weight Kg	Comments/Complexity
Mesoscopic Devices	MesoPower	20	1.95	0.91Kg methanol (1.15L)
Adaptive Materials Inc.	e20	20	2.06	0.5Kg (Solid Oxide)
Ultracell	XX25	25	4.68	10 cartridges: 3.45Kg
Mesoscopic Devices	MesoGen	75	5.21	2.2Kg Solid Oxide
MTImicro	MOBION 30M	30	7.10	3 Cartridges 2.7Kg
EFOY	600	25	7.85	1.5Kg methanol (1.98L)
Flexiva	LG2212	15	9.73	2 H$_2$ Tanks: 1 BL750, 1 BL250
EFOY	1200	50	10.58	3.09Kg methanol (3.9L)
EFOY	1600	65	11.61	4.02Kg methanol (5.1L)
Smart Fuel Cell	A50	50	11.70	3.7Kg Methanol (4.7L)
Altek	APS100	100	16.16	5 cartridges: 14.16Kg
MEU Millitary Version	VE100 v3	100	24.16	11 H$_2$ Tanks: CanV3
Jadoo	nGEN N-Stor360	100	48.70	20 H$_2$ Tanks: N-Stor360
Voller	RBC	50	50.70	8 H$_2$ Tanks: BL750
Jadoo	nGEN N-Stor130	100	52.70	55 H$_2$ Tanks: N-Stor360
Voller	ABC	50	53.73	8 H$_2$ Tanks: BL750
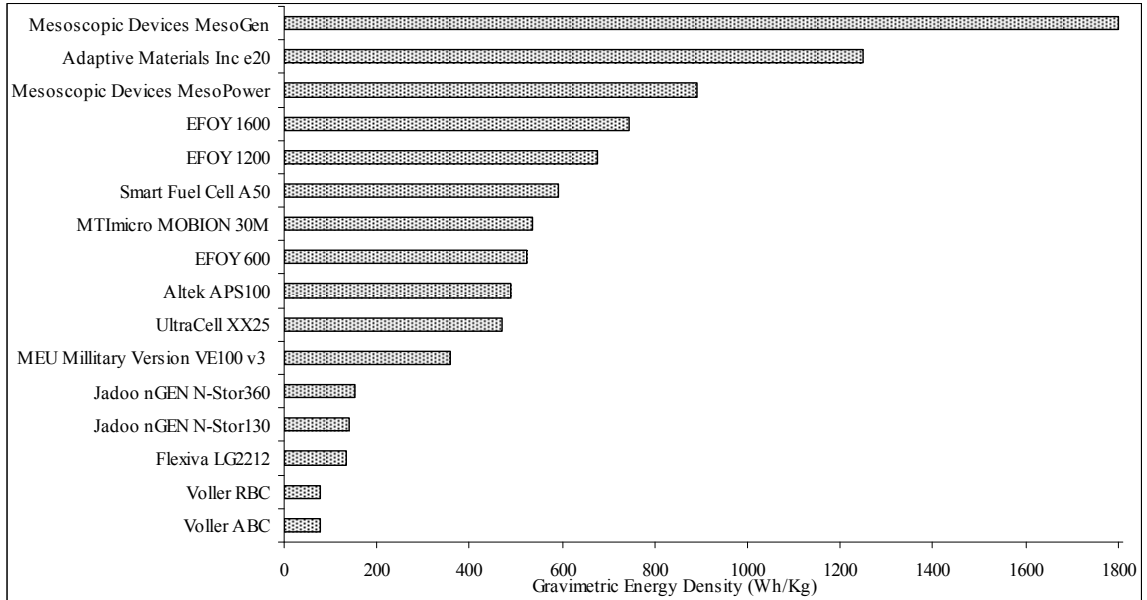
Figure 3-10: Gravimetric Energy Density for 240 Hour Operation at Rated Power.

50

Table 3-9: Total Weight (FC+Fuel) Required for 240 Hour Mission at Rated Power

Brand	Model	Power (W)	Weight Kg	Comments/Complexity
Adaptive Materials Inc.	e20	20	3.84	1.7Kg (Solid Oxide)
Mesoscopic Devices	MesoPower	20	5.39	3Kg methanol (3.8L)
Mesoscopic Devices	MesoGen	75	9.99	7.3Kg Solid Oxide
EFOY	600	25	11.47	5Kg methanol (6.6L)
Ultracell	XX25	25	12.72	33 cartridges:11.4Kg
MTImicro	MOBION 30M	30	13.40	10 Cartridges 9Kg
EFOY	1200	50	17.77	10.3Kg methanol (13L)
Smart Fuel Cell	A50	50	20.32	12.32Kg methanol (16.6L)
EFOY	1600	65	20.95	13.4Kg methanol (17L)
Flexiva	LG2212	15	27.07	5 H2 Tanks: 4 BL750,1 CL370
Altek	APS100	100	49.20	16 cartridges: 47Kg
MEU Millitary Version	VE100 v3	100	67.04	37 H_2 Tanks: CanV3
Voller	RBC	50	155.84	27 H_2 Tanks: BL750
Voller	ABC	50	155.84	27 H_2 Tanks: BL750
Jadoo	nGEN N-Stor360	100	156.97	67 H_2 Tanks: N-Stor360
Jadoo	nGEN N-Stor130	100	170.30	185 H_2 Tanks: N-Stor360

As it can be seen from tables 3-7 to 3-9, fuel cells in the power range of less than 30W can operate continuously for 24hrs with a total weight of less than 3Kg and at 240 hours still provide the least total weight. However, it is worth noting that a 100W FC at 240 hour continuous operation will provide 24000Wh whereas a 30W will only provide 7200Wh. For mobile applications both the weight and amount of energy should be considered when choosing the right power source for the mission. This analysis is offered in the next section where all suggested power sources will be compared for specific missions.

3.8 Final Suggestions for Power Sources for Mobile Applications

In this section, all power sources suggested in this study from primary, secondary Lithium Technologies as well as from fuel cells will be compared for specific missions. Finally the power sources which meet missions of 480Wh, 1440Wh and 4800Wh with the least weight will be highlighted. These results are shown in tables 3-10 to 3-12.

3.8.1 Final Suggestions for a 480Wh Mission

For a 480Wh capacity, as compared and summarized on table 3-10 there are a lot of choices for power sources with total weight of less than 3Kg. Top of the list is dominated by 3 primary lithium batteries. The lightest of all, the Lithopack by Saft, meets the energy requirement with only 0.93Kg. The 27 cells required could form a pack of 3 modules with 9 cells each and that would not increase the design complexity significantly. In the fuel cell category, the lightest solution is offered by e20 with a total weight of 1.73Kg.

Table 3-10: Suggestions for a 480Wh Mission

Brand	Model	Number Cells	Weight Kg	Volume Liters
Saft	Lithopack	27.21	0.93	0.84
Saft	PS 52 A	5.33	1.2	0.91
Saft	PS 53 B	1.83	1.32	0.99
Adaptive Materials Inc.	e20		1.73	NA
Mesoscopic Devices	MesoPower		1.85	1.53
Ben-tronics	BA-5347/U	8	2.16	1.88
Ultracell	XX25		2.3	NA
MIL Power	1794AS0953U	9.52	2.59	1.64
Saft	MP 176065	20	2.91	1.28
Saft	MP 174865	25.26	2.94	1.26
Saft	VL 34570	24	3	1.26
MIL Power	BB-2590/U	2.22	3.02	1.99
MIL Power	BB-2590/U	2.22	3.02	1.99
Mesoscopic Devices	MesoGen		3.2	6.05

3.8.2 Final Suggestions for a 1440Wh Mission

As shown in table 3-11, fuel cells offer the lightest solutions for the 1440Wh mission with approximately 2Kg. Following the fuel cells is a primary battery, Lithopack with a total weight of 2.79Kg. However, the 82 cells required for this amount of energy could complicate the design. Manufacturer recommendations should also be considered for such a design. It is worth noting that for a 1440Wh mission secondary batteries require a total weight of more than 7Kg.

Table 3-11: Suggestions for a 1440Wh Mission

Brand	Model	Number Cells	Weight Kg	Volume Liters
Mesoscopic Devices	MesoPower		1.95	2.30
Adaptive Materials Inc.	e20		2.06	NA
Saft	Lithopack	81.63	2.79	2.52
Saft	PS 52 A	15.99	3.60	2.73
Mesoscopic Devices	MesoGen		3.60	6.46
Saft	PS 53 B	5.49	3.96	2.97
Ultracell	XX25		3.99	NA
Bren-tronics	BA-5347/U	24.00	6.48	5.64
MIL Power	1794AS0953U	28.56	7.77	4.92
Saft	MP 176065	60.00	8.73	3.84
Saft	MP 174865	75.78	8.82	3.78
Saft	VL 34570	72.00	9.00	3.78
MIL Power	BB-2590/U	6.66	9.06	5.97
MIL Power	BB-2590/U	6.66	9.06	5.97

3.8.3 Final Suggestions for a 4800Wh Mission

For missions in the range of 4800Wh as shown in table 3-12, fuel cells dominate as the lightest power sources of choice. The e20 fuel cell by Adaptive Materials Inc can provide 4800Wh with 3.84Kg whereas the MesoGen by Mesoscopic Devices require 4.96. Primary and Secondary batteries require more than 8.4Kg for such a mission.

Table 3-12: Suggestions for a 4800Wh Mission

Brand	Model	Number Cells	Weight Kg	Volume Liters	Comments/Complexity
Adaptive Materials Inc.	e20		3.84	NA	Meets the mission with least weight
Mesoscopic Devices	MesoGen		4.96	7.81	
Mesoscopic Devices	MesoPower		5.39	4.95	
Saft	Lithopack	272.10	9.30	8.40	Too many cells and heavy
Ultracell	XX25		10.55	NA	More than 10Kg
Saft	PS 52 A	53.30	12.00	9.10	More than 10Kg
Saft	PS 53 B	18.30	13.20	9.90	More than 10Kg
Ben-tronics	BA-5347/U	80.00	21.60	18.80	More than 10Kg
MIL Power	1794AS0953U	95.20	25.90	16.40	More than 10Kg

Table 3-12 (Continued)

Brand	Model	Number Cells	Weight Kg	Volume Liters	Comments/Complexity
Saft	MP 176065	200.00	29.10	12.80	More than 10Kg and too many cells
Saft	MP 174865	252.60	29.40	12.60	More than 10Kg and too many cells
Saft	VL 34570	240.00	30.00	12.60	More than 10Kg and too many cells
MIL Power	BB-2590/U	22.20	30.20	19.90	More than 10Kg
MIL Power	BB-2590/U	22.20	30.20	19.90	More than 10Kg

3.9 Discussion and Recommendations

In this chapter products were analyzed and compared aiming in determining the most optimum solution for mobile applications. Optimum is defined as maximum runtime which is directly proportional to energy, with the least possible weight. A linear approach was followed where the effect of capacity loss at high discharge current was ignored. Furthermore, with load voltage and power unknown it was assumed 100% efficiency for DC-DC conversion and the effect of step down voltage conversion was also ignored (see section 6.2.2 - DC to DC Conversion Modeling). Microsoft Excel was used and hybrid systems could not be configured and compared.

CHAPTER 4. SURVEY OF LITHIUM TECHNOLOGY BATTERIES FOR AERO-
MODELING APPLICATIONS

4.1 Introduction

In this chapter, Lithium technology batteries used for specialized applications such as
aero-modeling are compared and examined. The same assumptions and methodology
used in previous chapters are used. A linear approach is followed where the effect of
capacity loss at high discharge current is ignored. Once again, optimum is defined as
maximum runtime with the least possible weight since aero-modeling application have
very strict payload constraints. Unlike Chapter 3, where energy was compared and
voltage was not known, in this application load power, operating voltage and payload are
defined as 325W, 11.1V and 1.3Kg respectively.

4.2 Methodology

In aero-modeling, a common question would be how to choose a battery for an electric
airplane. The answer to this question starts with the airplane's engine rated power and
operating voltage specifications and also payload capability. For example, a motor with
rated power of 325W and operating voltage of 11.1V requires approximately 30A
(Current=Power/Voltage). This means that for this specific application and payload
limitations, our search is narrowed down to batteries with an operating voltage of 11.1V
and maximum current of at least 30A within the payload range. Since many
commercially available battery packs meet these criteria, the new question that arises is
which battery is best?

Data for commercially available products, obtained or derived from the various
companies' official specification sheets [1]-[6], are presented in table D-1. Products are

sorted based on gravimetric energy density (Wh/Kg). As it can be seen the "Tenergy – 18650-2600-4" pack provides the highest energy density of 209Wh/Kg, whereas the "ThunderPower – TP2200-4SX" provides the highest rated power density of 3734W/Kg and the "ThunderPower TP9000-6S2PX" provides the highest burst power density of 7500W/Kg.

The "ThunderPower TP9000-6S2PX" pack as its name shows has a capacity of 9000mAh (9Ah) and it is composed of 2 parallel modules each made of 6 cells in series. The pack voltage of 22.2V and the 6 series connected cells indicate individual cell voltage of 3.7V, whereas the 9Ah capacity and 2 parallel modules indicate an individual module capacity of 4.5Ah. Furthermore, looking at a maximum power of 3996W, 22.2V operating voltage and 9Ah capacity it can be calculated that this pack can provide a maximum continuous current of 180A (3996/22.2) or 20C (180/9) and a discharge time of 3 minutes (1/20 hours*60 minutes). Furthermore, burst power of 9990W and 22.2V gives a burst current of 450A or 50C whereas burst power density of 7500W/Kg gives a current density of 339A/Kg. Something worth mentioning at this point is that different manufacturers have different burst duration times. For example most Saft products provide burst duration of 10 and 20 seconds, whereas ThunderPower and Tenergy have burst duration in the range of 5 to 10 seconds.

So, which battery pack should be selected among all packs that meet the criteria for operating voltage and maximum continuous current? The battery pack offering the highest energy density should be selected for runtime maximization and weight minimization.

Starting with products analyzed in table D-1, the list is narrowed down by excluding the batteries that have operating voltages higher than 11.1V. For battery packs or cells with lower voltages an adjustment was made to meet the required operating voltage. For example the Saft cell (MP174865) has an operating voltage of 3.75V. This means that 3 cells are needed to be connected in series. The following adjustment would be forming a

matrix of connections in order to increase the available amount of energy and power with payload capability of 1.3Kg. For example, the same Saft cell has a weight of 0.124Kg. As mentioned earlier, 3 cells were needed for the required operating voltage thus raising the weight to 0.372Kg. Furthermore, for a payload of up to 1.3Kg, then 3 such modules are connected in parallel forming a matrix of 3x3 which totals 9 such cells, which can provide total power of 386W, total energy of 189Wh and total weight of 1.16Kg. The same analysis was carried out on all products of table D-1 thus eliminating products that did not meet the criteria of 11.1V, 325W and 1.3Kg payload.

In table D-2, the new results are tabulated. Some products are highlighted with 50% grey color. These products were rejected, because even though they met the requirements, the number of cells required is too high. The more cells used the higher the possibility of failure, so it is advisable to avoid such configurations. Finally, highlighted with 40% grey color are the products with a total weight less than 1.3Kg and total energy between 178 and 231Wh. The products that made it in the final cut are presented in table 4-1.

4.3 Final Recommendations

So, starting with 94 products of table D-1, after all the analysis we end up with 13 products of table 4-1 that meet all requirements. The "ThunderPower TP8000-3S4PL" offers the lowest weight of 0.95Kg and number of cells but at the same time it offers the lowest energy of 178Wh. On the other hand the "Tenergy 18650 2600" offers the highest energy of 231Wh, with total weight of 1.11Kg but at the same time with available data it is the second most expensive solution with $768 and requires a matrix of 28 cells total. The cheapest and second highest energy solution is offered by the Tenergy Li18650-2200T with $163 and 229Whr but it requires a matrix of 28 cells.

Most of the 18650 cell averages to $2.47/Wh whereas the Lithium Polymer averages to $3.04. Total Power Solution [3] which offers the Tenergy products was recently offering their products at discounts of up to 50% which dropped their Lithium Polymer average to $2.21/Wh whereas ThunderPower was more expensive with an average of $3.64/Wh.

Table 4-1: Products With Total Weight Less Than 1.3Kg and Energy Between 178 and 231Wh

Brand	Model	Voltage (Volts)	Capacity (Ah)	Total Number Cells	Total Weight (Kg)	Total Power (W)	Total Energy (Wh)	Burst Power (W)	Total Price US$
Thunder Power	TP8000-3S4PL	11.1	8	2	0.95	1776	178	2398	510
Thunder Power	TP6000-3S3PL	11.1	6	3	1.14	1998	200	3596	630
Thunder Power	TP4000-3S2PL	11.1	4	5	1.28	2664	222	3996	750
Thunder Power	TP2100-3SPL	11.1	2.1	8	1.14	2797	186	4440	560
Saft	MP 174865	3.75	5.1 at 1.1A	9	1.16	386	189	737	NA
Saft	VL 34570	3.75	5.2 at 1.1A	9	1.17	386	187	737	NA
Thunder Power	TP2000-3SPL	11.1	2	10	1.20	2664	222	4440	730
Saft	MP 174865 IS	3.65	4.8 at 1A	10	1.29	381	181	761	NA
Saft	MP144350	3.75	2.48 at 0.5A	19	1.28	353	183	706	NA
Tenergy	18650-2600-4	3.7	2.6 at 0.5C	24	1.11	347	231	NA	768
Tenergy	18650-2600	3.7	2.6 at 0.5C	24	1.11	347	231	NA	240
Tenergy	Li18650-2200-4	3.7	2.2	28	1.29	343	229	NA	815
Tenergy	Li18650-2200T	3.7	2.2	28	1.29	343	229	NA	163

4.4 Discussion and Recommendations

It is important to note the difference between companies that specialize in aero-modeling applications (Thunder Power and Tenergy) and other leading lithium battery companies such as Saft, MILPower, Bren-tronics and Ultralife. The later companies specialize mostly in military applications and the fact that for this scenario most of their products were not selected does not make them inferior. Lithium batteries for military applications need to meet different packaging standards and regulations. More rigid and robust packaging adds extra weight which significantly decreases the overall energy and power

densities. Figure 4-1 and figure 4-2 represent the Normalized Weight and Volume of Lithium Packs used in Military and Aero-modeling applications respectively. As it can be seen, when 10 cells are packaged together then the total weight is not 10 times the cell weight; the packaging factor must also be taken into account. Therefore, for military applications the total weight for ten cells packed together would equal 14 times the cell weight (10*1.4*cell weight) whereas for aero-modeling applications the packaging factor is only 1.05 hence the total weight would be 10.5 times the cell weight.
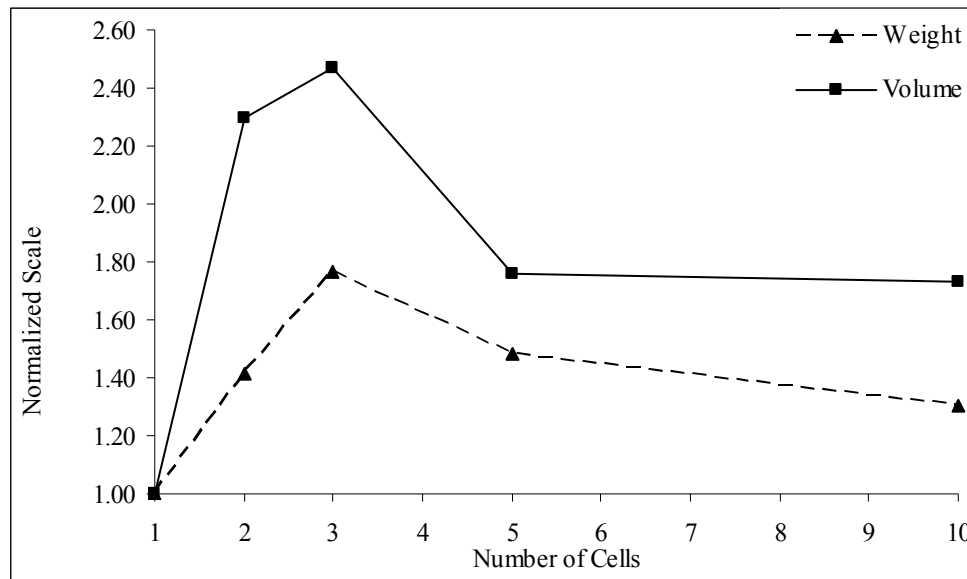
Figure 4-1: Normalized Weight and Volume for Lithium Packs Used in Military Applications.

From figure 4-1 it can be seen that energy densities would severely suffer when the pack is made of 3 to 5 cells and the packaging factor reaches 1.8 for military applications, whereas for aero-modeling applications 6 cells have the worst packaging factor of 1.05, which is still 58.3% less than the military application factor thus enabling higher energy densities. Packaging factors were not taken into consideration in this analysis. The graphs of figure 4-1 and figure 4-2 are for specific cells and can not be generalized. The purpose

is to introduce the reader with the packaging factor concept and show the major weight difference between enclosures.
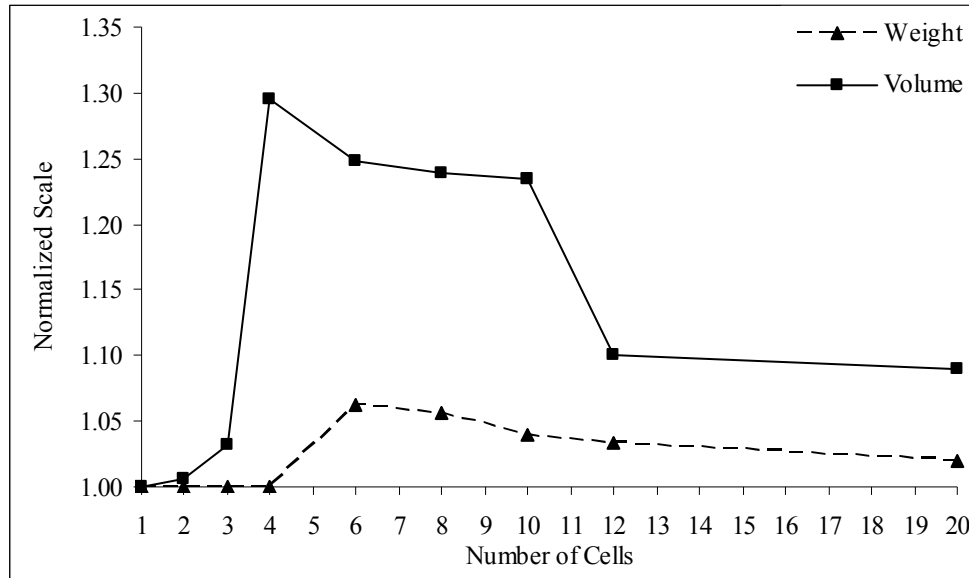
Figure 4-2: Normalized Weight and Volume for Lithium Polymer Packs Used in Aero-Modeling.

4.5 List of References

[1]   Thunder Power RC, "Extreme and Prolite Lipoly Packs", Online Posting: http:// thunderpowerrc.com/html/products.html (September 18, 2007).

[2]   Total Power Solution, "Li-Polymer Packs: High Rate and Heavy Duty", Online Posting: https://www.all-battery.com/index.asp (September 18, 2007).

[3]   UltraLife Batteries, "Rechargeable Batteries: Lithium Ion and Polymer", Online Posting: http://www.ultralifebatteries.com/ (October 28, 2007).

[4]   MIL Power Ltd, "Quality Military Batteries", Online Posting: http://milpower.co.uk/ (October 28, 2007).

[5]   Bren-tronics Inc., "Rechargeable Batteries: Lithium Ion and Polymer", Online Posting: http://www.bren-tronics.com/solutions.asp (October 28, 2007).

[6]   Tadiran Batteries, "Rechargeable Batteries: Lithium Ion", Online Posting: http://www.tadiranbat.com/home.php (October 28, 2007).

CHAPTER 5. IMPROVING ENDURANCE AND RANGE OF A UGV WITH GIMBALLED LANDING PLATFORM FOR LAUNCHING SMALL UNMANNED HELICOPTERS

5.1 Introduction

The quest for enhanced autonomy of unmanned vehicles, coupled with the complexity of the missions they are being used for, on one hand, and the operational restrictions due to low payload capabilities and small battery capacities, on the other hand, justify the need for novel solutions that improve unmanned vehicle endurance and range without adversely affecting their autonomy and functionality.

Unmanned aerial vehicles are widely used due to their ability to cover large areas and reach points not easily approachable by conventional ground vehicles [1]. As a consequence, runtime limitations of such systems are very important. In particular, small man portable unmanned VTOL vehicles, electric or not, although capable of taking off and landing anywhere, with the ability to hover over areas of interest, suffer tremendously from limited flying times that seldom exceed 30 minutes. This restricts the operational range, admissible mission profiles and on-board sensors and processors.

UGV and UAV power requirements are mostly determined by the manufacturer for a specific vehicle configuration, ignoring the impact of possible upgrades, off-the-self add on sensors and other custom made accessories, such as multiple cameras, IMU, GPS, compass, laser range finders and sonar sensors in addition to computer controlled servos, navigation systems and cooling fans. For UAVs, in addition to the above, the very low payload capabilities offer no room for major improvements.

Therefore, it is the central objective of this work to overcome said limitations by presenting specifications for an integrated UGV - gimballed landing platform - unmanned VTOL vehicle system with optimal power consumption and low power sensors that improves the UGV endurance by more than 500% and, indirectly, increasing the VTOL vehicle operational range since the VTOL vehicle is transported to the mission site without the need to fly. The proposed gimballed platform, which will be a power source itself, rotates around two axes perpendicular to each other, allowing the VTOL to take-off and land, regardless of the position of the UGV, while securing it during transportation.

The idea of landing a VTOL vehicle on a mobile platform is not new. The problem of autonomously landing a full size helicopter on a ship has already been investigated in [2]. It is a dangerous and difficult problem to solve even for manned helicopters with experienced crews. However, the topic has not been researched for miniature VTOL vehicles. In fact, a literature search has revealed only one design for autonomous launching, retrieval and refueling of UAVs, developed by SPAWAR Systems Center and Allied Aerospace as part of the Autonomous UAV Mission System (AUMS) project [3]. An initial demonstration of the capabilities of this system was done in 2003. This system was specifically designed to be used with Allied Aerospace's iSTAR UAV and SSC San Diego's MDARS UGV. However, adaptation to other systems is not possible, as compared to the design presented in this paper.

A detailed analysis is carried out for an ATRV-Jr UGV with custom made components and a gimballed landing platform suitable for small VTOL vehicles like the Raptor 90 or the Maxi Joker 2. However, the same analysis / design may be followed for any UGV/VTOL combination. Requirements for energy storage devices are set for 10 hours of continuous operation under maximum load (as compared with the 1 hour of the currently used custom made mobile platform) and two recharges of electric unmanned VTOL. Since improved endurance is of the highest priority set, requirements are coupled with recommendations for very low power efficient sensors that do not limit functionality

and flexibility. Before proceeding, it must be stated that it is beyond the scope of this paper to study how the VTOL will take off / land autonomously or how it will be controlled.

5.2 ATRV-Jr and Maxi Joker 2 Specifications: Power Consumption and Endurance

Current UGV power sources are almost exclusively re-chargeable lead-acid and nickel cadmium (NiCad) batteries due to the fact that both technologies are mature, well understood and cheaper compared to more recent technologies such as lithium batteries and fuel cells.

Recent concerns about energy and environmental problems and advances in material and manufacturing engineering have enabled a wider commercial product selection in lithium batteries and fuel cells. For example, Proton Exchange Membrane Fuel Cells (PEMFC) have already been tested and used in Autonomous Underwater Vehicles (AUVs) [4]-[7] and mobile robots [8], [9]. As stated in [5], Direct Methanol Fuel Cells (DMFC) are a better choice for mobile robots, but wide power range units are only in the first steps of their commercialization.

New generation VTOLs, such as the Raptor 90, use a gas motor and batteries such as NiCd and Lithium Polymer (LiPo) for the servos and computer. Similarly, electric VTOLs, such as the Maxi Joker 2, use NiMH and NiCad batteries with runtime of 5 - 12 minutes for 28-32 cells (5.2-5.5Kg) whereas 10-12 cells (4.5-5Kg) of LiPo can increase runtime to 8-20 minutes respectively.

The ATRV-Jr is manufactured by the iRobot Corporation and it has the following characteristics, as specified by the manufacturer [10]:

- Speed (m/s): 1

- Height (cm/in): 51/20

- Length (cm/in): 78/30.7

- Width (cm/in): 63/24.8

- Weight (kg/lbs): 50/110

- Payload (kg/lbs): 25/55

- Endurance: 3-5 hr (terrain dependent)

The Maxi Joker 2 is a middle sized, remote-controlled, electric, miniature helicopter. It can be modified to operate as an autonomous system by the incorporation of a lightweight vision system, a processing system as well as a communications platform. Its characteristics according to the manufacturer are:

- All-up weight (kg/lbs): 8/17.6

- Payload (kg/lbs): 2/4.4

- Endurance: up to 20 min

Based on manufacturer specifications the ATRV-Jr is powered by two lead-acid batteries, 12Kg (27lbs) and 4dm^3 (343in^3) each, with a total capacity of 672 W-hr. Without any upgrades or other additions, only the computer and vehicle motors are connected directly to the batteries. The Pentium 3, 800MHz computer requires 1.25A at 24V, whereas the two motors require 5.44A total (2.72A each). Taking into account the inefficiencies of the computer power supply and the motors, the full load current is estimated to be 7.5-8A and as a consequence the runtime is approximately 3.5 hours. Terrain dependency, smaller loads like cooling fans and 17 sonar sensors and losses result in runtime variation between 3-5 hours.

With current upgrades and added sensors, 2 DC-DC converters and a 300W ATX power supply are connected directly to the batteries to provide regulated voltages to power the

sensors and the on-board computer. The processor was upgraded to a 3 GHz Pentium 4 requiring 120W. Considering a 70% ATX power supply efficiency (built for desktops) and the power consumption of the other subsystems (storage, communications, etc.) the total computer power consumption is estimated to be 214W. Total peak sensor power demand is 86W increased to 107W when considering 80% efficiency for the DC-DC converters and voltage regulators. This analysis gives a full load of 452W and a corresponding current of 18.8A.

Figure 5-1 depicts the performance of the battery pack with respect to the discharge current. At a discharge current of 1.65A, the battery pack has a capacity of 33Ah or 20h runtime, whereas at a current of 19.7A the capacity drops to 19.7Ah or 1h of runtime. Therefore, for the previously estimated load current of 18.8A, the runtime is estimated to be barely over 1 hour. This runtime does not take into account any capacity loss due to aging.
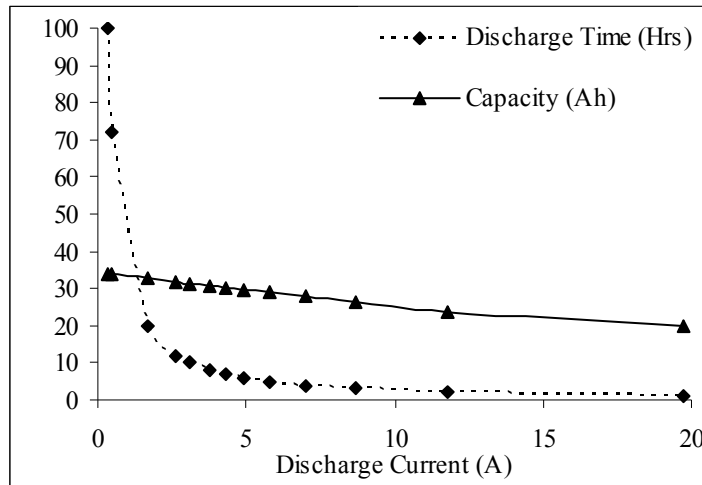
Figure 5-1: Capacity (Ah) and Discharge Time (Hours) Versus Discharge Current of Deep Cycle DCS-33H Lead Acid Batteries.

The flight time of the Maxi Joker 2 is determined by the battery pack used and it can go up to 20 minutes. In the case of the Raptor 90, maximum fly runtime is determined by the

amount of available fuel and vision system operation; as shown in [1] available fuel limits maximum runtime to 18 minutes. The vision system with CPU utilization between 98 and 100 percent and a wireless connection providing GPS coordinates to an external system, was operated continuously for 35 minutes. With low power, an efficient vision system already in use, and with payload capability reached, the options for endurance improvements are extremely limited for miniature VTOLs.

5.3 Increasing VTOL Endurance & Range

It has been already demonstrated that improving the endurance of VTOL vehicles is not possible due to payload limitations, high energy demands and the power storage technology currently employed. Nevertheless it is possible to indirectly increase the range of VTOLs by transporting them to the area of interest and using their runtime over the target rather than en route. This is achieved with the installation of a gimbaled landing platform on top of a UGV.

This gimbal-based design has been used extensively, albeit in a relatively smaller scale. The gimbal usually consists of 2 or 3 concentric rings that are connected with each other by axes, each of which is driven by an individual motor. As a result each ring can rotate independently of the other, keeping the inner gimballed platform horizontal and free from vibrations. This is usually achieved with installation of gyros, which calculate the angles of rotation of the platform providing the necessary information to the motors to counter any movement of the gimbal support [11]. Currently the main application of gimbaled systems is the stabilization of cameras on helicopters.

Gimbaled platforms allow for 1, 2 or 3-axes rotation, but a 2-axes gimballed system is sufficient for landing purposes. There is no need to install gyros, since altitude data can be supplied by the IMU of the UGV itself. This design is chosen because it levels the landing pad with no limitation with respect to the pose of the UGV. The cross section of the platform is seen in figure 5-2 and a 3D representation of the platform on top of an ATRV-Jr is depicted in figure 5-3. Platform rotation can be achieved with the use of two

motors connected via a geared system to the two rotation axes. The gears will take most of the load off the motors and make the platform more resistant to movement due to weight imbalance. The power requirements of the motors are estimated to be approximately 25W.
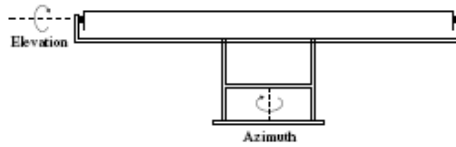
Figure 5-2: Cross Section of a 2-Axis Gimbaled Platform Design.
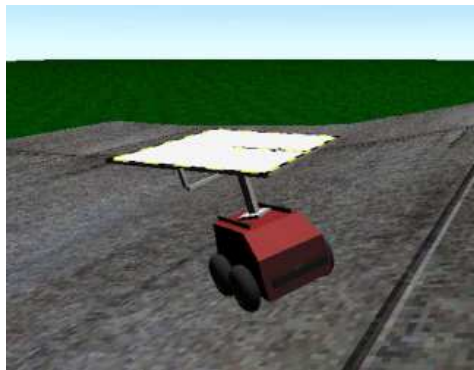
Figure 5-3: 3D Representation of the Platform Installed on Top of an ATRV-Jr.
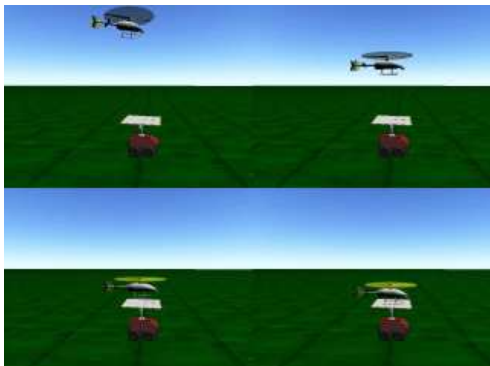
Figure 5-4: Screenshots Every 2 Seconds of a Simulated VTOL Landing.

5.4 UGV with Take Off/Landing Platform: Lower Power Demand, Higher Efficiency & Endurance

It is true that for most UGV outdoor applications, payload needs sensor suite utilization and as a consequence energy requirements are a-priori unpredictable. This makes proper sizing of energy storage devices a rather difficult task. However, this research considers a wide range of outdoor applications related to search and rescue, surveillance, mapping, de-mining threat identification and patrolling and, therefore, the requirements for energy storage devices have been sized for 10 hours of continuous operation under maximum load. This also includes the operation of the landing platform and two recharges of an electric unmanned VTOL. Since improved endurance is of high priority, set requirements are coupled with recommendations for more efficient sensors.

Table 5-1: ATRV-Jr Current Sensors

Sensor Type	Voltage (V)	Power (W)
Laser	24	17.5
Fans (two)	24	4.1
IMU	12	3
Fan	12	0.2
Sony Cameras (two)	12	60
GPS	9	0.6
Compass	5.1	0.1
Total Consumption		85.5

Table 5-2: Proposed Low Power Sensors

Sensor Type	Power (W)
Sony CCTV Camera – FCB (2)	6
GPS-Carmin 18, 12 channel	0.3
IMU – ETB	0.5
Range Finder HOKUYO URG-04X	2.5
Total Consumption	9.3

5.5 Sensors & Processing Platform

The current configuration of the ATRV-Jr with all sensors and power consumption requirements is presented in table 5-1. The cameras alone consume up to 60W out of the

total consumption that is about 85.5W! As a first step to save energy, lower power sensors that offer the same capabilities with the existing ones are proposed as shown in table 5-2. These sensors consume only 9.3W, resulting in a significant reduction of 90% and 13% in the sensor and total power consumption respectively.

The proposed new sensors have been selected with low power consumption in mind. As a result, some of the sensors have limited capabilities compared to the older sensors. However, these limitations do not affect the overall system performance and applications. For example the older laser (SICK LMS200) has a range of 80m but consumes 17.5W whereas the new proposed one (Hokuyo URG-04LX) has a range of 4m and consumes only 2.5W. However, for applications such as collision avoidance at speeds of 1m/s, the older laser was oversized and unnecessary. The new proposed laser can meet the application at much lower power consumption.

Table 5-3: Processor Power Consumption from [12]-[14]

Processor Type	Power Demand (Watts)	
	Idle State	Max Work Load
Intel Pentium D 820	50	134.3
Intel Pentium 4	49	130.6
Intel Pentium M	20.8 at 1.2GHz	30 at 2.66GHz
Intel Pentium 0.13 μm	30 at 1.6GHz	76 at 3.2GHz
Intel Pentium 90nm	30 at 1.866GHz	88 at 3.33GHz
AMD Athlon64, +3500	11.6	45.6

As a second step, a comparative study of processor power consumption (for processors with 3 GHz clock speed) shown in table 5-3 has revealed that the Pentium 4 processor with 3GHz clock speed consumes as much power as the two motors of the ATRV-Jr.

As observed in table 5-3, the two Intel processors tested at 3 to 3.4GHz for maximum work load required 131W and 134W respectively [12]. At idle state, Intel speed step technology reduces the power consumption to 50W by running the processor at 2.865GHz. On the other hand the AMD processor at the same clock speeds consumes only 45.6W under load and 11.6W in idle mode. Furthermore, the Pentium M processor,

specifically designed for mobile applications, has a maximum power consumption of 30W at 2.66GHz clock speed, whereas at idle state the demand drops to 21W by reducing the clock speed to 1.2GHz.

The recommendation is to use a Pentium M 2.66GHz and Compact Flash memory for storage. Compact Flash memory has the advantage of low power consumption [15], vibration resistance and plug in - plug out capability. The latter feature makes programming of the ATRV-Jr easier and allows for storage of various mission scenarios in different memory modules, loading them as needed.

With the proposed configuration, maximum power demand of the processor including that of the proposed sensors is about 40W. The use of a high efficiency power supply like the M1-ATX with 80-90% efficiency is proposed, as opposed to the currently used desktop power supply with 60-70% efficiency. As a result the total estimated power consumption of the sensors and processing platform is reduced from 321W to 50W only. In summary, following the stated recommendation for low power sensors, processor and power supply, results in a decrease of the total full load power demand (including the motors) by 60% (from 452 to 181W) and as a consequence a runtime increase from 1 to more than 3 hours.

5.6 Powering the ATRV-Jr with Lithium Batteries

Before determining the energy requirements for accomplishing the 10 hours runtime goal, the consumption due to platform operation and VTOL recharging needs to be estimated. The take off/landing platform on top of the UGV has an estimated power consumption of 25W, which will not be taken into account since it will operate only for a few minutes and therefore its contribution to the total power consumption is minimal. On the other hand VTOL recharging needs approximately 100Wh for every recharge. Thus the total required energy to achieve the set goal is estimated to be 2kWh resulting in a required battery capacity of 84Ah.

Table 5-4: Comparison of Lead Acid and Li-Ion Battery Packs

	DCS-33 Lead Acid	Li-Ion VL45E Cells, 7x2 matrix, by Saft
Capacity (Ah)	26 at C/3	90 at C/3
Voltage (V)	24	25.2
Weight (Kg)	24	15
Total Energy (Wh)	624	2268
Specific Energy (Wh/Kg)	26	151
Energy Density (Wh/dm^3)	78.6	318
Specific Power (W/Kg)	208	664
Power Density (W/dm^3)	604	1392
Worst case runtime1 (hr)	3.2	11
Average runtime2 (hr)	4.2	14

1 – Under maximum load   2 - For a mixed cycle of 30% stationary and 70% moving operation

By comparing the current lead acid with a high energy Li-Ion battery pack in table 5-4, it is evident that the set goal can be achieved with a significant reduction in the on board battery weight. Specifically a decrease of more than 37% (from 24 to 15kg) is possible which will allow an equivalent increase in the payload capacity of the system.

However, lithium batteries may not be the best available choice; current commercial scale up lithium batteries require at least 2 to 3 hours to be charged. For this reason fuel cells offer a better choice for powering the ATRV, due to their easy refueling process. This recommendation is justifiable since as stated in [7] the Urashima AUV had an increase in travel distance of 65.4% when powered by a fuel cell system instead of lithium ion batteries.

5.7 Using a Combination of Lithium Batteries and a Fuel Cell

Since most commercially available DMFCs do not meet the required power demand, an alternative approach is to combine a system like the 250W iGen system, provided by Idatech, with Li-Ion cells. This hybrid system's capacity depends on the on board fuel storage. Table 5-5 shows the characteristics of the hybrid system for 2.5 and 7.5 kg of fuel for a total system weight between 19 and 24 kg (the latter being equal to the currently installed battery pack.

Finally, the high energy density DMFC and high power density Li-Ion design can be classified as a hybrid system similar to battery and super-capacitor hybrid systems. An active hybrid system is proposed instead of a passive hybrid system. The introduction of a control system, DC-DC converter [16], eliminates all the negative aspects of a passive hybrid system and gives more design flexibility. Furthermore, it has been shown that a multilevel DC-DC converter can provide optimum fuel cell utilization [17].

5.8 Using a Solar Array

In order for the VTOL to safely perform an autonomous vision-based landing, significant margins of error need be accommodated and therefore the actual area of the landing platform is chosen to be $1m^2$, which is 4 times that of the footprint of the Maxi Joker 2. This free level surface can be covered with a photovoltaic array. Although a portion of the array will be shaded by the VTOL, it is estimated that about 50 to 70% will receive solar radiation at all times. The total area available on the landing platform is then used to provide up to 120W of energy under ideal conditions. Even with a more realistic performance of 50 to 60W, it is still adequate to cover the needs of the sensors and the on-board computer. As a result while the UGV is stationary it won't consume battery power and consequently its endurance will increase significantly.

Table 5-5: Alternative Solution (DMFC AND BATTERY)

	iGen DMFC by Idatech	Li-Ion VL45E Cells, 7x1 matrix, by Saft	Total Performance
Capacity (Ah)	56.3 - 168.8	45	101.3 - 213.8
Voltage (V)	24	25.2	24
Weight (Kg)	Unit 9.0Kg Fuel 2.5-7.5Kg	7.5	19 - 24
Total Energy (Wh)	1,351 - 4,050	1,134	2,485 - 5,184
Specific Energy (Wh/Kg)	117.5 - 245.5	151.2	130.8 - 216
Specific Power (W/Kg)	21.7 - 15.2	664	275.2 - 218
Worst case runtime1 (hr)	-	-	12.4 - 26
Average runtime2 (hr)	-	-	15.4 - 32

1 - Under maximum load   2 - For a mixed cycle of 30% stationary and 70% moving operation

Furthermore, when the VTOL is air-born the available rotation mechanism of the platform can be used to align the solar array with the sun, thus maximizing the former's performance and allowing battery recharging to take place. The energy output of the solar array was not taken into account in the sizing of the lithium battery pack and the fuel cell. This is because in the worst case, for example a rainy day, the solar array's contribution will be negligible. On the other hand on an average sunny day and during a 10 hour mission the solar array can produce up to 500Wh which is 25% of the total energy demand.

Even in the case where the motors of the rotation platform mechanism are assumed to be active at all times, then for a 10 hour operation, 250Wh power consumption would be required. In this case the photovoltaic array would cover this amount plus 12.5% of the total mission energy demand, thus extending runtime even more. Therefore, a conservative design and estimation is proposed.

5.9 Leveling the Platform

To derive the equations needed to level the platform, an orthogonal Cartesian system in 3D space is used, where the x axis is horizontal, the y axis is vertical, towards the sky and the z-axis is towards the viewer (figure 5-5 a). Using a matrix notation to represent the rotations of any object we have the following [18], [19]:

$$R(\phi) = \begin{bmatrix} 1 & 1 & 0 \\ 0 & \cos\phi & -\sin\phi \\ 0 & \sin\phi & \cos\phi \end{bmatrix} \tag{5.1}$$

$$P(\phi) = \begin{bmatrix} \cos\phi & -\sin\phi & 0 \\ \sin\phi & \cos\phi & 0 \\ 0 & 0 & 1 \end{bmatrix} \tag{5.2}$$

$$Y(\phi) = \begin{bmatrix} \cos\phi & 0 & \sin\phi \\ 0 & 1 & 0 \\ -\sin\phi & 0 & \cos\phi \end{bmatrix} \tag{5.3}$$

where R is the roll matrix, P is the pitch matrix and Y is the yaw matrix. The roll, pitch and yaw angles are defined by a rotation around the z, x and y axes, respectively (figure 5-5 b-d). Any rotated vector V can be calculated by a combination of the rotations mentioned above using the formula below:

$$V^{'} = R(\phi_1).P(\phi_2).Y(\phi_3).V \qquad (5.4)$$

where the sequence with which each operation is applied is important. Assuming that during its movement the robot reached a position where its roll, pitch and yaw angles are φ_1, φ_2, φ_3, respectively, then it follows that as a consequence the platform as well, has the same roll, pitch and yaw with respect to the horizontal. The landing platform is designed with the capability of rotating around two axes (figure 5-6), a vertical one and a horizontal one, which henceforth will be referred to as the azimuth axis and the elevation axis respectively. In order to level the platform suitable φ_4, φ_5 angles for the azimuth and elevation vectors, respectively, need to be calculated.
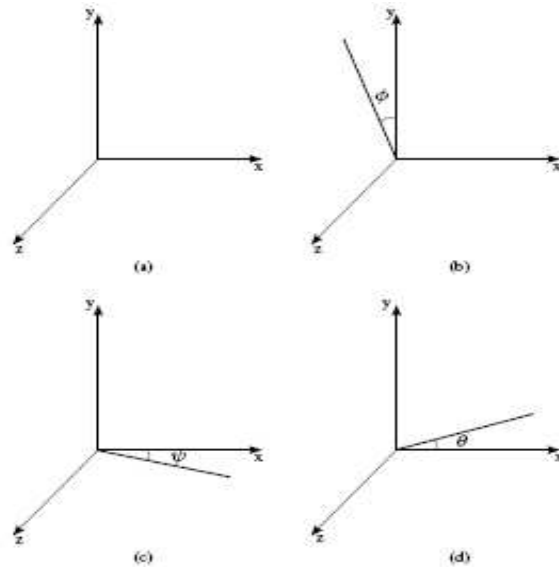
Figure 5-5: (a) The Cartesian System Used (b-d) Roll, Yaw and Pitch Angles Respectively.
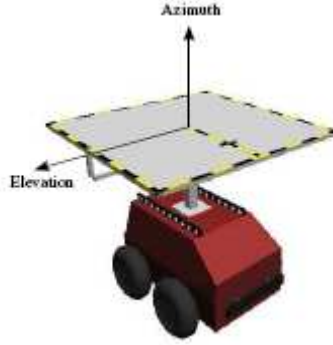
Figure 5-6: The Landing Platform Rotates Around Two Axes; a Vertical (Azimuth) and a Horizontal (Elevation).

The problem can be divided into two sub problems where the platform is first rotated around the azimuth axis until the elevation axis is horizontal. Then by rotating around the elevation axis until the azimuth axis is vertical, the platform assumes a horizontal pose. The initial elevation vector is given by:

$$V_{el} = R(\phi_1).P(\phi_2).Y(\phi_3).V_z \tag{5.5}$$

where V_z is the z-axis unitary vector and is equal to [0 0 1].

After the platform has been rotated around the azimuth vector, the new elevation vector becomes:

$$V_{el}' = Y(\phi_4).V_{el} \tag{5.6}$$

since a change of the azimuth corresponds to a change of the yaw of the platform. Since the elevation axis needs to be horizontal, the dot product of the elevation vector and the y-axis is set to zero and the $\varphi4$ angle is calculated.

$$V_{el}' \bullet V_y = 0 \Rightarrow$$

$$\phi_4 = \tan^{-1}\left(\frac{\cos\phi_2.\sin\phi_1}{\sin\phi_2}\right) \tag{5.7}$$

where Vy is the y-axis unitary vector and is equal to [0 1 0].

After the azimuth has been changed, the platform will be rotated around its new elevation vector, until the azimuth vector is vertical. The azimuth vector before this rotation is

$$V_{az} = R(\phi_1).P(\phi_2).Y(\phi_3).Y(\phi_4).V_y \tag{5.8}$$

Since the rotation above corresponds to a change of pitch for the platform, it will become:

$$V_{az}' = P(\phi_5).V_{az} \tag{5.9}$$

The angle φ_5 is calculated so that the V_{az} vector will be vertical by setting its dot product with either the x-axis or the z-axis to zero.

$$V_{az}' \bullet V_x = 0 \Rightarrow$$

$$\phi_5 = \tan^{-1}\left(\frac{\sin\phi_2 - \tan\phi_3.\tan\phi_1}{\tan\phi_3.\sin\phi_4 - \cos\phi_1.\cos\phi_2.\cos\phi_4}\right) \tag{5.10}$$

where V_x is the x-axis unitary vector.

5.10 Alignment of Solar Array With the Sun

The alignment of the solar array with the sun in order to maximize its performance is achieved using the methodology of the previous section. Initially the sun vector V_{sun} is calculated as the normalized vector with origin the center of the platform and destination the sun.

The calculation of the φ_4, φ_5 angles for azimuth and elevation respectively is done like in the previous section; in two steps. First the azimuth vector is changed until the elevation vector V_{el} is vertical to V_{sun}. Then the platform is rotated around the axis defined by the

elevation vector until the azimuth vector V_{az} is parallel to V_{sun}. The following two equations can be used to determine the final φ_4, φ_5 angles.

$$V_{sun} \bullet \left[R(\phi_1).P(\phi_2).Y(\phi_3).Y(\phi_4).V_z \right] = 0 \qquad (5.11)$$

$$V_{az} = R(\phi_1).P(\phi_2).Y(\phi_3).Y(\phi_4).P(\phi_5).V_y \qquad (5.12)$$

$$V_{sun} = \frac{V_{az}}{|V_{az}|} \qquad (5.13)$$

In order for the V_{sun} vector to be calculated it is possible to use geographical data from the region of operation of the system in combination with chronological data (day of year and time of day). Alternatively active sun tracking methods can also be employed using a vision system or other special purpose equipment, although that would further decrease the payload capabilities of the platform.

5.11 Simulation Results

In order to demonstrate the feasibility of the design, simulations of the robotic platform equipped with a landing platform were carried out, using the Gazebo 0.5.3(cvs121305) software [20]. This software is open source and is part of the Player/Stage/Gazebo software package. The object dynamics are calculated using the Open Dynamics Engine by Russel Smith [21], which is also used by several simulation applications as well as games.

The landing platform was simulated as a solid mass weighing 12kg and the moving understructure was modeled using several smaller geometries with a total mass of 3.2kg. The modeled weight of the platform corresponds to the weight of two readily available commercial solar panels, with an area equal to that of the platform and a total rated output of 120W (Sunwize SW60, [22]). Two motors are used to move the platform at low speeds. The elevation motor has a stop at $\pm 40^\circ$, while the heading motor is limited to

78

±90°. The controller instructs the motors to rotate the platform until the deviation from the predetermined angle is within ±1.7°.

In all test scenarios it was possible to rotate the platform until it was horizontal within the predetermined limits of error using only two axes of rotation. Further testing indicated that under the assumption of small and slow changes in the robot pose (roll, pitch and yaw), it is possible to control the platform so that it will remain horizontal while the robot was moving, without significant increase in the error. Finally, simulations also demonstrated that the installation of the platform resulted in moving the center of gravity of the robot higher, thus making it unstable in higher degrees of inclination.

A concept video demonstrating an unmanned helicopter landing as well as the operation of the securing mechanism can be found in the home page of the Unmanned Systems Lab (http://www.cse.usf.edu/USL/Videos/latch-pdemo.mpeg). A second video demonstrates how multiple platforms can be used for border patrol (http://www.cse.usf.edu/USL/Videos/patrol.mpg).

Figure 5-7: A 3D Representation of the Helicopter Landed on the Platform and Secured With a Latching Mechanism.

5.12 Discussion and Recommendations

This chapter examined and identified reasons for the reduced UGV endurance, and, in particular, of a custom made ATRV-Jr. As presented, the reasons were not only limited to the use of the inefficient lead acid batteries but also included an excessive power demand that exponentially decreased the battery discharge time. In order to achieve longer runtimes, it is recommended first to use lower power and more efficient sensors rather than over sizing the battery packs. Low power sensors, a Pentium mobile processor and a 90% efficient power supply may decrease power consumption by 60%. It has been shown that lithium ion technology meets the set energy requirements of the 10hr goal with only 15Kg whereas lead acid technology would require more than 72Kg. On the other hand, a combination of a DMFC and Li-Ion can achieve very high energy densities that can offer runtimes of over 24h. The proposed DMFC and Li-Ion solution also offers a refueling time of just a few minutes whereas Li-Ion batteries need several hours. Therefore, for outdoor applications such as search and rescue, DMFC combined with Li-Ion cells is the most suitable design considering refueling time, weight, volume and runtime.

It was also demonstrated that although increasing the endurance of modern miniature VTOL vehicles is not possible, it is possible to increase their operational range using a mobile landing platform. Additionally the landing platform provides the opportunity for on-site energy production from renewable energy sources, thus further increasing the VTOL's as well as the UGV's endurance.

5.13 List of References

[1]   R. Garcia R, K. Valavanis, M. Kontitsis, "A High Power, Inexpensive On-board Vision System for Miniature Unmanned VTOL Vehicles", Tech. Rep. 4, CRASAR, USF, 2005.

[2]   M. Storvik, "Guidance System for Automatic Approach to a Ship", Master's Thesis, Norwegian University of Science and Technology, 2003.

[3]   K. Mullens, E. Pacis, S. Stancliff, A Burmeister, T. Denewiler, M. Bruch, H. Everett, "An Automated UAV Mission System", In: AUVSI Unmanned Systems in International Security, SPAWAR Systems Center, Allied Aerospace, 2003.

[4]   G. Pappas, R. Rosenfeld, A. Beam, "The ARPA/Navy Unmanned Undersea Vehicle Program", Unmanned Systems, 11(2):41–44, 1993.

[5]   R. L. Rosenfeld, P. R. Prokopius, A. P. Meyer, "Fuel Cell Power System Development for Submersibles", In: Proc. of the 1992 Symposium on Autonomous Underwater Vehicle Technology, pp 184–188, 1992.

[6]   K. E. Swider-Lyons, R. T. Carlin, R. L. Rosenfeld, R. J. Nowak, "Technical Issues and Opportunities for Fuel Cell Development for Autonomous Underwater Vehicles", In: Proc. of the 2002 Workshop on Autonomous Underwater Vehicles, pp 61–64, 2002.

[7]   I. Yamamoto, T. Aoki, S. Tsukioka, H. Yoshida, T. Hyakudome, T. Sawa, S. Ishibashi, T. Inada, K. Yokoyama, T. Maeda, S. lshiguro, H. Hirayama, K. Hirokawa, A. Hashimoto, N. Hisatome, T. Tani, "Fuel Cell System of AUV Urashima" In: Proc. Of OCEANS'04 MTS/IEEE TECHNO-OCEAN '04, vol 3, pp 1732 – 1737, 2004.

[8]   Laboratories SN, "Robotics Online - Fuel Cell Powered Mobile Robots Case Study", Online Posting: http://www.roboticsonline.com/public /articles/index.cfm?cat=99 (January 21, 2006).

[9]   A. Wilhelm, J. Pharoah, B. Surgenor, "Fuel Cell Today - Fuel Cells and Mobile Robots", Online Posting: http://www.fuelcelltoday.com/FuelCellToday/ FCTFiles/FCTArticleFiles/Article_933_FuelCellsandMobileRobots.pdf (2006)

[10]   Space and Naval Warfare Systems Command, "Joint Robotics Program, Tech Database, Robotic Platforms, Unmanned Ground Vehicles ATRV-Jr Specifications", Online Posting: http://robot.spawar.navy.mil/images/database/ Platforms/UGV/doc/atrvjr_tech_2001.pdf (2005).

[11]   A. D. King, "Inertial Navigation - 40 years of evolution, GEC Review, vol. 13, no. 3, 2003", Online Posting: http://www.marconi.com/Home/aboutus/ Our%20History/Publications%20Archive/GEC%20Publications%20Archive/GEC%20Journals/GEC%20Review/v13n3s/p140.pdf (January 21, 2006).

[12]   I. Gavrichenkov, Xbit Labratories, "CPU Category - Intel Pentium D 820 CPU Review, Page 3, 05/27/2005", Online Posting: http://www.xbitlabs.com/articles/ cpu/display/pentiumd-820_3.html (January 21, 2006).

[13]   Intel United States, "Mobile Intel Pentium 4 ProcessorsM, Enhanced Intel SpeedStep Technology", Online Posting: http://www.intel.com/support/processors/mobile/pentium4/sb/cs-007499.htm (January 21, 2006).

[14]   Intel United States, "Mobile Intel Pentium 4 ProcessorsM, Voltage Requirements", Online Posting: http://www.intel.com/support/processors/mobile/pentium4/sb/cs-007501.htm (January 21, 2006).

[15]   Zheng, Garg, Sobti, Zhang, Joseph, Krishnamurthy, Wang, "Considering the Energy Consumption of Mobile Storage Alternatives", IEEE Symposium on Modeling, Analysis and Simulation of Computer Systems, 2003.

[16]   R. A. Dougal, S, Liu and R. E. White, "Power and Life Extension of Battery-Ultra-Capacitor Hybrids", IEEE, 25:120–131, March 2002.

[17]   B. Ozpineci, L. M. Tolbert, G. Su, Z. Du, "Optimum Fuel Cell Utilization with Multilevel DC-DC Converters", In: Proc. of Nineteenth Annual IEEE Applied Power Electronics Conference and Exposition (APEC'04), vol 3, pp 1572–1576, 2004.

[18]   M. Baker, "Euclidean Space", Online Posting: http://www.euclideanspace.com/ (October 18, 2008).

[19]   F. Dunn, "3D Math Primer for Graphics and Game Development", Wordware Publishing, Inc., 2002.

[20]   Sourceforgenet, "Project Page - Player/stage/gazebo", Online Posting: http://playerstage.sourceforge.net/ (2005)

[21]   R. Smith, "Open Dynamics Engine", Online Posting http://www.ode.org/ (October 18, 2008).

[22]   Sunwize Technologies, Inc., "Solar Electric Power Systems", Online Posting: http://www.sunwize.com/ (2005).

CHAPTER 6. OPTIMIZATION ALGORITHM FOR POWER AND ENERGY
SYSTEM CONFIGURATION

6.1 Introduction

In previous chapters, energy densities of commercially available lithium batteries (primary and secondary) and fuel cells were analyzed and compared which lead to suggestions on possible power sources for mobile applications. The suggestions were made solely on total weight required for various total mission energies. The entire analysis was performed by a linear approach where the total amount of energy was the product of battery capacity multiplied by the battery voltage, and the effects of discharge current and capacity were neglected. Furthermore, because for outdoor applications the load profile is unpredictable, only energy is considered. However, operating voltages are very important too because, for a particular application, the load current could be higher than the maximum continuous battery discharge capability in which case more battery packs would be required to be connected in parallel thus increasing the total weight. Microsoft Excel was used for all these calculations which were very time consuming. Furthermore, hybrid system configurations were very complicated to be configured and compared in an Excel environment.

In this chapter a method is developed and introduced that determines the optimal configuration of a power system for mobile applications under constraints relating to capacity/runtime, weight, volume, cost and number of battery cells or fuel cell refueling canisters. Finally, the solutions are displayed according to a "Score" value which is being calculated based on how well each solution met the requirements. All possible solutions are based on commercially available batteries and fuel cells to reduce cost and delivery time. This optimization algorithm is in a Matlab Graphical User Interface (GUI)

83

environment that can also configure hybrid systems. Primary lithium batteries will not be included in the database because for repetitive applications such as boarder patrol, mapping and localization the cost and logistics (order, storage, and disposal) would be higher than secondary batteries.

Mathematical modeling of power systems is not a new field, especially for batteries. Such mathematical models are divided into 4 major categories; physical, empirical, abstract and mixed models. Mathematical models are evaluated based on accuracy, computational complexity, configurability and analytical insight. Based on the application, design engineers have used these models for optimal power management algorithms as well as customizing power sources under volume and weight constraints [1]-[4].

Other software with graphical user interface is HOMER® and ADVISOR® both produced by the US Department of Energy (DOE) and the National Renewable Energy Laboratories (NREL). HOMER software is used for static applications and using a micro-power optimization model, it explores the role of generator sets in small solar power systems. With battery, photo-voltaic and diesel prices as inputs it explores the best cost effective solution at the present time for an increased load demand. For example, is it more cost-effective to include a diesel generator than to increase the size of the battery bank or photo-voltaic (PV) array? The Sri Lanka case study is an elaborate study available online [5].

ADVISOR on the other hand is a simulation tool for vehicle evaluation and testing [6], [7], [8]. With elaborate car models which include wheels, engine, power-train and other car components, ADVISOR helps engineers determine how to increase the life of components, improve vehicle performance, optimize vehicle system designs, and reduce development times. However, models already available on ADVISOR software are mostly for products used in the automotive industry where weight constraints are not as critical as in mobile applications; small unmanned ground and aerial vehicles (UGV and UAV).

6.2 Optimization Algorithm

6.2.1 User-Defined Requirements and Constraints

The algorithm takes a load and runtime requirement that is used to determine appropriate power system solutions and depends on the application. The load is defined as the nominal power in watts and operating voltage in volts. Although voltage and current would be an equivalent way to define the load, the power is preferred because most name tags for motor and various other applications include nominal power instead of current. The other user-defined requirement is the runtime, given in hours. This allows the algorithm to determine the total energy requirement using its product with power in watts. It should be noted that the algorithm does not attempt to achieve the exact runtime rather it determines solutions that meet the requirement with a minimum number of units (batteries and/or fuel cells).

In addition to the aforementioned requirements, optional constraints can also be defined such as weight in Kilograms (Kg), volume in Liters (Ltrs), cost in United States of America dollars (US$), number of battery cells and number of fuel cell re-fueling canisters. In the user interface these constraints are ignored when they are defined to be zero.

Finally, another option available is the linear voltage regulation or switched mode DC to DC conversion. This option is discussed in detail in Section 6.2.2.

6.2.2 DC to DC Conversion Modeling

In Alternate Current (AC) systems, current and voltages can be transformed to other values (higher or lower) with the use of transformers. Transformers, rely on electromagnetic induction between the primary and secondary windings. From Faraday's Law, an alternating magnetic field in the primary winding induces an electromotive force (EMF or alternating voltage) in the secondary winding.
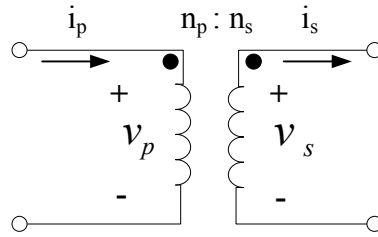
Figure 6-1: Schematic of an Ideal Transformer.

$$\frac{n_p}{n_s} = \frac{v_p}{v_s} = \frac{i_s}{i_p} \qquad (6.1)$$

Where subscript p denotes primary, s denotes secondary and n denotes the coil number of turns. For ideal transformers, the power on the primary and secondary windings will be the same. Therefore, a step up transformer ($n_s > n_p$), steps up the primary voltage but for power to be conserved then the current will be stepped down with the exact same ratio. Hence, $v_p < v_s$ and $i_p > i_s$.

For direct current (DC) applications transformers do not work due to lack of electromagnetic induction. However, DC to DC transformations or conversions can be achieved via linear voltage regulation or switched mode DC to DC conversion.

Linear voltage regulators can only step down a voltage by dissipating the extra energy in the form of heat. As a result they are very inefficient when the voltage difference is high or voltage regulation (v_{out}/v_{in}) is low. On the other hand, linear voltage regulators do not introduce any electronic noise.

DC to DC Converters on the other hand, temporarily store the energy in inductors or capacitors and then release this energy to the output at different voltage level; higher output voltage than input voltage can also be achieved. The voltage level is controlled by the ratio of how long the device stays on and off; also known as the duty cycle of pulsed width modulation (PWM). Because of this switched mode operation electronic noise is

introduced. However, because energy is stored in the form of magnetic and electric fields (inductors and capacitors respectively), then DC to DC conversion can provide higher efficiencies than linear voltage regulators (typically 80 to 98%).

In most applications runtime is of particular importance and as a result only step down voltage conversions will be considered. This is because for step down voltage conversions, the power system (battery or FC) current will be lower than the load current and hence its runtime will be higher.

Finally, a threshold point has to be determined when it is best to use a linear voltage regulator or a switched mode DC to DC converter. When the voltage difference (power system voltage minus the required application voltage) is very small then it can be said that voltage regulation (ratio of required application voltage to power system voltage) is high. Hence, for a switched mode DC to DC converter to be used the ratio of voltage regulation to DCDC efficiency has to be less than one. Otherwise, other means of regulation should be considered.

Therefore, for battery runtime maximization, a threshold parameter f can be defined, that when negative a DC to DC converter is required and when positive a linear regulator is more efficient. This threshold is calculated as:

$$f = \frac{V_{out}}{V_{in}} \frac{1}{e_{DC/DC}} - 1 \tag{6.2}$$

where $e_{DC/DC}$ is the efficiency of the DC to DC converter.

6.2.3 Design of the Battery Power System

First, an excel spreadsheet containing secondary lithium battery data is read and stored in the form of a matrix followed by the user inputs. The battery data includes information such as brand name and model, voltage, capacity and the specified discharge rate, weight, volume, price, maximum continuous discharge current and the Peukert's exponent. If any

information is missing then a predetermined value is used; 5 hours for discharge rate, $3 for cost and 1.1 for Peukert's exponent.

To meet the specified required application voltage, battery cells or packs need to be connected in series to form a string. The number of units (cells/packs) necessary is calculated by:

$$CS = \frac{V_L}{V_b} \qquad\qquad (6.3)$$

Where CS represents units connected in series, V_L is the load voltage and V_b is the unit's voltage. The series number is always rounded up. Hence the pack voltage is the product of series connected units and units' voltage.

$$V_{PA} = CS * V_b \qquad\qquad (6.4)$$

Pack voltages are always equal or higher than the specified required application voltage. Therefore, the DC to DC conversion parameters explained in section 6.2.2 are also checked and evaluated at this stage.

Load current is calculated from user input power and voltage.

$$I_L = \frac{P_L}{V_L} \qquad\qquad (6.5)$$

The calculated load current is compared to battery maximum continuous discharge current. If the load current is higher, then one more string is added in parallel. For every new parallel connection the new battery pack weight, volume etc are compared to the specified constraints. If any constraints are exceeded then the battery pack is rejected and the following product is evaluated.

Battery pack runtime is calculated with Peukert's equation;

$$t = \frac{t_{ref}\left(\dfrac{C_{PA}}{t_{ref}}\right)^{p}}{(I_L)^{P}} \tag{6.6}$$

Where p is Peukert's exponent, t_{ref} is battery discharge rate and all these are provided by the manufacturer and stored in the battery data sheet spread sheet. Pack capacity (C_{PA}) is the product of number of parallel modules and battery capacity. Strings increase the pack voltage but the capacity does not change, whereas parallel modules have the same voltage and increase the pack capacity. Runtime is a constraint that always has to be met.

When battery pack runtime is less than required runtime then one more parallel module is added, and new runtime, weight, volume etc are recalculated. The process is repeated utill runtime is met or exceeded while none of the other constraints are exceeded. Then the battery pack is added to the battery list of optimized solutions for this application.

6.2.4 Power System Score

In the case that more than one solution meet all the requirements then a measure should be available to compare which solution meets best the requirements and is the most optimized. For this reason a score of each solution is calculated, using the weight user inputs. Weight user inputs can be any number, representing constraints' importance. For example a runtime weight-factor (w_t) of 0.5 and a cost weight-factor (w_c) of 0.5 denotes that both runtime and cost constraints are as equally important. Hence the total score is the calculated by:

$$score_j = \frac{100}{w_t + w_m + w_v + w_c}\left[\frac{w_t t_j}{\max t_j} + \frac{w_m \min m_j}{m_j} + \frac{w_v \min v_j}{v_j} + \frac{w_c \min c_j}{c_j}\right] \tag{6.7}$$

Minimum and maximum values are found from the generated lists. For example for any battery solution the maximum runtime or minimum weight is found from the battery list,

whereas for fuel cell solution they are found from the fuel cell list and finally for the hybrid configuration they are found from the hybrid list. When all scores are calculated, then solutions are sorted in descending order according to their score and the three lists are displayed in the appropriate window. Hence, products with the highest score are on the top of the list whereas products with lower scores are at the bottom.

6.2.5 Design of the Fuel Cell Power System

Creating the Fuel Cell power system is more complicated that the battery system because every fuel cell depending on the technology and chemistry (DMFC, SOFC, etc) uses different forms of fuel and storage units. DMFC and SOFC systems use liquid and solid fuel respectively whereas hydrogen fuel cells use compressed H_2 which is stored in canisters, and to complicate matters even more, nearly every company uses different canisters, and even for some products there is more than one available canister type that needs to be evaluated. For these reasons, the fuel cell database uses different excel spreadsheets.

After the load current and system voltage are established as described in section 6.2.3, then total fuel cell runtime and constraints need to be calculated. It is possible to have a matrix for fuel cells to meet the design runtime and load current. Fuel cell weight, volume and costs include the fuel cell, the fuel required for the application and the fuel storage units.

For DMFC and SOFC systems, system runtime always equals to design runtime. This is because the exact fuel can be calculated for the desired runtime. Using manufacturer fuel consumption at rated power (usually rated power is where the fuel cell system works at optimal conditions) the amount of fuel necessary for a desired runtime is given by:

$$C_{FC} = t.P_{FC}.CS.CP.l \qquad (6.8)$$

Where l is the fuel cell gravimetric or volumetric consumption and P_{FC} is the fuel cell rated power. For example, the A50 by Smart Fuel Cell is a 50W DMFC which consumes

1.3 Liters of methanol per KWh. Using methanol density of 0.791Kg/L then it can be calculated that the power consumption comes to 1.028Kg/KWh.

For fuel cell systems that use compressed H_2 fuel, then the correct canister needs to be first identified. The canisters are divided into two major categories. A canister like the Nstore specify the amount of energy per canister (Wh/canister) whereas the second category canisters like BL and CL specify the canister volume in Liters.

Hence, for the Nstore, number of canisters required will be given by:

$$n_{can} = \frac{CS.CP.P_{FC}.t}{E_{can}}$$ (6.9)

Where E_{can} is the energy per canister. The number of canisters required is always rounded up hence for fuel cell systems higher runtimes can be achieved.

In the case of the BL and CL canisters, the required amount of fuel in Liters is found first from equation (6.8) and then the number of canisters required is calculated by dividing the fuel in Liters by each canister's volume:

$$n_{can} = \frac{C_{FC}}{v_{can}}$$ (6.10)

6.2.6 Design of the Hybrid Power System

The hybrid power systems configured are always a fuel cell system in parallel with a battery pack. First, for optimal results and higher system efficiencies the fuel cell system is always run at rated power. Then the hybrid systems are configured starting from a system made of just fuel cells, to gradually minimize the parallel fuel cells and add parallel batteries until the system is a configuration of just batteries. However, not all these simulated tests make it to the list. All assumptions and work explained in sections 6.2.3 to 6.2.5 are still the same.

The system runtime for a hybrid system is calculated in a different way than the battery and fuel cell systems. With known system voltage and fuel cell power the fuel cell load current contribution is calculated from equation (6.5). Hence, the battery current contribution is the difference of load current and fuel cell current.

$$I_b = I_L - I_{FC} \qquad (6.11)$$

Therefore, using equation (6.6) the battery runtime and energy are calculated for the calculated battery current contribution. This means that the necessary energy to be provided by the fuel cell is the difference of the total application energy and the battery contributed energy.

$$E_{FC} = E_T - E_b \qquad (6.12)$$

With the fuel cell required energy known the amount of fuel cell fuel necessary to meet this energy demand can be calculated as explained in section 6.2.5.

6.3 User Interface

The user may also define a desired maximum number of suggested solutions calculated before the simulation terminates. This option is useful for high power applications, because a very large number of configurations may be capable of meeting the load current requirements, especially in cases where most or all of the optional constraints are not defined.

Three different windows are provided for displaying results for battery-only solutions, fuel cell solutions and hybrid solutions. All results are displayed in descending order according to their score value.

When results are displayed, then the user can click on any of the lists, or any solution and then the individual solution's score, runtime, weight, volume and cost are displayed. Furthermore, the battery pack or fuel cell system are also divided in two more windows

representing the current contributed by the fuel cell or battery pack and the duty cycle of the DC to DC converter, if available.
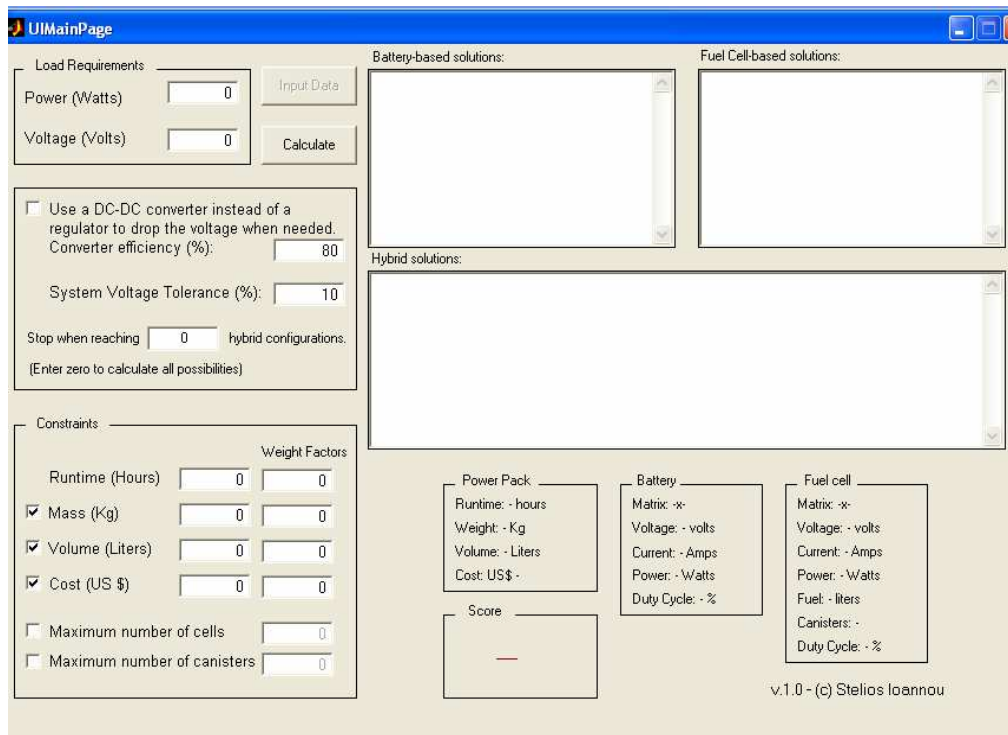
Figure 6-2: User Interface for Optimization Algorithm.

6.4 List of References

[1]   R. Rao, S. Vrudhula, D. N. Rakhamatov, "Battery Modeling for Energy Aware System Design", IEEE Computer Society, December 2003.

[2]   M. Chin and G. A. Rincon-Mora, " Accurate Electrical Battery model Capable of Predicting Runtime and I-V Performance", IEEE transactions of energy conversion, Vol.21, No. 2. June 2006.

[3]   S. Parchicha and S. R. Shaw, "A Dynamic PEM Fuel Cell Model", IEEE transactions of energy conversion, Vol.21, No. 2. June 2006.

[4]   F. Rafik, H. Gualous, R. Gallay, A. Crausaz and A. Berthon, "Super-Capacitors Characterization for Hybrid Vehicle Applications", IEEE, 2006.

[5]   T. Gilver and P. Lilienthal, "Using HOMER Software – Micropower Optimiztion Model, to Explore the Role of Gen-Sets in Small Solar Power Systems – Case Study: Sri Lanka", Technical Report, NREL/TP-710-36774, National Renewable Energy Laboratory (NREL), May 2005.

[6]   National Renewable Energy Laboratory (NREL), "Vehicle Systems Analysis", Online Posting: http://www.nrel.gov/vehiclesandfuels/vsa/ (October 15, 2008).

[7]   U.S. Department of Energy, "ADVISOR Simulation Tool for Vehicle Evaluation and Testing", Online Posting: http://www1.eere.energy.gov/vehiclesandfuels/pdfs/success/advisor_simulation_tool.pdf (October 15, 2008).

[8]   K. Wipke, M. Cuddy, D. Bharathan, S. Burch, V. Johnson, A. Markel and S. Sprik, "Advisor 2.0: A Second-Generation Advanced Vehicle Simulator for Systems Analysis", Technical Report, NREL/TP-540-25928, National Renewable Energy Laboratory (NREL), March 1999.

CHAPTER 7. MODEL FOR THE ELECTRICAL POWER CONSUMPTION OF
MOBILE GROUND VEHICLES

7.1 Introduction

This model has been developed to simulate the electrical power consumption of small to mid-sized electric robotic vehicles. To provide simulation ability and flexibility for various scenarios, this model can accommodate user inputs for road gradient, linear and angular velocity. Furthermore, this model assumes skid-steering.

Unmanned Ground and Aerial vehicles have gained a lot of popularity in recent years in applications such as boarder patrol, traffic monitoring, search and rescue, localization, mapping, de-mining etc. The high priced specialized ground vehicles such as the ATRV-Jr [1] and the Aerial Bergen Industrial Twin [2], has forced several research groups including the Unmanned Systems Lab (USL) at the University of South Florida, into exploring other options, such as transforming simple radio controlled (RC) toy trucks and helicopters into cost effective custom made platforms equipped with sensors such as stereo Visio, SICK laser, Inertia Measurement Unit (IMU), Global Positioning System (GPS), that enable them to carry out tasks such as autonomous navigation, collision avoidance mapping, localization and boarder surveillance.

UGV power sources were almost exclusively rechargeable lead-acid and NiCad batteries due to the fact that both technologies are mature and well understood, as well as cheaper compared to more recent technologies such as lithium batteries and fuel cells. Recent concerns about energy and environmental problems and advances in material and manufacturing engineering, have enabled a wider commercial product selection in lithium batteries and fuel cells. For example, Proton Exchange Membrane Fuel Cells (PEMFC) have already been tested and used in Autonomous Underwater Vehicles

(AUVs) [3]-[6] and mobile robots [7], [8]. As stated in [4], Direct Methanol Fuel Cells (DMFC) are a better choice for mobile robots, but wide power range units are commercially unavailable.

Recent small size UGV platforms due to limited payload and space availability are using Lithium Ion (Li-Ion) and Polymer (Li-Po) batteries. However, power requirements are mostly determined by the manufacturer for a specific vehicle configuration, ignoring the impact of possible upgrades, 'off-the-self' add on sensors and other custom made accessories, such as multiple cameras, Inertial Measurement Unit (IMU), GPS, compass, laser rangefinders and sonar sensors in addition to computer controlled processors and cooling fans. Given that a UGV has limited power availability, endurance and range are drastically affected by the on-board sensor suite and other peripherals. This dependence and restriction becomes even worse if and when the UGV needs serve as the 'base station' and take off/landing platform for small/miniature unmanned electrical vertical take off and landing (VTOL) vehicles that require recharging upon landing on the UGV to continue their mission [9].

It is true that for most UGV outdoors applications, payload needs, sensor suite utilization and energy requirements are apriori unpredictable. This makes proper sizing of energy storage devices a rather difficult task. Therefore, the thesis statement of this work assumes that the success of mobile robot improved endurance and range especially for outdoor applications depends on the accurate prediction of power and energy requirements for a wide of range of applications so that energy and power sources are properly sized. Therefore, in this chapter a Matlab based simulation model is presented that can estimate UGV power requirements for various user defined applications so that proper battery sizing is achieved. This model has been developed to simulate the electrical power consumption of small to mid-sized electric robotic vehicles. To provide simulation ability and flexibility for various scenarios, this model can accommodate user inputs for road gradient, linear and angular velocity. Furthermore, this model assumes skid-steering.

7.2 Vehicle Kinematics

Vehicle kinematics is the study of motion without the consideration of the masses or forces that bring out the motion. In the literature vehicle kinematics are separated into performance and handling characteristics [10], [11]. Performance characteristics involve the vehicle behavior (position, velocity, acceleration) in a straight line, whereas handling characteristics refer to the vehicle's response to steering. In this work, performance and handling characteristics are presented as longitudinal and angular models respectively. The following assumptions can be made based on the characteristics of small sized robotic vehicles.

- Vehicle longitudinal velocity is low and as a result aerodynamic drag is negligible.

- Vehicle lateral velocity is zero.

- No lateral load transfer occurs.

- No longitudinal load transfer occurs due to acceleration and deceleration.

- Rolling resistance is constant with respect to speed.

- Wheel/Ground contact area is rectangular and same for all wheels

- Slip angle is negligible. The mean slip angle for an experiment with a Pioneer AT on wet sand was 4.34 degrees. The wheel slip was 0.233 and 0.180 for the outer and inner wheels respectively.

- Centrifugal force is neglected.

- Rigid wheels in rigid mode; wheel sinkage and bulldozing are negligible.

7.2.1 Longitudinal Model

Newton's first law of motion says that the summation of all forces acting on a body equal to zero at a constant velocity. Hence, for any vehicle moving at a constant speed the sum of tractive forces or efforts has to be equal to all the forces resisting motion; aerodynamic drag, rolling resistance and road gradient. Aerodynamic drag is the friction force between the vehicle body and air, rolling is the friction force between vehicle tire and the road, whereas road gradient is the force necessary to go up a slope.

$$F_{tr} - F_{ad} - F_{rr} - F_\theta = 0 \qquad (7.1)$$

Newton's second law of motion says that for any vehicle moving at constant acceleration then the summation of all forces is not equal to zero but equal to the product of acceleration and weight.

$$m\frac{dv}{dt} = F_{tr} - F_{ad} - F_{rr} - F_\theta \qquad (7.2)$$
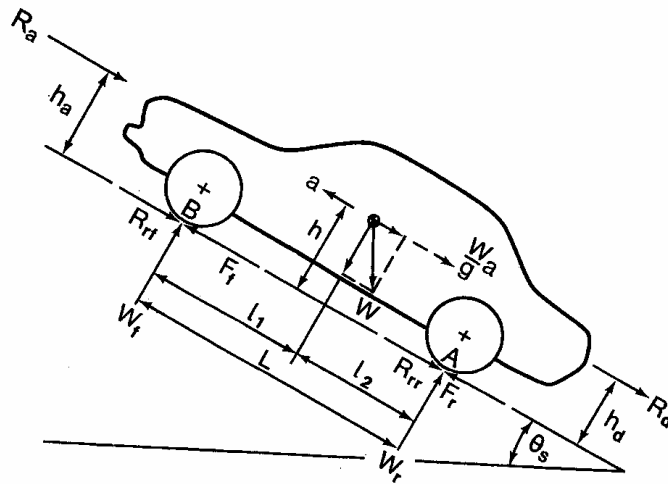
Figure 7-1: Forces Exerted on a Vehicle on a Slope from [10].

98

Hence, from the free body diagram of a 2 axle vehicle the equation can be written as:

$$m\frac{dv}{dt} = 2F_o + 2F_i - \frac{1}{2}\rho A C_D v^2 - \mu_{rr}mg\cos(\theta) - mg\sin(\theta) \tag{7.3}$$

Where ρ is the mass density of air, A is the surface area, C_D is the drag coefficient and v is the linear speed [10]. The aerodynamic drag force of the ATRV-Jr with maximum speed of 1m/s, front surface area of 0.164m^2, air mass density of 1.225Kg/m^3, and drag coefficient of 0.8 (worst case scenario) is only 0.08N which is considerably smaller than the force of rolling resistance of 47.1N, hence can be neglected. The rolling resistance coefficient, μ_{rr}, is empirically derived in [10] as a function of linear speed and type of tire. For the ATRV-Jr, μ_{rr} was experimentally determined to be 0.05.

7.2.2 Angular Model

Several types of steering are presented and analyzed in [10] and [12]. The ATRV-Jr that is the test-bed used in this work employs skid steering. In skid steering turning moment is achieved by means of speed differential between the inner and outer wheels. Similar to section (7.2.1) for any vehicle moving at a constant angular speed the sum of tractive forces is equal to the force of turning resistance.

$$F_{tr} - F_{turn} = 0 \tag{7.4}$$
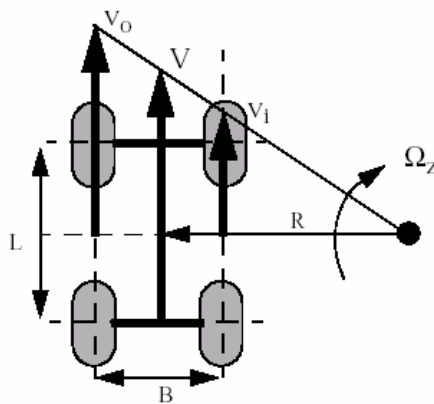
Figure 7-2: Skid Steering Kinematics from [13].

Hence to achieve angular acceleration the equation (7.4) can be re-written as:

$$I_z \frac{d\Omega_z}{dt} = \frac{B}{2}(F_o - F_i) - M_r \qquad (7.5)$$

Where Ω_z is the angular speed of the vehicle, B is the tread or width of the vehicle and I_z is the moment of inertia of the vehicle. Subscript z denotes the vertical axis that passes through the vehicle center of gravity. The center of gravity can be experimentally found with a procedure described in [14]. For the ATRV-Jr, the center of gravity was found at a height (h_{CG}) of 0.16m, at a distance of 0.23m from the front wheels and 0.27m from left side of the vehicle. Worth noting that datasheet lists the ATRV-Jr with weight of 50Kg and payload of 25Kg, whereas the vehicle under investigation had a total weight of 96Kg. Furthermore, in the literature [15] and [16], a total weight of 116Kg and a payload of 141.02Kg are listed respectively.

The vehicle moment of inertia, I_z is given by:

$$I_z = m\left[R'^2 + \left(\frac{l_1 - l_2}{2} \right)^2 \right] \qquad (7.6)$$

Where R' is the turning radius in meters and as shown in [10] can be calculated from similar triangles:

$$R' = \frac{B}{2}\left[\frac{r\omega_o(1-i_o) + r\omega_i(1-i_i)}{r\omega_o(1-i_o) - r\omega_i(1-i_i)} \right] \qquad (7.7)$$

Where i_i and i_o are the inner and outer wheel slippages respectively. Hence wheel speed in revolutions per minute (*rpm*) for the outer and inner wheels can be calculated by:

$$\omega_{o\_rpm} = \frac{2v + B\Omega}{2r(1-i_o)} \qquad (7.8)$$

$$\omega_{i\_rpm} = \frac{2v + B\Omega}{2r(1 - i_i)} \qquad (7.9)$$

In [10] the moment of turning resistance is derived for tracked vehicles whereas in [12] the moment of turning resistance for 4 wheeled vehicles is derived as:

$$M_r = \frac{\mu_t mgL}{2} \qquad (7.10)$$

Where μ_t is lateral turning resistance coefficient and L is the vehicle length in meters. As suggested in [10], [17] and [18], the lateral turning resistance is best represented as a function of linear, angular speeds and turning radius. Hence, for the ATRV-Jr, on firm ground with dry grass, the experimental data for lateral turning resistance was fitted using an inverse full quadratic function [19]:

$$\mu_t(v, \Omega_z) = \frac{1}{a + bv + c\Omega_z + dv^2 + e\Omega_z^2 + fv\Omega_z} \qquad (7.11)$$
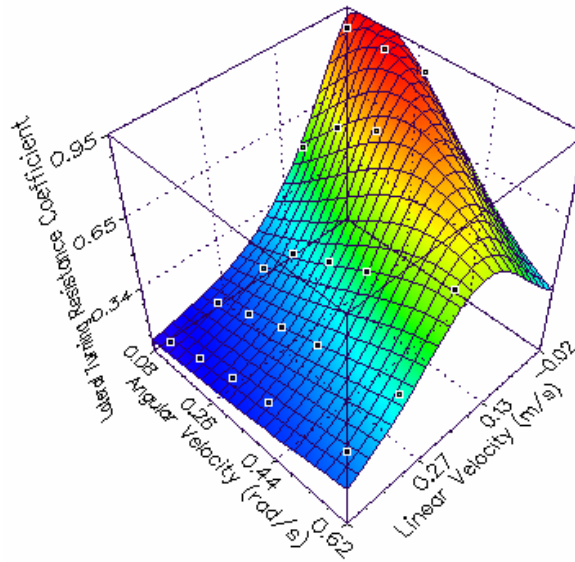
Figure 7-3: 3-D Surface Plot of Lateral Turning Resistance Coefficient as a Function of Linear and Angular Velocities.

As it can be seen from figure 7-3, at zero linear velocity the turning radius is zero and the coefficient of lateral resistance is highest.

At higher speeds and small turning radii the effects of centrifugal force and the load displacement should not be ignored [10]. Wheel slippage and skidding should also be empirically derived especially for point turns for more accurate kinematics model.

7.3 Electrical Power

Electrical power in watts (W) of any moving vehicle is the product of wheel rotating velocity in revolutions per minute (rpm) and torque in Newton-meters (Nm); where torque is the product of wheel radius in meters (m), wheel number and tractive force in Newton (N).

$$P = T(\omega_{rpm}) \tag{7.12}$$

Tractive forces F_o and F_i as well a wheel speeds can be calculated from the linear and angular models. The vehicle power system always delivers higher power because of motor inefficiencies.

$$P_{ps} = \frac{T(\omega_{rpm})}{e_m} \tag{7.13}$$

7.4 Motor Efficiency From Name Plate

Electric motors whether powered by Direct Current (DC) or Alternate Current (AC) sources convert electrical energy to mechanical. This conversion however is never 100% efficient. Motor losses for both AC and DC are mainly due to [20], [21], and [22]:

- Copper losses (I^2R_a) in the armature.

- Copper losses (I^2R_f) in the field windings.

- Brush Contact Losses.

- Friction losses due to brush and bearing and windage.

- Core losses due to hysteresis and Eddy current.

- Stray load loss.

Because motor losses are directly proportional to current and speed, motor efficiency is not constant. Usually, electric motors are designed to run between 50% and 100% of rated load with maximum efficiency being approximately at 75% of rated load [23], [24]. The efficiency of overloaded motors does not change whereas for underloaded motors efficiency severely decreases. Detailed procedures are provided in [21] and [22] that can be used to determine the motor characteristics and losses with precision.

Motor efficiency is rarely listed on the motor nameplate characteristics but it can be calculated from the listed motor characteristics. Usually, motor characteristics listed are, operating voltage (V) in volts, full load current (I_{FL}) in Amperes, torque (T) in Newton-meters (Nm), gear ratio, rotational speed in revolutions per minute (ω_{rpm}) and nominal input power or motor size in horse power (hp). It should be noted that when gear ratio (η) is given then the nameplate torque and RPM characteristics are given for the shaft not the motor.

Motor nominal input power in watts;

$$P_{nom} = P_{hp} \frac{746 watts}{1 hp}$$
(7.14)

Nominal power is not the full load power. Full load power is tehe product of full load current and operating voltage;

$$P_{FL} = V I_{FL}$$
(7.15)

At the shaft, revolutions per minute are converted to radians per second;

$$\omega_{rad/sec} = \omega_{rpm} \frac{1(\min)}{60(\sec)} \frac{2\pi(rads)}{1(rev)} = 0.105\omega_{rpm} \qquad (7.16)$$

At the motor side;

$$\omega_m = \eta\omega_{shaft} \qquad (7.17)$$

$$T_m = \frac{T_{shaft}}{\eta} \qquad (7.18)$$

Hence, full load efficiency can be found;

$$e_{FL} = \frac{T_m\omega_m}{P_{FL}}100\% \qquad (7.19)$$

7.4.1 ATRV-Jr Efficiency

The ATRV-Jr name plate characteristics are as follows; RPM = 168, Gear Ratio = 11:1,

Torque =9.82 Nm, Input = ¼ hp, I_{FL} = 10.78A, V = 24V.

Using equation (7.16), the shaft speed of 168 revolutions per seconds is converted to 17.59 radians per second. Hence, the shaft power is calculated by equation (7.12) to 172.73W. Worth noting that from equations (7.17) and (7.18) the motor torque and rpm are calculated to 0.893 Nm and 193.49 rad/sec respectively and the motor and shaft powers are equal.

From equation (7.15) input motor power for full load work is calculated at 258.72W. Hence, the ATRV-Jr motor efficiency using equation (7.19) is calculated to 66.77%.

7.5 List of References

[1] Sean Marshall Baity, "Development of a Next Generation Experimentation Robotic Vehicle (NERV) That Supports Intelligent and Autonomous Systems Research", Master of Science Thesis in Mechanical Engineering, Virginia Polytechnic Institute and State University, December 9, 2005.

[2] Unmanned Systems Lab (USL) Presentations December 4, 2006, "K. Valavanis, M. Labrador, W. Moreno, P. S. Lin, A. Weitzenfeld, N. Tsourveloudis, - Project Review UAV-UGV (ARO) Vision Based Traffic Monitoring (Hills. County)", Online Posting: http://www.cse.usf.edu/USL/uslpresentations.htm (September 21, 2008).

[3] I. Yamamoto, T. Aoki, S. Tsukioka, H. Yoshida, T. Hyakudome, T. Sawa, S. Ishibashi, T. Inada, "Fuel Cell of AUV Urashima", Japan Agency for Marine-Earth Science and Technology, Mitsubishi Heavy Industries, LTD, IEEE, 2004.

[4] G. Pappas, R. Rosenfeld, A. Beam, "The ARPA/Navy Unmanned Undersea Vehicle Program", Unmanned Systems, Spring 1993, pp. 41-44.

[5] K. E. Swider-Lyons, R. T. Carlin, R. L. Rosenfeld, R. J. Nowak, "Technical Issues and Opportunities for Fuel Cell Development for Autonomous Underwater Vehicles", IEEE, 2002.

[6] R. L. Rosenfeld, P. R. Prokopius, A. P. Meyer, "Fuel Cell Power System Development for Submersibles", IEEE Proceedings, Autonomous Underwater Vehicles Technology, IEEE AUV '92, 1992, pp. 184-188.

[7] Sandia National Laboratories, "Robotics Online - Fuel Cell Powered Mobile Robots Case Study", Online Posting: http://www.roboticsonline.com/public/articles/index.cfm?cat=99 (January 25, 2006).

[8] A. Wilhelm, J. Pharoah, B. Surgenor, "Fuel Cells and Mobile Robots, Fuel Cell Today, Online Posting: http://www.fuelcelltoday.com/FuelCellToday/Industry Information/IndustryInformationExternal/IndustryInformationDisplayArticle/0,15 88,933,00.html (January 25, 2006).

[9] K. Dalagkidis, S. Ioannou, K. Valavanis, E. Stefanakos, "A Mobile Landing Platform for Miniature Vertical Take-Off and Landing Vehicles", accepted 14th Mediterranean Conference on Control and Automation, sponsored by IEEE Control System Society, Ancona, Italy, presented on June 28-30, 2006.

[10] J. Y. Wong, "Theory of Ground Vehicles", John Wiley & Sons, Inc., 3rd edition, 2001.

[11]   J. Larminie, J. Lowry, "Eleric Vehicle Technology Explained", John Wiley & Sons, Ltd., 2003.

[12]   D. S. Apostolopoulos, "Analytical Configuration of Wheeled Robotic Locomotion", Dissertation, Robotics Institute, Carnegie Mellon University, Pittsburgh, Pennsylvania, April 2001.

[13]   Benjamin Shamah, "Experimental Comparison of Skid Steering Vs Explicit Steering for a Wheeled Mobile Robot", Master Thesis, The Robotics Institute, Carnegie Mellon University, Pittsburgh, Pennsylvania 15213, March 1999.

[14]   G. G. Lucas, "Road Vehicle Performance – Methods of Measurement and Calculation), Gordon and Breach, Science Publishers, Inc., 1986.

[15]   Shailesh Lakkad, "Modeling and Simulation of Steering Systems for Autonomous Vehicles", Master Thesis, Department of Mechanical Engineering, College of Engineering, Florida State University, 2004.

[16]   Sean Marshall Baity, "Development of a Next Generation Experimentation Robotic Vehicle (NERV) that Supports Intelligent and Autonomous Systems Research", Master Thesis, Department of Mechanical Engineering, Virginia Polytechnic Institute and State University, December 9, 2005.

[17]   Said Al-Milli, Kaspar Althoefer, Lakmal D. Seneviratne, "Dynamic Analysis and Traversability Prediction of Tracked vehicles on Soft Ground", Proceedings of the 2007 IEEE International Conference on Networking, Sensing and Control, London, UK, 15-17, April 2007.

[18]   T. H. Tran, N. M. Kwok, S. Scheding, and Q. P. Ha, "Dynamic Modeling of Wheel-Terrain Interaction of a UGV", Proceedings of the 3rd Annual IEEE Conference on Automation Science and Engineering, Scottsdale, AZ, USA, September 22-25, 2007.

[19]   ZunZun, "Online Curve Fitting and Surface Fitting Web Site", Online Posting: http://zunzun.com/ (September 22, 2008).

[20]   William H. Yeadon, Allan W. Yeadon, "Handbook of Small Electric Motors", McGraw Hill, 2001.

[21]   H. Wayne Beaty, James L. Kirtley, Jr., "Electric Motor Handbook", McGraw Hill, 1998.

[22]   Ronald Bullock, "Product Focus: Motors - Applying PMDC Motors", Bison Gear and Engineering Corp., Online Posting: http://fab.cba.mit.edu/classes/MIT/961.04/topics/permanentmagnetDC.pdf (September 26, 2008).

[23]   Motor Challenge Fact Sheet, "Determining Electric Motor Load and Efficiency", a Program of the U.S. Department of Energy, Online Posting: http://www.p2pays.org/ref/40/39569.pdf (September 26, 2008).

[24]   MicroMo Electronics – Faulhaber Group, "Technical Library – DC Motor Tutorials – Motor Calculations", Online Posting: http://www.micromo.com/n390432/n.html (September 26, 2008).

CHAPTER 8. EXPERIMENTAL SET UP

8.1 Introduction

Preliminary work on the reasons of reduced endurance of the ATRV-Jr presented on Chapter 5 and [1] showed load current as high as 28A and operating voltage of 24V. The data acquisition system (DAQ), USB-6008, by national instruments was chosen for the application. With 12-bit input resolution indicates input voltages as low as 2.44mV $(10V/10^{12} bits)$ whereas for both differential and single ended measurements with absolute accuracy of 14.7mV for input voltage of 10V [2]. Absolute accuracy is defined by National Instruments as the overall uncertainty of the measurement [3]. Another advantage of the DAQ was that it was USB powered.

The major limitation of the DAQ was that the maximum input voltage of 10V whereas the voltage of interest is 24V. To overcome this limitation, differential operational amplifiers were designed for measuring voltages and currents.

8.2 Differential Amplifier Design and Operational Amplifier Selection
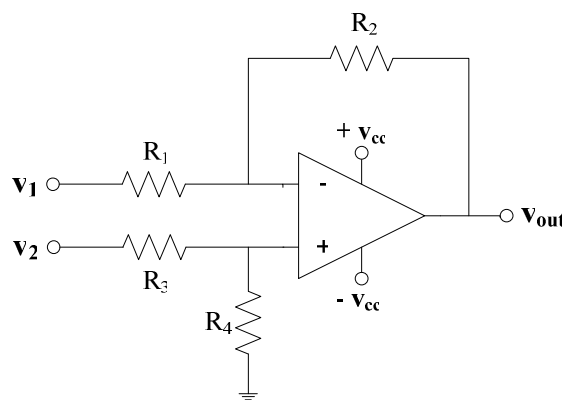
Figure 8-1: Differential Amplifier Design.

Building a differential amplifier is not a new research topic [4]. For the following design the output voltage can be found easily using superposition circuit analysis technique; Grounding v_2 leads to an inverting amplifier whereas grounding v_1 leads to a non-inverting amplifier. The total output voltage is given by:

$$V_{out} = v_1\left(\frac{-R_2}{R_1}\right) + v_2\left(1 + \frac{R_2}{R_1}\right)\left(\frac{R_4}{R_3 + R_4}\right) \tag{8.1}$$

Since it is desired that the output is the difference of v_2 and v_1, the two gains have to be the same as shown in (2):

$$\left(\frac{R_2}{R_1}\right) = \left(1 + \frac{R_2}{R_1}\right)\left(\frac{R_4}{R_3 + R_4}\right) \tag{8.2}$$

Solving for equation (8.2) leads to equation (8.3) where it can be concluded that, the two grains can be equal when:

$$\left(\frac{R_2}{R_1}\right) = \left(\frac{R_4}{R_3}\right) \tag{8.3}$$

Using the relationship of equation (8.3), then the output voltage simplifies to:

$$V_{out} = \left(\frac{R_2}{R_1}\right)(v_2 - v_1) \tag{8.4}$$

For the required application, operating voltage is 24V and maximum allowable input for the DAQ is 10V. Therefore, a gain of 1/3 is required. Resistances chosen $R_2=R_4=37.4K\Omega$ and $R_1=R_3=110K\Omega$ thus giving a theoretical gain of 0.34. With 1% component tolerance means that the theoretical design gain could vary between 0.3333 and 0.3469.

Batteries have small internal resistance in the milli-ohm range. By selecting resistors (R_1-R_4) in the range of kilo, gives a ratio in the mega range. Therefore, for the desired

application there is no need to use any "buffer" Op-Amps to provide high input impedance to minimize op-amp loading.

Another design constraint was the power supply. The ATRV-Jr is powered by two 12v batteries and no negative voltages. Therefore, for easier power for the differential amplifier design, the single supply, LM324 Op-Amp, was chosen [5]. Single supply op-amp designs eliminate the need of negative supply voltage and can be powered directly from the ATRV batteries. This further, eliminates the need of a new power supply and also the possibility of error due to ground loop currents. Without a negative supply voltage the output voltage will never be negative. When v_1 is greater than v_2, then the output voltage will go to the negative rail of the op-amp which in this case will be close to zero volts.

8.3 Measuring Current

Measuring current in not a new research area either; in fact there is a huge literature and many designs available. No matter how complicated and sophisticated the design is, the concept is simple and best described by Ohm's law where electrical current equals to the ratio between the voltage drop across a resistor and the resistance. In other words, use a sensing resistor of known value and then measure the voltage across it; the ratio equals to the current. However, there are a couple of design considerations. The current sensing resistor must be in series with the load. This means that the voltage drop across this sensing resistor must be small enough not to affect the load voltage and big enough to be recorded. So, a rule of thumb was used where the sensing voltage is 0.5% of the supply voltage. This means that the sensing voltage should be approximately 120mV. At a load current of 30A this means that the sensing resistance must be 4mΩ.

Furthermore, with a DAQ system with 2.44mV resolution, this means that at load currents of less than 1A there could be an error of 60% or higher. An amplifier with a gain between 50 and 100 could minimize the error to less than 1% since the specified DAQ has an absolute accuracy of 14.7mv at a 10V scale.
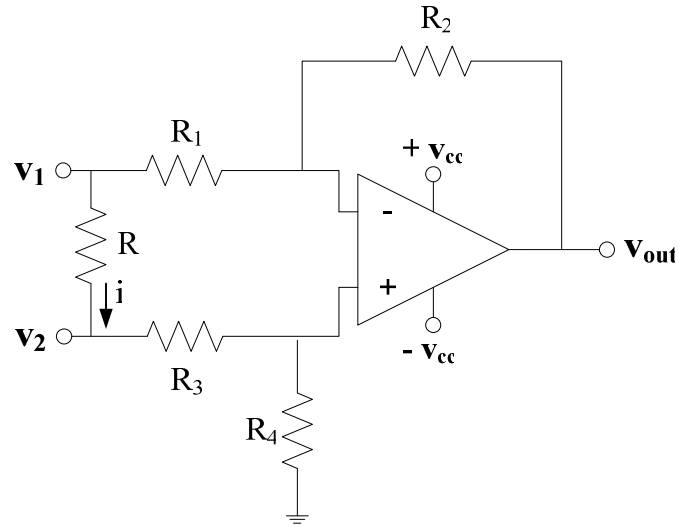
Figure 8-2: Differential Amplifier Design for Current Measurement.

The same differential amplifier described in section (8.2) was chosen for this application. Based on available 1% resistors, R_2 and R_4 were chosen to be 88.7KΩ whereas R_1 and R_3 to be 1KΩ thus giving a theoretical gain of 88.7. Furthermore, including the 1% component tolerance this means that the theoretical design gain could vary between 86.94 and 90.492. The sensing resistor was chosen to be 5mΩ with 4.5W rated power. This means that it can handle 30A current at which case the sensing voltage is 0.625% of the supply voltage.

Since a single supply amplifier is used for this application, providing only positive voltages, care should be taken on the design connections. For positive output voltages, since $V_{out}=Gain(v_2-v_1)$, the current direction should be flowing from v_2 to v_1, thus making v_2 the high potential so that $V_{sense}= v_2 - v_1$ is greater than zero and V_{out} is positive.

The experimental design is connected to the load as shown in figure 8-3.

$$v = Gain(v_2 - v_1)$$

$$I = \frac{(v_2 - v_1)}{(Gain * R_{sense})}$$
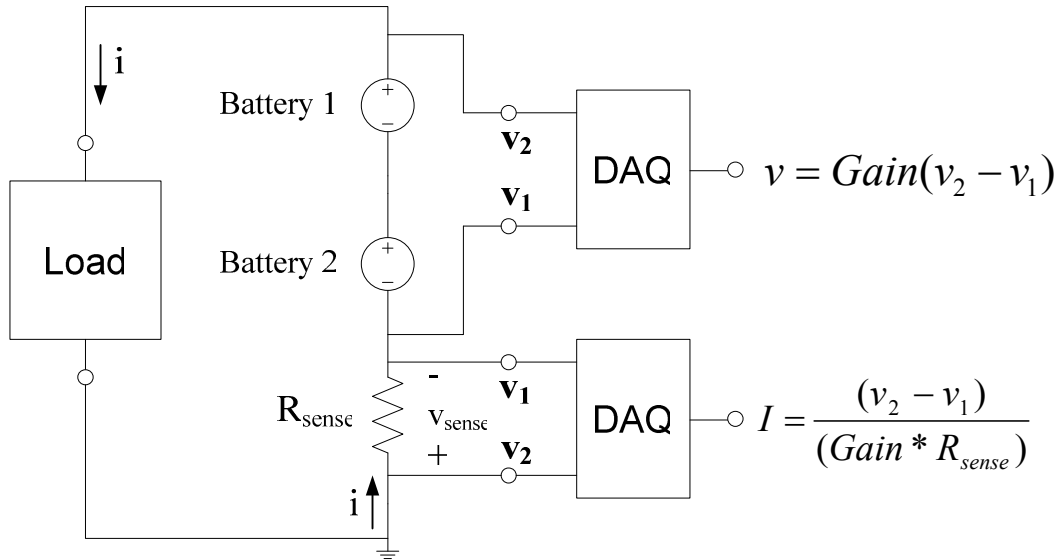
Figure 8-3: Complete Experimental Set Up.

8.4 Measuring Temperature

For recording the temperature, the LM335 precision temperature sensor was used in a temperature range between -40°C and +100°C. After calibration, an accuracy of ±1°C can be achieved.
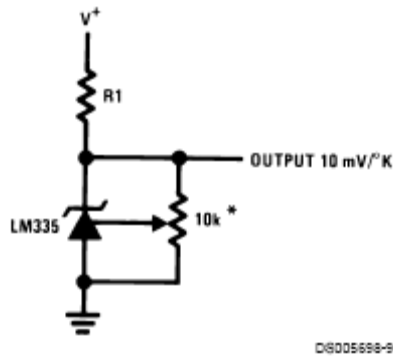
Figure 8-4: Calibrated Temperature Sensor from [6].

8.5 Voltage Regulation

The single supply operational amplifier (LM324) chosen for voltage and current monitoring has a power supply voltage range between 3 to 32V. However, the ATRV-Jr lead acid batteries could not power the LM324 directly as the terminal voltage varies, when fully charged and discharged, from 25.7V to 21V, respectively, which could potentially affect the operational amplifier output [8]. Therefore, a steady dc power supply was used with the LM7815 constant voltage regulator as proposed in the datasheet and application notes.
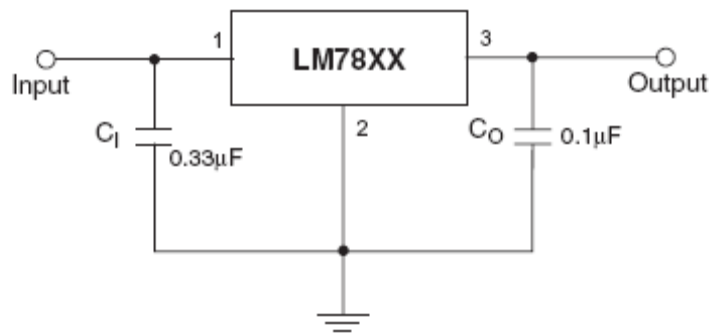
Figure 8-5: Typical Applications and DC Parameters from [7].

8.6 Experimental Set-Up Testing

The LM7815 voltage regulator was tested for a range of input voltages. From 20 to 26V input, the regulated output voltage was kept constant at 14.76V, whereas at 15.25V it dropped to 14V. As mentioned in section (8.5) the ATRV-Jr test-bed uses two series connected 12V lead acid batteries (6 cells each) which when fully charged or discharged the terminal voltage reaches 26.68V and 21V respectively. Deep cycle batteries can discharge to voltages less than 1.75 volts per cell making it possible for terminal voltages as low as 15V. However, this pack with a maximum discharge current of 600A is 20 times greater in magnitude than the estimated test-bed load currents making that possibility unlikely [8].

Following the manufacturer recommendations for accuracy in the range of ±1°C, the temperature sensor was calibrated at 25°C by varying the 10KΩ until the output voltage reached 2.982V [6].

The voltage and current differential amplifier gains were found to be 0.33875V/V and 87.5V/V respectively.

8.7 List of References

[1]   S. Ioannou, K. Dalamagkidis, K. P. Valavanis, E. K. Stefanakos and P. H. Wiley, "On Improving Endurace on Unmanned Ground Vehicles: The ATRV-Jr Case Study", 14th Mediterranean Conference on Control and Automation, sponsored by IEEE Control System Society, Ancona, Italy, presented on June 28-30, 2006.

[2]   National Instruments, "Product and Services - NI USB-6008 12-bit, 10KS/s, Low Cost Multifunction DAQ - Datasheet", Online Posting: http://sine.ni.com/nips/cds/view/p/lang/en/nid/14604 (September 7, 2008).

[3]   National Instruments, "Support – Specifications and Accuracy", Online Posting: http://www.ni.com/support/calibrat/accuracy.htm (September 7, 2008).

[4]   Sedra and Smith, "Microelectronic Circuits", 4th edition, Oxford University Press, 1998, pp. 86-92.

[5]   National Semiconductor, "Low Power Quad Operational Amplifier – LM324 Datasheet", Online Posting: http://cache.national.com/ds/LM/LM124.pdf (September 7, 2008).

[6]   National Semiconductor, "Precision Temperature Sensor – LM335 Datasheet", Online Posting: http://cache.national.com/ds/LM/LM335.pdf (September 7, 2008).

[7]   Fairchild Semiconductor, "Positive Voltage Regulator – LM7815 Datasheet", Online Posting: http://www.fairchildsemi.com/ds/LM%2FLM7805.pdf (September 7, 2008).

[8]   C&D Technologies Inc., "Standby Power – Deep Cycle Series – DCS-33", Online Posting: http://www.cdstandbypower.com/product/battery/vrla/dcs33h.html (September 7, 2008).

CHAPTER 9. POWER CONSUMPTION SIMULATION AND EXPERIMENTAL RESULTS

9.1 Introduction

It is true that for most UGV outdoor applications, payload needs, sensor suite utilization and energy requirements are apriori unpredictable. This makes proper sizing of energy storage devices a rather difficult task. Therefore, this work assumes that the success of mobile robot improved endurance and range especially for outdoor applications depends on the accurate prediction of power and energy requirements for specific applications so that the energy and power sources are properly sized. Hence, this work presents a Matlab based simulation model that can estimate UGV power requirements for various user defined applications so that proper battery sizing is achieved. This model has been developed to simulate the electrical power consumption of small to mid-sized electric robotic vehicles. To provide simulation ability and flexibility for various scenarios, this model can accommodate user inputs for road gradient, linear and angular velocity. Furthermore, this model assumes skid-steering.

9.2 Longitudinal and Angular Model Validation

Various experiments were performed with the ATRV-Jr used as test-bed for the validation of the kinematic equations presented in section (7.2).

First, as shown in figure 9-1, the ATRV-Jr power consumption was determined when the vehicle is powered, stationary and without any running applications. The background current consumption for the monitor and joystick controllers was found to be 1.24A which translates to an average power of 30.85W. The spike current of 22.32A and 1 milli-second duration is due to switching and power supply capacitor charging.

115
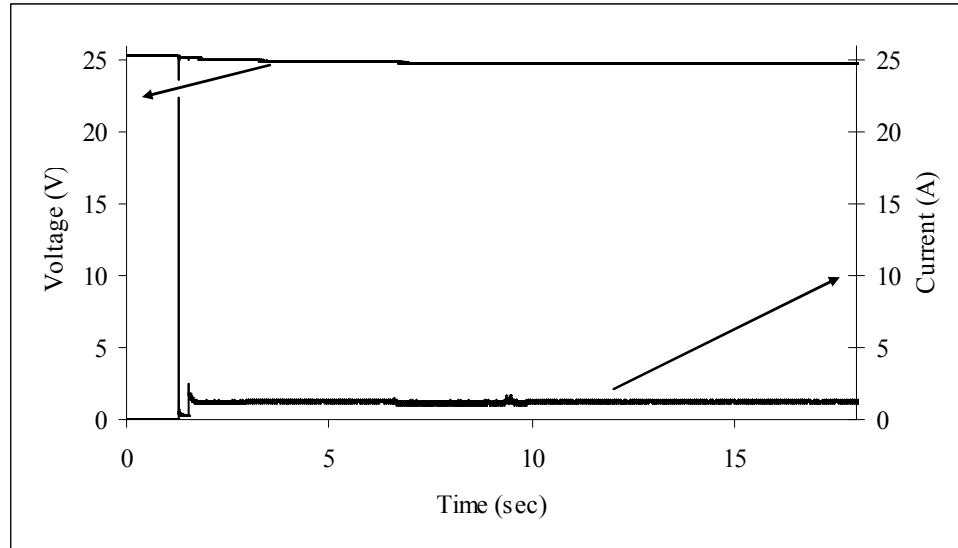
Figure 9-1: ATRV-Jr Background Power Consumption.

A second set of experiments, involved calculating the three pre-set modes of motion. Mode 1, linear and angular velocities of 0.2543m/s (0.92km/hr) and 0.419rad/sec respectively. Mode 2, 0.3984m/s (1.43km/hr) and 0.6283rad/sec. Mode 3, 0.7832m/s (2.83km/hr) and 1.257rad/sec. Only the Mode 3 linear velocity could be compared to the manufacturer's specified maximum linear velocity of 1m/s. The experimental linear velocity is 27.7% less than the maximum specified speed which is a result of customizations that significantly increased the vehicle's weight.

A third set of experiments, determined that the increased vehicle weight and new center of gravity, had no significant effect on turning the vehicle clockwise and counter-clockwise; the results of all the three modes of operations are shown in figures 9-2 to 9-4. From the same figures it can also be seen that turning the vehicle consumes the most power. Furthermore, it was found that the required power to achieve acceleration for modes 1 and 2 was not providing the maximum power required for turning the vehicle. For mode 3 on the other hand, achieving acceleration from 0 to 0.7832m/s requires 298W for 0.317 seconds whereas from 0 to 1.257rad/sec requires 423W for 0.317 seconds.
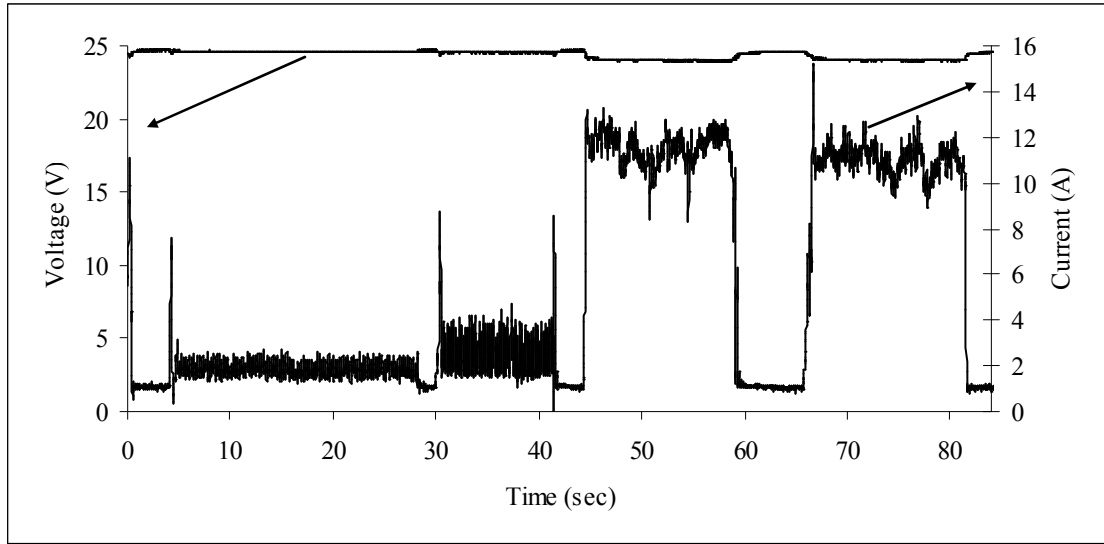
Figure 9-2: ATRV-Jr Power Consumption for Mode 1; Forward, Reverse, Clockwise and Counter Clockwise Motion.
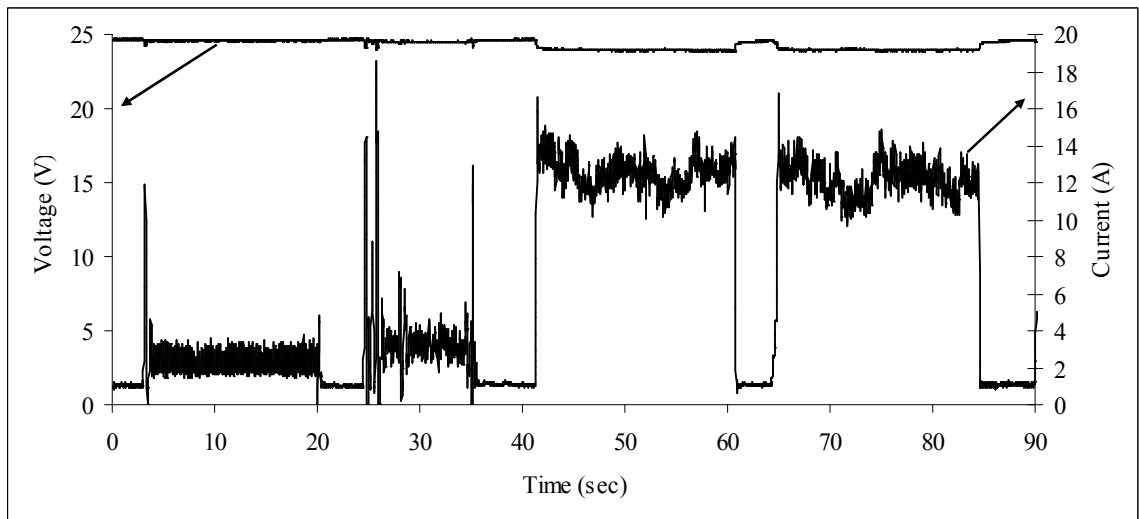
Figure 9-3: ATRV-Jr Power Consumption for Mode 2; Forward, Reverse, Clockwise and Counter Clockwise Motion.

117
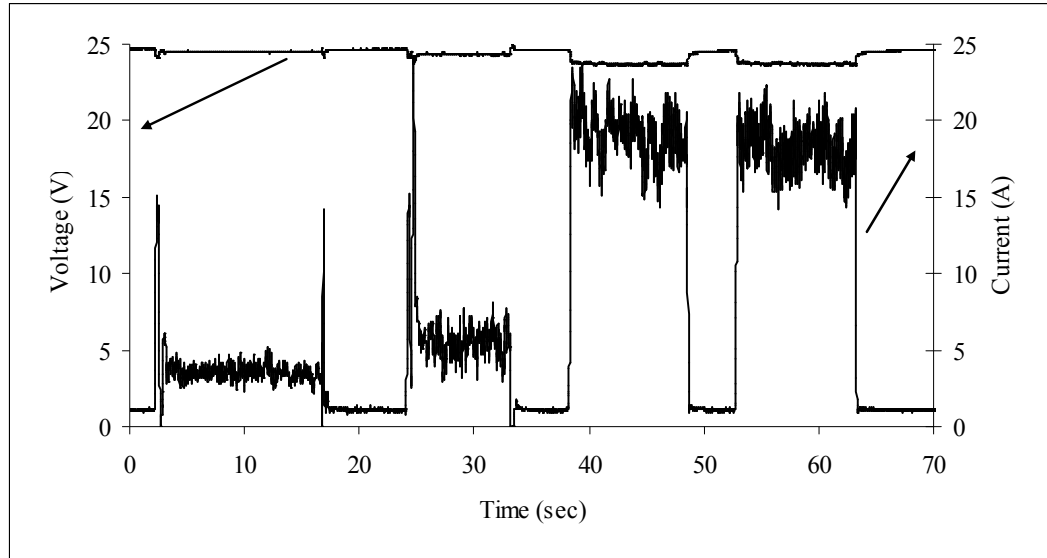
Figure 9-4: ATRV-Jr Power Consumption for Mode 3; Forward, Reverse, Clockwise and Counter Clockwise Motion.

9.2.1 Longitudinal Model Validation

Experimental and simulation results of the power consumption of a vehicle traveling on a straight line (zero angular velocity) are represented in figure 9-5. As can be seen, there is a ± 4.5% difference between simulation and experimental results when traveling on concrete and on a hard surface. This is due the fact that the rolling resistance coefficient as suggested in section 7.2.1 is a function of vehicle speed, tire type and road material, whereas a constant value of 0.05 was used in the simulation. However, depending on the application required accuracy, the experimental results suggest that for linear velocities lower than 1m/s the rolling resistance coefficient can be considered constant. At constant velocity and vehicle weight, from equation 7.3, it can be deduced that the power consumption is directly proportional to the rolling resistance coefficient, μ_{rr}; hence, from figure 9-5 a μ_{rr} increase of 20% results in a 20% increased power consumption. Experimental results validate the accuracy of the longitudinal model.
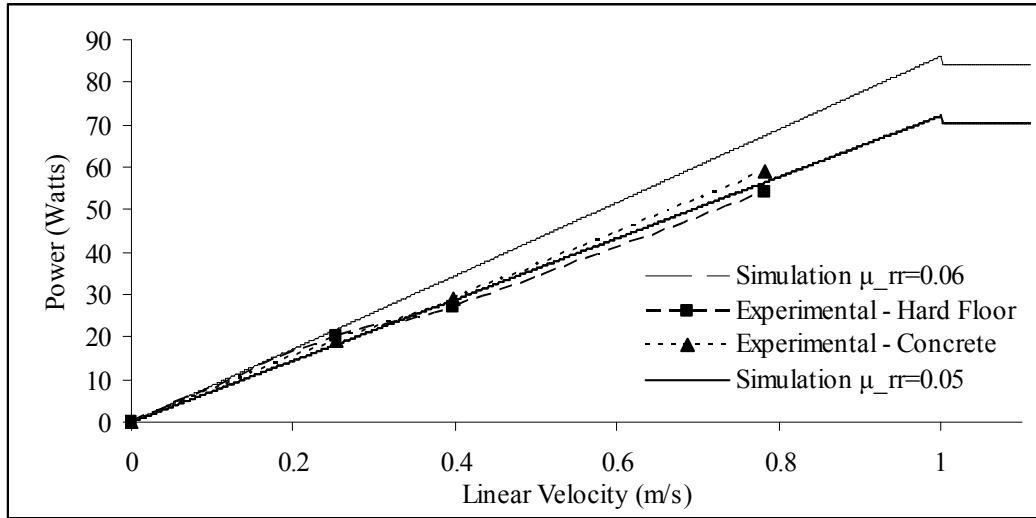
Figure 9-5: Linear Velocity Versus Power Consumption; Simulation and Experimental

Comparison Results.

9.2.2 Angular Model Validation

Experimental and simulation results of the power consumption versus linear and angular velocities are represented and compared in figures 9-6 to 9-8.
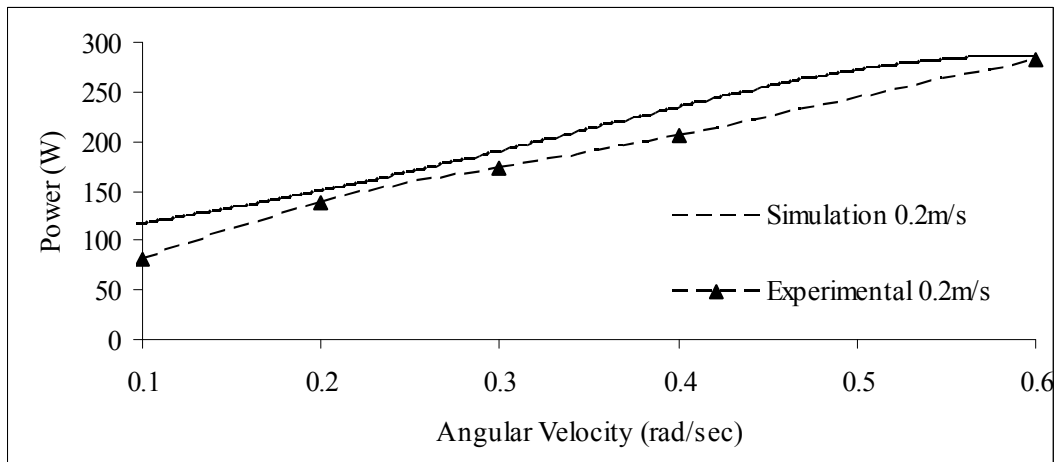
Figure 9-6: Angular Velocity Versus Power Consumption at Constant Linear Velocity of

0.2m/s; Simulation and Experimental Comparison Results.

119

As can be seen in figure 9-6 at constant linear velocity of 0.2m/s and varying angular velocity, the model gives a conservative average power consumption by an average of 7.65% compared to experimental values whereas from figure 9-7 and a constant linear velocity of 0.3m/s the model accuracy is about ±6%.
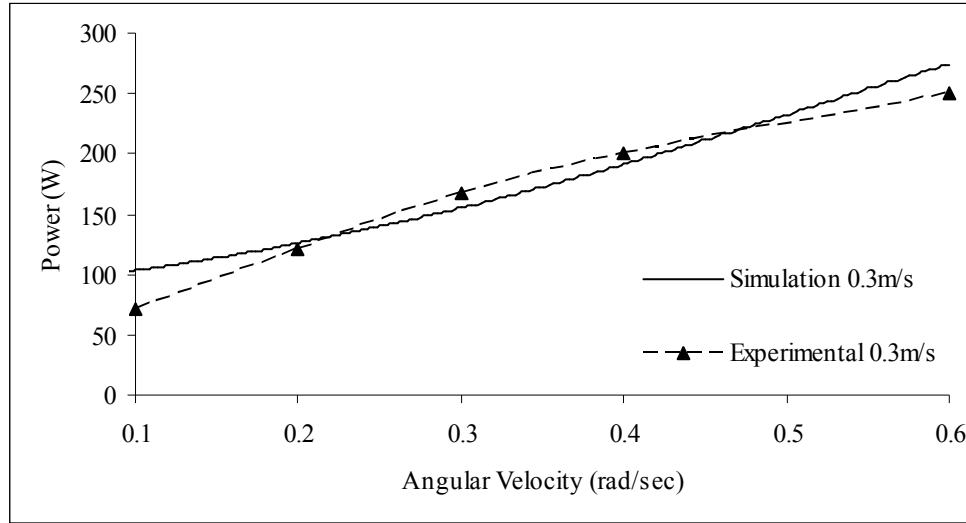
Figure 9-7: Angular Velocity Versus Power Consumption at Constant Linear Velocity of 0.3m/s; Simulation and Experimental Comparison Results.

Furthermore, from figure 9-8 at constant linear velocity of 0.4m/s and varying angular velocity, the simulated power consumption is lower compared to experimental values by an average of 20%. This is because lateral skidding and sliding were ignored. In addition, it is worth noting that from all three figures the model gives very conservative power consumption at an angular velocity of 0.1rad/sec; the simulated power consumption is at all instances 40% higher than the experimental results. This is due to the time step parameter used in the simulation.

Based on the results presented and compared in figures 9-6 to 9-8, it can be concluded that the angular model that simulates vehicle turning kinematics into electrical power is very accurate. With pre-set modes of operation, the ATRV-Jr can complete a turn in 5 to

15 seconds respectively which classifies the turning power consumption as instantaneous or burst power with burst duration of 15 seconds. Burst power does not affect the total mission energy requirement but provides an indication of the burst power and burst duration that the power system should be able to deliver.
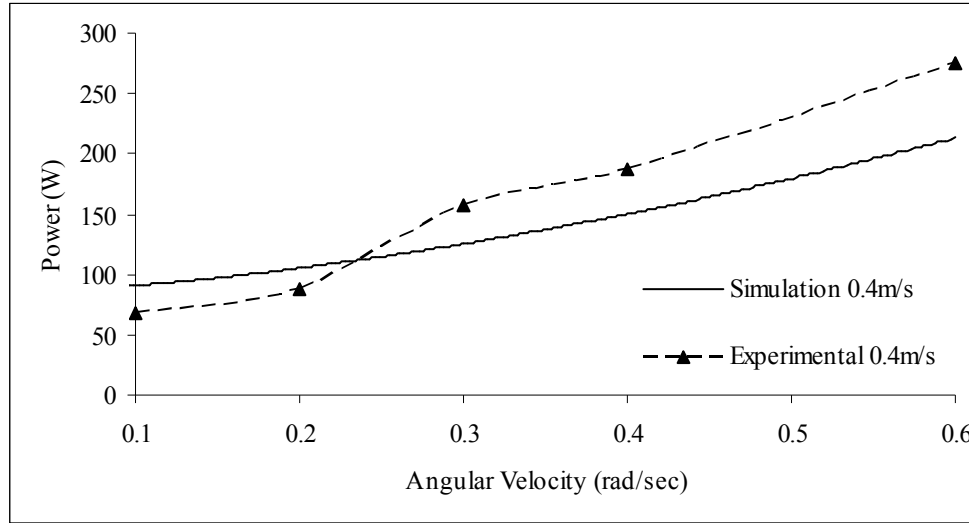
Figure 9-8: Angular Velocity Versus Power Consumption at Constant Linear Velocity of 0.4m/s; Simulation and Experimental Comparison Results.

9.3 Additional Payload Effects on Power Consumption

The longitudinal and angular models are verified in sections 9.2.1 and 9.2.2. In this section the effects of additional payload weight on electrical power consumption are analyzed. In the example under investigation the additional payload weight comes from the landing platform and the UAV. In section 5.11 the landing platform was simulated with total weight of 15.2Kg which included the weights of both the photovoltaic system and the rotating mechanisms, whereas the Maxi Joker 2 weighs 8Kg and has a 2Kg payload capability. Therefore, a worst case scenario of a 25.2Kg additional weight is assumed which is equivalent to 26.25% increase in total vehicle weight.

From the longitudinal model analyzed in section 7.2.1, at constant velocity and rolling resistance coefficient, μ_{rr}, it can be deduced that the power consumption is directly proportional to the vehicle weight. Hence, as expected from figure 9-9 a 26.25% increase in vehicle weight results in the same power consumption increase.
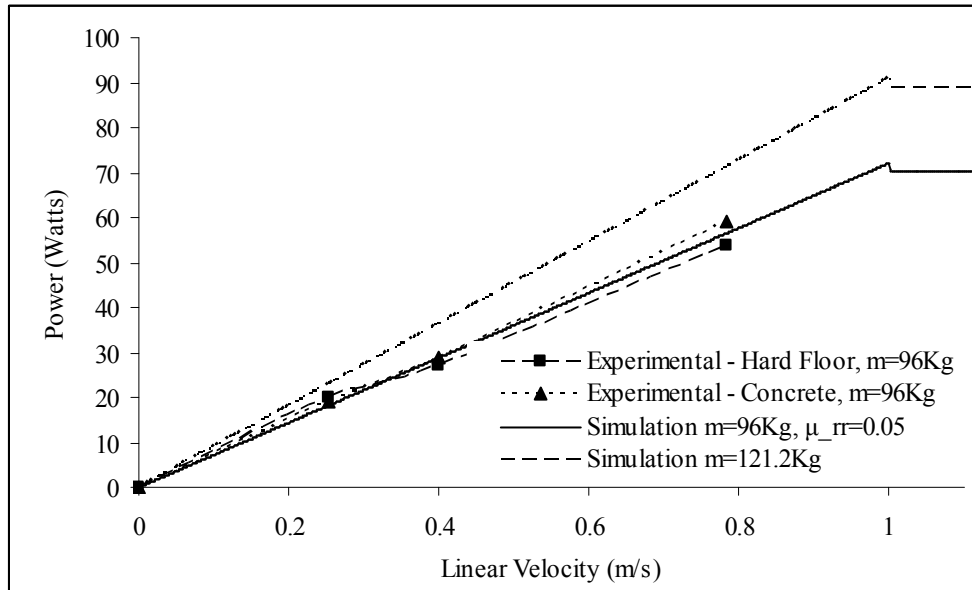
Figure 9-9: Effects of Landing Platform Additional Weight on Longitudinal Model Power Consumption.

On the other hand, the added weight affects the vehicle turning power consumption differently than the longitudinal power consumption. As the angular model equations (7.5) and (7.6) suggest, the moment of inertia is directly proportional to the squared of the turning radius. Hence, the amount of power required to achieve angular acceleration is directly proportional to the vehicle turning radius. These effects are clearly illustrated in figures 9-10 to 9-12.

The vehicle turning radius is the ratio of the linear and angular velocities. Therefore, from figures 9-10 to 9-12 the highest turning radius is at angular velocities of 0.1 rad/sec whereas the lowest turning radius is at angular velocities of 0.6 rad/sec. From these

figures it can be seen that at a turning radius of 2 meters the added weight does not affect the power consumption whereas at turning radii of 3 and 4 meters, power consumption increases by 15.90% and 41.44% respectively.
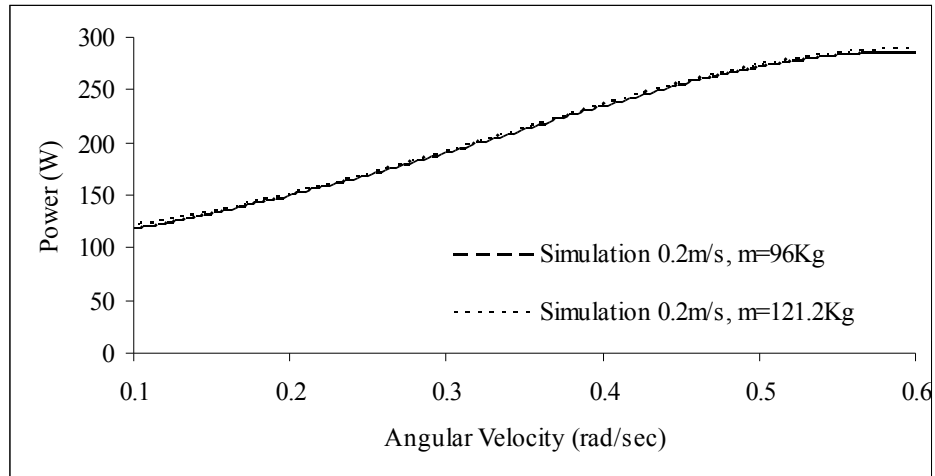
Figure 9-10: Effects of Landing Platform's Additional Weight on Angular Model Power Consumption; v=0.2m/s.
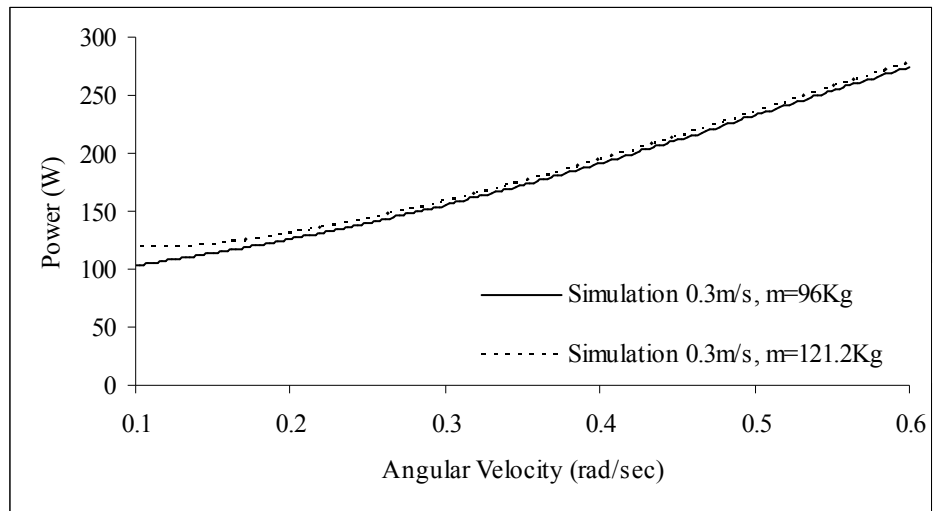
Figure 9-11: Effects of Landing Platform's Additional Weight on Angular Model Power Consumption; v=0.3m/s.
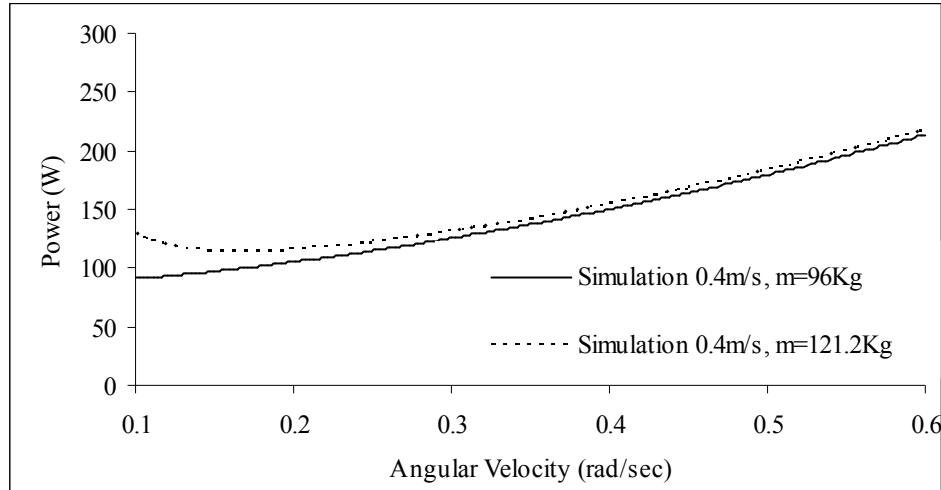
Figure 9-12: Effects of Landing Platform's Additional Weight on Angular Model Power Consumption; v=0.4m/s.

9.4 Sensor Package Profile

The quest for enhanced autonomy of unmanned vehicles UGV and UAV require sensor packages which include multiple cameras, IMU, GPS, compass, laser range finders and sonar sensors in addition to computer controlled servos, navigation systems and cooling fans. In this section the current ATRV-Jr sensors are characterized and power consumption is compared to manufacturer data presented on table 5-1. Characterization aims at sensor utilization which depends on the application algorithm such as autonomous navigation and localization.

From figure 9-13 the computer steady state consumption is 4.55A which at 24V operating voltage it translates to 109.05W. It is worth noting that the computer boots up takes 4 minutes and 55 seconds and requires an additional average current consumption of 6.63A or 161.31W whereas before reaching steady state, several boot up processes and peripherals cause repetitive spikes of 12ms duration at 7.76A or 188.1W.
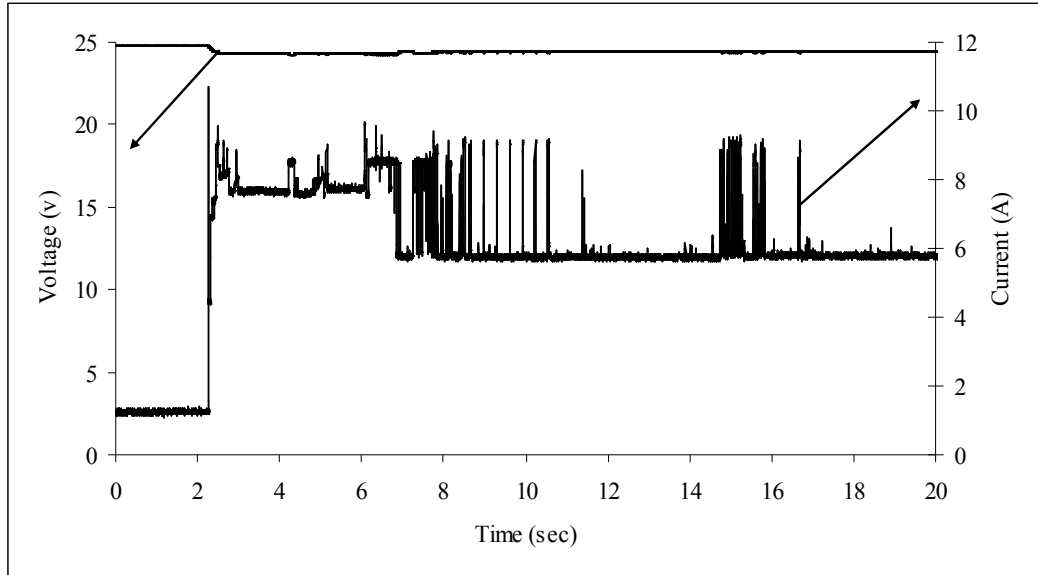
Figure 9-13: Computer Boot Up.
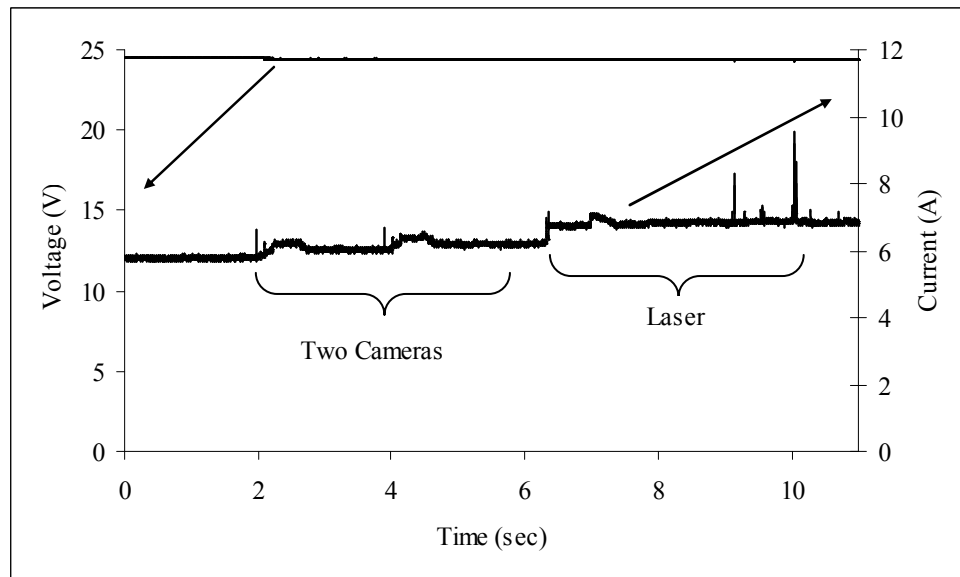
Figure 9-14: Cameras and Laser Power Consumption.

Cameras and laser power consumption are shown in figure 9-14. Each camera once powered on, has an instantaneous current consumption of 0.35A which translates to

8.54W whereas the steady state current consumption drops to 0.24A or 5.85W. Camera instantaneous power consumption has duration less than a second. The Laser has a steady state current consumption of 1.05A which translates to 25.61W, whereas when scanning the burst duration is in the range of 1ms and current consumption of 7A.
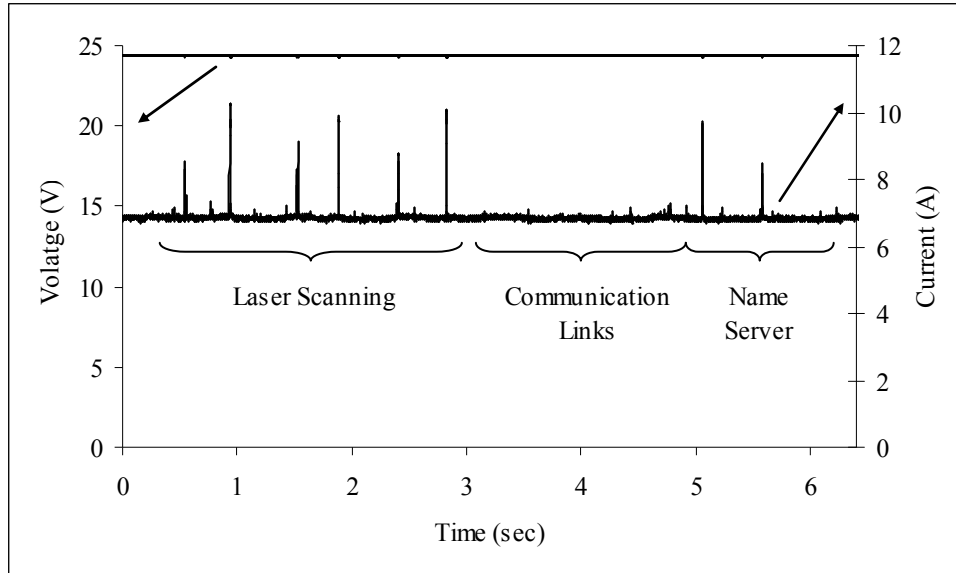
Figure 9-15: Laser Scanning and Communication Power Consumption.

The communication links and the name server presented in figure 9-15 do not consume significant power whereas the GPS and the IMU presented in figure 9-16 do not consume more than 4W.

Capturing images presented in figure 9-17 average a current consumption of 3.43A which translates to 81.63W with 0.1 second duration. The number of images per second required for autonomous navigation depends on the algorithm used.
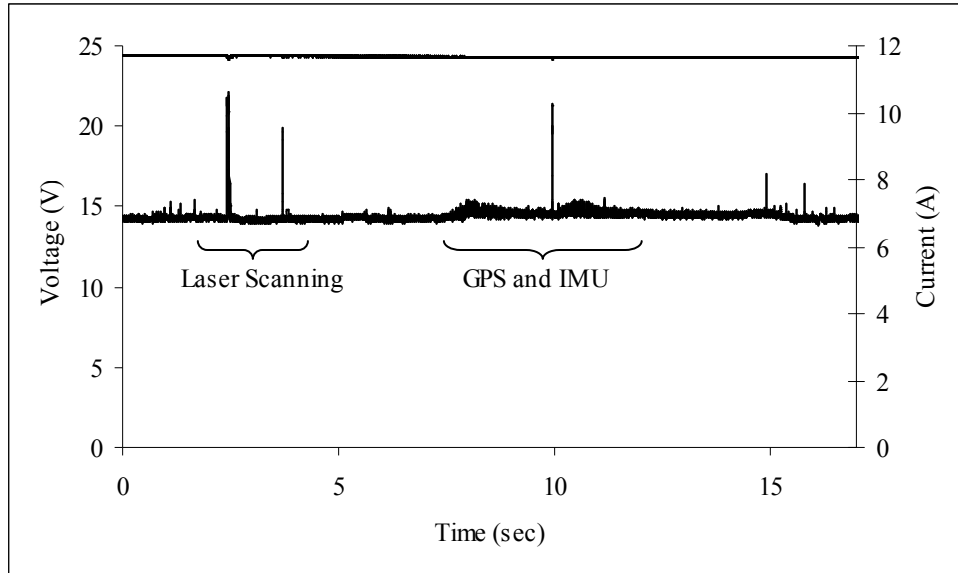
Figure 9-16: Laser Scanning, GPS and IMU Power Consumption.
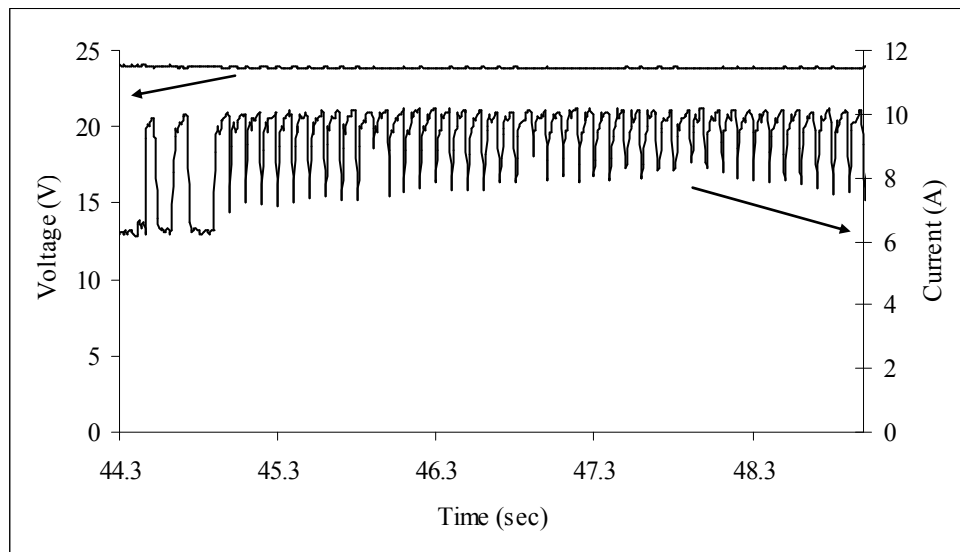
Figure 9-17: Current Consumption of Capturing and Processing 10 Images per Second.

Finally, a real application such as localization presented in figure 9-18 has an average power consumption of 240W. The power consumption of this application is more

realistic because not only the sensors previously presented are used but also the computer peripherals such as hard disk, memory and central processing unit (CPU) utilization.
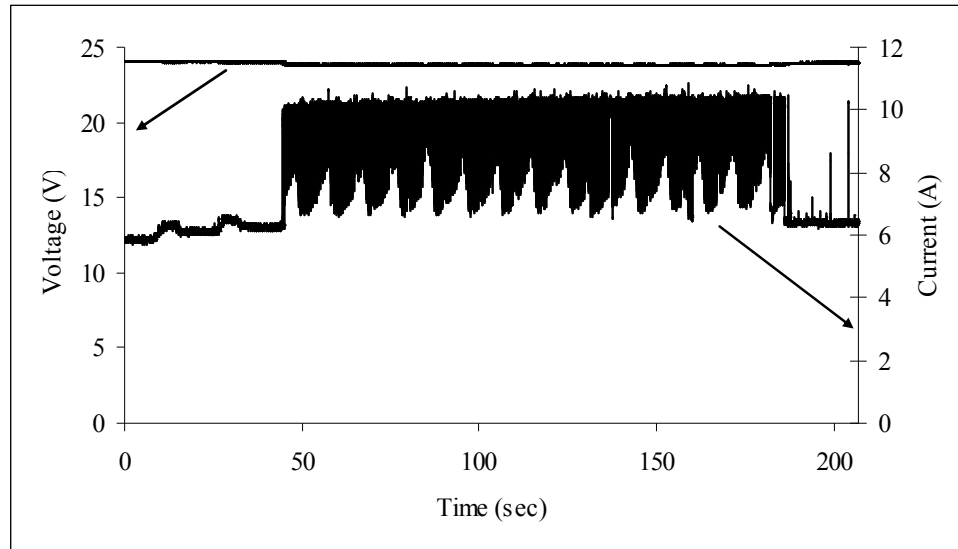
Figure 9-18: Localization Power Consumption.

In section 5.5 the sensors and processing platform power consumption including power supply efficiency, was found to be in the range of 321W because 100% utilization was assumed. However, from figure 9-18 it is concluded for a real application the application algorithm determines the sensor utilization and in the case of localization and autonomous navigation sensor utilization was only 74.77%.

9.5 Discussion and Recommendations

In section 5.6 it was estimated that the total required energy to achieve the 10 hour runtime set goal at full load was 2kWh resulting in a required battery capacity of 84Ah. The required energy consumption was calculated with motor full load power of 130W, low power sensors and processing platform with 100% utilization of 50W and total VTOL recharges of 200Wh.

Based on experimental findings presented in sections 9.2.1, 9.3 and 9.4 at full speed and low power sensors the energy requirement for the 10 hour goal would be 1468Wh which is 26.6% less than what was initially estimated using the traditional simplified method. Furthermore, a more realistic scenario would have the ATRV-Jr running at half speed which means that the new energy requirement for the 10 hour goal would be 1031Wh which is 49.45% lower. Finally, it can be concluded that the power system recommended in section 5.6 is oversized hence offering even higher runtimes that the ones reported.

CHAPTER 10. CAPACITY AND DISCHARGE CURRENT RELATIONSHIP FOR
LEAD ACID AND LITHIUM BATTERIES

10.1 Introduction

The relationship between battery capacity and discharge current is not a new research area. Schroder initially noted the phenomenon, between battery capacity and discharge current, but it was not until 1897, that W. Peukert established a mathematical relationship aimed specifically at lead acid batteries [1], [2]. The relationship is known and widely used to this day as Peukert's Equation or Peukert's Law.

The purpose of this chapter is to re-examine Peukert's Equation and understand the reasons why this relationship does not appear to be accurate for discharge times lower than 3 to 4 hours (high discharge rates). Does the fact that batteries today are completely different from 100 years ago account for this? For example, material and manufacturing advancements today enable lead acid batteries to achieve higher discharge rates (5 to 10C) and faster recovery from at deep discharges. These advancements enables end of discharge voltages down to 1.37 volts per cell instead of 1.75 volts per cell [3].

Experts claim that Peukert's equation gives the total amount of energy obtained from a battery at a specific discharge current when it is discharged, then left to rest, and then discharged a little bit more [1]. Therefore, Peukert's equation can not predict the amount of energy released from a single discharge. Even though a literature review did not reveal any evidence on the topic, it makes sense because as shown in figure 10-1 using a battery's datasheet to calculate Peukert's exponent, it turns out that for a single discharge Peukert's exponent is only constant in the region of 20 to 4 hour discharge time. At higher discharge rates Peukert's exponent is no longer constant but it dependents on battery capacity and discharge current.

This work proposes a reformulation of the relationship between battery capacity and discharge current using an exponent value which is a function of battery capacity and discharge current. The reformulated law provides an accurate prediction of the total energy for single discharge applications using only the battery name plate information such as capacity and the corresponding discharge time.

10.2 Peukert's Equation

In 1897, W. Peukert established a relationship between battery capacity and discharge current for lead acid batteries. His equation predicts the amount of energy you can extract from a battery. At higher discharge currents (high discharge rate) the battery efficiency decreases and as a result less energy is delivered. The Peukert equation is expressed as:

$$C_p = I^p t \tag{10.1}$$

where I is the discharge current in Amperes (A), t is runtime in hours (hr), p is Peukert's exponent which depends on the battery chemistry and C_p is Peukert's battery capacity in Ampere-hours (Ah) which is constant; hence $I^p t = constant$.

Solving for the discharge time,

$$t = \frac{C_p}{I^p} \tag{10.2}$$

Experts in the area have recently shed some light on how to correctly use Peukert's equation [1]. Peukert's battery capacity is the capacity recorded at 1A of discharge current, whereas, today, battery capacity for lead acid batteries is usually recorded for 20 hour discharge time. Therefore, for capacities other than 1A, Peukert's equation needs to be adjusted to accommodate the other discharge currents.

From Peukert's assumption that $I^p t = constant$ [2] then for different discharge currents it can be said that:

$$I_1{}^p t_1 = I_2{}^p t_2 \qquad (10.3)$$

Solving for runtime:

$$t_2 = \frac{I_1{}^p t_1}{I_2{}^p} \qquad (10.4)$$

Battery capacity is the product of discharge current and time:

$$C_1 = I_1 t_1 \qquad (10.5)$$

Hence, substituting for the discharge current then equation 10.4 can be re-written as:

$$t_2 = \frac{\left(\dfrac{C_1}{t_1}\right)^p t_1}{I_2{}^p} \qquad (10.6)$$

Where subscript *1* is for reference or advertised values and subscript *2* is for new discharge values. Hence, the equation can be written and seen in the following ways:

$$t = \frac{t_{ref}{}^{1-p} C^p}{I^p} = \frac{t_{ref}\left(\dfrac{C}{t_{ref}}\right)^p}{I^p} = \frac{C\left(\dfrac{t_{ref}}{C}\right)^{1-p}}{I^p} = \frac{C\left(\dfrac{C}{t_{ref}}\right)^{p-1}}{I^p} \qquad (10.7)$$

Where C is the battery capacity and t_{ref} is the discharge time as listed in the datasheet or battery nameplate.

Using any of the above expressions in Eq. (10.7), the Peukert's exponent can be calculated as follows:

$$p = \frac{\log(t_2) - \log(t_1)}{\log\left(\dfrac{C_1}{t_1}\right) - \log\left(\dfrac{C_2}{t_2}\right)} = \frac{\log(t_2) - \log(t_1)}{\log(I_1) - \log(I_2)} \qquad (10.8)$$

132

Care should be taken when calculating Peukert's exponent from the battery datasheet because some times the listed battery capacities and discharge rates are at different end-voltages.

10.3 New Approach With Variable Exponent

Energy and power systems with batteries have been well studied and understood by engineers. As a result, experts in the area follow empirical models and solutions derived mostly from their experience but at the same time Peukert's Law is widely used to explain phenomena such as battery capacity loss at higher discharge currents.
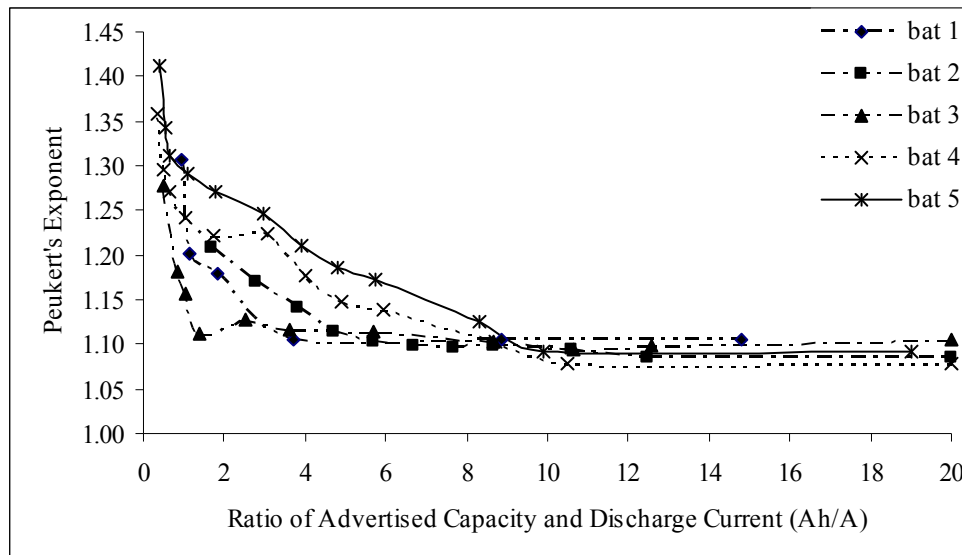
Figure 10-1: Peukert's Exponent Versus Ratio of Advertised Capacity and Discharge Current (Ah/A).

The exponent values shown in figure 10-1 were calculated using equation (10.8) by keeping fixed R_2 and I_2 (datasheet values for 20 hours discharge time) and varying the next data point. As it can be seen, Peukert's exponent has a relatively constant value up to 4 hours of discharge time and after that it increases exponentially. The reformulated

law takes advantage of the variable exponent value which is related to the battery's advertised capacity and discharge load current, as:

$$t = \frac{t_{ref}\left(\dfrac{C}{t_{ref}}\right)^{a-b\ln\left(\frac{C}{I}\right)}}{I^{a-b\ln\left(\frac{C}{I}\right)}} = t_{ref}\left(\dfrac{\dfrac{C}{t_{ref}}}{I}\right)^{a-b\ln\left(\frac{C}{I}\right)} \tag{10.9}$$

Where a and b depend on the specific battery and as before t_{ref} and C are the nameplate values for the discharge time and capacity, respectively.

10.4 Comparison of Results

First, the new approach of a variable exponent is compared to other ways of estimating battery runtime, such as, the linear approach, Peukert's equation and two different ways of calculating the exponent value. The datasheet of 6 batteries from 5 different companies were used and one battery was tested in the laboratory. Second, the new approach is taken a step further where an accurate runtime is calculated from running only a one hour test in order to obtain a very good approximation of values a and b for any battery.

10.4.1 Power Sonic PS1212

The first battery under test is a rechargeable sealed lead acid (SLA) battery from Power Sonic, PS1212 which is 12 volts, 1.2Ah at 20 hour. The constant discharge current characteristics shown in table 10-1 were either obtained or derived directly from the battery datasheet.

Furthermore, following the recommendations from [4] on battery modeling, by plotting the discharge time versus the discharge current on logarithmic scales, shown in figure 10-2 the slope of the best line-fit is Peukert's exponent value which in this case is 1.3438.

Table 10-1: Constant Discharge Current to End Voltage of 1.75V per Cell from Power Sonic PS1212 Datasheet

Capacity (Ah)	Runtime (hr)	Current (A)	C-Rate (hr^{-1})
1.22	20.0000	0.061	0.05
1.16	10.0000	0.116	0.10
1.12	8.0000	0.14	0.12
1.03	5.0000	0.206	0.17
0.992	4.0000	0.248	0.21
0.918	3.0000	0.306	0.26
0.8	2.0000	0.4	0.33
0.71	1.0000	0.71	0.59
0.595	0.5000	1.19	0.99
0.48	0.2500	1.92	1.60
0.41	0.1667	2.46	2.05
0.288333	0.0833	3.46	2.88

$$y = -1.3438x - 0.2453$$
$$R^2 = 0.9958$$
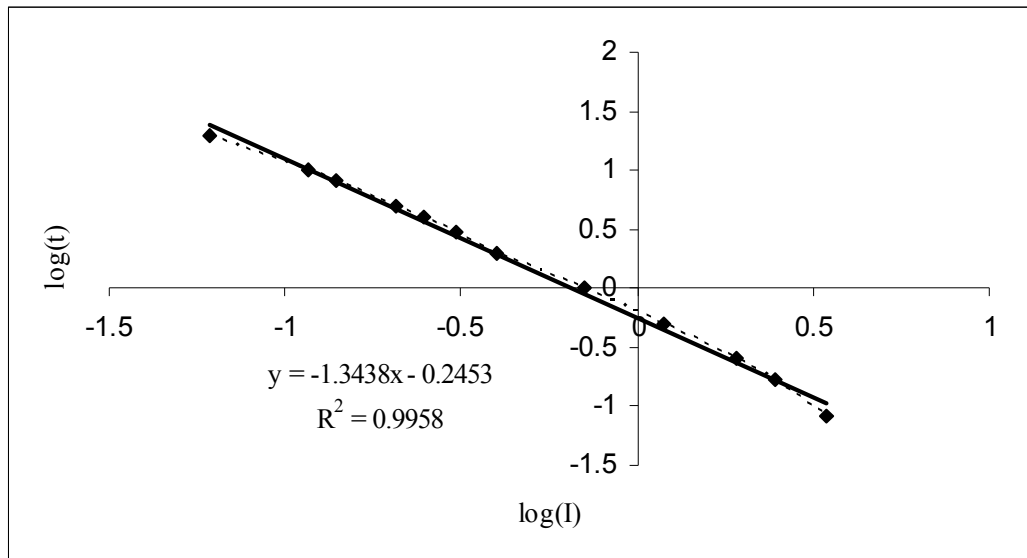
Figure 10-2: Runtime Versus Current on Logarithmic Scales for Peukert's Exponent Estimation for PS1212.
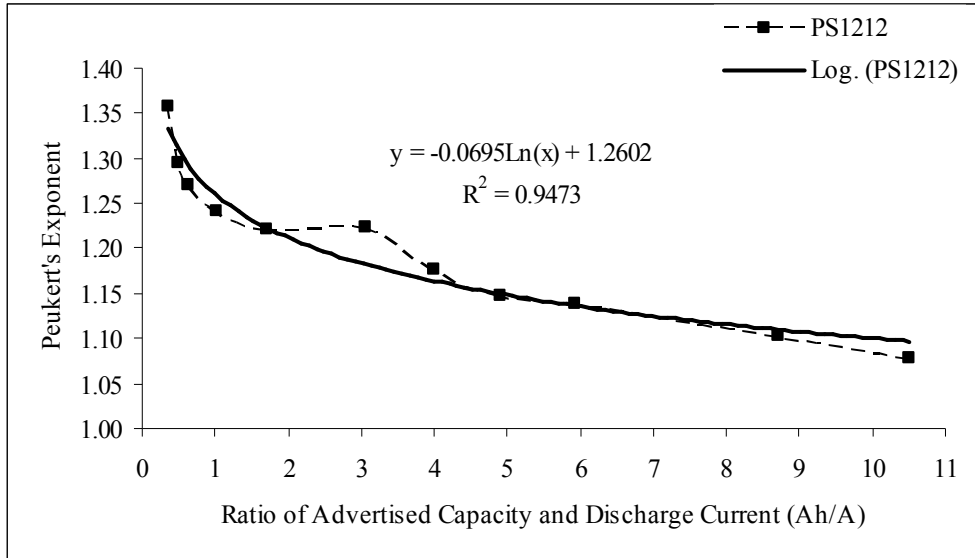
Figure 10-3: Peukert's Exponent Versus Capacity and Current Ratio for a and b-values Estimation for PS1212.

From equation (10.8), Peukert's exponent can be calculated from two discharge times and currents. Therefore, using only the 20 hour and 10 hour points, p is calculated to:

$$p = \frac{\log(20) - \log(10)}{\log\left(1.16/10\right) - \log\left(1.22/20\right)} = 1.0785$$

The linear approach assumes that Peukert's exponent has a value of unity and hence runtime is the ratio of advertised capacity and discharge current.

From table 10-2 it can be seen that the linear and the two data point methods have the worst accuracy especially for discharge times lower than 2 hours with errors reaching up to 200 and 300%, whereas when additional data points are used in calculating Peukert's exponent the accuracy significantly improves. Furthermore, as shown in both table 10-2 and figure 10-4 the reformulated law with a variable exponent value has significantly smaller error for a 20 hour discharge time down to 5 minutes whereas Peukert's law using additional data points has a uniform error in the range of 20%.

136

Table 10-2: Comparison of Results for PS1212

Datasheet Runtime (hr)	Linear t = C/ I % Error	$t=t_{ref}[(C/t_{ref})/I]$^1.3438 % Error	$t=t_{ref}[(C/t_{ref})/I]$^1.078 % Error	Reformulated Law % Error
20.0000	1.64%	2.20%	1.77%	0.00%
10.0000	-3.45%	17.53%	1.77%	1.16%
8.0000	-7.14%	19.93%	-0.25%	0.56%
5.0000	-16.50%	23.76%	-5.75%	-0.31%
4.0000	-20.97%	25.73%	-8.22%	0.28%
3.0000	-30.72%	25.34%	-15.03%	-2.00%
2.0000	-50.00%	21.87%	-29.25%	-8.16%
1.0000	-69.01%	27.72%	-39.21%	0.49%
0.5000	-101.68%	27.79%	-59.52%	4.86%
0.2500	-150.00%	24.06%	-90.45%	7.07%
0.1667	-192.68%	18.36%	-118.67	5.04%
0.0833	-316.18%	-3.25%	-202.73	-10.43%
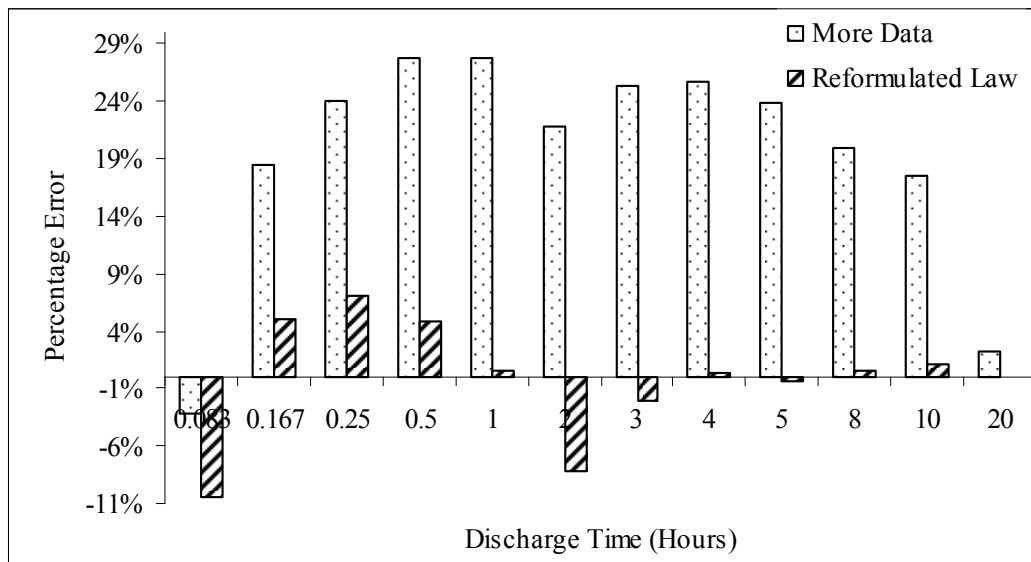
Figure 10-4: Comparison % Error Between the Reformulated Law and Peukert's Law Using More Data Points for PS1212.

10.4.2 C&D Technologies, Inc. DCS-33

The second battery to be tested was a rechargeable deep cycle sealed lead acid (SLA) battery from C&D Technologies, Inc., and is rated at 33Ah at 20 hour discharge time.

Table 10-3: Constant Discharge Current to End Voltage of 1.75V per Cell from C&D Technologies, Inc. DCS-33 Datasheet

Capacity (Ah)	Runtime (hr)	Current (A)	C-Rate (hr^{-1})
33	20	1.65	0.05
31.7	12	2.64	0.08
31.1	10	3.11	0.09
30.4	8	3.80	0.12
30.1	7	4.30	0.13
29.6	6	4.93	0.15
29	5	5.80	0.18
28	4	7.00	0.21
26.1	3	8.70	0.26
23.6	2	11.80	0.36
19.7	1	19.70	0.60
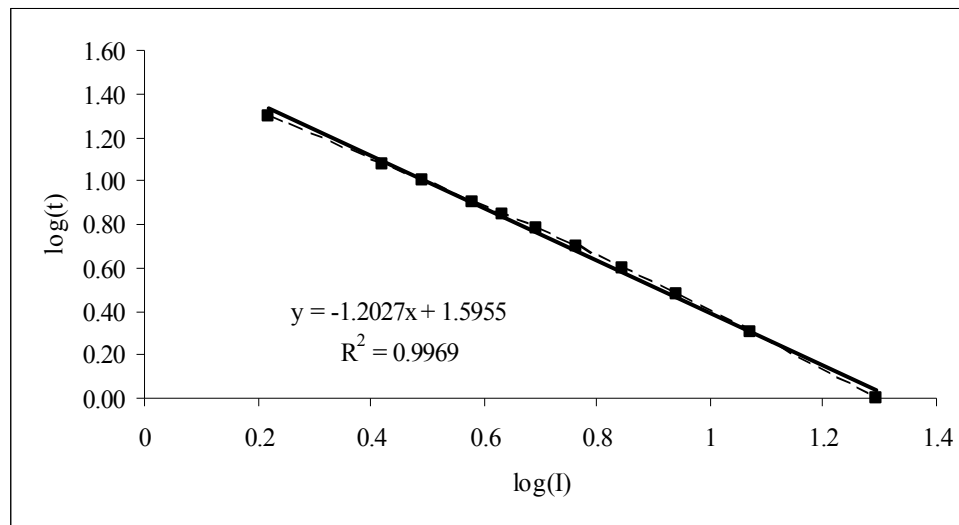
Figure 10-5: Runtime Versus Current on Logarithmic Scales for Peukert's Exponent Estimation for DCS-33.

Figure 10-6: Peukert's Exponent Versus Capacity and Current Ratio for a and b-values Estimation for DCS-33.

Table 10-4: Comparison of Results for DCS-33

Datasheet	Linear t = C/ I	$t=t_{ref}[(C/t_{ref})/I]^{\wedge}1.2027$	$t=t_{ref}[(C/t_{ref})/I]^{\wedge}1.0854$	Reformulated Law
Runtime (hr)	% Error	% Error	% Error	% Error
20	0.00%	0.00%	0.00%	0.00%
12	-4.10%	5.37%	0.00%	-0.93%
10	-6.11%	6.68%	-0.52%	-1.09%
8	-8.55%	8.34%	-1.09%	-0.74%
7	-9.63%	9.71%	-1.02%	0.16%
6	-11.49%	10.71%	-1.53%	0.81%
5	-13.79%	11.80%	-2.21%	1.82%
4	-17.86%	12.07%	-4.17%	2.30%
3	-26.44%	9.74%	-9.70%	0.49%
2	-39.83%	6.15%	-18.21%	-1.24%
1	-67.51%	-1.33%	-35.54%	-2.56%

The comparison of results presented on figure 10-7 shows that the reformulated approach offers higher accuracy than all the other three methods.
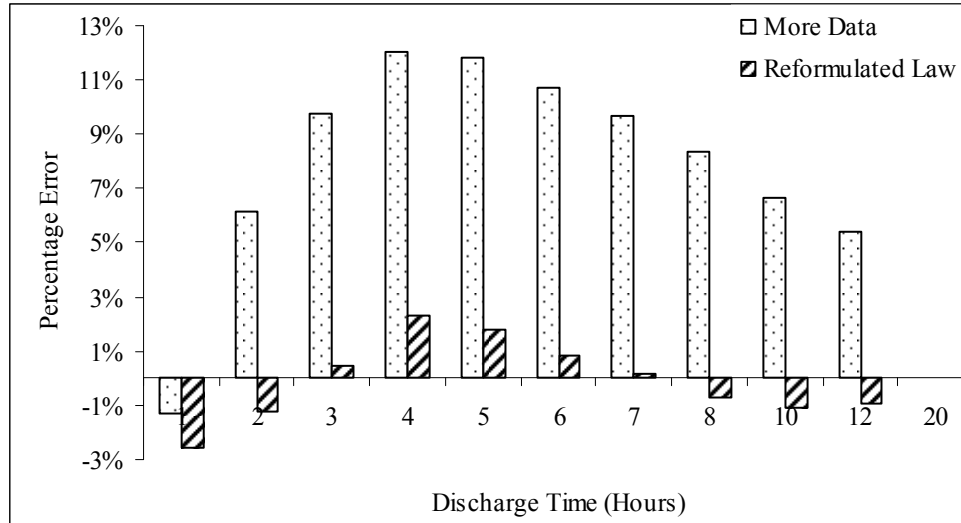
Figure 10-7: Comparison % Error Between the Reformulated Law and Peukert's Law Using More Data Points for DCS-33.

10.4.3 Power Sonic PS12380

The third battery to be tested was a rechargeable seal lead acid (SLA) battery from Power Sonic, PS12380 which is 12 volt, 38Ah at 10 hour.

Table 10-5: Constant Discharge Current to End Voltage of 1.75V per Cell from Power Sonic PS12380 Datasheet

Capacity (Ah)	Runtime (hr)	Current (A)	C-Rate (hr^{-1})
40.00	20.0000	2	0.05
38.30	10.0000	3.83	0.10
36.64	8.0000	4.58	0.12
33.15	5.0000	6.63	0.17
31.56	4.0000	7.89	0.21
29.16	3.0000	9.72	0.26
25.80	2.0000	12.9	0.34
21.40	1.0000	21.4	0.56
17.70	0.5000	35.4	0.93
14.35	0.2500	57.4	1.51
11.97	0.1667	71.8	1.89
8.20	0.0833	98.4	2.59
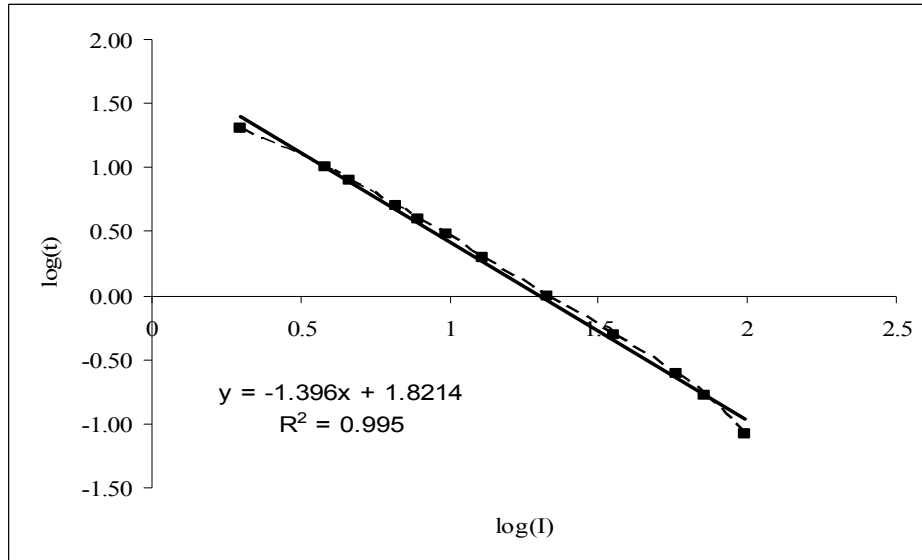
Figure 10-8: Runtime Versus Current on Logarithmic Scales for Peukert's Exponent Estimation for PS12380.
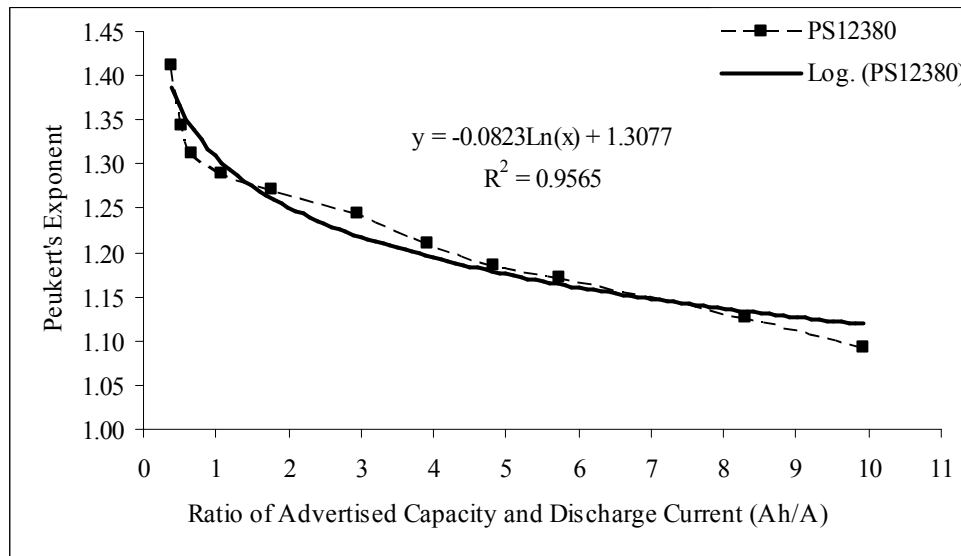
Figure 10-9: Peukert's Exponent Versus Capacity and Current Ratio for a and b-values Estimation for PS12380.

Table 10-6: Comparison of Results for PS12380

Datasheet Runtime (hr)	Linear t = C/ I % Error	$t=t_{ref}[(C/t_{ref})/I]^{\wedge}1.396$ % Error	$t=t_{ref}[(C/t_{ref})/I]^{\wedge}1.0919$ % Error	Reformulated Law % Error
20.000	0.00%	0.00%	0.00%	0.66%
10.000	-4.44%	19.25%	1.61%	0.88%
8.0000	-9.17%	21.37%	-1.17%	-1.08%
5.0000	-20.66%	24.93%	-8.08%	-4.39%
4.0000	-26.74%	26.40%	-11.72%	-5.37%
3.0000	-37.17%	26.66%	-18.62%	-8.03%
2.0000	-55.04%	25.89%	-30.63%	-12.15%
1.0000	-86.92%	26.88%	-50.33%	-12.39%
0.5000	-126%	27.57%	-73.54%	-8.43%
0.2500	-178.8%	26.23%	-104.75%	-3.55%
0.1667	-234.3%	19.04%	-140.53%	-8.86%
0.0833	-387.8%	-4.29%	-241.00%	-30.18%

Once again, from the comparison of results shown in figure 10-10 and table 10-6, it is clearly shown that the reformulated law offers higher accuracy than the other three methods.
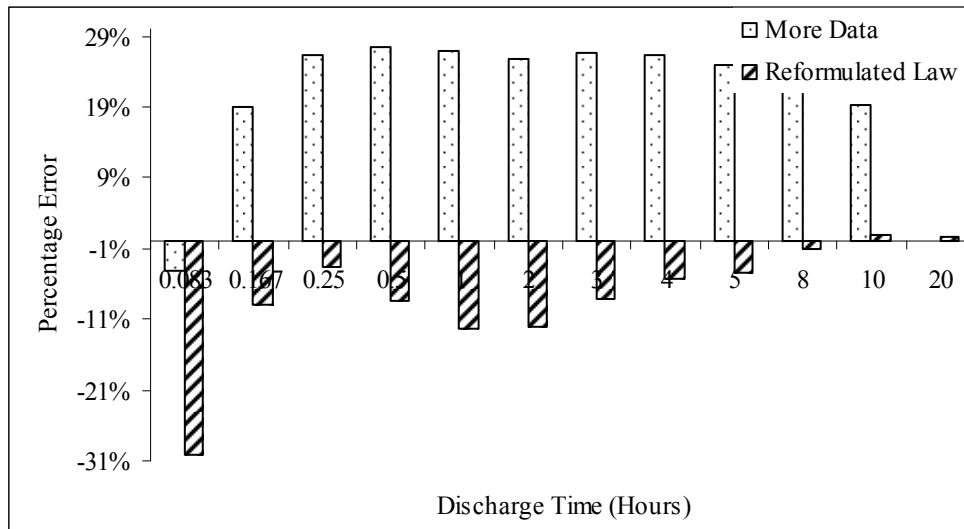
Figure 10-10: Comparison % Error Between the Reformulated Law and Peukert's Law Using More Data Points for PS12380.

10.4.4 USA Power Company Inc, PRC-6200S

Before introducing the next battery to be tested it would be a good idea to introduce the difference between constant current and constant power discharge. For constant current discharge as the name implies the discharge current is kept constant by monitoring the voltage and adjusting the load resistance (i.e. control the biasing of a power MOSFET). On the other hand, for constant power, as the battery voltage drops then the discharge current increases (use of a DC-DC converter with constant output load) so that the power is kept constant. Many lead acid battery manufacturers are providing the constant power ratings because this information is necessary for back up applications. However, care must be taken when calculating the discharge current from constant power discharge data. For example, the constant power discharge test at 724W for a 6V battery, implies that the starting current is 724W / 6V=120.7 Amperes, whereas at the end of the experiment, when approaching the cut off voltage of 1.75V per cell (10.5V), the current will actually be 724/5.25=137.9 Amperes. However, the average current can not be calculated unless the duration of each discharge current is known.
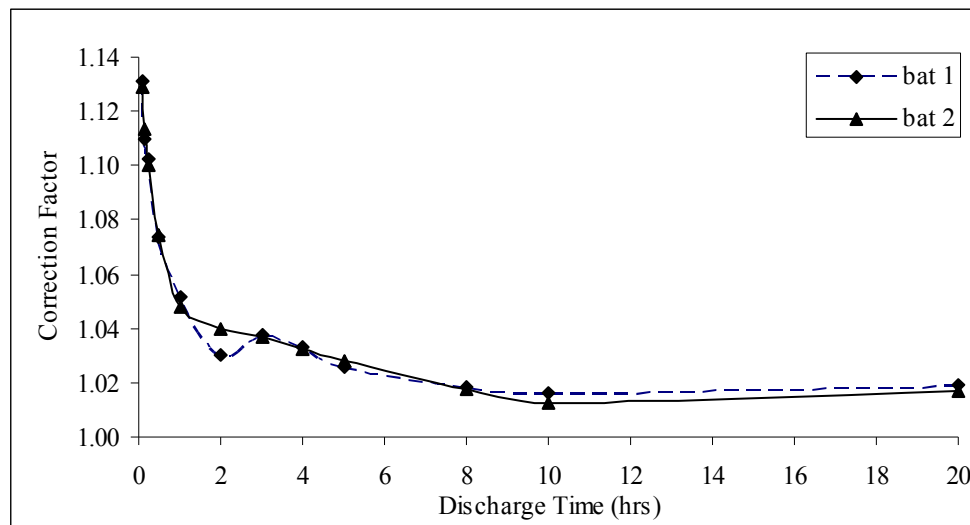
Figure 10-11: Constant Discharge Power to Current Correction Factor.

143

Comparing the datasheet from the Power Sonic products where both constant current and constant power discharge data is available for the same discharge times, then from figure 10-11 it can be seen that a common correction factor is required to find the average current from constant power discharge data.

For example, for a 6V battery at constant power of 724W and runtime of 1 hour, from figure 10-11 the correction factor is 1.05. This means that the average discharge current is 724/6*1.05=126.7A.

To complete the comparison, the fourth battery chosen for the test was a valve regulated rechargeable lead acid (VRLA) with absorbed glass mat (AGM) technology battery from USA Power Company Inc, PRC-6200S, which is rated at 6 volt, 208Ah at 20 hour.

Table 10-7: Derived Constant Discharge Current to End Voltage of 1.75V per Cell from USA Power Company Inc. PRC-6200S Datasheet

Capacity (Ah)	Runtime (hr)	Current (A)	C-Rate (hr^{-1})
213.60	24.0000	8.90	0.04
193.20	12.0000	16.10	0.08
188.00	10.0000	18.80	0.09
182.40	8.0000	22.80	0.11
175.20	6.0000	29.20	0.14
170.50	5.0000	34.10	0.16
165.20	4.0000	41.30	0.20
157.50	3.0000	52.50	0.25
144.80	2.0000	72.40	0.35
138.32	1.5000	92.21	0.44
126.70	1.0000	126.70	0.61
121.11	0.8333	145.34	0.70
118.32	0.7500	157.76	0.76
113.54	0.6667	170.31	0.82
103.79	0.5000	207.58	1.00
90.08	0.3333	270.24	1.30
80.62	0.2500	322.48	1.55
63.86	0.1667	383.14	1.84
43.03	0.0833	516.41	2.48
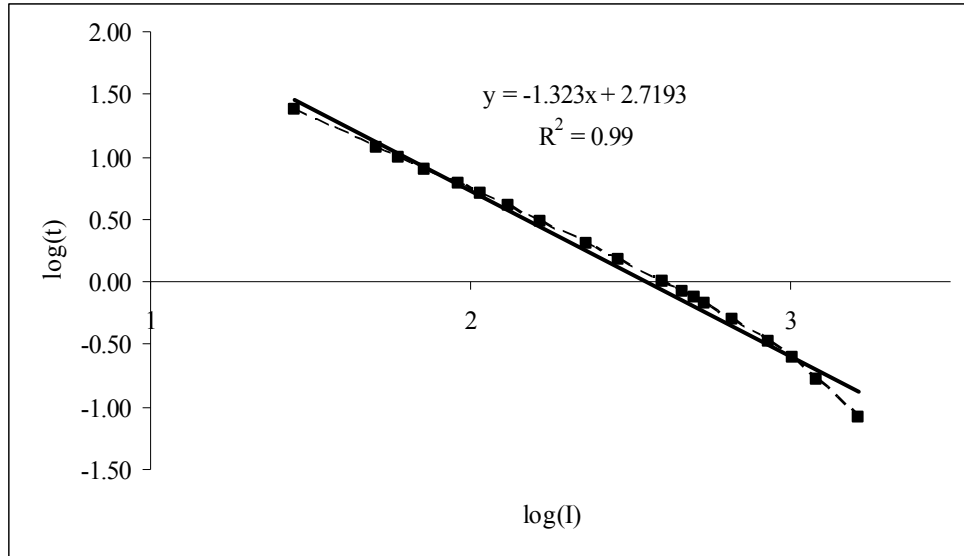
Figure 10-12: Runtime Versus Current on Logarithmic Scales for Peukert's Exponent Estimation for PRC-6200S.
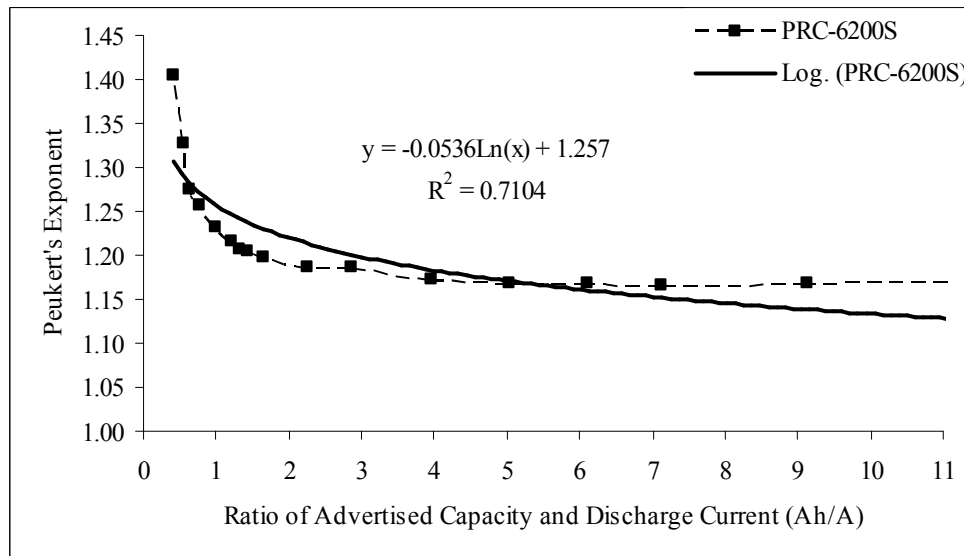
Figure 10-13: Peukert's Exponent Versus Capacity and Current Ratio for a and b-values Estimation for PRC-6200S.

145

Table 10-8: Comparison of Results for PRC-6200S

Datasheet Runtime (hr)	Linear t = C/ I % Error	t=t$_{ref}$[(C/t$_{ref}$)/I]^1.323 % Error	t=t$_{ref}$[(C/t$_{ref}$)/I]^1.1689 % Error	Reformulated Law % Error
24.0000	2.62%	-2.40%	0.03%	1.28%
12.0000	-7.66%	6.51%	0.00%	-2.17%
10.0000	-10.64%	8.62%	-0.11%	-2.55%
8.0000	-14.04%	11.50%	0.12%	-2.29%
6.0000	-18.72%	14.94%	0.28%	-1.50%
5.0000	-21.99%	16.87%	0.18%	-0.87%
4.0000	-25.91%	19.35%	0.25%	0.45%
3.0000	-32.06%	21.72%	-0.47%	1.83%
2.0000	-43.65%	23.25%	-3.51%	2.64%
1.5000	-50.38%	25.69%	-4.02%	5.61%
1.0000	-64.17%	26.79%	-7.62%	7.72%
0.8333	-71.74%	26.73%	-10.01%	8.27%
0.7500	-75.79%	26.96%	-11.05%	9.01%
0.6667	-83.19%	25.75%	-14.24%	7.98%
0.5000	-100.4%	23.80%	-20.87%	7.12%
0.3333	-130.9%	19.37%	-33.19%	4.50%
0.2500	-158.0%	14.91%	-44.45%	1.54%
0.1667	-225.7%	-1.61%	-77.14%	-14.56%
0.0833	-383.3%	-36.9%	-149.92%	-46.46%
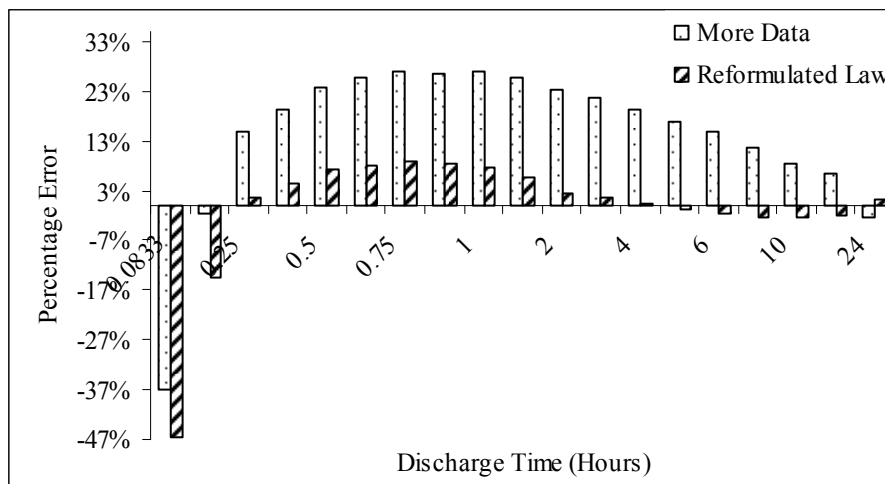
Figure 10-14: Comparison % Error Between the Reformulated Law and Peukert's Law Using More Data Points for PRC-6200S.

146

10.4.5 Lab Characterized, 6.654Ah at 14.786 hours

The fifth battery to be tested was an old lead acid battery found in the lab which was characterized having a capacity of 6.654Ah at a discharge time of 14.786 hours.

Table 10-9: Constant Discharge Current to End Voltage of 1.75V per Cell from Lab Characterization Data

Capacity (Ah)	Runtime (hr)	Current (A)	C-Rate (hr^{-1})
6.654	14.786	0.45	0.07
6.303	8.404	0.75	0.11
5.749	3.194	1.8	0.27
4.590	1.274	3.6	0.54
3.970	0.685	5.8	0.87
2.854	0.396	7.2	1.08
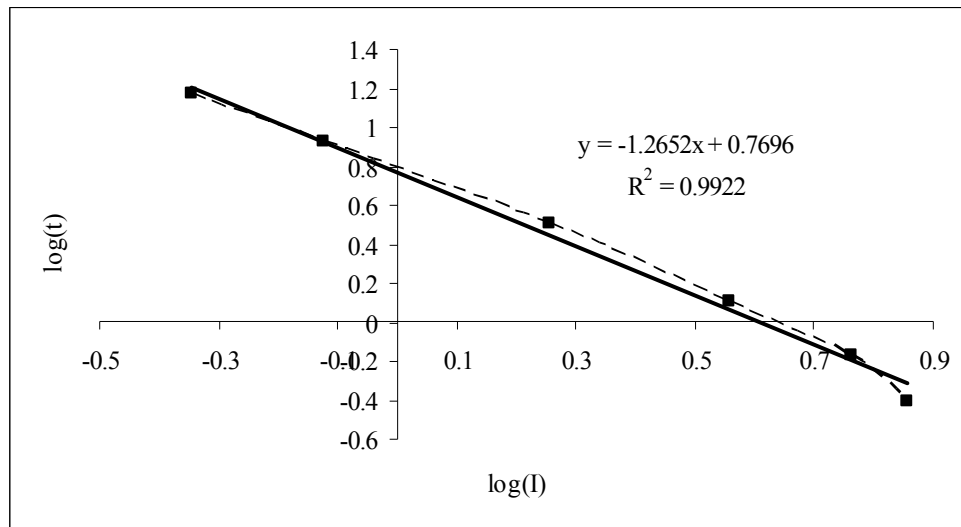
Figure 10-15: Runtime Versus Current on Logarithmic Scales for Peukert's Exponent Estimation for Lab Characterized LA Battery.

147
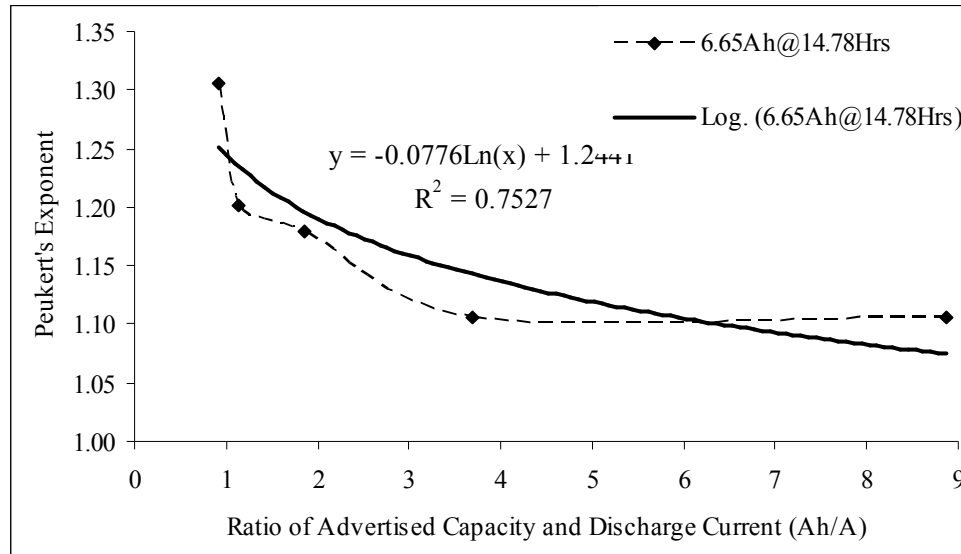
*Figure 10-16: Peukert's Exponent Versus Capacity and Current Ratio for a and b-values
Estimation for Lab Characterized LA Battery.*

Table 10-10: Comparison of Results for Lab Characterized LA Battery

Datasheet Runtime (hr)	Linear $t = C/I$	$t = t_{ref}[(C/t_{ref})/I]^{1.265}$	$t = t_{ref}[(C/t_{ref})/I]^{1.106}$	Reformulated Law
	% Error	% Error	% Error	% Error
14.786	0.00%	0.00%	0.00%	0.00%
8.404	-5.57%	7.81%	0.00%	-1.61%
3.194	-15.74%	19.87%	0.08%	5.03%
1.274	-45.08%	16.42%	-16.38%	3.57%
0.658	-67.48%	14.98%	-32.96%	7.79%
0.396	-133.4%	-11.87%	-73.94%	-16.61%

Once again, from the comparison of results shown in figure 10-10 and table 10-6, it is
clearly shown that the reformulated law offers higher accuracy than the other three
methods.
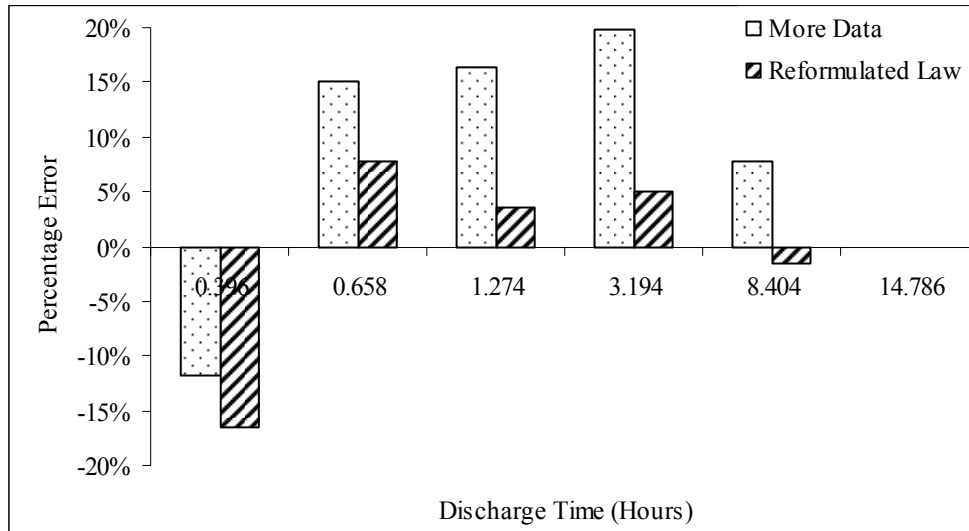
*Figure 10-17: Comparison % Error Between the Reformulated Law and Peukert's Law
Using More Data Points for Lab Characterized LA Battery.*

10.4.6 Power Sonic PSH-12180FR

Another problem which comes from using battery datasheets is the fact that a number of tests and battery characterizations are done at different end voltages. Usually, the end voltage for lead acid batteries is 1.75 volts per cell. However, as mentioned earlier advancements in material science enables nowadays Deep Cycle lead acid batteries which means that lead acid batteries can be discharged down to lower voltages such as 1.5 volts per cell etc. Deep cycle discharging usually is performed at low discharge rates (high discharge current) because the damage on the electrodes from deep discharging is completely different and less severe when discharge currents last a few minutes rather than few hours [3]. Therefore, many times on datasheet the listed capacity at 20 hour discharge rate is at an end voltage of 1.75 volts per cell whereas the capacity at 5 minute discharge time could at 1.6 volts per cell or lower.

The reformulated equation assumes an end voltage of 1.75 volts per cell for the calculated runtimes. Therefore, for any other voltages a correction factor is necessary.

149

From table 10-11 it can be see that at 20 hour discharge time discharging your battery down to 1.6 volts per cell increases delivered energy by 3.28% whereas at 5 minutes discharge time the gain can be as high as 33.82%. Similarly, discharging the battery at voltages higher than 1.75v (ie 1.85v/cell) then less energy is delivered. Similarly, at 1 hour discharge time and end voltage of 1.5 volts per cell, the correction factor can be extrapolated to 1.16 (16%) whereas at 15 minutes discharge time the correction factor is 1.35 (35%).

Table 10-11: Runtime and Final Voltage Correction Factors

F.V/Time	5MIN	10MIN	15MIN	30MIN	1HR	3HR	4HR	5HR	10HR	20HR
1.6	33.82%	28.05%	21.35%	15.97%	9.86%	10.46%	9.27%	7.77%	4.31%	3.28%
1.67	15.32%	14.23%	9.90%	7.56%	4.23%	5.23%	4.03%	2.43%	1.72%	1.64%
1.7	10.12%	9.35%	6.77%	4.20%	2.82%	2.94%	2.42%	1.46%	0.86%	1.64%
1.75	0.00%	0.00%	0.00%	0.00%	0.00%	0.00%	0.00%	0.00%	0.00%	0.00%
1.8	-11.27%	-8.94%	-8.33%	-3.36%	-4.23%	-1.96%	-2.42%	-3.40%	-0.86%	-1.64%
1.85	-33.82%	-28.86%	-24.48%	-18.49%	-15.49%	-8.82%	-8.47%	-10.19%	-6.90%	-3.28%

The following battery is a Power Sonic which is a high rate series rechargeable SLA, 12 volts and rated 21Ah at 20 hours (PSH-12180FR).

Table 10-12: Constant Power Discharge from Power Sonic PSH-12180FR Datasheet

Runtime (hr)	Power (W)	C-Rate (hr -1)	End Voltage (V)	EV/cell (V)	Power to Current C. F	EV -1.67v C. F
1.000	162	1.00	10.02	1.67	1.05	1.0423
0.750	228	1.33	10.02	1.67	1.06	1.0590
0.500	310	2.00	10.02	1.67	1.07	1.0756
0.333	402	3.00	10.02	1.67	1.09	1.0912
0.250	492	4.00	10.02	1.67	1.10	1.0990
0.167	648	6.00	10.02	1.67	1.11	1.1423
0.083	864	12.00	10.02	1.67	1.13	1.1532

The correction factors will be applied to all techniques used to calculate runtime.

Table 10-13: Constant Current Discharge from Power Sonic PSH-12180FR Datasheet

Capacity (Ah)	Runtime (hr)	Current (A)	C-Rate (hr^{-1})	End Voltage (V)	EV/cell (V)
21.00	20	1.05	0.05	10.50	1.75
20.00	10	2.00	0.10	10.50	1.75
18.50	5	3.70	0.18	10.20	1.70
13.00	1	13.00	0.62	9.00	1.50
10.00	0.25	40.00	1.91	9.00	1.50

Table 10-14: Derived Constant Current Discharge from PSH-12180FR Datasheet

Capacity (Ah)	Runtime (hr)	Current (A)	C-Rate (hr^{-1})
21.00	20	1.05	0.05
20.00	10	2.00	0.10
18.50	5	3.70	0.18
14.18	1.000	14.18	0.68
15.11	0.750	20.14	0.96
13.82	0.500	27.64	1.32
12.16	0.333	36.52	1.74
11.28	0.250	45.10	2.15
10.01	0.167	59.94	2.85
6.75	0.083	81.36	3.87
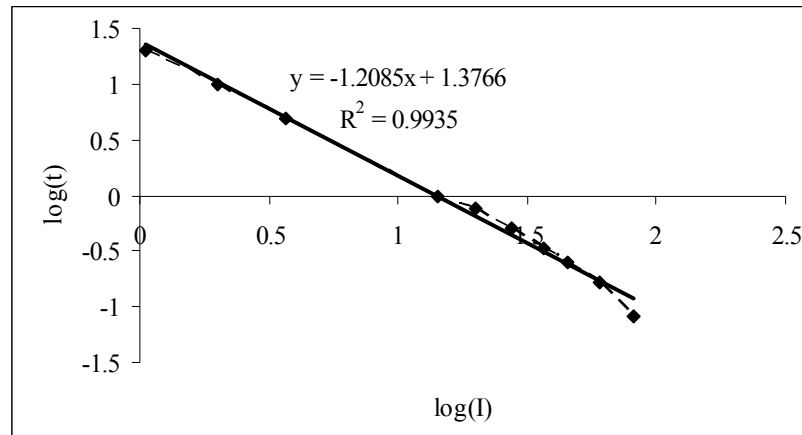
Figure 10-18: Runtime Versus Current on Logarithmic Scales for Peukert's Exponent Estimation for PSH-12180FR.
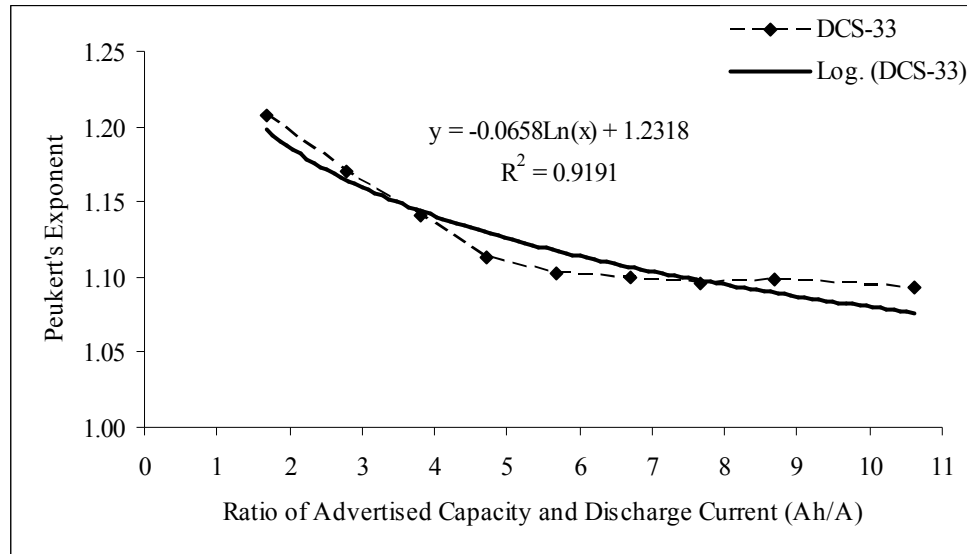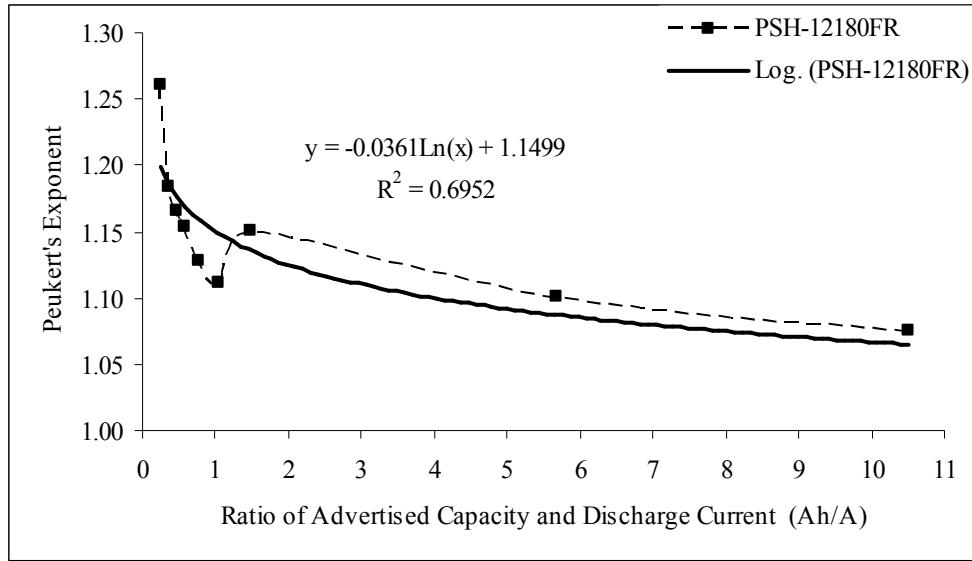
Figure 10-19: Peukert's Exponent Versus Capacity and Current Ratio for a and b-values Estimation for PSH-12180FR.

Table 10-15: Comparison of Results for PSH-12180FR

Datasheet Runtime (hr)	Linear t = C/ I % Error	$t=t_{ref}[(C/t_{ref})/I]^{\wedge}1.2085$ % Error	$t=t_{ref}[(C/t_{ref})/I]^{\wedge}1.0757$ % Error	Reformulated Law % Error
20	0.00%	0.00%	0.00%	0.00%
10	-5.00%	8.20%	-0.05%	-0.69%
5	-13.51%	12.70%	-3.28%	-1.70%
1.000	-55.50%	9.63%	-27.92%	-9.22%
0.750	-47.37%	20.40%	-18.08%	4.93%
0.500	-62.58%	17.79%	-27.22%	3.60%
0.333	-88.25%	10.18%	-44.26%	-3.02%
0.250	-104.88%	6.46%	-54.53%	-5.11%
0.167	-132.87%	-0.20%	-71.94%	-8.97%
0.083	-251.41%	-41.88%	-153.58%	-47.99%
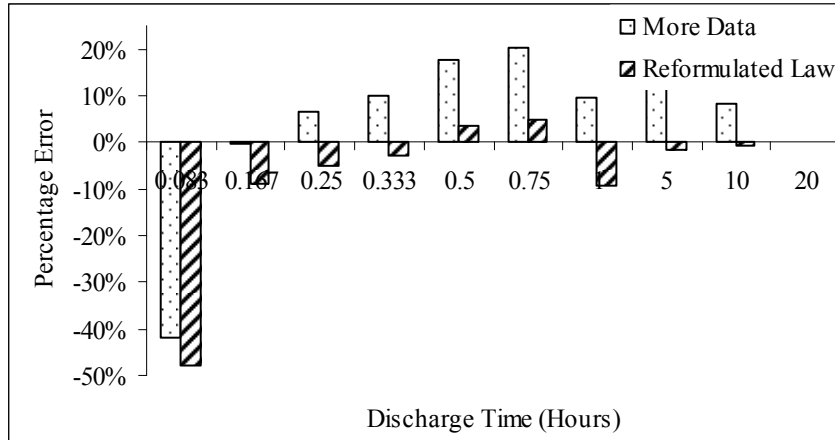
Figure 10-20: Comparison % Error Between the Reformulated Law and Peukert's Law Using More Data Points for PSH-12180FR.

10.5 Estimating *a* and *b*-values From the 0.5 Hour Experiment

A reformulated law that takes advantage of a variable exponent value which relates the battery advertised capacity and discharge load current has been presented and tested in section 10.3. It was shown that this approach predicts the battery runtime under constant discharge current more accurately than Peukert's Law. The reformulated law requires some estimates for *a* and *b*-values which are battery depended. Similarly, in calculating Peukert's exponent value, higher accuracy can be achieved with a larger number of data points which is time consuming.

In this section a new approach will be introduced that can be used to calculate *a* and *b*-values in less than an hour. As it can be seen, every single battery examined has different *a* and *b*-values. Test results of four additional batteries are as follows:

- BBA-160RT (88Ah at 20hrs) by C&D Technologies Inc, Dynasty Division. a=1.2236 and b=-0.043.

- DCS-100L (100Ah at 20hrs) by C&D Technologies Inc, Dynasty Division. a=1.396 and b=-0.1146.

- DCS-75IT (75Ah at 20hrs) by C&D Technologies Inc, Dynasty Division. a=1.264 and b=-0.0822.

- MPS12-50 (50Ah at 20hrs) by C&D Technologies Inc, Dynasty Division. a=1.1904 and b=-0.0418.

One can see that all four batteries examined have one parameter in common. The *a*-value is represented by Peukert's exponent at the half hour discharge time. Therefore, when no data is available then the battery pack can be discharged once for 0.5 hours and the *a*-value is given by:

$$a = \frac{\log(t_2) - \log(0.5)}{\log(I_{0.5}) - \log\left(\frac{C_2}{t_2}\right)} = \frac{\log(20) - \log(0.5)}{\log(I_{0.5}) - \log(0.05C_2)} \tag{10.10}$$

where C_2 is the advertised capacity mostly given at 20 hours discharge time. Care should be taken when estimating the discharge current to achieve an actual runtime of 0.5 hours. Using the linear approach for a 5Ah battery, the discharge current would be 2C or 10A, whereas from the manufacturer datasheet it can be seen that the discharge current is at approximately 1 to 1.5C which would indicate 5 to 7.5A. For aged lead acid batteries experimental results show that the discharge current is between 0.9 and 1.1C.

Unlike the *a*-value being determined with the 0.5 hour test, the *b*-value for the batteries examined has no correlation with the battery capacity and/or discharge current. The *b*-values obtained for the batteries examined ranges between -0.0361 to -0.1146, and a mean value of -0.0667. A sensitivity analysis is performed to evaluate the bias and variance effects of the *b*-value on the model. From experimental data, the *b*-value is assumed as a random variable with uniform distribution.

Therefore, if

$$b \sim U(b_{min}, b_{max}) \tag{10.11}$$

then the probability density function is given by

$$f(b) = \frac{1}{b_{max} - b_{min}}$$

(10.12)

where $b_{min} \leq b \leq b_{max}$.

The expected value of a function $g(C, I, R, a, b)$ with distribution $f(b)$ is given by;

$$E[g(C, I, R, a, b)] = \int_{-\infty}^{+\infty} g(C, I, R, a, b) f(b) db$$

(10.13)

Using the expectation of $g(b)$ then the bias is calculated by

$$bias[g(C, I, R, a, b)] = g(\mu) - E[g(C, I, R, a, b)]$$

(10.14)

where μ is the true value of b, and the variance is

$$Var[g(C, I, R, a, b)] = E[g^2(C, I, R, a, b)] - E[g(C, I, R, a, b)]^2$$

(10.15)
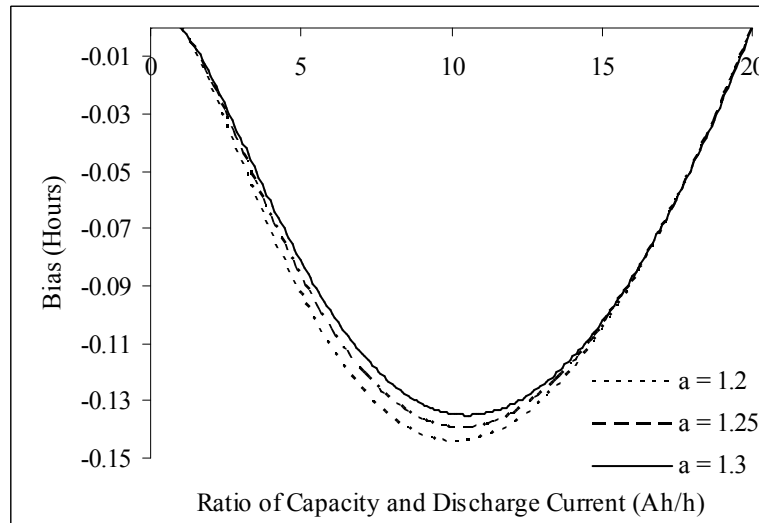
Figure 10-21: Bias Difference Between an Estimator's Expectation and the True Runtime.

The bias effect examined and presented in figure 10-21 shows a maximum difference of 1.5% between an estimator's expectation and the true runtime value whereas the variance effect examined and presented in figure 10-22 shows a maximum deviation of 1.3% between an estimator's expectation and the true runtime value.
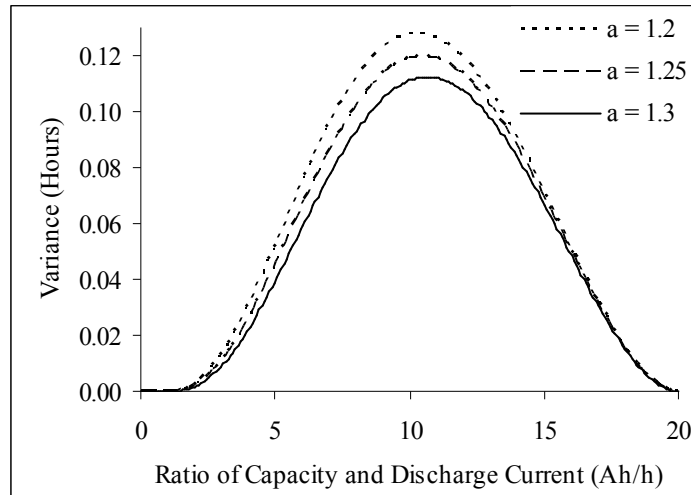
Figure 10-22: Variance Versus Ratio of Capacity and Discharge Current.
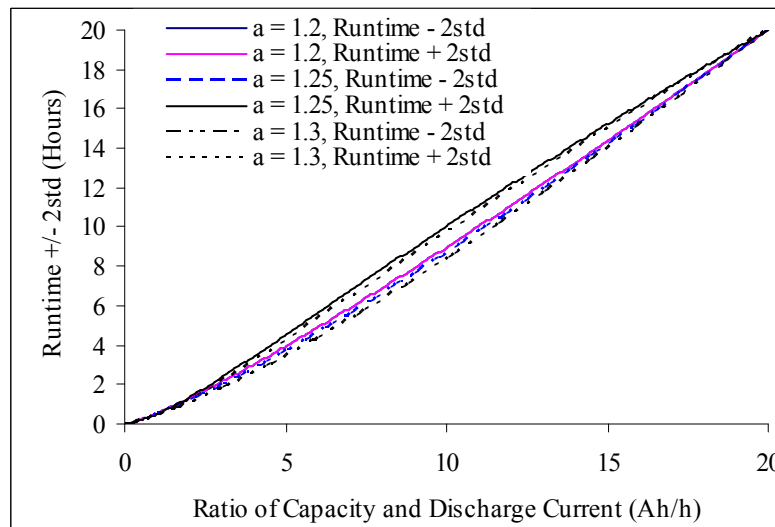
Figure 10-23: Runtime ± 2σ.

As shown in figure 10-23, with a 95% confidence, the true runtime will fall between the envelope of plus or minus 2 standard deviations from the mean value. Hence, since bias and variance deviations are small when no data is available then an average *b*-value of -0.0667 can be selected.

10.6 Peukert's Law for Lithium Batteries

Unlike lead acid batteries where Peukert's exponent can vary between 10 to 27% as shown in figure 10-1, lithium batteries shown in figure 10-24 have a Peukert's exponent variation of only 2 to 3%.
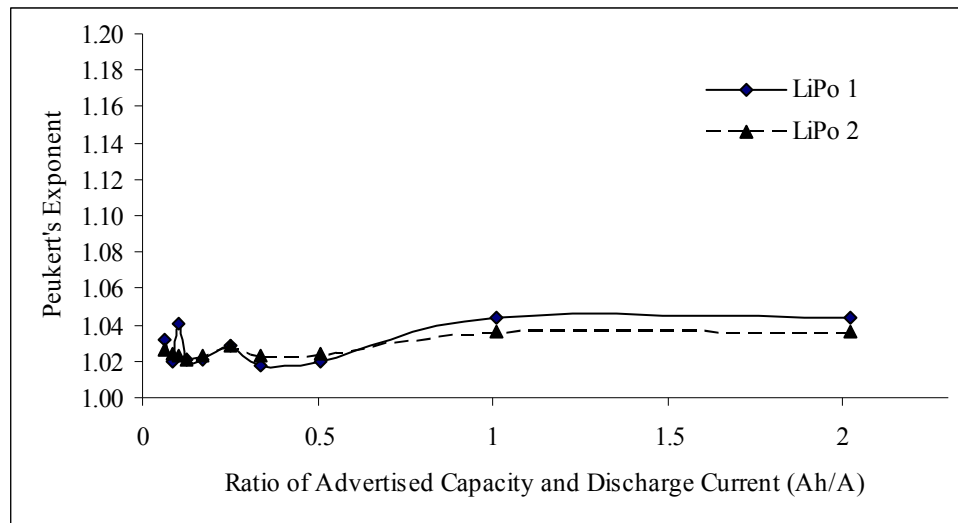
Figure 10-24: Peukert's Exponent Versus Ratio of Advertised Capacity and Discharge Current (Ah/A) for Lithium Batteries.

In addition, at discharge times as low as 3 to 5 minutes, lithium batteries show much higher efficiencies with the Peukert's exponent decreasing instead of increasing like in lead acid batteries. This could be attributed to the very high temperatures generated at high discharge currents which are significantly greater than those in lead acid batteries. From the experimental results it was found that for lead acid batteries discharged at 1.1C there was a 9.2% increase in the battery pack temperature whereas for lithium polymer

batteries tested when discharged at 1C there was 22.1% increase in temperature. In addition, when lithium batteries were discharged at 16C, there was a 136.8% increase in temperature whereas lead acid batteries could not be tested at such high discharge rates. Hence, it can be concluded that in the case of lithium batteries, the heat generated from I^2R battery losses improves the overall battery efficiency by increasing the pack temperature to such levels where the heat losses are compensated by temperature capacity gains.

In [5] it is concluded that Peukert's law is only applicable to batteries that are discharged at constant load current and temperature. In addition, for lithium batteries under high discharge currents there is a significant temperature increase and Peukert's law is not applicable. However, this research concludes that because of this increase in temperature, Peukert's exponent value is more constant and Peukert's law is a very accurate method for the prediction of runtime and capacity even for lithium batteries without any reformulation. The same methodology is followed as that in section 10.4 with the exception that no reformulation is used because it is not necessary due to very small variations in the exponent value.

Table 10-16: Constant Discharge Current to End Voltage of 3V per Cell from Lab Characterization Data

Capacity (Ah)	Runtime (hr)	Current (A)	C-Rate (hr^{-1})
0.91	2.027	0.45	0.5
0.89	0.988	0.9	1.0
0.88	0.490	1.8	2.0
0.87	0.324	2.7	3.0
0.86	0.239	3.6	4.0
0.86	0.159	5.4	5.9
0.86	0.119	7.2	7.9
0.85	0.094	9	9.9
0.85	0.078	10.8	11.9
0.83	0.058	14.4	15.8
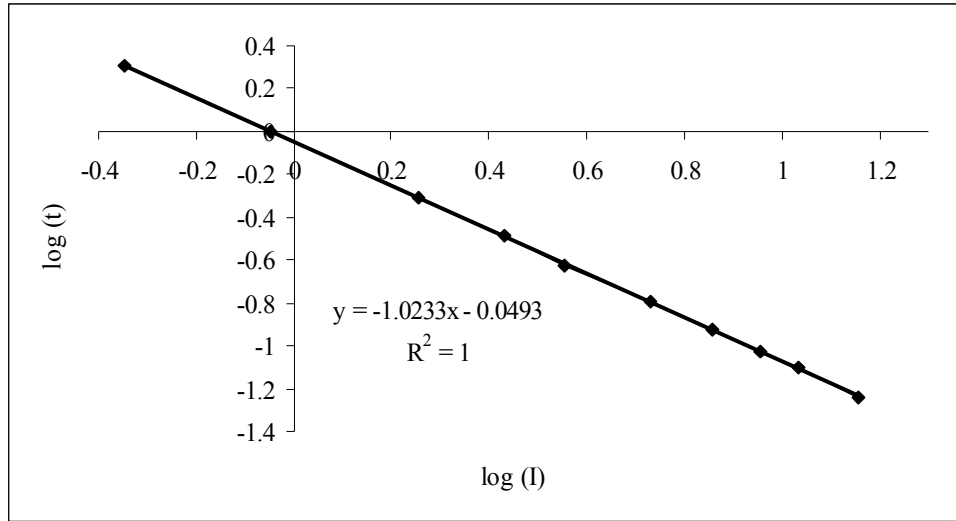
Figure 10-25: Runtime Versus Current on Logarithmic Scales for Peukert's Exponent Estimation for Lithium Batteries.

Table 10-17: Comparison of Results for Lithium Batteries

Datasheet Runtime (hr)	Linear $t = C/I$ % Error	$t=t_{ref}[(C/t_{ref})/I]^{\wedge}1.0233$ % Error	$t=t_{ref}[(C/t_{ref})/I]^{\wedge}1.0367$ % Error
2.027	0.23%	0.00%	0.00%
0.988	-2.33%	-0.93%	0.00%
0.490	-3.17%	-0.13%	1.71%
0.324	-4.06%	-0.04%	2.33%
0.239	-5.81%	-1.05%	1.73%
0.159	-5.69%	0.02%	3.29%
0.119	-5.81%	0.57%	4.20%
0.094	-7.06%	-0.08%	3.86%
0.078	-7.57%	-0.12%	4.05%
0.058	-9.37%	-1.13%	3.46%

As it can be seen from the comparison results of table 10-17 and figure 10-26 calculating the Peukert's exponent even with 2 data points, maximum error is only 4.2% whereas with additional data points, the runtime error can be reduced to 1.13%. It is worth noting

that the linear approach has a maximum error of 9.37% which for a 3 minute discharge time the runtime deviation is only 280 milliseconds.
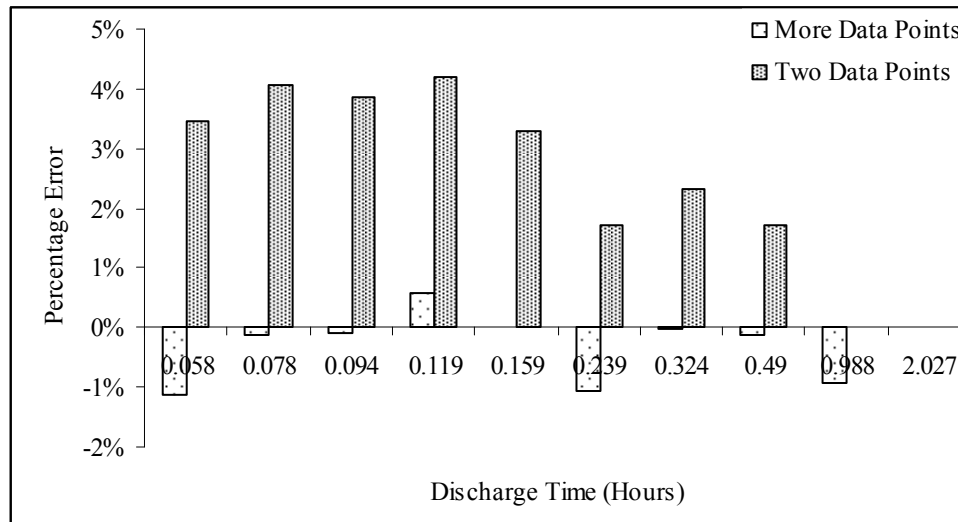
Figure 10-26: Comparison % Error Between the Reformulated Law and Peukert's Law Using More Data Points for Lithium Batteries.

It is worth noting that experimental results also showed that for the lithium batteries examined, discharging down to 2.9 volts per cell there is on average a 1% energy gain whereas the highest energy gain of 2.7% is obtained at a 16C discharge current.

10.7 List of References

[1]   Smart Gauge, "A proper explanation of Peukert's Equation", Online Posting: http://www.smartgauge.co.uk/peukert.html (January 20, 2008).

[2]   W. Peukert, "About the Dependence of the Capacity of the Discharge Current Magnitude and Lead Acid Batteries", Elektrotechnische Zeitschrift, Volume 20, 1897.

[3]   Power Sonic, "Technical Literature - Sealed Lead Acid Batteries – Technical Handbook", Online Posting: http://www.power-sonic.co.uk/uploads/files/techman.pdf (August 22, 2008).

[4]   James Larminie and John Lowry, "Electric Vehicle Technology Explained", 1st Edition, John Wiley and Sons Ltd., pp. 65, ISBN 0-470-85163-5, 2003.

[5]   Dennis Doerffel and Suleiman Abu Sharkh, "A Critical Review of Using the Peukert Equation for Determining the Remaining Capacity of Lead Acid and Lithium Ion Batteries", Journal of Power Sources, pp 395 – 400, 155, 2006.

CHAPTER 11. REMAINING BATTERY ENERGY ESTIMATION

11.1 Introduction

There are three main models of measuring energy delivered by a battery and hence estimating the remaining battery capacity [1]. The first model assumes a linear approach by neglecting the battery capacity loss due to high discharge currents. Hence, it is assumed that the advertised capacity is always delivered independent of discharge current, as

$$C_{remain} = C_{total} - \int_0^t i(t)dt \qquad (11.1)$$

The second model accounts for the loss of battery capacity due to a discharge current by introducing a battery efficiency factor, e, which is a function of load and rated battery currents and can be derived from battery datasheets. More data can lead to more accurate efficiency estimation, as

$$C_{remain} = eC_{total} - \int_0^t i(t)dt \qquad (11.2)$$

The third model accounts for the battery relaxation effect which gives the battery the chance to recover the high current lost capacity. This model however, is very analytical and difficult to implement.

11.2 New Proposed Model

The new proposed model suggests that the remaining battery capacity depends on the present load current. Hence, the present battery capacity is calculated based on the

present load current and estimated runtime. The remaining capacity will be the difference between present capacity and total battery delivered energy.

$$C_{remain} = ti_{LOAD} - \int_0^t i_{total}(t)dt \qquad (11.3)$$

Where t is the runtime and is given by the reformulated equation (10.9). This new method can give the real time capacity estimation depending on the present load current and taking advantage of the variable exponent which leads to more accurate runtime calculations.

11.3 Results for Lead Acid Batteries

Runtime of constant load applications can easily be estimated because the load current and/or power are kept constant from start to finish. As is can been from   figure 11-1, at a constant discharge current of 0.45A, the 6.65Ah battery gives a runtime of 14.786 hours whereas at 7.2A the runtime drops to 0.396 hours and hence the delivered capacity is 2.854Ah.
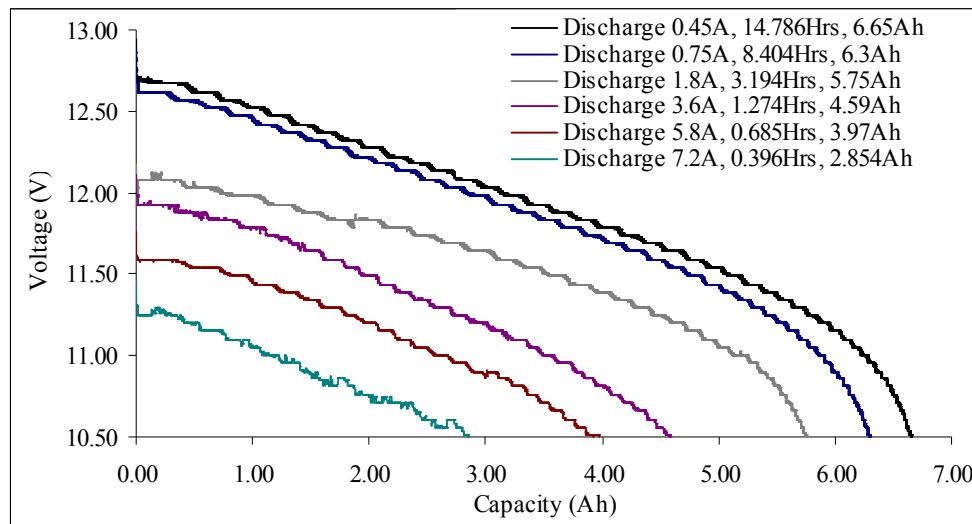
Figure 11-1: Constant Current Discharge Profile of 12V, 6.65Ah at 14.786Hrs Lead Acid Battery.

For applications where the load is unknown and unpredictable then runtime and remaining energy are more difficult to estimate. Models and techniques reviewed in section (11.1) use an average load current to do so. However, in many applications the question that arises after the battery delivers a certain amount of energy at various discharge currents (which makes the remaining battery capacity uncertain), for the next load current is how much runtime can be achieved. As shown in figure 11-2 and figure 11-8, and also reported in [1]-[3], when a battery is discharged at high discharge currents down to the end voltage then the battery is not completely drained as more energy can be supplied by the battery at lower discharge currents. Furthermore, it can be seen that the new or final current is the one that determines the remaining available energy.
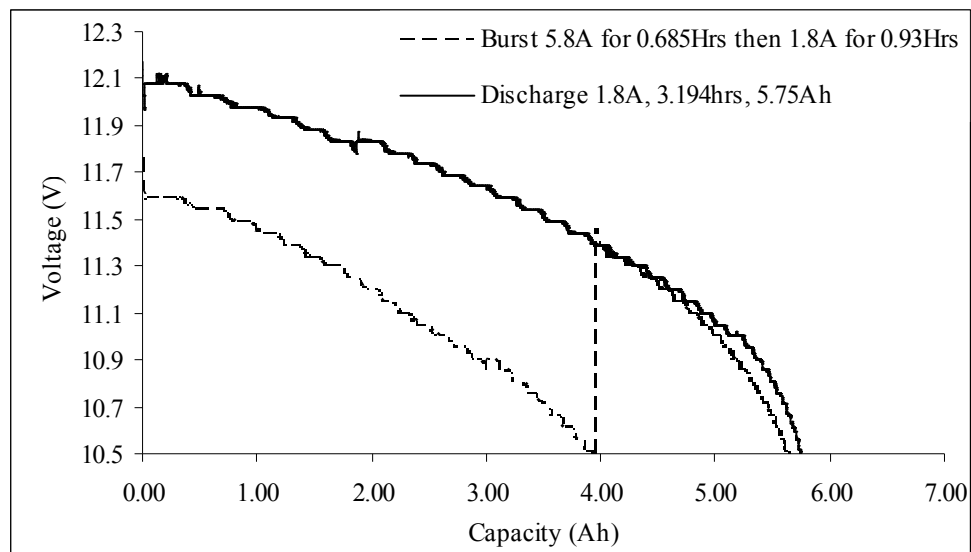
Figure 11-2: Burst Current at 5.8A and Then Constant Current Discharge at 1.8A.

The first battery under test to prove this point is a lead acid battery presented in section (10.4.5) characterized as a 6.65Ah at 14.786 hours with *a* and *b*-values equal to 1.2441 and -0.0776 respectively. In this experiment the battery was pulsed for 0.685 hours at 5.8A hence delivering 3.97Ah. Right after, it was discharged at a constant current of 1.8A for 0.93 hours. Therefore, the question to be answered here is the following; how

much energy can be obtained by pulsing this battery at 5.8A delivering 3.97Ah and then for the next current of 1.8A?

The methodology for the answer is as follows. Since the final current is 1.8A, then using equation (10.9) it can be found that for a constant discharge current of 1.8A the runtime is 3.03 hours and the total energy is 5.46Ah. Since, 3.97Ah has already been removed by pulsing at 5.8A this means that the remaining capacity is 1.49Ah and the runtime is 0.83 hours whereas the experimental results show a total energy of 1.67 Ah and runtime of 0.93 hours. The 12% difference between the results show a conservative approach to energy and runtime estimation for an application where the load is unpredictable and the average load current can not be calculated.
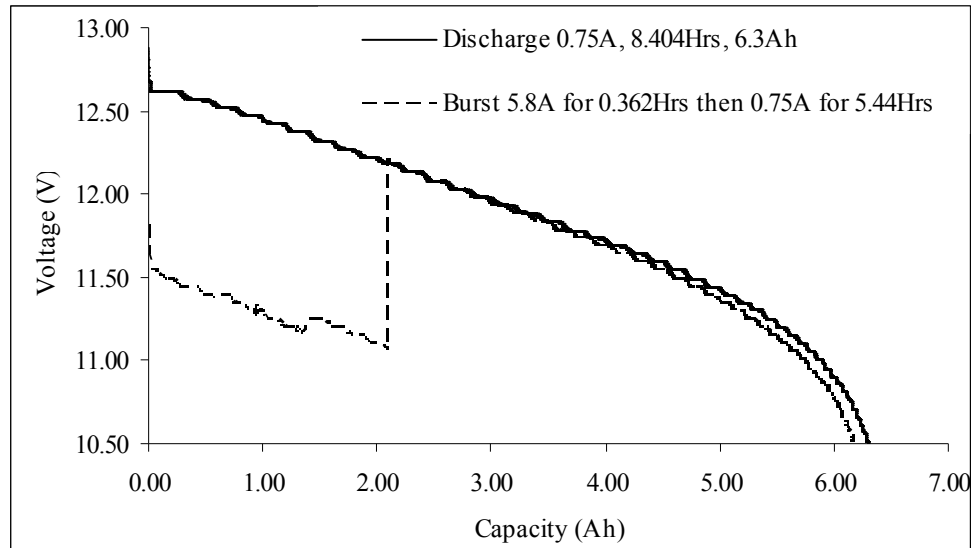
Figure 11-3: Burst Current at 5.8A and Then Constant Current Discharge at 0.75A.

In the second experiment of figure 11-3, the battery was pulsed to 5.8A for 0.362 hours and then discharged at a constant current of 0.75A. Hence, using equation 10.9 the runtime for 0.75A is calculated to be 8.54 hours with a total energy of 6.4Ah. Hence, after 2.1Ah delivered pulsed energy, the battery can still deliver 4.3Ah under a constant

load current of 0.75A. Experimental results give 4.08Ah. The 5.4% difference translates to a runtime difference of 17.6 minutes in 326.4 minutes (5.44 hours) operation.

In the third experiment of figure 11-4, the battery was pulsed to 3.6A for 0.81 hours and then discharged at a constant current of 1.8A. Hence, using equation 10.9 the runtime for 1.8A is calculated to be 3.03 hours with a total energy of 5.45Ah. Hence, after 2.92Ah delivered pulsed energy, the battery can still deliver 2.53Ah under a constant load current of 1.8A. Experimental results give 2.74Ah. The 8.14% difference translates to a runtime difference of 7.44 minutes out of 91.33 minutes (1.52 hours) of operation.
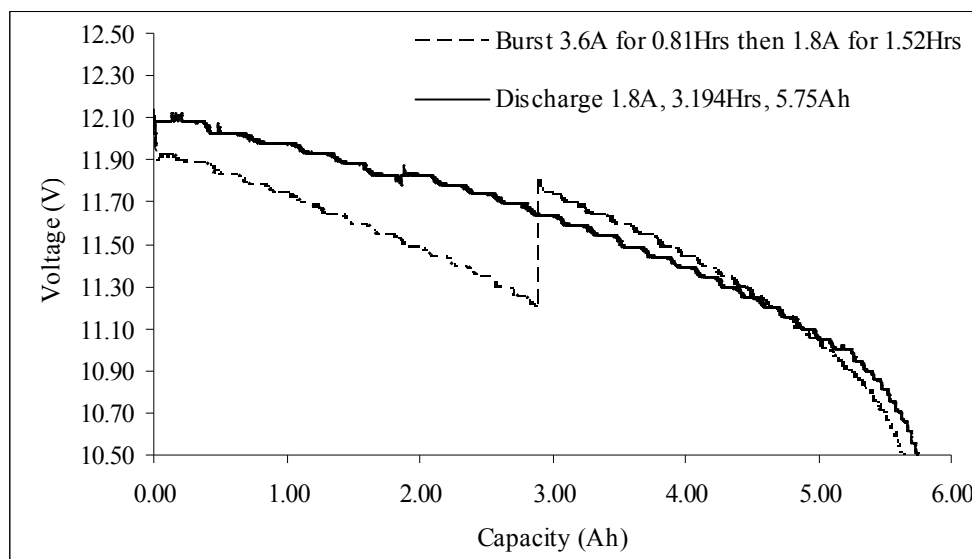
Figure 11-4: Burst Current at 3.6A and Then Constant Current Discharge at 1.8A.

11.4 Verification of the 0.5 Hour Test

To take this a step further, another lead acid battery was tested in the lab and it was characterized by a single test as 6.4Ah at the 14.22 hour rate. Then in order to determine the *a*-value the 0.5 hour test, proposed in section (10.5), was performed by discharging the battery between 0.9 and 1.1C or 5.76A and 6.4A respectively. Two experiments were performed and since the actual 0.5 hour discharge time was not achieved it was

extrapolated. Then by using equation 10.10 the *a*-values for the actual 0.4 and 0.6 hours were found as

$$a_{0.4Hrs} = \frac{\log(14.22) - \log(0.416)}{\log(6.4) - \log(0.45)} = 1.3303 \tag{11.4}$$

$$a_{0.6Hrs} = \frac{\log(14.22) - \log(0.582)}{\log(5.76) - \log(0.45)} = 1.2536 \tag{11.5}$$

By averaging the 0.4 and 0.6 hour values the 0.5 hour is found to be 1.2902. Hence, following the recommendations in section (10.5) *b* = -0.0667 and by substituting in equation 10.9 the runtime and remaining energy of this battery can be estimated by:

$$t = 14.22 \left(\frac{0.45}{I} \right)^{1.2902 - 0.0667 \ln\left(\frac{6.4}{I} \right)} \tag{11.6}$$
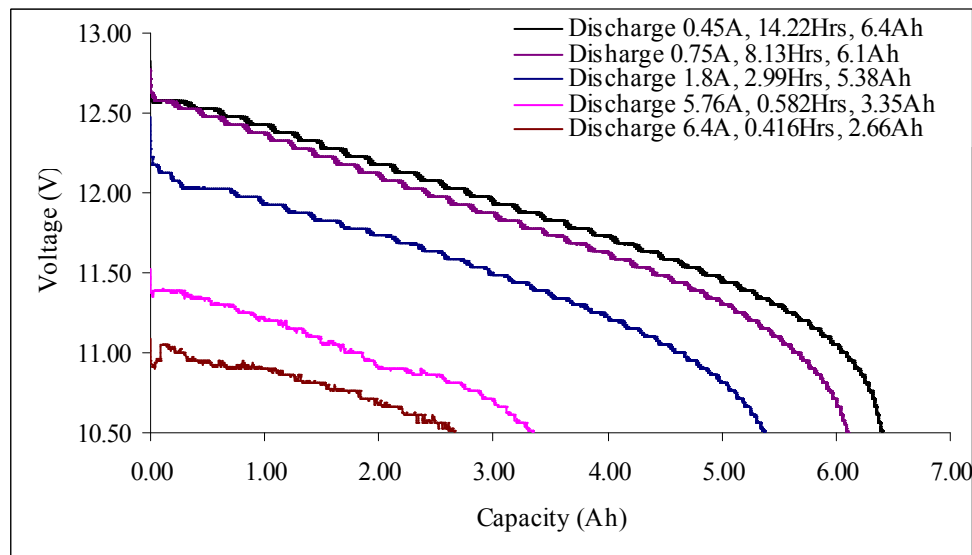
Figure 11-5: Discharge Characterization of 6.4Ah at 14.22Hrs Rate Lead Acid Battery.

By comparing the accuracy of this equation with the experimental values shown in figure 11-5 at a constant discharge current of 0.75A, the estimated runtime is calculated as 7.91

167

hours indicating a 2.78% difference from the experimental runtime; at 1.8A the estimated runtime is 2.67 hours with a 11.82% difference from the experimental runtime; at 5.76A the estimated runtime is 0.54 hours with a 7.78% difference from the experimental runtime and at 6.4A the estimated runtime is 0.463 hours with a 9% difference from the experimental runtime.

The multi-pulsing discharge scenario applied to this battery is presented in figure 11-6 was as follows: 0.75A for 0.33 hours, 7.6A for 0.07 hours, 1.8A for 0.42 hours, 5.4A for 0.19 hours, 7.2A for 0.1 hours, 0.75A for 0.33 hours, 1.8 for 0.18 hours, 3.6 for 0.17 hours, 1.8A for 0.42 hours and finally 0.75A for 0.73 hours. The same methodology, as that in section (11.3), applied with a final current of 0.75A gave a maximum estimated energy of 5.94Ah and a total delivered pulsed energy of 5.35Ah. Hence, this method suggests that after the described pulsing scenario then at a final discharge current of 0.75A runtime it can continue for 0.887 hours whereas the experimental results show a runtime of 0.973 hours and a 9.73% difference.
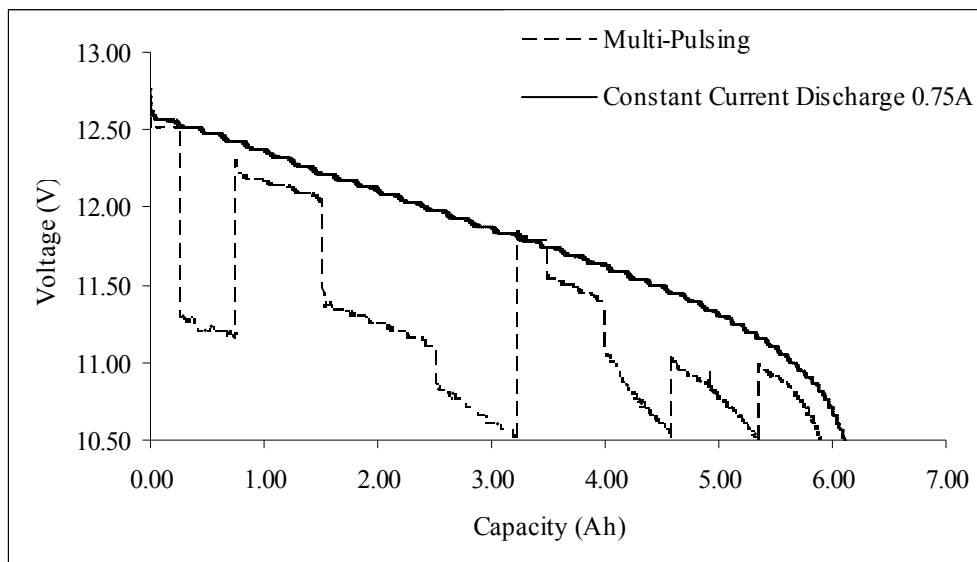
Figure 11-6: Multi-Pulsing and Then Constant Current Discharge at 0.75A.

168

Similar pulsing scenario is presented in figure 11-7 with the difference that the final load current is 1.8A. The pulsed energy delivered is 4.58Ah whereas the maximum possible energy for a 1.8A discharge current is 4.81Ah. Hence, this method suggests that after the described pulsing scenario at a final discharge current of 1.8A the runtime can continue for 0.128 hours (7.73 minutes) whereas the experimental results show a runtime of 0.42 hours (25.2 minutes). The big deviation between experimental and estimated results is contributed to battery relaxation effects between pulses.

The multi-pulsing discharge scenario used on this battery is presented in figure 11-8, as follows: 0.75A for 0.33 hours, 7.6A for 0.07 hours, 1.8A for 0.42 hours, 5.4A for 0.19 hours and finally 7.2A for 0.1 hours. The same methodology, presented in section (11.3), was applied with the final current of 7.2A and produced a maximum estimated energy of 2.8Ah and a total delivered pulsed energy of 2.5Ah. Hence, this method suggests that by applying this pulsing scenario at a final discharge current of 7.2A the runtime can continue for 2.5 additional minutes whereas experimental results show runtime of 6 minutes.
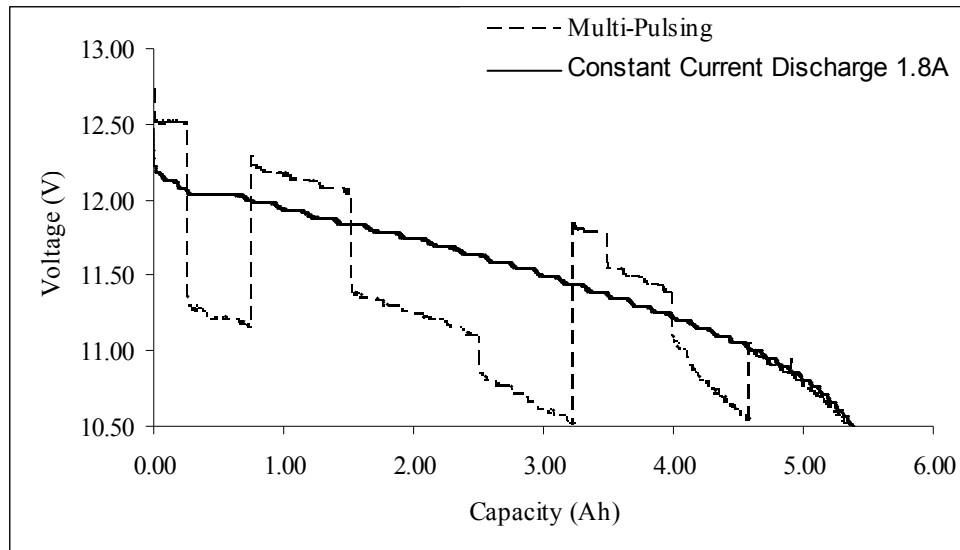
Figure 11-7: Multi-Pulsing and Then Constant Current Discharge at 1.8A.
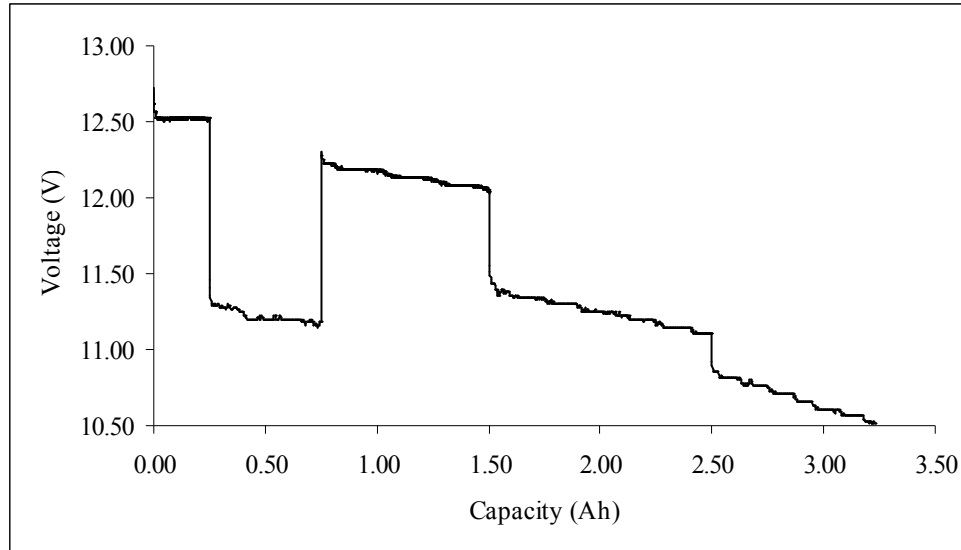
Figure 11-8: Multi-Pulsing Scenario.

In the case of multi-pulsing scenarios presented in fugures 11-6 to 11-8, the experimental results show higher runtimes by a few minutes than those estimated. This deviation is due to battery relaxation effects. A commercial battery discharger was used that required the experiment to be stopped between pulses for the results to be saved and the new settings to be adjusted. Every pause was no longer than 1 minute but for runtimes in the range of 6 minutes the relaxation contributed increased battery runtime of 2-3 minutes giving an error of 100%. This effect was insignificant for the single pulsing presented in figures 11-2 to 11-4. Nine pauses were required for the multi-pulsing of figure 11-7 and four for the multi-pulsing of figure 11-8.

11.5 Results for Lithium Batteries

The lithium battery under test was first discharged under constant discharge current of 0.93A; the runtime was 0.95 hours with 0.88Ah total energy delivered. Then the same battery was fully charged in one hour and then discharged with a burst current of 4.65A for 0.085 hours and then discharged to the end of voltage with a constant current of 0.93A.
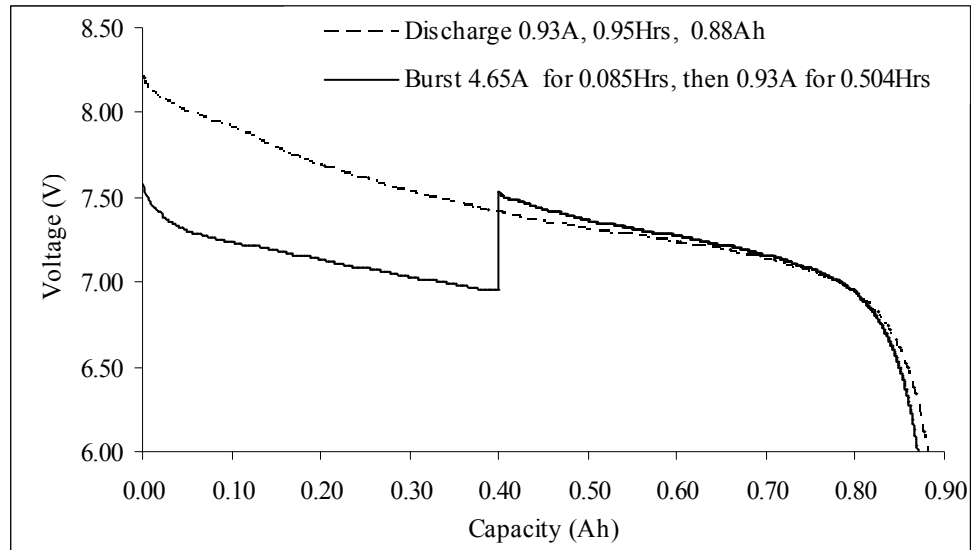
Figure 11-9: Burst Current at 4.65A and Then Constant Current Discharge at 0.93A.

At a discharge current of 0.93A, from section 10.6, the runtime and energy is estimated to be 0.964 hours and 0.897Ah respectively. Hence, with a removed pulse energy of 0.395Ah it is estimated that at a 0.93A discharge current the runtime is 0.54 hours with 7% difference from the experimental results.

11.6 List of References

[1]   Sung Park, Andreas Savvides and Mani B. Srivastava, "Battery Capacity Measurement and Analysis using Lithium Coin Cell battery", Low Power Electronics and Design, International Symposium on, 6-7 Aug. 2001 Page(s):382 – 387.

CHAPTER 12. OPTIMIZED ENERGY AND POWER SOLUTIONS

12.1 Introduction

In chapters 3 to 5 a comparative analysis of several commercially available energy and power sources was carried out, resulting in proposed solutions to a number of different applications. In this chapter, the aforementioned solutions are compared with the configurations proposed by the optimization algorithm described in chapter 6. It should be noted that the optimization algorithm has a larger product database and takes into account losses in the DC to DC conversion and the loss of battery capacity due to high discharge currents, both of which were not taken into account in the analysis in chapters 3 to 5. Additionally an investigation is carried out on the effect of changing the operating voltage on the application energy and the suggested solutions.

12.2 Aero-Modeling Application 325W, 11.1V and 1.3Kg

Chapter 4 deals with a comparative analysis of energy and power systems that are used in specialized applications such as aero-modeling with design requirements and restrictions specified by power, operating voltage and payload. Thirteen solutions are suggested and their characteristics are summarized on table 4-1 where for the lowest and highest listed energies the runtime is estimated to be between 0.548 and 0.711 hours, respectively.

Hence the input user parameters for the optimization calculations, also shown in figure 12-1 are 325W power, 11.1V operating voltage, 0.548 hours runtime and 1.3Kg payload. In addition, because cost, weight and runtime are equally important the same weight factor of 0.5 is given to each (for the same positive real number weight factors as inputs, the score is unaffected). In addition, the system voltage tolerance is 10% which indicates that DC to DC conversion is not required when the power system voltage is between 11.1

and 12.21V. As explained in see section 6.2.2 (DC to DC Conversion Modeling) it is not desirable for the power system to have a voltage lower than 11.1V because in that case a higher current will be delivered thus reducing runtime. Finally, improved runtime accuracy is achieved when user input parameters include a DC to DC converter.
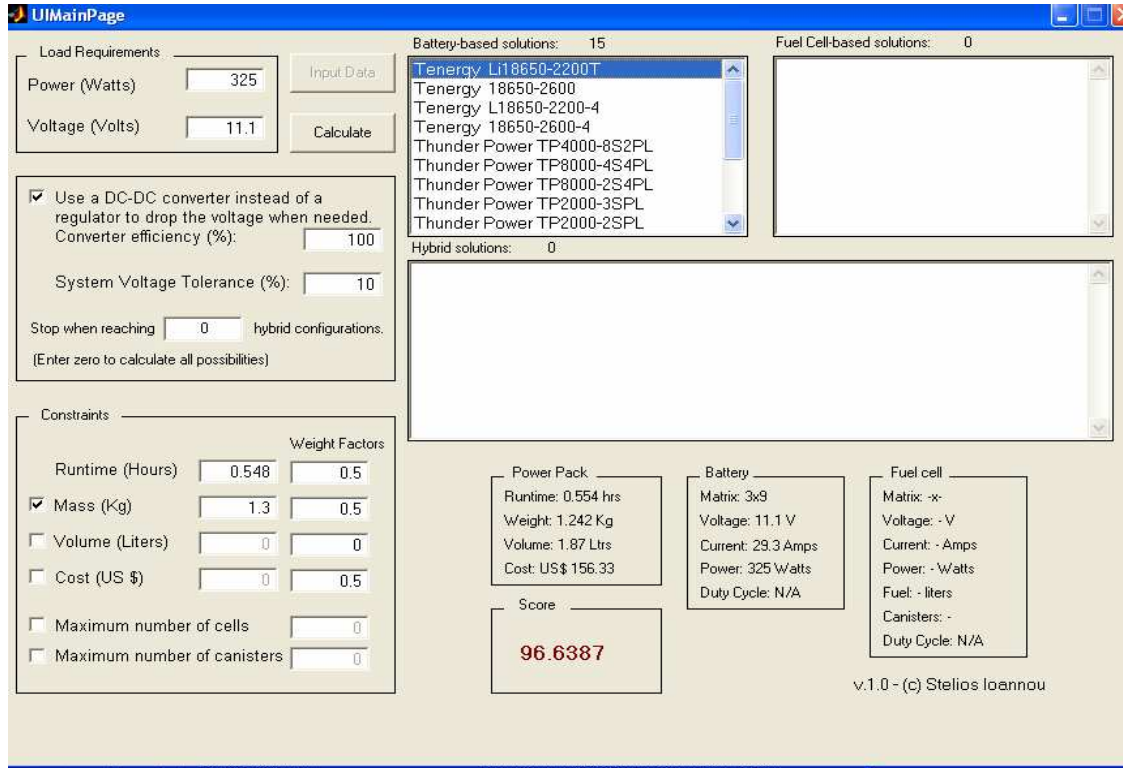
Figure 12-1: User Interface With Input Parameters and Output Results.

With the aforementioned user input parameters, 15 optimized solutions are summarized on table 12-1. As can be seen in the table, the best output based on runtime, cost and weight is provided by the Tenergy Li18650-2200T with 0.554 hours, $156.33 and 1.242Kg, respectively. The same pack is listed in table 4-1 with a total energy of 229Wh when using the linear approach. By including the loss of capacity at higher discharge currents, a more conservative and accurate energy of 180Wh is obtained from table 12-1. For the same reasons several products listed in table 4-1 are not part of the optimized

solutions listed in table 12-1. Since the required weight to meet the designed runtime exceeded the payload capability those solutions were rejected by the optimization algorithm.

Table 12-1: List of Optimized Solutions for 325W, 11.1V, 0.548 Hours and 1.3Kg

Score	Brand / Model	Voltage (Volts)	Matrix s x p	Total Weight (Kg)	Runtime (Hrs)	Total Price US$	Volume (Ltrs)	Duty Cycle %
96.64	T/Li18650-2200T	11.1	3 x 9	1.242	0.554	156.33	1.87	Na
90.62	T/18650-2600	11.1	3x8	1.104	0.584	239.76	1.61	Na
90.10	T/Li186502200-4	14.8	1x7	1.187	0.576	216.65	0.652	75
75.68	T/18650-2600-4	11.1	3x8	1.104	0.584	767.04	1.61	Na
73.58	TP4000-8S2PL	29.6	1x2	1.244	0.601	699.90	0.735	38
73.52	TP8000-4S4PL	14.8	1x2	1.266	0.601	659.90	0.74	75
72.75	TP8000-2S4PL	14.8	2x2	1.28	0.601	699.90	0.742	75
71.86	TP2000-3SPL	11.1	1x10	1.2	0.56	729.50	0.65	Na
71.83	TP2000-2SPL	14.8	2x8	1.28	0.601	799.20	0.676	75
71.82	TP2000-4SPL	14.8	1x8	1.28	0.601	799.60	0.65	75
71.82	TP4000-2S2PL	14.8	2x4	1.28	0.601	799.60	0.87	75
71.29	TP6000-5S3PL	18.5	1x2	1.254	0.56	659.90	0.748	60
71.09	TP4000-5S2PL	18.5	1x3	1.248	0.56	689.85	0.778	60
69.96	T/Li186502200-4	11.1	3x9	1.242	0.554	782.73	1.81	Na
69.86	TP4000-3S2PL	11.1	1x5	1.275	0.56	749.75	0.786	Na

T – Tenergy, TP – Thunder Power

Since runtime is inversely proportional to discharge current then, as expected at higher voltage and fixed power, the discharge current decreases and therefore the runtime increases. Higher runtimes listed in table 12-1 are achieved by solutions that use DC to DC conversion. However, higher costs and weights associated with these solutions yield lower scores. With a more realistic DC to DC converter efficiency of 90%, then all the solutions that require the use of a voltage converter do not meet the design criteria and are rejected by the algorithm. Because of the application criticality and strict payload capability, a 10% discharge current increase can make the difference between accepting or rejecting a solution. These sorts of calculations and options are much more difficult to implement using Microsoft Excel.
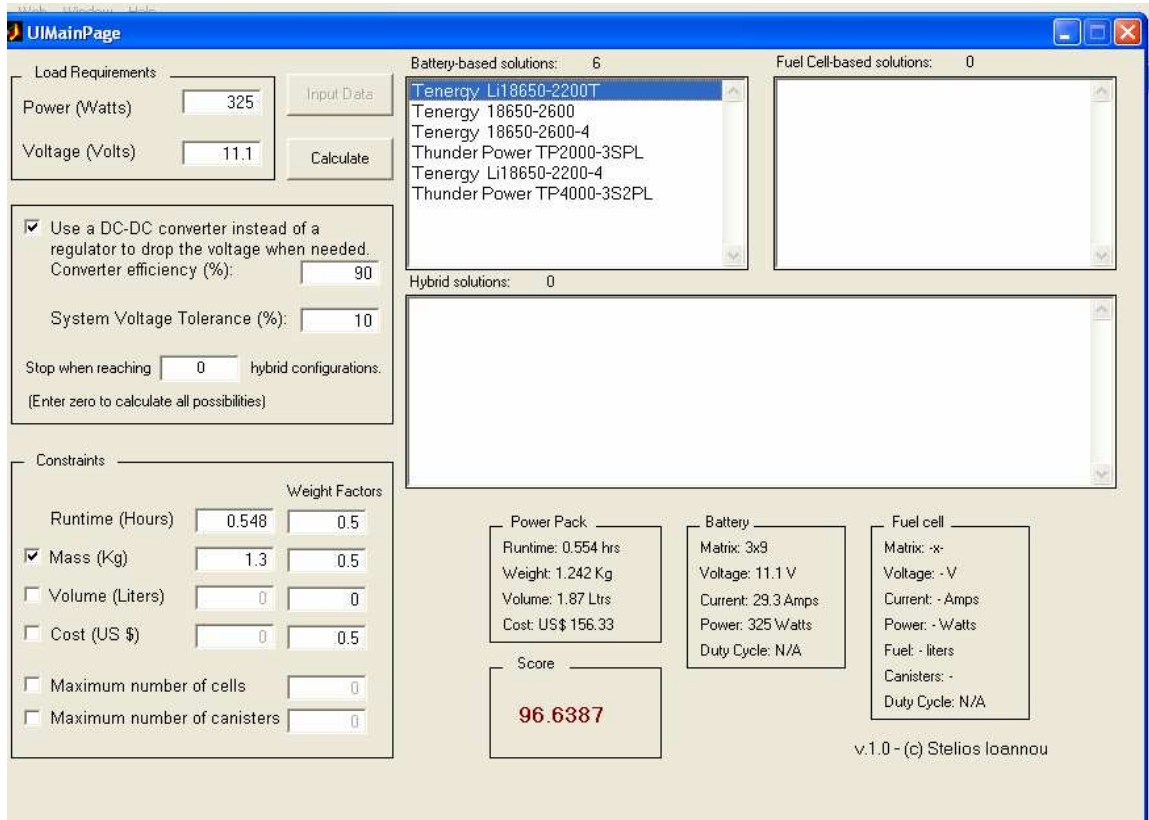
Figure 12-2: User Interface With 90% DC-DC Converter Efficiency.

Table 12-2: List of Optimized Solutions for 325W, 11.1V, 0.548 Hours, 1.3Kg and 90% DC-DC Converter Efficiency

Score	Brand / Model	Voltage (Volts)	Matrix s x p	Total Weight (Kg)	Runtime (Hrs)	Total Price US$	Volume (Ltrs)	Duty Cycle %
96.64	T/Li18650-2200T	11.1	3 x 9	1.242	0.554	156.33	1.87	Na
90.62	T/18650-2600	11.1	3x8	1.104	0.584	239.76	1.61	Na
75.68	T/18650-2600-4	11.1	3x8	1.104	0.584	767.04	1.61	Na
71.86	TP/TP2000-3SPL	11.1	1x10	1.2	0.56	729.50	0.65	Na
69.96	T/Li186502200-4	11.1	3x9	1.242	0.554	782.73	1.81	Na
69.86	TP/TP40003S2PL	11.1	1x5	1.275	0.56	749.75	0.786	Na

T – Tenergy, TP – Thunder Power

175

The low payload constraint is the reason that fuel cell or hybrid solutions were not proposed for this application. If the payload load could be increased to 2Kg, then 68 hybrid solutions would also be made available with the highest score solution composed of a battery pack (3x8 Tenergy 18650-2600-4) and the MesoPower fuel cell (by Mesoscopic Devices).

12.3 ATRV-Jr Application 10 Hour, 180W, 24V, 25Kg

In Chapter 5 a comparative analysis was presented when the ATRV-Jr was powered with lead acid and lithium batteries in a hybrid system. The recommendations and comparisons were based on a 180W required power, 10 hour desired runtime and limited battery and fuel cell product list. In this section all the suggested energy and power sources are compared with the optimization algorithm suggested solutions.

Table 12-3: List of Battery Optimized Solutions for 180W, 24V, 10 Hours and 25Kg

Score	Brand / Model	Voltage (Volts)	Matrix s x p	Total Weight (Kg)	Runtime (Hrs)	Total Price US$	Volume (Ltrs)	Duty Cycle %
92.69	T/Li18650-2200T	25.9	7x33	10.63	10.3	1337.49	16	Na
91.88	T/Li18650-14.6V4400BL	29.6	2x13	8.845	10	15559.74	4.58	81
91.08	T/Li186502200-4	29.6	2x26	8.82	10	1609.40	4.84	81
86.67	T/Li18650-2600	25.9	7x28	9.02	10.4	1958.04	13.2	Na
86.54	T/PL-787285	25.9	7x6	9.53	10.9	1995.00	4.36	Na

T – Tenergy, TP – Thunder Power

For this application there are a total of 5108 optimized solutions; 92 battery solutions, 11 fuel cell and 5005 hybrid solutions. The VL45E cell by Saft that was the suggested solution in section 5.6, is now listed as the 23rd choice with a 70.15 score, 13.8 hours runtime, 14.98Kg weight and $6804.00 cost whereas from table 12-3 the highest score is 92.69. On the other hand the solution with the highest scores requires a matrix of 7x33 which translates to a total of 231 cells. A similar pattern is observed with all of the first 5 choices. Hence to keep the design complexity simple the number of cells will be limited to a total of 21, as shown in figure 12-3 and the results are summarized in table 12-4.

Comparing the optimized solutions with the highest scores, T/Li18650-2200T from table 12-3 and T/PL7521223 from table 12-4 it can be noticed that the system simplicity came at the expense of the weight and cost.   In the T/Li18650-2200T case the weight is 10.63Kg and the cost is $1337.49 while in the T/PL7521223 case the weight is 13.65Kg and the cost is $2519.79.   On the other hand, the simpler solution offers 4% higher runtime. This is always a trade off that depends on user input parameters. The algorithm can carry out the tedious calculations but the user will have to make the final decision on which option to choose.

Table 12-4: List of Battery Optimized Solutions With Number of Cells Constraint

Score	Brand / Model	Voltage (Volts)	Matrix s x p	Total Weight (Kg)	Runtime (Hrs)	Total Price US$	Volume (Ltrs)	Duty Cycle %
88.43	T/PL7521223	25.9	7x3	13.65	10.7	2519.79	7.45	Na
87.85	T/ PL9521223	25.9	7x3	21	15.5	3569.79	9.52	Na
87.67	T/ TEN7872185	29.6	2x2	14.4	14.5	3999.90	7.16	81
87.51	T/ PL13212223	25.9	7x2	19.6	14.7	3359.86	9.02	Na
80.60	TP/8000-5S4PL	37	2x6	9.48	10.6	4799.40	5.66	65

T – Tenergy, TP – Thunder Power
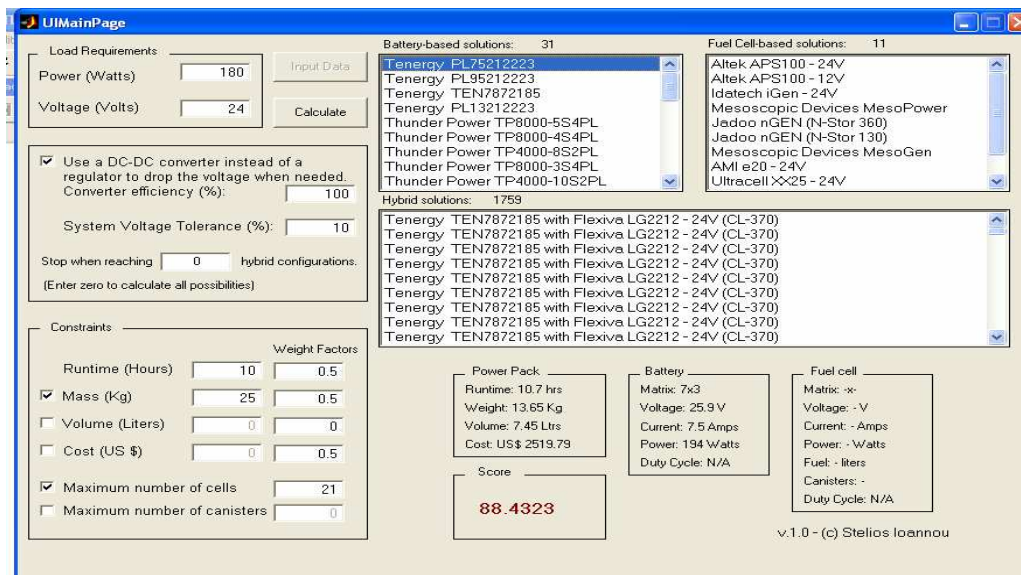
Figure 12-3: User Interface Including Maximum Number of Cells Restriction.

As seen from figure 12-3, with the maximum number of cells restricted to only 21 the battery and hybrid solutions decreased to 31 and 1759 respectively; the fuel cell solution are not affected. In addition, it should be noted that with 180W load power and 24V voltage the load current is 7.5A. The optimization algorithm sizes the power system to deliver the required load current. Furthermore, in this case because the battery pack voltage is within the design voltage tolerance of 10%, no DC to DC converter is used. As a result the battery system is listed as contributing 194W from which 7.92% of the energy is dissipated as heat.

The top five fuel cell solutions are summarized in table 12-5. It is worth noting that in the fuel cell solutions presented if the fuel is in liquid or solid form then the exact runtime can be achieved. While if the fuel is compressed H_2 then, since the number of canisters is rounded up, higher runtimes can be achieved. For example the Idatech iGen unit uses liquid methanol whereas Jadoo devices use H_2.

Table 12-5: List of Fuel Cell Optimized Solutions With Number of Cells Restriction

Score	Brand / Model	Voltage (Volts)	Matrix s x p	Total Weight (Kg)	Runtime (Hrs)	Total Price US$	Volume (Ltrs)	Fuel
66.67	A/ APS100 (24V)	24	1x1	7.93	10	na	Na	5.9Kg
62.15	I / iGen (24V)	24	1x1	12.96	10	10000	35	5L
60.14	MD / MesoPower	24	2x5	9.87	10	na	13.1	1.6L
57.23	J/nGen NStor 360	24	2x1	18.51	10.8	12092	9.66	6cans
54.40	J/nGen NStor 130	24	2x1	19.15	10.4	14182	10.4	16can

A – Altek, I – Idatech, MD – MesoScopic Devices and J – Jadoo

In the case of hybrid systems the first solution is a system composed of the Tenergy TEN7872185 battery pack and the Flexiva LG2212-24V fuel cell. The system characteristics are as follows: 77.38 score, 15.9 hours runtime, 19.46 Kg weight, 19.7 liters volume and $7899.80 price.

The hybrid power system individual contributions can be observed in figure 12-4. The battery pack contributes 165W with a matrix of 2x10, voltage of 44.4V and a DC to DC

converter duty cycle of 54% whereas the fuel cell contributes 15W, 24V and uses one H_2 canister of 370 Liters.

Figure 12-4 verifies that the algorithm output results are correct. For optimum conditions a fuel cell runs at rated power, hence the fuel cell produces a current of 0.625A (15W/24V). However, the current contributed by the battery pack is more difficult to calculate because of the higher voltage that is required due to the use of a DC to DC converter. On the battery side the voltage is 29.6V and the current is 5.57A whereas after the DC to DC converter the voltage is 24V (29.6*Duty Cycle of 81%) and the current translates to 6.87A. Hence, the load current is the sum of the battery and fuel cell current contributions which comes to 7.50A.
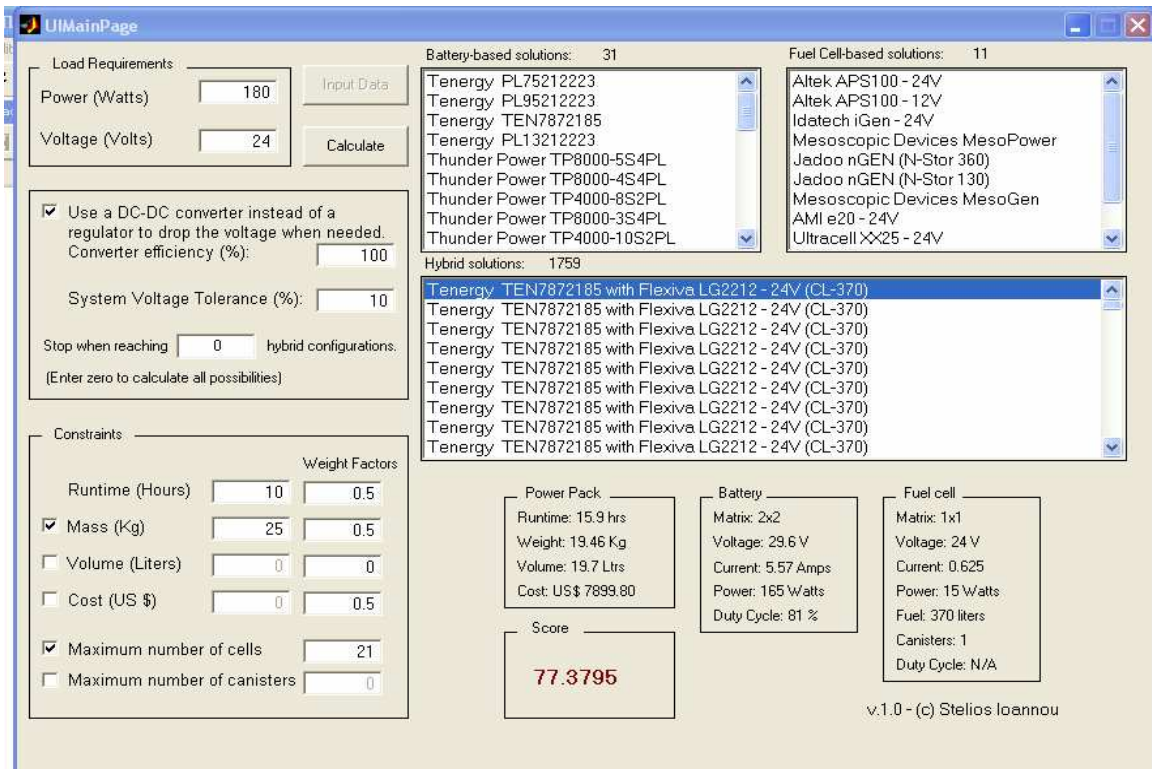
Figure 12-4: Hybrid System Power Contributions.

12.4 Voltage Effects on Suggested Solutions for the 20 to 100W Power Range

In Chapter 3 products were analyzed and compared for the purpose of determining the most optimum solution for mobile applications with only the required energy known. Optimum was defined as the maximum runtime, which is directly proportional to energy, with the least possible weight. A linear approach was followed where the effect of capacity loss at high discharge currents was ignored. Furthermore, with the load voltage and power unknown it was assumed 100% efficiency for DC-DC conversion and the effect of step down voltage conversions were also ignored (see section 6.2.2 - DC to DC Conversion Modeling). Microsoft Excel was used and hybrid systems could not be configured and compared.

The main purpose of this section is to show how the optimized solutions are affected from variations in operating voltage and hence discharge current. The total amount of energy without specifying power or voltage is not a good measure for properly sizing and selection of an energy and power system. Primary batteries are not included in the analysis. User input parameters will include power of 20 and 100W and runtimes between 24 and 240 hours. Constraints will change based on the energy requirements. For the 480Wh application the weight is constraint is only 3.2Kg whereas for 4800Wh it is 10Kg. The maximum number of cells is limited to 27 and the DC to DC converter efficiency is 100%.

12.4.1 Mobile Applications of 480Whr

For the 480Whr energy application only 20W power at operating voltages of 5, 12 and 24V are investigated and the results are presented in figures 12-5 to 12-7. As it can be seen, by changing the operating voltage the suggested optimized solutions change. First, for the 5V voltage presented in figure 12-5, there are 38 battery solutions, 0 fuel cell solutions and 0 hybrid solutions, whereas for the 12V voltage presented in figure 12-6, there are 37 battery solutions, 3 fuel cell solutions and 84 hybrid solutions and finally for the 24V voltage presented in figure 12-7, there are 27 battery solutions, 3 fuel cell

solutions and 0 hybrid solutions. Furthermore, not only the number of available solutions change but also the order and scores; from figure 12-5 at 5V, Tenergy PL68135170 has a 106.27 score followed by Tenergy PL7872185 having a 104.88 score, whereas from figure 12-6 at 12V the order of the first two batteries are reversed with Tenergy PL7872185 having a 91.39 score followed by Tenergy PL68135170 with a 88.48 score. Finally, at 24V presented in figure 12-7 Tenergy PL68135170 is the 18th choice with a 87.76 score whereas the Tenergy PL7872185 has the highest score of 102.52.
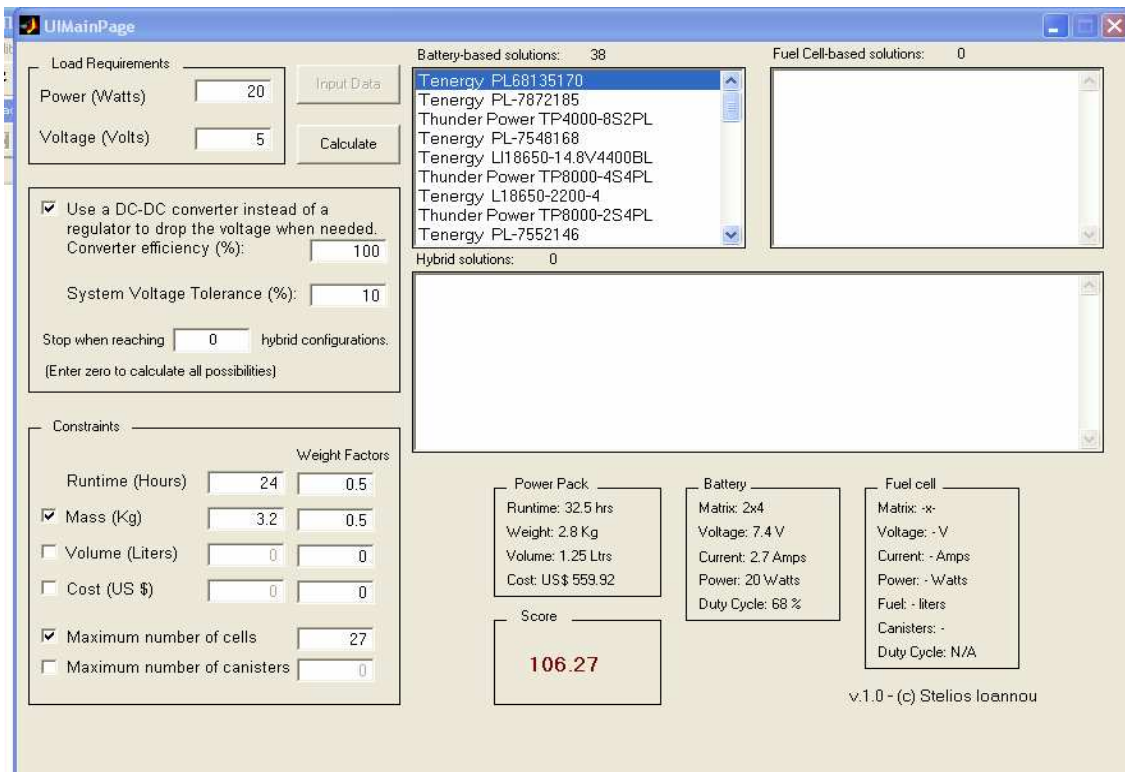
Figure 12-5: Optimized Solutions for 20W, 24 Hours and 5V Application.

Results presented in figures 12-5 to 12-7 demonstrate that the algorithm output results are correct. In figure 12-5 the battery voltage is 7.4V which is 67.7% higher than the load voltage; hence the DC to DC converter duty cycle is 68% rounded up. The load current

181

is 4A whereas the battery contributed current is lower by 68% which comes to 2.72A. Once again the difference is less than 1% due to the rounding of the displayed numbers.

From figure 12-6 the hybrid configuration results can be verified with a design voltage of 12V. The AMI e20 fuel cell with an output voltage of 24V requires a DC to DC converter duty cycle of 50% whereas the battery pack at 15.4V requires a 78% duty cycle. Hence, the fuel cell and battery contributed currents are 1.666 and 0.002A which total 1.668A and 20.002W. This simulation identifies an extra feature to be added to the optimization algorithm. The suggested hybrid solution is mathematically correct but it is not practical and wise to have additional equipment that only contribute one thousandth of the required power. Hence, in this application only the fuel cell system is required to supply the load power.
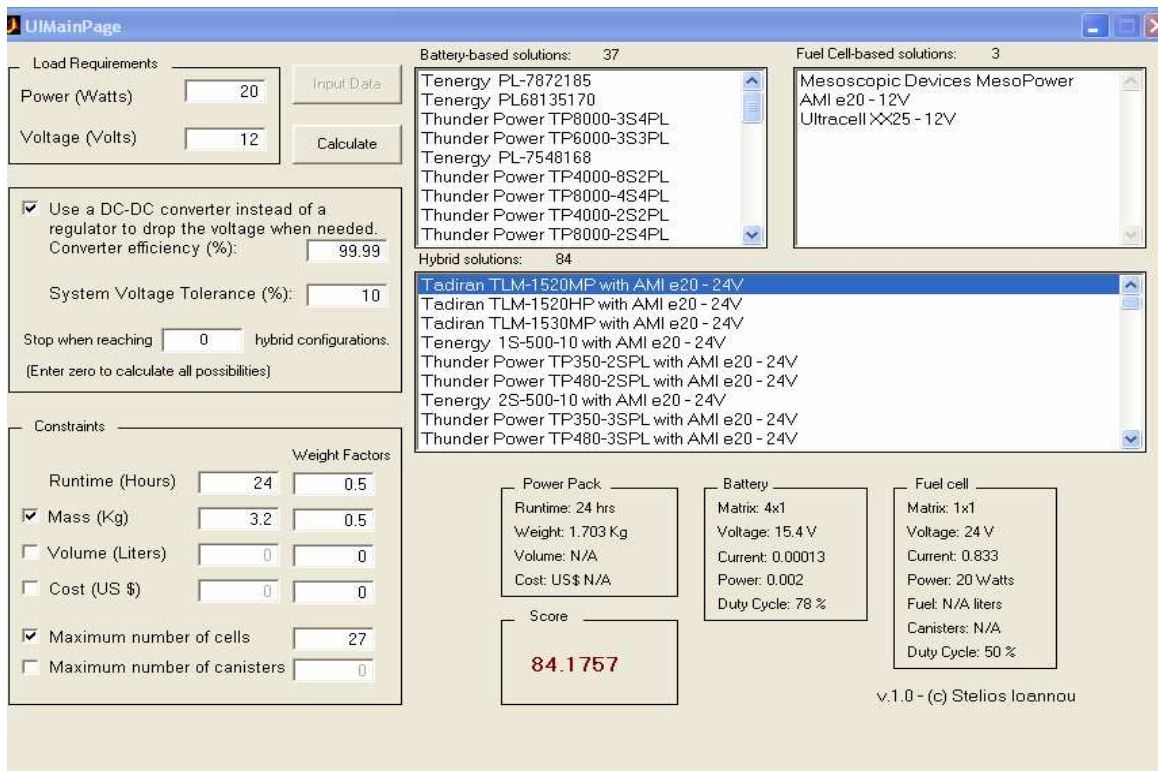
Figure 12-6: Optimized Solutions for 20W, 24 Hours and 12V Application.
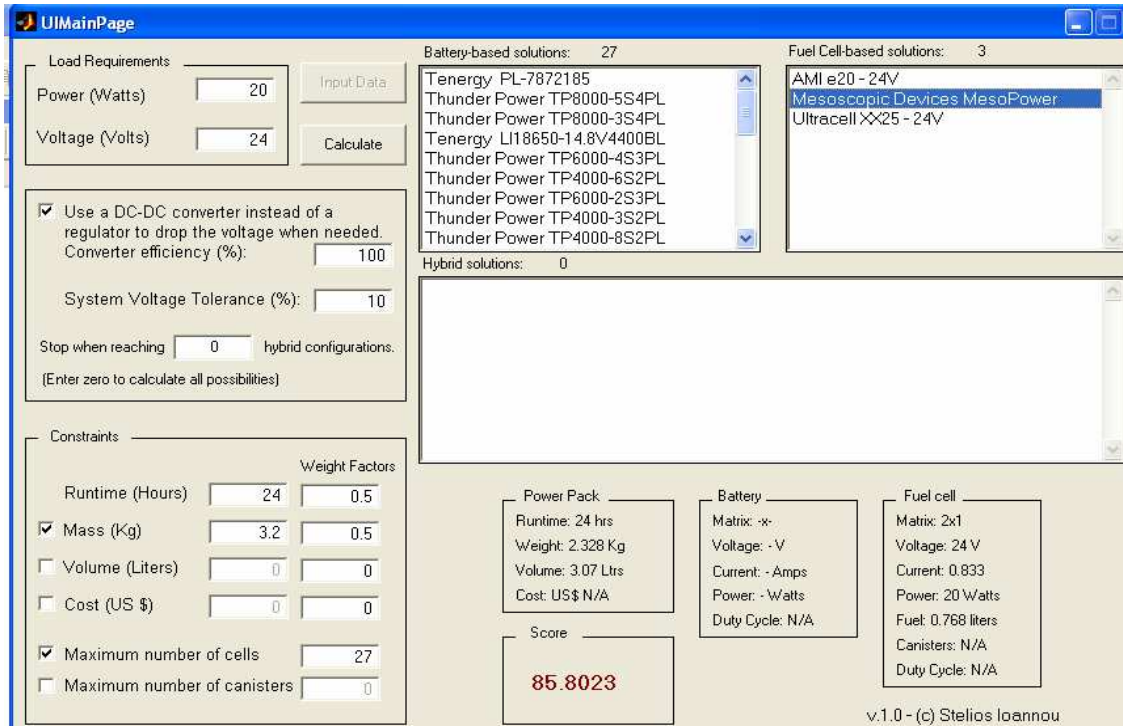
Figure 12-7: Optimized Solutions for 20W, 24 Hours and 24V Application.

12.4.2 Mobile Applications of 4800Wh

For the 4800Wh energy application, investigated powers are 20W and 100W at operating voltages of 5, 12 and 24V. The results are presented in figures 12-8 to 12-13.

12.4.2.1 Mobile Applications 20W and 240 Hours

As expected for 240 hour runtime results presented in figures 12-8 to 12-10, there are no battery solutions that meet the design criteria, since the best battery solution requires a 20Kg total weight. Furthermore, for a 240 hour operation, which is equivalent to ten days, the battery self discharge must also be taken into consideration when the runtime is calculated.
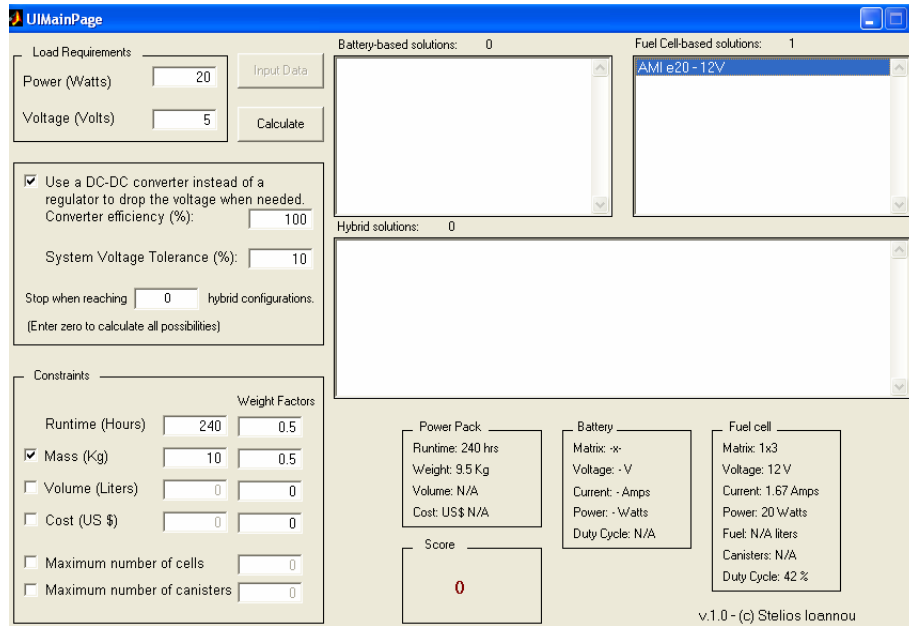
Figure 12-8: Optimized Solutions for a 20W, 240 Hours and 5V Application.
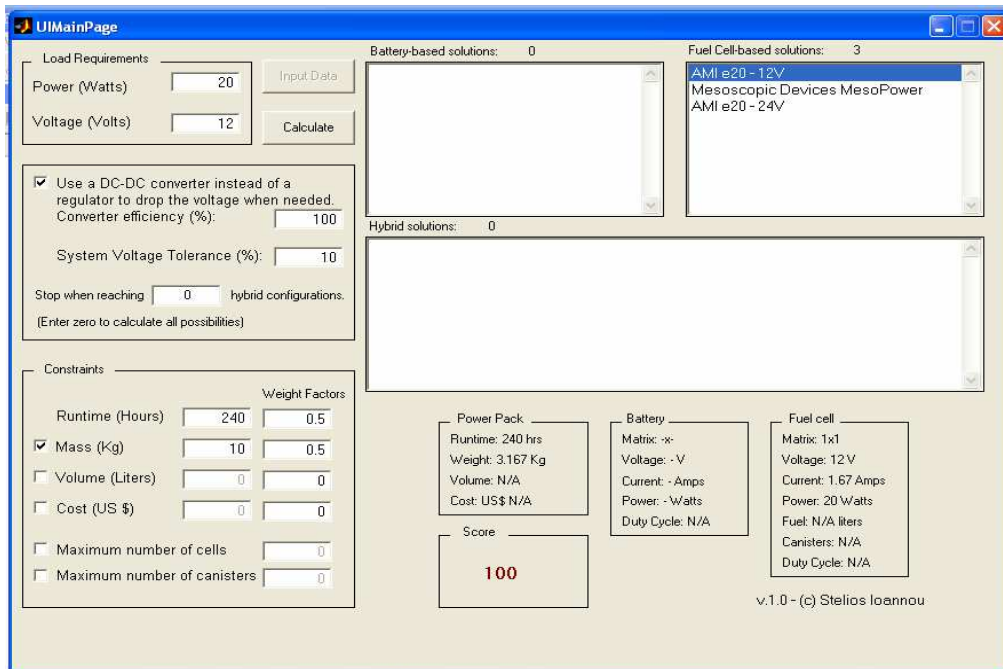
Figure 12-9: Optimized Solutions for a 20W, 240 Hours and 12V Application.

From figure 12-8 it can be seen that only one fuel cell can meet the application criteria with a total weight of 9.5Kg. The score for this solution is shown as zero because only one solution is available and there is no comparative data, however, from figure 12-9 where three solutions are available corresponding scores are provided.

It is worth noting from figures 12-8 to 12-10 that at higher operating voltages less weight is required to meet the mission requirements. This is because lower load currents and hence less fuel is required.

The calculated scores are verified using the suggested optimized solutions for the 24V application presented in figure 12-10 and the results tabulated in table 12-6. The 24V fuel cell system e20 by AMI earns the highest score of 100 followed by the 12V fuel cell systems e20 and MesoPower that require two series connected units to meet the design voltage hence earning the lower scores of 75 and 70.31 respectively.
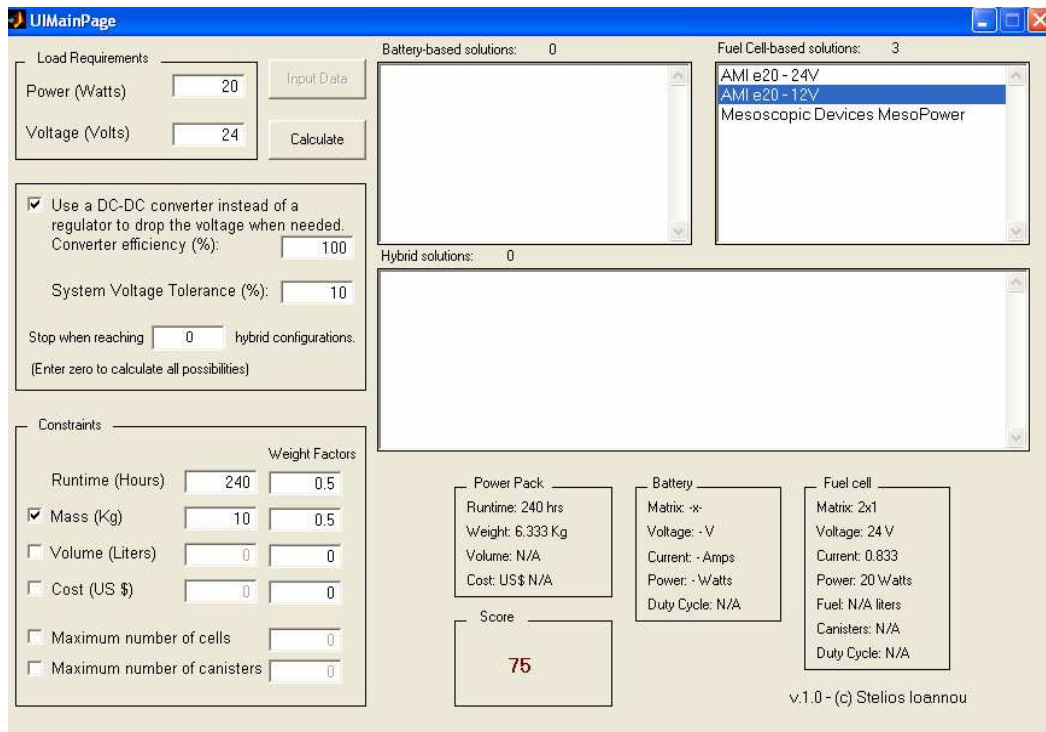
Figure 12-10: Optimized Solutions for 20W, 240 Hours and 24V Application.

Score	Brand / Model	Voltage (Volts)	Matrix s x p	Total Weight (Kg)	Runtime (Hrs)
100	AMI / e20-24V	24	1x1	3.167	240
75	AMI / e20-12V	12	2x1	6.333	240
70.31	MD / MesoPower	12	2x1	7.796	240

From table 12-6 all solutions offer 240 hour runtime whereas the maximum and minimum required weights are 3.167Kg and 7.796Kg respectively. Furthermore, the user input parameters weights for runtime, weight, volume and cost are 0.5, 0.5, 0 and 0 respectively. Therefore, using equation (6.7) the scores are calculated as follows:

$$score_1 = \frac{100}{0.5+0.5}\left[\frac{(0.5)(240)}{240} + \frac{(0.5)(3.167)}{3.167} + \frac{0(\min v_j)}{v_j} + \frac{0(\min c_j)}{c_j}\right] = 100$$

$$score_2 = \frac{100}{0.5+0.5}\left[\frac{(0.5)(240)}{240} + \frac{(0.5)(3.167)}{6.333} + \frac{0(\min v_j)}{v_j} + \frac{0(\min c_j)}{c_j}\right] = 75$$

$$score_3 = \frac{100}{0.5+0.5}\left[\frac{(0.5)(240)}{240} + \frac{(0.5)(3.167)}{7.796} + \frac{0(\min v_j)}{v_j} + \frac{0(\min c_j)}{c_j}\right] = 70.31$$

Therefore, this is a validation that the algorithm works as expected.

12.4.2.2 Mobile Applications 100W and 48 Hours

The effects of operating voltage on suggested solutions are observed from the results represented in figures 12-11 to 12-13. At a constant 100W power and 5, 12 and 24V operating voltages the load currents are 20, 8.33 and 4.17A, respectively.

Only hybrid systems can supply 20A at 5V for 48 hours as shown in figure 12-11 with the MesoGen and MesoPower fuel cell systems dominating. The highest score of 100 indicates that the solution has met all requirements by offering the highest runtime and

lowest weight. Scores higher than 100, are possible when the suggested solutions achieve runtimes higher than the design runtime
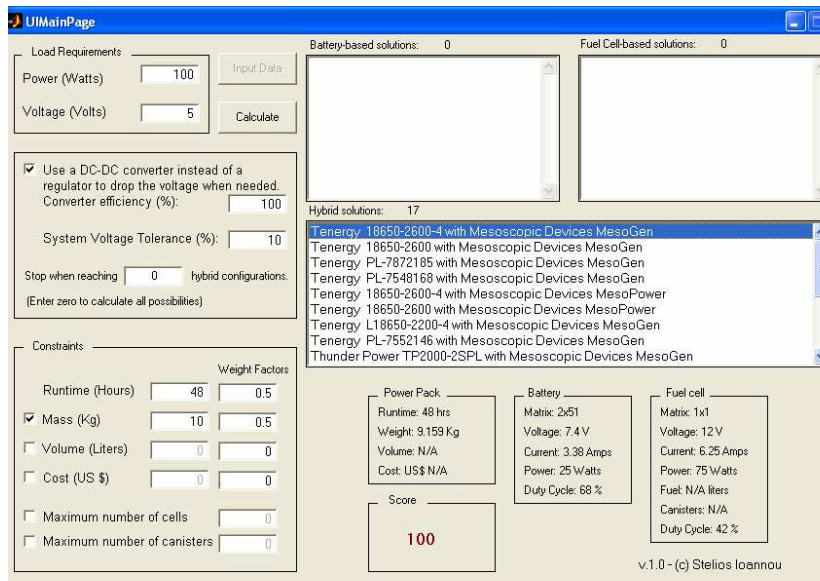
Figure 12-11: Optimized Solutions for 100W, 48 Hours and 5V Application.
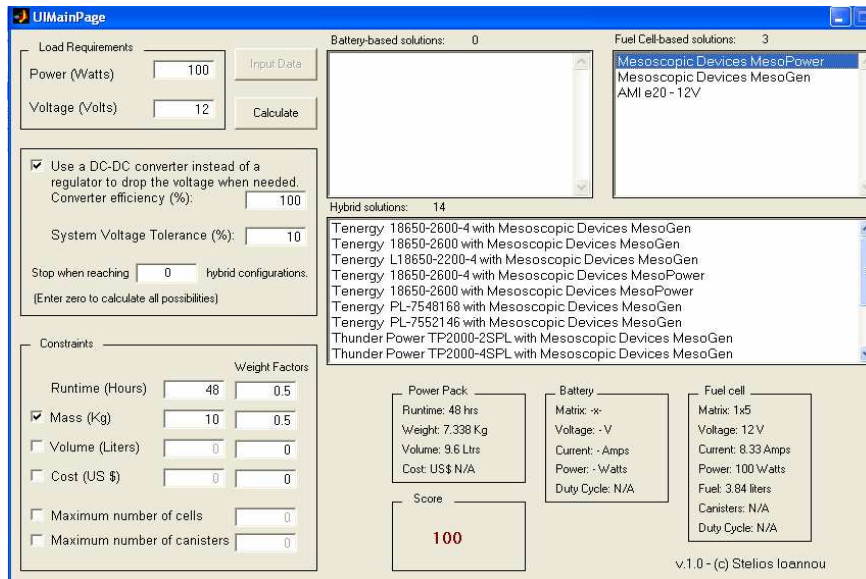
Figure 12-12: Optimized Solutions for 100W, 48 Hours and 12V Application.

The MesoPower fuel cell system shown in figure 12-12 offers the lightest solution despite the fact it requires a matrix of five parallel connected units to meet the load current demand. For the 24 voltage application shown in figure 12-13, only three fuel cell solutions are available with the lightest solution and higher score offered by the MesoPower.

Figure 12-13: Optimized Solutions for 100W, 48 Hours and 24V Application.

CHAPTER 13. DISCUSSION AND FUTURE WORK

13.1 Discussion

The success of any unmanned mobile application depends on the accurate prediction of the energy required to carry out the mission and on the precise, real time state of charge indication. The energy prediction helps to properly select and size the power system, whereas the state of charge indicates the remaining on-board energy. The latter directly corresponds to the remaining runtime and is important for mission planning.

This work proposes a novel way that significantly increases the accuracy of battery runtime estimation, the latter being a significant factor in power system selection and sizing. In addition, this work proposes a novel, optimal way to size power systems including hybrid systems. Both proposed methods are compared with several traditional techniques of calculating battery runtime and of sizing power systems.

Peukert's law is a dominant approach for battery runtime prediction and a way to represent battery capacity loss at higher discharge currents. However, Peukert's law accuracy depends on Peukert's exponent which has been traditionally assumed to be a constant value. There are several methodologies for its calculation with an accuracy that is directly dependent on the length of experimental characterization, a procedure that is time consuming. Furthermore, some research studies claim that Peukert's law is not applicable to lithium battery technology. This is because at high discharge rates, the heat produced is significant and as a result battery temperature can no longer be considered constant.

This work reformulates Peukert's law by proposing a variable exponent which is a function of battery capacity and discharge current. The concept is compared with other

traditional techniques of calculating battery runtime and in every case the reformulated approach yields significantly more accurate results.

Another significant contribution of this work is that it provides a method for estimating the constants of the proposed Peukert's exponent using a single experimental measurement, without compromising accuracy. This measurement typically does not require more than one hour and is referred to as the "half hour test". Additionally, the proposed variable exponent approach can be used to calculate the remaining energy stored in the battery. Unlike other techniques the variable exponent method offers higher accuracy without extensive battery characterization.

Experimentation with different batteries suggests that Peukert's law is also applicable to lithium batteries. This can be attributed to the fact that although there is an increase in capacity due to the increase in temperature, this is offset by a decrease due to polarization occurring at high discharge rates.

In the area of power system selection and sizing for mobile applications this work proposes a novel optimization algorithm which is suitable for sizing hybrid systems as well. The optimal solutions take advantage of a wider database of commercially available products and the suggested solutions depend on user-defined parameters representing application requirements and constraints. All simulation results were compared and verified with the suggested solutions produced by the traditional methodology.

From the survey of power sources between 20 and 100W presented in chapter 3 it was concluded that the linear approach which ignores the loss of capacity at higher discharge currents does not yield an accurate runtime. In addition, the optimization algorithm verifies that for better power system selection and sizing, the operating voltage should be known and taken into consideration whereas from the ATRV-Jr case study it was verified that a wider product selection can improve the probability of finding solutions that can meet user requirements.

Finally, this work presents a Matlab model that estimates the energy demand as a function of time for small to mid-sized robotic vehicles in both indoor and outdoor applications. A comparison of the results of this model with the traditional methodology presented in the case study found that the traditional methodology oversized the system by as much as 50%.

13.2 Conclusions and Recommendations for Future Work

This work has made some major contributions and set a milestone in the area of battery runtime estimation and power system selection and sizing. However, there are some possible future improvements that can be made:

- Extension of the reformulated variable exponent law for Nickel Cadmium (NiCd) batteries.

- Improvement of the accuracy of the b-value estimation procedure. This may involve an examination of the relationship between the b-value and the slope between the 20 hour and other data points.

- Extension of the optimization algorithm by including the effect of burst power and burst duration.

- Extension of the optimization algorithm to size different types of hybrid systems, such as those including a super-capacitor or more than one battery models.

APPENDICES

Appendix A

Table A-1: List of Primary Lithium Batteries Sorted by Highest Energy Density

Brand	Model	Power W/Kg	Density W/L	Energy Density (Wh/Kg)	Energy Density (Wh/L)	Number of Cells for 480Wh	Total Weight Kg	Total Volume Liters
Saft	Lithopack C	5	6	572	628	24.69	0.84	0.76
Saft	Lithopack	28	30	519	570	27.21	0.93	0.84
Saft	PS 52 A	58	76	400	529	5.33	1.20	0.91
Saft	LSC 9V	5	2	372	175	44.44	1.29	2.74
Saft	PS 53 B	53	70	365	485	1.83	1.32	0.99
Saft	LS 9V	12	6	341	161	48.48	1.41	2.99
Saft	PS 48 B	55	60	274	298	1.52	1.75	1.61
Saft	PS 42 A	55	79	274	394	7.62	1.75	1.22
Saft	G15-127	24	28	272	315	0.50	1.76	1.52
Saft	G15-127	24	28	272	315	0.50	1.76	1.52
UltaLife	BA5390U	46	68	256	377	1.44	1.87	1.27
UltaLife	BA5390U	46	68	256	377	1.44	1.87	1.27
Saft	BA 5590HC	68	77	246	279	1.95	1.95	1.72
Saft	BA 5590HC	68	77	246	279	1.95	1.95	1.72
Saft	PS 40 A	64	53	226	187	7.45	2.12	2.56
Bren-tronics	BA-5347/U	78	89	222	256	8.00	2.16	1.88
MIL Power	C0109	34	42	218	266	1.00	2.20	1.80
UltaLife	U2550HCE-CF-UFA	60	136	215	488	37.21	2.23	0.98
MIL Power	BA-5590/U	59	66	211	239	2.22	2.28	2.01
MIL Power	BA-5590/U	59	66	211	239	2.22	2.28	2.01
Saft	G6-104	70	110	210	330	11.43	2.29	1.45

Table A-1 (Continued)

Brand	Model	Power W/Kg	Density W/L	Energy Density (Wh/Kg)	Energy Density (Wh/L)	Number of Cells for 480Wh	Total Weight Kg	Total Volume Liters
Saft	(/C,D,E,F,G,H)	70	110	210	330	11.43	2.29	1.45
MIL Power	BA5290/U	45	65	205	291	1.78	2.35	1.65
MIL Power	BA5290/U	45	65	205	291	1.78	2.35	1.65
Saft	BA5590B/U	66	77	199	230	2.37	2.42	2.09
Saft	BA5590B/U	66	77	199	230	2.37	2.42	2.09
MIL Power	MIL/C4430	63	71	188	213	2.13	2.56	2.25
MIL Power	BA-5600/U	62	96	186	289	7.11	2.58	1.66
MIL Power	1794AS0953U	132	208	185	292	9.52	2.59	1.64
Saft	BA 5800A/U	60	104	181	313	12.08	2.66	1.54
Saft	G30-102/B	34	47	179	253	1.07	2.68	1.90
UltaLife	BA-5367/U	52	118	177	405	123.08	2.71	1.18
UltaLife	BA-5347U	47	77	175	283	7.21	2.74	1.70
Saft	BT 5791	58	82	175	246	2.29	2.74	1.95
Saft	BA 5567A/U	175	348	175	348	171.43	2.74	1.38
Saft	PS 31 A	58	196	173	588	111.11	2.78	0.82
UltaLife	5380	38	117	171	521	7.21	2.81	0.92
Saft	G9-124	59	57	170	164	7.62	2.82	2.92
Saft	BA 5600A/U	56	89	169	268	7.90	2.84	1.79
MIL Power	BA5598/U	55	67	168	202	4.21	2.86	2.37
Saft	BT 5790	56	79	167	236	4.57	2.88	2.03
Saft	BA 5588A/U	95	105	166	183	9.80	2.89	2.62

Table A-1 (Continued)

Brand	Model	Power W/Kg	Density W/L	Energy Density (Wh/Kg)	Energy Density (Wh/L)	Number of Cells for 480Wh	Total Weight Kg	Total Volume Liters
Saft	BA 5847B/U	55	57	166	170	12.08	2.90	2.82
Saft	BT 5313	92	NA	165	NA	2.65	2.91	NA
Saft	BA 5598A/U	51	58	165	187	4.29	2.91	2.57
Saft	G6-105	127	162	163	207	26.79	2.95	2.32
UltaLife	Sophie	42	42	160	160	6.37	2.99	3.00
UltaLife	BA-5368/U	51	104	158	324	40.00	3.04	1.48
UltaLife	BA-5372/U	48	138	150	430	160.00	3.20	1.12
UltaLife	1/2AA	48	109	150	340	320.00	3.20	1.41
Saft	BA 5372/U	90	255	150	425	160.00	3.20	1.13
Saft	G18-115	49	37	148	112	3.81	3.24	4.29
Bren-tronics	BA-5374/U	NA	NA	148	617	57.14	3.24	0.78
MIL Power	BA-5374/U	NA	NA	147	617	57.14	3.26	0.78
Bren-tronics	BA-5372/U	90	255	144	408	166.67	3.33	1.18
Saft	BA 5112A/U	124	129	143	148	18.63	3.35	3.24
MIL Power	BA-5800/U	46	122	141	375	10.39	3.40	1.28
Saft	Li/3	47	173	140	520	7.62	3.43	0.92
Saft	G30-101	49	67	140	194	2.29	3.43	2.48
Tadiran	TLM-1550MP	776	1770	136	310	176.73	3.53	1.55
Saft	PS 38 A	45	59	135	177	22.86	3.54	2.72
Saft	BA 5599A/U	45	55	135	164	7.90	3.56	2.92
MIL Power	BA-5567/U	150	407	129	350	186.05	3.72	1.37

Appendix A (Continued)

Table A-1 (Continued)

Brand	Model	Power W/Kg	Density W/L	Energy Density (Wh/Kg)	Energy Density (Wh/L)	Number of Cells for 480Wh	Total Weight Kg	Total Volume Liters
Saft	BA 5557A/U	112	322	123	354	7.79	3.90	1.36
Saft	BA 5557A/U	112	141	123	155	7.79	3.90	3.09
Tadiran	TLM-1530MP	696	1626	104	244	417.75	4.60	1.97
Saft	G15-114	52	54	99	103	18.05	4.87	4.68
Tadiran	TLM-1550HP	970	2212	97	221	247.42	4.95	2.17
Brentronics	BA-5368/U	59	93	80	127	80.80	5.98	3.77
Saft	BA 5368/U	33	111	74	250	44.44	6.44	1.92
Tadiran	TLM-1520MP	428	1120	73	190	733.38	6.60	2.52
Saft	XSG 1493/1	62	90	70	102	40.34	6.86	4.71
MIL Power	MIL-150483	NA	NA	63	138	29.72	7.58	3.47
Tadiran	TLM-1520HP	525	1374	53	137	1015.87	9.14	3.49
MIL Power	BA-5347/U	14	104	15	116	17.65	31.76	4.14
Tadiran	TLM-1530HP	87.05	2032.33	8.01	186.97	544.90	59.94	2.57

Grey 10% - Less Than 20W/Kg
Grey 20% - Can meet a 3 day mission for less than 4 Kg
Grey 30% - With 3Kg it provides 1557Wh (3 day mission with 22W loads or 31 hour mission with 50W load)
Grey 35% - Between 3 and 10Kg for 480Whr
Grey 40% - More than 80 cells required
Grey 50% - Heaviest Solution

Appendix B

Table B-1: List of Secondary Lithium Technology Batteries

Model	(V)	(Ah)	Crate	(W)	W/Kg	W/L	Wh/Kg	Wh/L	(Kg)	(Ltr)
					UltraLife					
UBBL09	11.1	18.4	C/20	66.6	46	75	142	227	1.44	0.885
UBBL09	22.2	9.2	C/20	66.6	46	75	142	227	1.44	0.885
UBBL01	15.2	8	C/5	98.8	107	153	131	195	0.925	0.646
UBBL02	14.4	12	C/12	172.8	120	193	120	200	1.44	0.896
UBBL02	28.8	6	C/12	172.8	120	193	120	200	1.44	0.896
UBBL03	15.2	7.5	C/5	45.6	48	69	120	175	0.944	0.660
UBBL06	15.2	9.4	C/5	76	74	1914	140	200	1.021	0.040
					MIL Power					
BB-2590/U	30	7.2	C/4	180	132	201	159	241	1.36	0.896
BB-2590/U	15	14.4	C/4	180	132	201	159	241	1.36	0.896
BB-2812/U	12	2.4	NA	36	132	208	106	167	0.272	0.173
MIL/RF5800	10.8	3.6	NA	27	69	113	100	163	0.39	0.238
					Bren-tronics					
BB-2590/U	28.8	6.2	NA	57.6	41	65	128	203	1.4	0.883
BB-2590/U	14.4	12.4	NA	57.6	41	65	128	203	1.4	0.883
BB-2600A/U	7.2	4.6	NA	18	57	79	106	146	0.314	0.227
BB-2800/U	7.2	3.7	NA	18	71	142	106	212	0.255	0.127
BB-2557/U	28.8	2.2	NA	57.6	105	148	115	162	0.55	0.389
BB-2557/U	14.4	4.4	NA	57.6	105	148	115	162	0.55	0.389
					Saft					
VL45E	3.6	45	C/3	360	336	701	149	313	1.07	0.514
VLE 22-42	21.6	42	C/3	2160	270	379	110	158	8	5.702

Appendix B (Continued)

Table B-1 (Continued)

Model	(V)	(Ah)	Crate	(W)	W/Kg	W/L	Wh/Kg	Wh/L	(Kg)	(Ltr)
VLE 11-84	10.8	84	C/3	2160	270	379	110	158	8	5.702
VL41M	3.6	41	C/3	540	505	1051	136	285	1.07	0.514
VM27M	3.6	27	C/3	396	514	1050	124	252	0.77	0.377
VL7P	3.6	7	C	360	973	1881	67	131	0.37	0.191
VL20P	3.6	20	C	900	1125	2386	89	187	0.8	0.377
VL30P	3.6	30	C	1080	982	2102	97	209	1.1	0.514
Intensium 1 (P1500)	48	3.5	C/8	1680	373	512	41	56	4.5	3.280
Intensium 1 (P3000)	48	7	C/8	3360	420	512	46	56	8	6.560
Intensium 1 (E350)	48	5.7	C/8	576	125	176	65	92	4.6	3.280
Intensium 1 (E700)	48	11.4	C/8	1152	134	176	70	92	8.6	6.560
Intensium 3 (E2000)	48	45	C/8	3600	171	214	108	136	21	16.831
MP144350	3.75	2.48	C/5	18.75	276	601	143	344	0.068	0.031
MP 174865	3.75	5.1	C/5	41.25	333	696	163	380	0.124	0.059
MP 174865 IS	3.65	4.8	C/5	36.5	294	616	140	335	0.124	0.059
MP 176065	3.75	6.45	C/5	52.5	343	687	165	375	0.153	0.076
VL 34570	3.75	5.2	C/5	41.25	330	758	160	380	0.125	0.054

Appendix B (Continued)

Table B-2: List of Highest Energy and Less Weight for a 480Wh Mission

Brand	Model	C - Rate	W/Kg	W/L	Wh/Kg	Wh/L	480Whr mission Number Cells	Weight (Kg)	Volume (L)
Saft	MP 176065	C/5	343	687	165	375	20.00	2.91	1.28
Saft	MP 174865	C/5	333	696	163	380	25.26	2.94	1.26
Saft	VL 34570	C/5	330	758	160	380	24.00	3.00	1.26
MIL Power	BB-2590/U	C/4	132	201	159	241	2.22	3.02	1.99
MIL Power	BB-2590/U	C/4	132	201	159	241	2.22	3.02	1.99
Saft	VL45E	C/3	336	701	149	313	2.96	3.22	1.53
Saft	MP144350	C/5	276	601	143	344	48.00	3.36	1.40
UltraLife	UBBL09	C/20	46	75	142	227	2.35	3.38	2.11
UltraLife	UBBL09	C/20	46	75	142	227	2.35	3.38	2.11
UltraLife	UBBL06	C/5	74	1914	140	200	3.36	3.43	2.40
Saft	MP 174865 IS	C/5	294	616	140	335	26.67	3.43	1.43
Saft	VL41M	C/3	505	1051	136	285	3.24	3.53	1.68
UltraLife	UBBL01	C/5	107	153	131	195	3.97	3.66	2.46
Bren-tronics	BB-2590/U	NA	41	65	128	203	2.68	3.75	2.36
Bren-tronics	BB-2590/U	NA	41	65	128	203	2.68	3.75	2.36
Saft	VM27M	C/3	514	1050	124	252	4.95	3.87	1.90
UltraLife	UBBL02	C/12	120	193	120	200	2.77	4.00	2.40
UltraLife	UBBL02	C/12	120	193	120	200	2.77	4.00	2.40
UltraLife	UBBL03	C/5	48	69	120	175	4.21	4.00	2.74
Bren-tronics	BB-2557/U	NA	105	148	115	162	7.62	4.17	2.96
Bren-tronics	BB-2557/U	NA	105	148	115	162	7.62	4.17	2.96
Saft	VLE 22-42	C/3	270	379	110	158	0.53	4.36	3.04
Saft	VLE 11-84	C/3	270	379	110	158	0.53	4.36	3.04
Saft	Intensium 3 (E2000)	C/8	171	214	108	136	0.21	4.44	3.53
MIL Power	BB-2812/U	NA	132	208	106	167	16.55	4.53	2.87
Bren-tronics	BB-2600A/U	NA	57	79	106	146	14.55	4.53	3.29
Bren-tronics	BB-2800/U	NA	71	142	106	212	17.78	4.53	2.26
MIL Power	MIL/RF5800	NA	69	113	100	163	12.31	4.80	2.94
Saft	VL30P	C	982	2102	97	209	4.44	4.95	2.30

Appendix B (Continued)

Table B-2 (Continued)

Brand	Model	C - Rate	W/Kg	W/L	Wh/Kg	Wh/L	480Whr mission		
							Number Cells	Weight (Kg)	Vol.ume (L)
Saft	VL20P	C	1125	2386	89	187	6.67	5.39	2.57
Saft	Intensium 1 (E700)	C/8	134	176	70	92	0.80	6.86	5.22
Saft	VL7P	C	973	1881	67	131	19.20	7.16	3.66
Saft	Intensium 1 (E350)	C/8	125	176	65	92	1.60	7.38	5.22
Saft	Intensium 1 (P3000)	C/8	420	512	46	56	1.30	10.43	8.57
Saft	Intensium 1 (P1500)	C/8	373	512	41	56	2.59	11.71	8.57

Grey 10% - High Power density and low weight for a 480Wh mission

Appendix C

Table C-1: Commercially Available Fuel Cell Systems

Adaptive Materials Inc, e20
Operating temperature -20°C to 50°C
Lightweight portable SOFC for military applications
Functions regardless of orientation
Unassisted cold start
Low thermal signature
Rugged, impact-resistant design

Altek APS 100
Operating temperature -25°C to 45°C
200W maximum
Scalable to up to 10kW
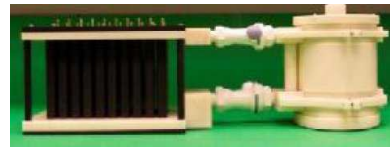
Jadoo nGen
Operating temperature 0°C to 40°C
Lightweight, portable H2 FC for cameras
State of fuel indication

Appendix C (Continued)

Table C-1 (Continued)

Mesoscopic Devices MesoGen 75
Operating temperature -20°C to 60°C
Burns JP-8 or propane
Contains battery that can provide up to 10 Wh

Mesoscopic Devices MesoPower 20
Operating temperature 0°C to 40°C
Orientation independent
Contains battery that can provide up to 3.3 Wh
40 Wh worth internal fuel storage

MTImicro MOBION30
Operating temperature -10°C to 40°C
Doesn't require diluted methanol
120W peak power

Smart Fuel Cell A50
Operating temperature -20°C to 40°C (-35°C for special
applications)
Works well with other power sources (e.g. solar panels)

Appendix C (Continued)

Table C-1 (Continued)

Ultracell XX25
Operating temperature -20$^{\text{o}}$C to 50$^{\text{o}}$C
Lightweight portable RMFC for military applications
Functions under any orientation
Rugged design
Standard military connectors available

Voller ABC 75
Operating temperature 5$^{\text{o}}$C to 40$^{\text{o}}$C
Independent DC/AC outputs
Contains battery for peak loads
USB charging socket built in

Voller RBC 70
Operating temperature 5$^{\text{o}}$C to 40$^{\text{o}}$C
Frost sensor turns unit on at low temperatures
Autonomous battery charging mode

Voller VE 100
Operating temperature 5$^{\text{o}}$C to 40$^{\text{o}}$C
Independent DC/AC outputs
Contains 4Ah battery for peak loads

Appendix C (Continued)

Table C-2: List of Commercially Available Fuel Cells' Characteristics

Brand	Model	Power (W)	Voltage (V)	Weight (Kg)	Dimensions (cm)	Technology	Price (US$)
Adaptive Materials Inc.	e20	20	24/12	1.5	28x9x13	SOFC	NA
Adaptive Materials Inc.	e50	50	NA	NA	NA	NA	NA
Altek	APS100	100	24/12	2	35x13x12	AFC	NA
BCS Fuel Cells, Inc.	FCS 1020	30	12	NA	15x10x9	H2	NA
BCS Fuel Cells, Inc.	FCS2520	80	12	NA	24x13x12	H2	NA
BCS Fuel Cells, Inc.	FCS5018	100	12	3.2	15x10x14	H2	2,910
EFOY	600	25	12	6.3	44x20x28	DMFC	
EFOY	1200	50	12	7.5	44x20x28	DMFC	
EFOY	1600	65	12	7.6	44x20x28	DMFC	
Flexiva	LG2212	15	24/12	2.2	32x21x17	H2	3,899
Jadoo	nGEN	100	12	2.3	11x11x19	H2	1,000
Mesoscopic Devices	MesoGen	75	12	3	13x18x25	SOFC	
Mesoscopic Devices	MesoPower	20	12	0.86	6x12x16	DMFC	
MEU Millitary Version	VE100 v3	100	12	6	20x28x19	H2	custom order
MTImicro	MOBION 30M	30	24/12	4.4	9x25x17	DMFC	
Smart Fuel Cell	A50	50	12	8	39x16x26	DMFC	3,898
SRE	100SR4	100	32/96	0.9	11x11x11	H2	2,425
SRE	25SR4-A	25	24/12	0.196	10x6x2	H2	765
SRE	HW-125	100	24	2	33x27x27	H2	2,695
Ultracell	XX25	25	24/12	1.23	15x23x4	RMFC	
Voller	ABC	70	12	9	38x30x20	H2	7,308
Voller	RBC	65	12	8	18x45x41	H2	6,804

Appendix C (Continued)

Table C-3: Commercially Available Hydrogen Storage Units and Regulators

	Model	Capacity (Liters)	Weight (Kg)	Volume (cm^3)	Volume (Liters)	Price (US$)
1	High Pressure Cylinder SP22017-1	330	5.5	4239	4.239	280
2	BL-18 Metal Hydride	18	0.329	62.30938	0.062	333
3	Extra CANv3 - Metal Hydride Canister	504	1.65	588.75	0.589	1,125
	300Whr per cylinder which is 504 litter of H2					
4	BL-120 Metal Hydride	120	1.067*	367.38	0.367	1,495.00
	*Hydride Mass: 907gr, Container Mass * : 160 gr, Total Mass: 1067gr.					
5	BL-60 Metal Hydride	60	0.63*	232.7635	0.233	991
6	BL-20 Metal Hydride	20	0.3	51.025	0.051	650
7	BL-30 Metal Hydride	30	0.5	78.5	0.079	650
8	BL-250 Metal Hydride	250	2	740.2282	0.740	2,299
9	CL-370 Metal Hydride	370	2.86	1105.28	1.105	505
10	BL-750 Metal Hydride	750	5.5	2147.76	2.148	3,699
Regulators						
1	BL & CL Regulator		0.18	576	0.576	150
2	High Pressure Regulator 3910-15-350			NA	NA	324

Appendix C (Continued)

Table C-4: Fuel Consumption

Brand	Model	Comments
Adaptive Materials Inc.	e20	Total Weight=(1.5+0.5Kg/3days)
Smart Fuel Cell	A50	1.3L methanol/KWh=1.028Kg/KWhr
Flexiva	LG2212	14sl H2 per hour at nominal output power
Voller	VE100	With a 50 Watt load, the unit consumes 1.4 standard liters of hydrogen per minute (SLPM).
Voller	VE100 v3	1.3 l/min at 100% load
Ultracell	XX25	Capacity: 180 Whr, 9hrs at 20W, full weight 345gr and container 131grs. Optimal power of 25W was used in calculations.
EFOY	600	1,1 l/kWh, and 1.3L per 1200Whr
EFOY	1200	1,1 l/kWh, and 1.3L per 1200Whr
EFOY	1600	1,1 l/kWh, and 1.3L per 1200Whr
MTImicro	MOBION 30M	3 day mission at 30W total weight=7.1Kg, Cartridge 0.9Kg, 720Wh
Voller	ABC	With a 50 Watt load, the unit consumes 1.4 standard liters of hydrogen per minute (SLPM).
Voller	RBC	With a 50 Watt load, the unit consumes 1.4 standard liters of hydrogen per minute (SLPM).
Altek	APS100	Total 35.0x12.5x12, Fuel 2.95Kg gives 1500Wh
Jadoo	nGEN	N-Stor130 ($449), capacity 130wh, 2lb, 2.5x4.5inch
Jadoo	nGEN	N-Stor360 ($849), capacity 360Wh, 5.1lb, 2.5x10.5 inch
Mesoscopic Devices	MesoGen	5.2 kg (11.5 lb) with fuel for 3 days
Mesoscopic Devices	MesoPower	1580 W-hr/kg methanol, 1.81 kg (4.0 lb) with fuel for 3 days

Appendix D

Table D-1: List of Secondary Lithium Batteries for Aero-Modeling Applications

Brand	Model	Voltage (Volts)	Capacity (Ah)	Power (W)	Power Density (W/Kg)	(W/L)	Energy Density (Wh/Kg)	(Wh/L)	Burst Power (W)	Burst Power Density (W/Kg)	(W/L)	Weigh (Kg)	Vol. (L)	Price US$/Wh
Tenergy	18650-2600-4	3.7	2.6	14	314	215	209	143	NA	NA	NA	0.046	0.067	$3.32
Tenergy	18650-2600	3.7	2.6	14	314	215	209	143	NA	NA	NA	0.046	0.067	$1.04
Tenergy	PL-7548168	3.7	6.35	23	196	355	196	355	NA	NA	NA	0.120	0.066	$1.09
Tenergy	L18650-2200-4	14.8	2.2	74	436	794	192	350	NA	NA	NA	0.170	0.093	$0.95
Tenergy	LI18650-4400BL	14.8	4.4	96	283	546	191	369	NA	NA	NA	0.340	0.176	$0.92
Thunder Power	TP4000-8S2PL	29.6	4	1421	2284	3866	190	322	2131.2	3426	5799	0.622	0.368	$2.96
Tenergy	PL-7552146	3.7	5.7 at 1.14	21	190	373	190	373	NA	NA	NA	0.111	0.057	$1.09
Thunder Power	TP8000-5S4PL	18.5	8	1480	1873	3141	187	314	1998	2529	4240	0.79	0.471	$2.70
Thunder Power	TP8000-3S4PL	11.1	8	888	1873	3310	187	331	1198.8	2529	4469	0.474	0.268	$2.87
Thunder Power	TP8000-4S4PL	14.8	8	1184	1870	3202	187	320	1598.4	2525	4323	0.633	0.370	$2.79
Thunder Power	TP8000-2S4PL	7.4	8	592	1850	3190	185	319	799.2	2498	4306	0.32	0.186	$2.96
Thunder Power	TP2000-4SPL	14.8	2	355	2220	4372	185	364	592	3700	7286	0.16	0.081	$3.38
Thunder Power	TP4000-2S2PL	7.4	4	355	2220	3265	185	272	532.8	3330	4897	0.16	0.109	$3.38
Thunder Power	TP2000-3SPL	11.1	2	266	2220	4098	185	342	444	3700	6831	0.12	0.065	$3.29

Appendix D (Continued)

Table D-1 (Continued)

Brand	Model	Voltage (Volts)	Capacity (Ah)	Power (W)	Power Density (W/Kg)	Power Density (W/L)	Energy Density (Wh/Kg)	Energy Density (Wh/L)	Burst Power (W)	Burst Power Density (W/Kg)	Burst Power Density (W/L)	Weigh (Kg)	Vol. (L)	Price US$/Wh
Thunder Power	TP2000-2SPL	7.4	2	178	2220	4204	185	350	296	3700	7006	0.08	0.042	$3.38
Thunder Power	TP6000-4S3PL	14.8	6	888	1820	3028	182	303	1598.4	3275	5451	0.488	0.293	$3.04
Thunder Power	TP4000-10S2PL	37	4	1776	2176	3882	181	323	2664	3265	5823	0.816	0.458	$2.84
Tenergy	PL-7872185	3.7	11 at 11	41	179	392	179	392	NA	NA	NA	0.227	0.104	$1.17
Thunder Power	TP4000-6S2PL	22.2	4	1066	2148	3840	179	320	1598.4	3223	5760	0.496	0.278	$3.04
Thunder Power	TP4000-5S2PL	18.5	4	888	2135	3425	178	285	1332	3202	5138	0.416	0.259	$3.11
Thunder Power	TP6000-5S3PL	18.5	6	1110	1770	2970	177	297	1998	3187	5346	0.627	0.374	$2.97
Tenergy	Li18650-2200-4	3.7	2.2	12	265	182	177	121	NA	NA	NA	0.046	0.067	$3.56
Tenergy	Li18650-2200T	3.7	2.2	12	265	176	177	118	NA	NA	NA	0.046	0.069	$0.71
Thunder Power	TP4000-4S2PL	14.8	4	710	2102	3411	175	284	1065.6	3153	5117	0.338	0.208	$3.21
Thunder Power	TP6000-3S3PL	11.1	6	666	1748	3130	175	313	1198.8	3146	5635	0.381	0.213	$3.15
Thunder Power	TP2100-4SPL	14.8	2.1	466	2619	5274	175	352	740	4157	8371	0.178	0.088	$3.22
Thunder Power	TP6000-2S3PL	7.4	6	444	1741	3016	174	302	799.2	3134	5429	0.255	0.147	$3.38
Thunder Power	TP4000-3S2PL	11.1	4	533	2089	3388	174	282	799.2	3134	5082	0.255	0.157	$3.38

Appendix D (Continued)

Table D-1 (Continued)

Brand	Model	Voltage (Volts)	Capacity (Ah)	Power (W)	Power Density (W/Kg)	(W/L)	Energy Density (Wh/Kg)	(Wh/L)	Burst Power (W)	Burst Power Density (W/Kg)	(W/L)	Weigh (Kg)	Vol. (L)	Price US$/Wh
Tenergy	PL6813517 0	3.7	16 at 16	59	169	379	169	379	NA	NA	NA	0.350	0.156	$1.18
Tenergy	1S-500-10	3.7	0.5	19	1682	3003	168	300	28	2523	4505	0.011	0.006	$3.22
Saft	MP 176065	3.75	6.45 at 1.4A	52.5	343	687	165	375	101	662	1325	0.153	0.076	NA
Tenergy	TEN78721 85	14.8	40	592	164	331	164	331	NA	NA	NA	3.600	1.791	$1.69
Thunder Power	TP2100-3SPL	11.1	2.1	350	2462	5142	164	343	555	3908	8162	0.142	0.068	$3.00
Thunder Power	TP2100-2SPL	7.4	2.1	233	2454	5274	164	352	370	3895	8371	0.095	0.044	$3.21
Saft	MP 174865	3.75	5.1 at 1.1A	41.25	333	696	163	380	79	635	1328	0.124	0.059	NA
Saft	VL 34570	3.75	5.2 at 1.1	41.25	330	758	160	380	79	630	1446	0.125	0.054	NA
MIL Power	MIL/BB-2590/U	30	7.2 at 2A	180	132	201	159	241	540	397	603	1.36	0.896	NA
MIL Power	MIL/BB-2590/U	15	14.4 at 4A	180	132	201	159	241	540	397	603	1.36	0.896	NA
Thunder Power	TP480-3SPL	11.1	0.48	80	2351	4403	157	294	116.55	3428	6421	0.034	0.018	$7.50
Thunder Power	TP480-2SPL	7.4	0.48	53	2317	4194	154	280	77.7	3378	6116	0.023	0.013	$8.43
Thunder Power	TP9000-6S2PX	22.2	9	3996	3000	5848	150	292	9990	7500	14621	1.332	0.683	$3.00
Thunder Power	TP2200-4SX	14.8	2.2	814	3734	7204	149	288	1628	7468	14408	0.218	0.113	$3.38
Saft	VL45E	3.6	45 at 15	360	336	701	149	313	900	841	1752	1.07	0.514	NA
Thunder Power	TP6600-5S2PX	18.5	6.6	2442	2978	5952	149	298	6105	7445	14881	0.82	0.410	$3.03

Appendix D (Continued)

Table D-1 (Continued)

Brand	Model	Voltage (Volts)	Capacity (Ah)	Power (W)	Power Density (W/Kg)	(W/L)	Energy Density (Wh/Kg)	(Wh/L)	Burst Power (W)	Burst Power Density (W/Kg)	(W/L)	Weigh (Kg)	Vol. (L)	Price US$/Wh
Thunder Power	TP6600-6S2PX	22.2	6.6	2930	2978	6000	149	300	7326	7445	15000	0.984	0.488	$3.00
Thunder Power	TP9000-5S2PX	18.5	9	3330	2942	5832	147	292	8325	7354	14581	1.132	0.571	$3.00
Thunder Power	TP2200-2SX	7.4	2.2	407	3634	6992	145	280	814	7268	13984	0.112	0.058	$3.68
Thunder Power	TP2200-5SX	18.5	2.2	1018	3608	6861	144	274	2035	7216	13722	0.282	0.148	$3.49
Thunder Power	TP2200-3SX	11.1	2.2	611	3591	6916	144	277	1221	7182	13832	0.17	0.088	$3.48
Saft	MP144350	3.75	2.48 at 0.5A	18.75	276	601	143	344	38	551	1203	0.068	0.031	NA
Tenergy	PL-0550100	3.7	2.7 at 0.54	10	143	400	143	400	NA	NA	NA	0.070	0.025	$1.70
Tenergy	2S-2000-10	7.4	2	148	1423	3039	142	304	222	2135	4558	0.104	0.049	$1.89
Tenergy	PL7521222 3	3.7	25 at 5	93	142	261	142	261	NA	NA	NA	0.650	0.355	$1.30
UltraLife	UBBL09	11.1	18.4 at 1A	66.6	46	75	142	227	400	278	452	1.44	0.885	NA
UltraLife	UBBL09	22.2	9.2 at 0.5A	66.6	46	75	142	227	400	278	452	1.44	0.885	NA
UltraLife	UBBL06	15.2	9.4 at 1.88A	76	74	1914	140	200	NA	NA	NA	1.021	0.040	NA
Saft	MP 174865 IS	3.65	4.8 at 1A	36.5	294	616	140	335	73	589	1231	0.124	0.059	NA
Tenergy	Li18500-1300T-4	3.6	1.3	9	254	170	138	92	NA	NA	NA	0.034	0.051	$2.84
Tenergy	Li14500-800T-4	3.6	0.8	7	343	239	137	95	NA	NA	NA	0.021	0.030	$4.86

Appendix D (Continued)

Table D-1 (Continued)

Brand	Model	Voltage (Volts)	Capacity (Ah)	Power (W)	Power Density (W/Kg)	(W/L)	Energy Density (Wh/Kg)	(Wh/L)	Burst Power (W)	Burst Power Density (W/Kg)	(W/L)	Weigh (Kg)	Vol. (L)	Price US$/Wh
Tenergy	Li14500-800	3.6	0.8	7	343	239	137	95	NA	NA	NA	0.021	0.030	$4.86
Saft	VL41M	3.6	41 at 13.7A	540	505	1051	136	285	1080	1009	2102	1.07	0.514	NA
Tadiran	TLM-1550MP	3.88	0.7 at 0.5A	15.52	776	1770	136	310	58	2,910	6,637	0.02	0.0088	NA
Tenergy	LP-2S-2000-15	7.4	2	229	2085	3874	135	250	311	2825	5248	0.110	0.059	$3.04
Tenergy	PL13212223	3.7	50 at 10	185	132	287	132	287	NA	NA	NA	1.400	0.644	$1.30
UltraLife	UBBL01	15.2	8 at 1.6A	98.8	107	153	131	195	NA	NA	NA	0.925	0.646	NA
Tenergy	PL95212223	3.7	35 at 7	130	130	286	130	286	NA	NA	NA	1.000	0.453	$1.31
Tenergy	2S-1250-10	7.4	1.25	93	1285	3220	128	322	133	1850	4636	0.072	0.029	$1.89
Brentronics	BB-2590/U	28.8	6.2	57.6	41	65	128	203	NA	NA	NA	1.4	0.883	NA
Brentronics	BB-2590/U	14.4	12.4	57.6	41	65	128	203	NA	NA	NA	1.4	0.883	NA
Tenergy	2S-500-10	7.4	0.5	37	1276	3003	128	300	56	1914	4505	0.029	0.012	$3.50
Saft	VM27M	3.6	27 at 9A	396	514	1050	124	252	1080	1403	2863	0.77	0.377	NA
Tenergy	LP-2S-1500-15	7.4	1.5	167	1850	2565	123	171	222	2467	3420	0.090	0.065	$3.06
UltraLife	UBBL03	15.2	7.5 at 1.5	45.6	48	69	120	175	NA	NA	NA	0.944	0.660	NA
UltraLife	UBBL02	14.4	12 at 1A	172.8	120	193	120	200	518	360	578	1.44	0.896	NA

Table D-1 (Continued)

Brand	Model	Voltage (Volts)	Capacity (Ah)	Power (W)	Power Density (W/Kg)	(W/L)	Energy Density (Wh/Kg)	(Wh/L)	Burst Power (W)	Burst Power Density (W/Kg)	(W/L)	Weigh (Kg)	Vol. (L)	Price US$/Wh
UltraLife	UBBL02	28.8	6 at 0.5A	172.8	120	193	120	200	518	360	578	1.44	0.896	NA
Thuner Power	TP350-2SPL	7.4	0.35	47	2119	3669	118	204	66.6		5242	0.022	0.013	$6.54
Thuner Power	TP350-3SPL	11.1	0.35	70	2119	3853	118	214	99.9	3027	5504	0.033	0.018	$6.42
Brentronics	BB-2557/U	28.8	2.2	57.6	105	148	115	162	NA	NA	NA	0.55	0.389	NA
Brentronics	BB-2557/U	14.4	4.4	57.6	105	148	115	162	NA	NA	NA	0.55	0.389	NA
Tenergy	LP-2S-1100-15	7.4	1.1	122	1720	3573	115	238	163	2293	4764	0.071	0.034	$3.19
Tenergy	20c-2s-1000	7.4	1	148	2145	3463	107	173	185	2681	4329	0.069	0.043	$4.45
Power MIL	BB-2812/U	12	2.4	36	132	208	106	167	NA	NA	NA	0.272	0.173	NA
Brentronics	BB-2800/U	7.2	3.7	18	71	142	106	212	NA	NA	NA	0.255	0.127	NA
Brentronics	BB-2600A/U	7.2	4.6	18	57	79	106	146	NA	NA	NA	0.314	0.227	NA
Tenergy	LP-2S-700-15	7.4	0.7	78	1586	3777	106	252	104	2114	5036	0.049	0.021	$3.27
Tadiran	TLM-1530MP	3.83	0.3 at 0.25	7.66	696	1626	104	244	19	1,741	4,065	0.011	0.0047	NA
Power MIL	MIL/RF5800	10.8	3.6	27	69	113	100	163	NA	NA	NA	0.39	0.238	NA
Saft	VL30P	3.6	30 at 30A	1080	982	2102	97	209	1800	1636	3503	1.1	0.514	NA
Tadiran	TLM-1550HP	3.88	0.5 at 0.5	19.40	970	2212	97	221	58	2,910	6,637	0.02	0.0088	NA

Appendix D (Continued)

Table D-1 (Continued)

Brand	Model	Voltage (Volts)	Capacity (Ah)	Power (W)	Power Density (W/Kg)	(W/L)	Energy Density (Wh/Kg)	(Wh/L)	Burst Power (W)	Burst Power Density (W/Kg)	(W/L)	Weigh (Kg)	Vol. (L)	Price US$/Wh
Saft	VL20P	3.6	20 at 20A	900	1125	2386	89	187	1800	2250	4771	0.8	0.377	NA
Tadiran	TLM-1520MP	3.85	0.17 at 0.125	3.85	428	1120	73	190	10	1,069	2,799	0.009	0.0034	NA
Saft	VL7P	3.6	7 at 7A	360	973	1881	67	131	900	2432	4704	0.37	0.191	NA
Tadiran	TLM-1520HP	3.78	0.125 at 0.125	4.73	525	1374	53	137	13	1,470	3,847	0.009	0.0034	NA

Table D-2: Data Analysis for a 325W and 11.1V Application

Brand	Model	Voltage (Volts)	Capacity (Ah)	Power Density (W/Kg)	Energy Density (Wh/Kg)	Burst Power Density (W/Kg)	Weig. (Kg)	Price US$/Wh	For 11.1V and 325W Application			
									Total Number Cells	Total Weig. (Kg)	Total Power (W)	Total Energy (Wh)	Burst Power (W)
UltraLife	UBBL09	11.1	18.4 at 1A	46	142	278	1.44	NA	5	7.75	358	1100	2150
Brentronics	BB-2600A/U	7.2	4.6	57	106	NA	0.314	NA	19	5.91	339	627	NA
MIL Power	MIL/RF5800	10.8	3.6	69	100	NA	0.39	NA	13	4.89	339	489	NA
Tenergy	PL13212223	3.7	50 at 10	132	132	NA	1.400	$1.30	3	4.20	555	555	NA
Tenergy	PL75212223	3.7	25 at 5	142	142	NA	0.650	$1.30	6	3.90	555	555	NA
Tadiran	TLM-1530HP	3.83	0.23 at 0.23	87	8	226	0.11	NA	35	3.89	339	31	881
Saft	VL30P	3.6	30 at 30A	982	97	1636	1.1	NA	3	3.39	3330	329	5550
Saft	VL45E	3.6	45 at 15	336	149	841	1.07	NA	3	3.30	1110	492	2775
Saft	VL41M	3.6	41 at 13.7A	505	136	1009	1.07	NA	3	3.30	1665	449	3330
Tenergy	PL95212223	3.7	35 at 7	130	130	NA	1.000	$1.31	3	3.00	389	389	NA
Saft	VL20P	3.6	20 at 20A	1125	89	2250	0.8	NA	3	2.47	2775	220	5550
Tenergy	PL68135170	3.7	16 at 16	169	169	NA	0.350	$1.18	7	2.45	414	414	NA
Tenergy	PL-0550100	3.7	2.7 at 0.54	143	143	NA	0.070	$1.70	34	2.38	340	340	NA
Saft	VM27M	3.6	27 at 9A	514	124	1403	0.77	NA	3	2.37	1221	294	3330
Tenergy	PL-7872185	3.7	11 at 11	179	179	NA	0.227	$1.17	9	2.15	386	386	NA
Tenergy	PL-7552146	3.7	5.7 at 1.14	190	190	NA	0.111	$1.09	17	1.88	357	357	NA
Tenergy	PL-7548168	3.7	6.35	196	196	NA	0.120	$1.09	15	1.84	360	360	NA
Tenergy	Li18500-1300T-4	3.6	1.3	254	138	NA	0.034	$2.84	39	1.33	338	183	NA
Tenergy	18650-2600-4	3.7	2.6	314	209	NA	0.046	$3.32	24	1.11	347	231	NA!

Table D-2 (Continued)

Brand	Model	Voltage (Volts)	Capacity (Ah)	Power Density (W/Kg)	Energy Density (Wh/Kg)	Burst Power Density (W/Kg)	Weig. (Kg)	Price US$/Wh	For 11.1V and 325W Application				
									Total Number Cells	Total Weig. (Kg)	Total Power (W)	Total Energy (Wh)	Burst Power (W)
Tenergy	18650-2600	3.7	2.6	314	209	NA	0.046	$1.04	24	1.11	347	231	NA
Tenergy	Li18650-2200-4	3.7	2.2	265	177	NA	0.046	$3.56	28	1.29	343	229	NA
Tenergy	Li18650-2200T	3.7	2.2	265	177	NA	0.046	$0.71	28	1.29	343	229	NA
Thunder Power	TP2000-3SPL	11.1	2	2220	185	3700	0.12	$3.29	10	1.20	2664	222	4440
Thunder Power	TP4000-3S2PL	11.1	4	2089	174	3134	0.255	$3.38	5	1.28	2664	222	3996
Thunder Power	TP6000-3S3PL	11.1	6	1748	175	3146	0.381	$3.15	3	1.14	1998	200	3596
Saft	MP 176065	3.75	6.45 at 1.4A	343	165	662	0.153	NA	9	1.38	403	194	777
Saft	MP 174865	3.75	5.1 at 1.1A	333	163	635	0.124	NA	9	1.16	386	189	737
Saft	VL 34570	3.75	5.2 at 1.1a	330	160	630	0.125	NA	9	1.17	386	187	737
Thunder Power	TP2100-3SPL	11.1	2.1	2462	164	3908	0.142	$3.00	8	1.14	2797	186	4440
Saft	MP144350	3.75	2.48 at 0.5A	276	143	551	0.068	NA	19	1.28	353	183	706
Saft	MP 174865 IS	3.65	4.8 at 1A	294	140	589	0.124	NA	10	1.29	381	181	761
Thunder Power	TP8000-3S4PL	11.1	8	1873	187	2529	0.474	$2.87	2	0.95	1776	178	2398
Tenergy	1S-500-10	3.7	0.5	1682	168	2523	0.011	$3.22	95	1.05	1758	176	2636
Thunder Power	TP2200-3SX	11.1	2.2	3591	144	7182	0.17	$3.48	7	1.19	4274	171	8547
Tenergy	Li14500-800T-4	3.6	0.8	343	137	NA	0.021	$4.86	47	0.98	336	134	NA

Appendix D (Continued)

Table D-2 (Continued)

Brand	Model	Voltage (Volts)	Capacity (Ah)	Power Density (W/Kg)	Energy Density (Wh/Kg)	Burst Power Density (W/Kg)	Weig. (Kg)	Price US$/Wh	For 11.1V and 325W Application				
									Total Number Cells	Total Weig. (Kg)	Total Power (W)	Total Energy (Wh)	Burst Power (W)
Tenergy	Li14500-800	3.6	0.8	343	137	NA	0.021	$4.86	47	0.98	336	134	NA
Tadiran	TLM-1530MP	3.83	0.3 at 0.25	696	104	1,741	0.011	NA	88	0.97	674	101	1685
Saft	VL7P	3.6	7 at 7A	973	67	2432	0.37	NA	3	1.14	1110	76	2775
Tadiran	TLM-1520HP	3.78	0.125 at 0.125	525	53	1,470	0.009	NA	140	1.26	662	66	1852
Tadiran	TLM-1550MP	3.88	0.7 at 0.5A	776	136	2,910	0.02	NA	22	0.45	347	61	1302
Tadiran	TLM-1520MP	3.85	0.17 at 0.125	428	73	1,069	0.009	NA	86	0.77	331	56	826
Tadiran	TLM-1550HP	3.88	0.5 at 0.5	970	97	2,910	0.02	NA	18	0.36	353	35	1058
Thunder Power	TP480-3SPL	11.1	0.48	2351	157	3428	0.034	$7.50	5	0.16	365	24	532
Thunder Power	TP350-3SPL	11.1	0.35	2119	118	3027	0.033	$6.42	5	0.17	360	20	514

Grey 10% - Adjustments required to meet voltage and power requirements
Grey 20% - Since weight was too low then adjustment was made to have more energy
Grey 30% - Both of the above
Grey 40% - Weight <1.3Kg AND 178Wh<Toral Energy<231Wh
Grey 50% - More than 80 cells required

216

Appendix E

Table E-1: Battery Database for Optimization Algorithm

Brand	Model	(Volts)	(Ah)	Discharge Rate	(W)	(Kg)	Liters	US $	max amps	p
Default				5				3		1.1
Bren-tronics	BB-2590/U	28.8	6.2		57.6	1.4	0.8831529		2	
Bren-tronics	BB-2590/U	14.4	12.4		57.6	1.4	0.8831529		4	
Bren-tronics	BB-2557/U	28.8	2.2		57.6	0.55	0.3885		2	
Bren-tronics	BB-2557/U	14.4	4.4		57.6	0.55	0.3885		4	
Bren-tronics	BB-2800/U	7.2	3.7		18	0.255	0.1271246		2.5	
Bren-tronics	BB-2600A/U	7.2	4.6		18	0.314	0.2266601		2.5	
MIL Power	MIL/BB-2590/U	30	7.2	3.6	180	1.36	0.896112		6	
MIL Power	MIL/BB-2590/U	15	14.4	3.6	180	1.36	0.896112		12	
MIL Power	BB-2812/U	12	2.4		36	0.272	0.1730093		3	
MIL Power	MIL/RF5800	10.8	3.6		27	0.39	0.238		2.5	
Saft	MP 176065	3.75	6.45	4.607143	52.5	0.153	0.07644		14	
Saft	MP 174865	3.75	5.1	4.636364	41.25	0.124	0.05928		11	
Saft	VL 34570	3.75	5.2	4.727273	41.25	0.125	0.0544473		11	
Saft	VL45E	3.6	45	3	360	1.07	0.5138334		100	
Saft	MP144350	3.75	2.48	5	18.75	0.068	0.031175		5	
Saft	MP 174865 IS	3.65	4.8	4.8	36.5	0.124	0.05928		10	
Saft	VL41M	3.6	41	2.992701	540	1.07	0.5138334		150	
Saft	VM27M	3.6	27	3	396	0.77	0.377274		110	
Saft	VL30P	3.6	30	1	1080	1.1	0.5138334		300	
Saft	VL20P	3.6	20	1	900	0.8	0.377274		250	
Saft	VL7P	3.6	7	1	360	0.37	0.1913398		100	
Tadiran	TLM-1550MP	3.88	0.7	1.4	15.52	0.02	0.0087693		4	

Appendix E (Continued)

Table E-1 (Continued)

Brand	Model	(Volts)	(Ah)	Discharge Rate	(W)	(Kg)	Liters	US $	max amps	p
Default				5				3		1.1
Tadiran	TLM-1530MP	3.83	0.3	1.2	7.66	0.011	0.0047113		2	
Tadiran	TLM-1550HP	3.88	0.5	1	19.40	0.02	0.0087693		5	
Tadiran	TLM-1520MP	3.85	0.17	1.23	3.85	0.009	0.0034389		1	
Tadiran	TLM-1520HP	3.78	0.125	1	4.73	0.009	0.0034389		1.25	
Tadiran	TLM-1530HP	3.83	0.23	1	9.58	0.11	0.0047113		2.5	
Tenergy	18650-2600-4	3.7	2.6		14	0.046	0.0672056	31.96	3.9	
Tenergy	18650-2600	3.7	2.6		14	0.046	0.0672056	9.99	3.9	
Tenergy	PL-7548168	3.7	6.35		23	0.12	0.066248	25.5	6.35	
Tenergy	L18650-2200-4	14.8	2.2		74	0.1696	0.0931441	30.95	5	
Tenergy	LI18650-14.8V4400BL	14.8	4.4		96	0.3402	0.176256	59.99	6.5	
Tenergy	PL-7552146	3.7	5.7	5	21	0.111	0.05655	22.95	5.7	
Tenergy	PL-7872185	3.7	11	1	41	0.227	0.103896	47.5	11	
Tenergy	Li18650-2200-4	3.7	2.2		12	0.046	0.0672056	28.99	3.3	
Tenergy	Li18650-2200T	3.7	2.2		12	0.046	0.0692422	5.79	3.3	
Tenergy	PL68135170	3.7	16	1	59	0.35	0.15606	69.99	16	
Tenergy	1S-500-10	3.7	0.5		19	0.011	0.00616	5.95	5	
Tenergy	TEN7872185	14.8	40		592	3.6	1.79075	999.95	40	
Tenergy	PL-0550100	3.7	2.7	5	10	0.07	0.025	16.95	2.7	
Tenergy	2S-2000-10	7.4	2		148	0.104	0.048708	27.95	20	
Tenergy	PL75212223	3.7	25	5	93	0.65	0.35457	119.99	25	
Tenergy	Li18500-1300T-4	3.6	1.3		9	0.034	0.0509134	13.29	2.4	
Tenergy	Li14500-800T-4	3.6	0.8		7	0.021	0.0301835	13.99	2	

Appendix E (Continued)

Table E-1 (Continued)

Brand	Model	(Volts)	(Ah)	Discharge Rate	(W)	(Kg)	Liters	US $	max amps	p
Default				5				3		1.1
Tenergy	Li14500-800	3.6	0.8		7	0.021	0.0301835	13.99	2	
Tenergy	LP-2S-2000-15	7.4	2		229	0.11	0.05922	44.95	31	
Tenergy	PL13212223	3.7	50	5	185	1.4	0.64395	239.99	50	
Tenergy	PL95212223	3.7	35	5	130	1	0.45315	169.99	35	
Tenergy	2S-1250-10	7.4	1.25		93	0.072	0.02873	17.5	12.5	
Tenergy	2S-500-10	7.4	0.5		37	0.029	0.01232	12.95	5	
Tenergy	LP-2S-1500-15	7.4	1.5		167	0.09	0.064906	33.95	22.5	
Tenergy	LP-2S-1100-15	7.4	1.1		122	0.071	0.03417	25.95	16.5	
Tenergy	20c-2s-1000	7.4	1		148	0.069	0.042735	32.95	20	
Tenergy	LP-2S-700-15	7.4	0.7		78	0.049	0.02057	16.95	10.5	
Thunder Power	TP4000-8S2PL	29.6	4		1421	0.622	0.3675	349.95	48	
Thunder Power	TP8000-3S4PL	11.1	8		888	0.474	0.26825	254.95	80	
Thunder Power	TP8000-5S4PL	18.5	8		1480	0.79	0.47125	399.95	80	
Thunder Power	TP8000-4S4PL	14.8	8		1184	0.633	0.36975	329.95	80	
Thunder Power	TP2000-2SPL	7.4	2		178	0.08	0.04225	49.95	24	
Thunder Power	TP2000-3SPL	11.1	2		266	0.12	0.065	72.95	24	
Thunder Power	TP2000-4SPL	14.8	2		355	0.16	0.08125	99.95	24	
Thunder Power	TP4000-2S2PL	7.4	4		355	0.16	0.1088	99.95	48	

Appendix E (Continued)

Table E-1 (Continued)

Brand	Model	(Volts)	(Ah)	Discharge Rate	(W)	(Kg)	Liters	US $	max amps	p
Default				5				3		1.1
Thunder Power	TP8000-2S4PL	7.4	8		592	0.32	0.1856	174.95	80	
Thunder Power	TP6000-4S3PL	14.8	6		888	0.488	0.29325	269.95	60	
Thunder Power	TP4000-10S2PL	37	4		1776	0.816	0.4575	419.95	48	
Thunder Power	TP4000-6S2PL	22.2	4		1066	0.496	0.2775	269.95	48	
Thunder Power	TP4000-5S2PL	18.5	4		888	0.416	0.25925	229.95	48	
Thunder Power	TP6000-5S3PL	18.5	6		1110	0.627	0.37375	329.95	60	
Thunder Power	TP4000-4S2PL	14.8	4		710	0.338	0.20825	189.95	48	
Thunder Power	TP6000-3S3PL	11.1	6		666	0.381	0.21275	209.95	60	
Thunder Power	TP2100-4SPL	14.8	2.1		466	0.178	0.0884	99.95	31.5	
Thunder Power	TP6000-2S3PL	7.4	6		444	0.255	0.1472	149.95	60	
Thunder Power	TP4000-3S2PL	11.1	4		533	0.255	0.15725	149.95	48	
Thunder Power	TP2100-3SPL	11.1	2.1		350	0.142	0.068	69.95	31.5	
Thunder Power	TP2100-2SPL	7.4	2.1		233	0.095	0.0442	49.95	31.5	
Thunder Power	TP480-3SPL	11.1	0.48		80	0.034	0.01815	39.95	7.2	
Thunder Power	TP480-2SPL	7.4	0.48		53	0.023	0.012705	29.95	7.2	

Appendix E (Continued)

Table E-1 (Continued)

Brand	Model	(Volts)	(Ah)	Discharge Rate	(W)	(Kg)	Liters	US $	max amps	p
Default				5				3		1.1
Thunder Power	TP9000-6S2PX	22.2	9		3996	1.332	0.68328	599.99	180	
Thunder Power	TP2200-4SX	14.8	2.2		814	0.218	0.112992	109.99	55	
Thunder Power	TP6600-5S2PX	18.5	6.6		2442	0.82	0.410256	369.99	132	
Thunder Power	TP6600-6S2PX	22.2	6.6		2930	0.984	0.4884	439.99	132	
Thunder Power	TP9000-5S2PX	18.5	9		3330	1.132	0.57096	499.99	180	
Thunder Power	TP2200-2SX	7.4	2.2		407	0.112	0.058208	59.99	55	
Thunder Power	TP2200-5SX	18.5	2.2		1018	0.282	0.148302	141.99	55	
Thunder Power	TP2200-3SX	11.1	2.2		611	0.17	0.088275	84.99	55	
Thunder Power	TP350-2SPL	7.4	0.35		47	0.022	0.012705	16.95	6.3	
Thunder Power	TP350-3SPL	11.1	0.35		70	0.033	0.01815	24.95	6.3	
UltraLife	UBBL09	11.1	18.4	18.4	66.6	1.44	0.8847328		6	
UltraLife	UBBL09	22.2	9.2	18.4	66.6	1.44	0.8847328		3	
UltraLife	UBBL06	15.2	9.4	5	76	1.021	0.0397155		5	
UltraLife	UBBL01	15.2	8	5	98.8	0.925	0.645568		6.5	
UltraLife	UBBL02	14.4	12	12	172.8	1.44	0.896112		12	
UltraLife	UBBL02	28.8	6	12	172.8	1.44	0.896112		6	
UltraLife	UBBL03	15.2	7.5	5	45.6	0.944	0.659792		3	

Table E-2: Fuel Cell Database for Optimization Algorithm

Brand	Model	Wattag	Voltage	Weight	Vol (L)	Technology	Price	$/W	Consumption Kg/Wh	Consumption L/Wh	H2 L/Wh	Camister	BL	CL	CAN V3	N-Stor
AMI	e20 - 24V	20	24	1.5	3.276	SOFC		0	0.0003	-1	-1		-1	-1	-1	-1
AMI	e20 - 12V	20	12	1.5	3.276	SOFC		0	0.0003	-1	-1		-1	-1	-1	-1
Altek	APS100 - 24V	100	24	2	5.46	AFC		0	0.002	-1	-1		-1	-1	-1	-1
Altek	APS100 - 12V	100	12	2	5.46	AFC		0	0.002	-1	-1		-1	-1	-1	-1
EFOY	"600"	25	12	6.3	24.64	DMFC	2900	116	0.0009	0.0011	-1		-1	-1	-1	-1
EFOY	"1200"	50	12	7.5	24.64	DMFC	4300	86	0.0009	0.0011	-1		-1	-1	-1	-1
EFOY	"1600"	65	12	7.6	24.64	DMFC	4600	70.8	0.0009	0.0011	-1		-1	-1	-1	-1
Flexiva	LG2212 - 24V	15	24	2.2	11.424	H2	3,395	226	-1	-1	0.933	2	-1	1	-1	-1
Flexiva	LG2212 - 12V	15	12	2.2	11.424	H2	3,395	226	-1	-1	0.933	2	-1	1	-1	-1
Jadoo	nGEN	100	12	2.3	2.299	H2	3499	35	-1	-1	-1	4	-1	-1	-1	1
Mesoscopic Devices	MesoGen	75	12	3	5.85	SOFC		0	0.0004	-1	-1		-1	-1	-1	-1
Mesoscopic Devices	MesoPower	20	12	0.86	1.152	DMFC		0	0.0006	0.0008	-1		-1	-1	-1	-1
MEU Mil Ver	VE100 v3	100	12	6	10.64	H2		0	-1	-1	0.78	3	-1	-1	1	-1
MTImicro	MOBION 30M - 24V	30	24	4.4	3.825	DMFC		0	0.0013	0.0016	-1		-1	-1	-1	-1
MTImicro	MOBION 30M - 12V	30	12	4.4	3.825	DMFC		0	0.0013	0.0016	-1		-1	-1	-1	-1
Smart Fuel Cell	A50	50	12	8	16.224	DMFC	3,898	78	0.001	0.0013	-1		-1	-1	-1	-1
Ultracell	XX25 - 24V	25	24	1.23	1.38	RMFC		0	0.0026	-1	-1		-1	-1	-1	-1
Ultracell	XX25 - 12V	25	12	1.23	1.38	RMFC		0	0.0026	-1	-1		-1	-1	-1	-1
Voller	ABC	70	12	9	22.8	H2	7,308	104	-1	-1	1.68	1	1	-1	-1	-1
Voller	RBC	65	12	8	33.21	H2	#####	105	-1	-1	1.68	1	1	-1	-1	-1

Table E-2 (Continued)

Brand	Model	Wattage	Voltage	Weight	Vol (L)	Technology	Price	$/W	Consumption Kg/Wh	Consumption L/Wh	H2 L/Wh	Camister	BL	CL	CAN V3	N-Stor
Idatech	iGen - 24V	250	24	9	30	DMFC	10,000		0.0016	0.002	-1		-1	-1	-1	-1
Idatech	iGen - 12V	250	12	9	30	DMFC	10,000		0.0016	0.002	-1					

Appendix E (Continued)

Table E-3: Fuel Cell Canister Database for Optimization Algorithm

Canister Model	BL-18	BL-20	BL-30	BL-60	BL-120	BL-250	BL-750	CL-370	CANv3	N-Stor 130	N-Stor 360
Canister type	1	1	1	1	1	1	1	2	3	4	4
Capacity (Liters)	18	20	30	60	120	250	750	370	504	-1	-1
Weight (Kg)	0.329	0.3	0.5	0.63	1.067	2	5.5	2.86	1.65	0.909	2.318
Volume (Liters)	0.062	0.051	0.08	0.233	0.367	0.74	2.148	1.105	0.589	0.362	0.844
Price (US $)	333	650	650	991	1495	2299	3699	505	1125	449	849
Energy (Whr)	-1	-1	-1	-1	-1	-1	-1	-1	-1	130	360

ABOUT THE AUTHOR

Stelios Ioannou (MSc'02) is a student member of IEEE. He was born in Nicosia, Cyprus on June 29, 1976. He received the Higher National Diploma (HND) in the field of Electrical and Electronics Engineering from Higher Technical Institute (HTI), Nicosia, Cyprus, and then transferred to University of South Florida (USF) where he received a BSEE and an MSEE with Minor in Engineering Management. As a PhD candidate for the Clean Energy Research Center (CERC) and Unmanned Systems Lab (USL) at USF, he is involved in improving endurance on Unmanned Ground Vehicles (UGVs) and Unmanned Aerial Systems (UAS). Specializations include power and energy demand of unmanned systems, prediction of available onboard energy, battery characterization and state of art energy storage devices including lithium, fuel cell and super-capacitor technologies. Other research interests include the design of high voltage testing equipment and the diagnostic analysis of electronic components via a high impulse current generator.